Development of native electrophoretic techniques for the isolation and characterization of mitochondrial complexes

Dissertation

zur Erlangung des Doktorgrades
der Naturwissenschaften

vorgelegt beim Fachbereich Biowissenschaften
der Johann Wolfgang Goethe-Universität
in Frankfurt am Main

von

Zibirnisa Kadeer

aus Kashgar, China

Frankfurt am Main 2012

(D30)

vom Fachbereich Biowissenschaften der Johann Wolfgang Goethe-Universität als Dissertation angenommen.

Dekanin :   Prof. Dr. Anna Starzinski-Powitz

Gutachter: Prof. Dr. Heinz D. Osiewacz

                            Prof. Dr. Hermann Schägger

Datum der Disputation: 09.04.2013

Teile der vorliegenden Arbeit wurden unter meinem früheren Namen *Zibiernisha Wumaier* veröffentlicht:

Original articles:

Wumaier, Z., Nübel, E., Wittig, I., and Schägger, H. (2009) Two-dimensional native electrophoresis for fluorescent and functional assays of mitochondrial complexes. *Methods Enzymol.* **456**:153-168

Zickermann, V.*, **Wumaier, Z.***, Wrzesniewska, B., Hunte, C., and Schägger, H. (2010) Native immunoblotting of blue native gels (NIBN) to identify conformation-specific antibodies. *Proteomics* **10**, 1959-1963   *** equal contribution**.

Wittig, I., Meyer, B., Heide, H., Steger, M., Bleier, L., **Wumaier, Z.**, Karas, M., and Schägger, H. (2010) Assembly and oligomerization of human ATP synthase lacking mitochondrial subunits a and A6L. *Biochim. Biophys. Acta* **1797**, 1004-1011

Wittig, I., Beckhaus, T., **Wumaier, Z.**, Karas, M. and Schägger, H. (2010) Mass estimation of native proteins by blue native electrophoresis: principles and practical hints. *Mol. Cell. Proteomics* **9**, 2149-2161

Strecker, V., **Wumaier, Z.**, Wittig, I., and Schägger, H. (2010) Large pore gels to separate mega protein complexes larger than 10 MDa by blue native electrophoresis: Isolation of putative respiratory strings or patches. *Proteomics* **18**, 3379-3387

Angerer, H., Zwicker, K., **Wumaier, Z.**, Sokolova, L., Heide, H., Steger, M., Kaiser, S., Nübel, E., Brutschy, B., Radermacher, M., Brandt, U., and Zickermann, V. (2011) A scaffold of accessory subunits links the peripheral arm and the distal proton pumping module of mitochondrial complex I. *Biochem. J.* **437**, 279-288

Kadeer, Z., Cruciat, M., Strecker, V., Angerer, H., Pfeiffer, K., Schägger, H., Stuart, R. A., and Wittig, I. (2012) Respirasome-associated Cox26 protein binds to cytochrome *c* oxidase subunit Cox2. *Manuscript in preparation*

Supplements / Abstracts :

Poster Talk: 18th July 2010

Wumaier, Z.: "Assembly and oligomerization of human ATP synthase lacking mitochondrial subunits a and A6L". 16th European Bioenergetics Conference - Warsaw, 17-22 July 2010

Abstract:

Wumaier, Z., Wittig, I., Meyer, B., Heide, H., Steger, M., Bleier, L., Karas, M., and Schägger, H. (2010) Assembly and oligomerization of human ATP synthase lacking mitochondrial subunits a and A6L. *Biochim. Biophys. Acta* **1797**, 39-40

Die vorliegende Arbeit wurde in der Zeit von September 2007 bis Mai 2012 im Gustav-Embden Zentrum der Biologischen Chemie, Molekulare Bioenergetik, des Fachbereichs Medizin der Goethe Universität in Frankfurt am Main unter Anleitung von Prof. Dr. Hermann Schägger durchgeführt.

Acknowlegments

Table of Contents

I.A.   Zusammenfassung

Das erste Ziel dieser Arbeit war die Entwicklung eines neuen zwei-dimensionalen Elektrophoresesystems, bei dem der native Zustand von Proteinen und Proteinkomplexen in beiden aufeinanderfolgenden Laufrichtungen erhalten bleiben sollte. Damit sollte die proteinchemische und biochemische Untersuchung riesiger Proteinkomplexe, wie der Superkomplexe der mitochondrialen Atmungskette, wesentlich erleichtert werden. Gleichzeitig sollten die gravierenden Nachteile der bisher bekannten zwei-dimensionalen Blau-Nativ Elektrophorese (2-D BN/BN Elektrophorese) vermieden werden. Dieses System hat nämlich den Nachteil, dass der verwendete Coomassie-Farbstoff in der zweiten Dimension der Elektrophorese die In-Gel-Farbreaktionen und die Detektierbarkeit von Fluoreszenz-markierten Proteinen beträchtlich stört. Deswegen wurde im neuen 2-D Elektrophoresesystem (2-D BN/hrCNE) die sogenannte "high-resolution clear native electrophoresis" (hrCNE) für die zweite Laufrichtung verwendet, die eine ungestörte Proteinidentifizierung im Gel über Fluoreszenzmarkierung und enzymatische Tests erlaubt. Diese neue Kombination zweier Nativ-Elektrophoresen (BNE und hrCNE) vereinfacht proteomische und biochemische Analysen von Superkomplexen, weil BNE zur Isolierung von Superkomplexen geeignet ist und die nachfolgende hrCNE, Einzelkomplexe aus den Superkomplexen abspaltet und voneinander trennt. Damit wird die Komplexität des Systems beträchtlich reduziert. Das System eignet sich besonders für die Identifizierung von Membranproteinkomplexen anhand spezifischer Fluoreszenzmarkierungen oder anhand ihrer enzymatischen Eigenschaften, die direkt im Nativ-Gel analysiert werden können. Verwendung fand dieser Ansatz vor allem bei der Identifizierung und Charakterisierung von Superkomplexen der mitochondrialen Atmungskette aus unterschiedlichen Spezies und Geweben. Die Analyse der obligat aeroben Hefe *Yarrowia lipolytica* führte zur Identifizierung bisher nicht bekannter Typen von Superkomplexen.

Ein zweites Ziel der Arbeit war die Entwicklung einer Methode für das Native Immunoblotting von Blau-Nativen Gelen (NIBN). Die neue Technik sollte die Identifizierung von konformationsspezifischen Antikörpern ermöglichen und die Unterscheidung von Antikörpern erlauben, die lineare Epitope von denaturierten Proteinen erkennen. Dies wird immer wichtiger für die elektronenmikroskopische Identifizierung von nativen Proteinen und generell für Strukturuntersuchungen. Zu diesem Zweck wurde ein allgemein verwendetes Protokoll für den Western Blott von Blau-Nativen Gelen auf solche Art und Weise

modifiziert, dass der native Zustand von Proteinen und Protein-Komplexen in jedem Teilschritt des Protokolls bewahrt wurde. Anstelle des in Western Blott üblicherweise verwendeten Methanols, der leicht zur Proteindenaturierung führt, wurden milde Detergenzien wie Tween 20, Digitonin oder Brij 35 zur Entfärbung des Blotts verwendet. Als Modell für die Methodenentwicklung diente der größte und komplizierteste Atmungskettenkomplex aus *Y. lipolytica*, die NADH:Ubichinon Oxidoreduktase (Komplex I). Der native Zustand des Enzyms auf der Blott-Membran wurde anschließend durch Aktivitätsfärbung überprüft. Aktivitätsfärbungen des Komplex I auf der Membran, die mit milden Detergentien gewaschen wurden zeigten, dass die NADH Oxidationsdomäne des Enzymes nach Entfernung des Coomassie-Farbstoffes immer noch funktionell blieb. Dies wurde auch durch Verwendung monoklonaler Antikörper, die ausschließlich unter nativen Bedingungen an Komplex I binden, bestätigt. NIBN kann als eine einfache alternative Methode an Stelle des technisch anspruchsvollen und aufwändigen nativen ELISA verwendet werden, wenn ein Fundus von Antikörpern nach konformationsspezifischen Antikörpern für strukturelle, meist elektronenmikroskopische Studien durchsucht werden soll. Im Vergleich zur aufwändigen Probenvorbereitung beim nativen ELISA mit Affinitätschromatographie und Proteinaufreinigung, spart NIBN viel Zeit, weil keine "affinity-tags" in Proteine eingebaut werden müssen und keine Affinitätschromatograpie gebraucht wird. Die native Elektrophorese übernimmt selbst die Isolierung des interessierenden Proteins oder Proteinkomplexes. Besonders wertvoll ist die NIBN-Technik für Proben, die nicht leicht einer genetischen Manipulation und der Einführung von "affinity-tags" zugänglich sind.

Der dritte Teil der Arbeit hatte zum Ziel, die direkten Protein-Protein Kontakte von Cox26, einem hydrophoben Protein, zu ermitteln, das Schägger und Kollegen in Hefe-Superkomplexen (Respirasome) identifiziert hatten. Die Superkomplexe von *S. cerevisiae,* die aus den Komplexen III und IV zusammengesetzt sind, enthalten mindestens 21 Untereinheiten. Zehn Untereinheiten davon sind dem Komplex III zuzurechnen und elf Untereinheiten dem Komplex IV. All diese Untereinheiten waren zunächst als potentielle Nachbarn des Cox26 Proteins anzusehen. Um die tatsächlich vorliegenden Topologien zu ermitteln, wurden multi-dimensionale elektrophoretische Techniken angewendet, die geeignet sind kovalente und nicht-kovalente Protein-Protein Wechselwirkungen von Cox26 zu identifizieren. Drei-dimensionale Elektrophorese (BN/BN/SDS-PAGE) zeigte, dass der Hauptanteil aller Cox26 Proteine nicht-kovalent an die Komplex IV-Komponente der Respirasome gebunden war. Vier-dimensionale Elektrophorese (BN/BN/SDS/SDS-PAGE) unter reduzierenden und nicht-reduzierenden Bedingungen zeigte, dass ein geringer Anteil der

Cox26 Proteine an einen Cysteinrest der Cox2-Untereinheit des Komplex IV unter Ausbildung einer Disulfid-Brücke gebunden war. Dies legte nahe, dass Cox26 eine spezielle Rolle für den Komplex IV spielt, obwohl bisher keine konkrete Funktion nachgewiesen werden konnte und bei Cox26-Defizienz kein spezieller Phänotyp auftritt. Auf der Grundlage eines Strukturmodells des Hefe-Respirasoms und mit der neuen Erkenntnis, dass eine Disulfid-Brücke zwischen Cox2 und Cox 26 existiert, wurde eine strukturelle Rolle des Cox26 Proteins für die Assemblierung und/oder Stabilität von respiratorischen Ketten oder Netzen vorgeschlagen.

Der vierte Abschnitt dieser Arbeit hatte die Isolierung und Charakterisierung von nativen und morphologisch intakten Nucleoiden aus Rinderherzmitochondrien zum Ziel. Mitochondrien besitzen eine eigene mitochondriale DNA (mtDNA), die im Matrixraum lokalisiert ist. Die mtDNA ist innerhalb des mitochondrialen Netzwerks nicht homogen verteilt, sondern ausschließlich in den sogenannten Nucleoiden konzentriert. Unter der Annahme, dass ein Nucleoid eine Kopie des mtDNA Genoms (16.6 kb; 10.7 MDa) und vergleichbar große Massen von gebundenen Proteinen und auch von RNA enthält, besitzt ein mt-Nucleoid eine molekulare Masse von mindestens 30 MDa. Dies ist viel größer als die 1-3 MDa von Atmungsketten-Superkomplexen und auch größer als der 10 MDa Pyruvat-Dehydrogenase Komplex. Damit stellen Nucleoide die größten Komplexe in einem Mitochondrium dar, die bisher identifiziert wurden. Die meisten publizierten Studien zu mitochondrialen Nucleoiden wurden an Xenopus-Oozyten und an sich ständig teilenden Krebszell-Linien durchgeführt. Nucleoide von ausdifferenzierten Geweben, wie Säugetiergeweben, wurden bisher kaum untersucht. Deswegen lag der Focus in diesem Teil der Arbeit auf der Isolierung und Charakterisierung intakter Nucleoide aus Rinderherzmitochondrien. Basis für die erfolgreiche Isolierung nativer mt-Nucleoide waren unsere umfangreichen Vorarbeiten zur Optimierung der Bedingungen für eine möglichst milde Reinigung und die Nachreinigung der riesigen Nucleoid-Komplexe mit der neu entwickelten Blau-Nativ Elektrophorese an "large pore" Gelen. Für die Solubilisierung der mitochondrialen Membranen wurde das Detergens Dodecylmaltosid verwendet, das mitochondriale Superkomplexe vollständiger in die Einzelkomplexe dissoziiert als die Detergenzien Triton X-100 oder Nonidet NP-40, die bisher fast ausschließlich für die Isolierung von Nucleoiden verwendet wurden.

Die elektronmikroskopischen Analysen von nativen Nucleoiden, die von Dr. Karen Davies vom Max-Planck-Institut für Biophysik, Abteilung Strukturbiologie in Frankfurt, durchgeführt wurden, zeigten eine beeindruckende Homogenität der Nucleoid-Partikel, was

auf eine bisher nie so offensichtlich erkennbare Nativität einer Präparation hindeutet. Die Analyse im "negative stain" zeigte Partikel mit einer einheitlichen Größe von 85x100 nm während mit der Cryo-Elektronenmikroskopie eine homogene Partikelgröße von 100x150 nm festgestellt wurde. Die Größenunterschiede dürften auf den unterschiedlichen Dehydratationsgrad der Partikel bei Anwendung der beiden unterschiedlichen Techniken zurückzuführen sein, wobei die Cryo-Technik die geringere Dehydratation und damit die exakteren Werte ergeben sollte. Daneben waren nur wenige Hantel-förmige Strukturen sichtbar, die auf eine Dimerisierung von Nucleoiden hindeuteten. Bei Anwendung härterer Bedingungen wurden auch 70 nm Partikel in Cryo-Tomogrammen identifiziert, die vermutlich instabile und teilweise desintegrierte Kern-Strukturen von Nucleoiden darstellen.

Die Homogenität der isolierten Nucleoide wurde auch mittels Blau-Nativ Elektrophorese an "large pore" Gelen bestätigt. Mit dieser Technik wurden allerdings auch gewisse Unterschiede in der Wanderungsstrecke und damit in der Partikelgröße von Nucleoiden aus verschiedenen Fraktionen erkennbar. Die Abschätzung der Masse von Nucleoiden auf BN Gelen zeigte, dass die Partikelgröße ungefähr bei 30-36 MDa lag. Unter der Vorraussetzung, dass diese abgeschätzte Masse in etwa der tatsächlichen Masse entspricht und dass Nucleoide vergleichbar große Massen an DNA, Protein und RNA enthalten, sollten die isolierten nativen Nucleoide nur eine einzige doppelsträngige mtDNA mit einer berechneten Masse von 10.7 MDa enthalten.

Die Protein-Zusammensetzung der mt-Nucleoide aus Rinderherz wurde auf verschiedenen Präparationsstufen und durch verschiedene Ansätze analysiert, um fest gebundene und leichter abdissoziierende Komponenten zu identifizieren. Hierzu wurden native und denaturierende Elektrophorese-Techniken mit der nano-LC-Massenspektrometrie (LC-MS) kombiniert. Die qualitative MS-Analyse der mit Blau-Nativ Elektrophorese nachgereinigten Nucleoide identifizierte mehr als 400 Proteine, unter anderem gesicherte Nucleoid-Komponenten wie den mitochondrialen Transkriptions-Faktor A (TFAM), die mitochondrialen Dimethyladenosin Transferasen 1 und 2 (TFB1M und TFB2M), die Untereinheit Gamma-2 der mitochondrialen DNA Polymerase (POLG2), das mitochondriale Einzelstrang-DNA-bindende Protein (mtSSB), und die mitochondriale Helikase C26H10ORF2 (Twinkle). Diese Proteine wurden nach Mascot Scores gelistet und in verschiedene funktionelle Gruppen eingeteilt. Die meisten massenspektrometrisch identifizierten Proteine konnten der Gruppe der an der Protein-Synthese beteiligten Proteine zugeordnet werden, die fast alle bekannten Untereinheiten von mitochondrialen Ribosomen

enthielt. Dies legt die Vermutung nahe, dass die isolierten nativen Nucleoide erhebliche Mengen von mitochondrialen Ribosomen enthielten. Die Identifizierung von 66 der insgesamt etwa 100 Proteine der oxidativen Phosphorylierung lässt darauf schließen, dass native Nucleoide auch erhebliche Menge von OXPHOS-Proteinen enthalten.

Nach der Identifizierung folgte die Quantifizierung der Nucleoid-Proteine. Zu diesem Zweck wurde eine zentrale Fraktion des Sucrosedichtegradienten mit 2-D IEF/SDS-Gelen analysiert, mit DeepPurple bzw. SyproRuby gefärbt und die Fluoreszenz aller Protein-Spots quantifiziert. Nach massenspektrometrischer Identifizierung der Spots wurde eine Liste der 90 häufigsten Nucleoid proteine erstellt. Interessanterweise wurde TFAM, der als ein wichtiger mtDNA-Verpackungsfaktor in Säugetierzellen bekannt ist, zwar identifiziert; er zählte jedoch nicht zu den 90 häufigsten Nucleoid-proteinen. Die Western-Blott Analyse der zentralen Sucrosedichtegradienten Fraktionen zeigte außerdem die Anreicherung einer potentiellen TFAM-Isoform in den Nucleoid-Fraktionen. Unerwartet wurde das uncharakterisierte mitochondriale Protein Es1 als das häufigste Nucleoid-Protein in Rinderherzmitochondrien identifiziert. Das deutet darauf hin, dass die Nucleoid-Organisation in postmitotischem Gewebe sich erheblich von den bisher untersuchten mitotischen Zellen unterscheiden kann. Eine funktionelle Charakterisierung von Es1 ist erforderlich, um seine Rolle in Säugetier-Nucleoiden aufzuklären.

I.B. Summary

In the first part of this work, the development of a novel two-dimensional native gel electrophoretic system (2-D BN/hrCNE) is described. This new system simplifies proteomics and biochemical analysis of mega protein complexes that are dissociated into the constituent complexes during 2-D electrophoresis, thereby reducing the complexity of the system considerably. This technique is exceptionally well suited for the in-gel detection of fluorescence-labeled proteins and the identification of individual enzymes and protein complexes by specific in-gel assays on native gels.

In the second part, a new technique for the native immunoblotting of blue native gels (NIBN) was developed. This new technique allows for the identification of conformation-specific antibodies and the discrimination of antibodies recognizing linear epitopes of denatured proteins. Identification of conformation-specific antibodies is becoming increasingly important not only for the electron microscopic identification of native proteins but also for structural investigations in general. For this purpose, a commonly used protocol for Western blotting of blue native gels was modified in such a way that the native state of proteins and protein complexes was retained throughout the complete protocol. Instead of using the denaturing methanol in Western blotting protocols, mild detergents such as Tween 20, digitonin and Brij 35 were used for the obligatory removal of protein bound Coomassie-dye. The detection of respiratory complex I by activity staining on the blot membrane demonstrated that all three non-ionic detergents preserved the native state of complex I. The native state of the enzyme on the blot membrane was also monitored and confirmed with the help of a set of conformation-specific antibodies. NIBN can be used as a simple alternative method to the demanding native ELISA to screen for conformation-specific antibodies for structural studies. Unlike the time consuming native ELISA, NIBN does not require introduction of appropriate affinity tags and purification of the target protein by chromatography. Thus, the NIBN technique is especially useful for microscale projects and for proteins not easily accessible to genetic manipulation.

The third part aimed at identification of the immediate protein interaction partners of Cox26, a hydrophobic protein that has been identified by our group as a novel component of yeast respiratory supercomplex. Multi-dimensional electrophoretic techniques were applied to identify non-covalent and covalent protein-protein interactions of Cox26. Three-dimensional

electrophoresis (BNE/BNE/SDS-PAGE) gave both qualitative and quantitative information on covalent and non-covalent interactions of Cox26 and subunits of cytochrome *c* oxidase (complex IV), and showed that most of the Cox26 protein was non-covalently bound to the complex IV moiety of the respirasomes. Four-dimensional electrophoresis (BNE/BNE/SDS/SDS-PAGE) applying reducing and non-reducing conditions revealed that a minor fraction of Cox26 used a single cysteine residue in the center of a predicted transmembrane helix to form a disulfide bond with the Cox2 subunit of complex IV. A structural role of Cox26 protein in the assembly/stability of respiratory strings or patches has been suggested.

The last part of this work focused on the isolation and characterization of native and morphologically intact nucleoids from bovine heart mitochondria, since only a few studies on nucleoid organization and composition have been carried out on mammalian tissues. The nucleoids appeared as distinct bands (apparent mass around 30-36 MDa) in blue native-PAGE on large pore gels. The moderate variation in particle size seems to reflect variations in the binding of loosely nucleoid-associated components like respiratory chain complexes. The estimated 30-36 MDa mass of nucleoids on native gels suggested that each nucleoid contains one mtDNA molecule provided that nucleoids contains equal amounts of DNA, protein and RNA (Miyakawa et al., 1987).

Electron microscopic analysis of native nucleoids, which was performed by Dr. Karen Davies from the Max-Planck-Institute of Biophysics, Department of Structural Biology, Frankfurt, showed homogenous pool of particles with dimensions in 85x100 nm (in negative stain) and 100x150 nm (in cryo-tomography). Some of the nucleoids showed dumbbell-shape indicating dimerization of nucleoids. Recent EM and high-resolution light microscopy analysis of mammalian nucleoids have reported that nucleoids have a size of 70 nm in average. We also observed the same size of 70 nm in cryo-tomogramms when we applied harsher treatment of the native nucleoid particles with dimensions 100x150 nm. This observation is in agreement with published nucleoid sizes from both EM and high-resolution light microscopy, if we assume that native nucleoids have been dissociated under harsher treatment.

The protein composition of bovine heart mt-nucleoids was analyzed by a number of complementary approaches to identify low and highly abundant, easily dissociating and tightly bound proteins, and to rank the 90 most abundant mt-nucleoid proteins. Native and denaturing gel electrophoresis techniques were coupled to LC-MS/MS to achieve a comprehensive protein component analysis. Qualitative MS analysis of highly purified

nucleoids identified more than 400 proteins, including well known nucleoid proteins such as mitochondrial transcription factor and mtDNA-binding protein (TFAM), mitochondrial single-stranded DNA-binding protein (mtSSB), mitochondrial DNA polymerase subunit gamma-2 (POLG2) and mitochondrial helicase C26H10ORF2 protein (Twinkle). These proteins were ranked according to Mascot scores, and sorted according to presumed functional properties. A large group of proteins involved in protein synthesis comprised an almost complete set of subunits of mitochondrial ribosomes suggesting that the nucleoids contained significant amounts of mitochondrial ribosomes. Identification of sixty six proteins from the oxidative phosphorylation (OXPHOS) system comprising around 100 proteins in total suggested that OXPHOS proteins are also associated with mt-nucleoids.

Interestingly, TFAM, described as a main mtDNA packaging factor in human and other mammalian cells, was not confirmed here as a major nucleoid component from bovine heart mitochondria. Fluorescence staining of protein spots on 2-D IEF/SDS gels clearly identified TFAM, but according to the stain intensity, this protein did not rank in the list of the 90 most abundant nucleoid proteins. Western blot analysis of sucrose gradient fractions revealed an enrichment of putative TFAM isoform in nucleoid fractions. Unexpectedly, the uncharacterized mitochondrial protein Es1 was identified as the most abundant nucleoid protein in bovine heart nucleoids instead. This implicates that nucleoid organization may differ between species and tissues. A functional characterization of Es1 is required to clarify its role in mammalian nucleoids.

II.   Introduction

1.   Mitochondria and mitochondrial complexes

The ubiquitous occurrence of intracellular structures that represented mitochondria was first recognized by Altmann, 1890. He believed that these structures, which he termed "bioblasts", were organisms that live inside the cells and perform vital functions (reviewed by Ernster and Schatz, 1981). The name mitochondrion was introduced by Benda, 1898. The existence of mitochondria has been explained by the so called endosymbiotic theory, which has been proposed based on the similarities between mitochondria and bacteria (Margulis, 1970).

Mitochondria are dynamic organelles found in most eukaryotic cells. Mitochondria are organized in networks and undergo fusion and fission (Bereiter-Hahn and Vöth, 1994; Rizzuto et al., 1998). Only a few groups of unicellular eukaryotes such as diplomonads, trichomonads, and pelobionts lack mitochondria. They possess organelles called mitosomes or hydrogenosomes (Andersson and Kurland, 1999; Embley et al., 2003).

The most prominent role of mitochondria is to produce adenosine triphosphate (ATP), an energy equivalent of the cell, through respiration. In addition to supplying cellular energy, mitochondria participate in key metabolic reactions, e.g., citric acid cycle, fatty acid oxidation and urea cycle. Certain reactions in heme synthesis, steroid synthesis, iron sulfur synthesis and amino acid degradation take place also in mitochondria. Mitochondria play a crucial role in many other tasks, such as apoptosis, aging, calcium signaling and regulation of cellular metabolism.

Mitochondria have a double membrane: a pretty smooth outer membrane and a highly convoluted inner membrane forming folds called cristae. The cristae enormously increase the inner membrane surface area, making it possible for a high amount of membrane to be packed into the mitochondrion (Palade, 1952; Paumard et al., 2002; reviewed by Mannella et al., 2006). Among many other membrane proteins located in the cristae membranes the four complexes of the respiratory chain (complexes I-IV) and the ATP synthase (complex V) are the most abundant ones. In the process of oxidative phosphorylation, protons are pumped from the mitochondrial matrix across the mitochondrial inner membrane through respiratory complexes I, III, and IV, generating an electrochemical potential. When protons return to the

mitochondrial matrix down their electrochemical gradient, ATP is synthesized via complex V (reviewed by Saraste, 1999).

Mitochondria have their own genetic system located in the matrix. The mitochondrial DNA (mtDNA) was first visualized by electron microscopy (EM) in mitochondria isolated from chicken (Nass and Nass, 1963a, b; Nass, 1966) and mouse cells (Bruggen et al., 1966). The mammalian mtDNA encodes a few protein subunits of the mitochondrial OXPHOS complexes as well as transfer RNAs (tRNA) and ribosomal RNAs (rRNA) for their intramitochondrial translation. The vast majority of mitochondrial proteins are encoded by the nuclear genome and synthesized in the cytosol. They are further imported into mitochondria by the translocase of the outer membrane (TOM complex, Paschen et al., 2001; Perry et al., 2008), the sorting and assembly machinery (SAM) of the outer membrane (Bolender et al., 2008; Chan and Lithgow, 2008), and the translocases of the inner membrane (TIM22 and TIM23 complexes, Neupert and Brunner 2002; Herrmann, 2003; Rehling et al., 2003).

It has been discovered that mtDNA is not homogenously distributed within the mitochondrial compartment, but concentrated in structures called mitochondrial nucleoids (Nass, 1969; Kuroiwa et al., 1976). Mitochondrial nucleoids represent the largest macromolecular complexes in mitochondria identified so far.

1.1.   Respiratory chain and oxidative phosphorylation

The mitochondrial respiratory chain consists of four multi-subunit protein complexes located in the inner mitochondrial membrane of eukaryotic cells (Fig. 1): complex I (NADH:ubiquinone oxidoreductase), complex II (succinate:ubiquinone oxidoreductase), complex III (ubiquinol:cytochrome *c* oxidoreductase) and complex IV (cytochrome *c* oxidase). The electron transfer between complexes is initiated by reducing equivalents produced in the Krebs cycle and the β-oxidation (NADH, $FADH_2$) and uses ubiquinone and the soluble cytochrome *c* as electron carriers (Hatefi, 1985).

Complex I transfers electrons from NADH to ubiquinone thereby pumping two protons per electron across the inner mitochondrial membrane (Wikström, 1984; Galkin et al., 1999; Brandt, 2006, 2011). In contrast to most eukaryotes, the yeast *Saccharomyces cerevisiae* does not possess complex I but rather contains three so called alternative NADH dehydrogenases associated with the inner membrane (De Vries and Marres, 1987; Joseph-Horne et al., 2001). Complex II is a member of both, the respiratory chain and the citric acid cycle. It transfers

electrons from succinate via FAD to ubiquinone, but does not pump protons. Complex III transfers electrons from ubiquinol to cytochrome *c* and pumps one proton per electron (Wikström et al., 1981; Brandt, 1996).

Complex IV transfers electrons from cytochrome *c* onto molecular oxygen, the ultimate electron acceptor, converting it to water and translocates two protons per electron (Michel, 1998). The electron transfer is coupled to a vectorial proton translocation across the inner mitochondrial membrane performed by complexes I, III and IV to establish a proton gradient. Thus, the energy of the exergonic electron transfer reaction is stored into a proton motive force (PMF) across the membrane. The PMF is utilized by the F_1F_O-ATP synthase (complex V) for the regeneration of ATP from ADP and phosphate. This process is called oxidative phosphorylation (OXPHOS).

The fundamental principle of coupling the energy-generating electron transfer to ATP synthesis by means of an electrochemical proton gradient across the membrane, known as the chemiosmotic theory, was first described by Peter Mitchell (Mitchell, 1961, 2011 (reprinted)). The mitochondrial respiratory chain also contributes to the production of reactive oxygen species (ROS) such as the superoxide anion ($O_2^{\cdot-}$) (Fridovich, 1978). Complex I (Turrens and Boveris, 1980; Kushnareva et al., 2002; Galkin and Brandt, 2005; Kussmaul and Hirst, 2006) and complex III (Boveris et al., 1976; Cadenas et al., 1977; Dröse and Brandt, 2008; Borek et al., 2008; Dröse et al., 2011) are the main sources of ROS formation within the respiratory chain. It has been suggested that low levels of ROS play a role in cellular signaling (Bell et al., 2007; Starkov, 2008), whereas higher rates of ROS result in oxidative stress involved in apoptosis, cellular injury during ischemia and reperfusion, aging as well as several neurodegenerative diseases including Parkinson's, Huntington's and Alzheimer disease (Benzi and Moretti, 1995; Finkel and Holbrook, 2000; Emerit et al., 2004; Lin and Beal, 2006; Zhou et al., 2008; Dröse and Brandt, 2008).

Detailed crystal structures of complex II from *E. coli* (Yankovskaya et al., 2003), of complex III dimer from chicken (Zhang et al., 1998), bovine heart (Iwata et al., 1998; Huang et al., 2005) and yeast *S. cerevisiae* (Lange et al., 2001; Solmaz and Hunte, 2008), and of complex IV from bovine heart mitochondria (Tsukihara et al., 1996; Yoshikawa et al., 1998) have already been determined. The structures of complex I from *E. coli* (Efremov et al., 2010; Efremov and Szanov, 2011) and *Y. lipolytica* (Hunte et al., 2010), and of complex V from bovine heart mitochondria (Abrahams et al., 1994; Stock et al., 1999; Watt et al., 2010) are only partially available.
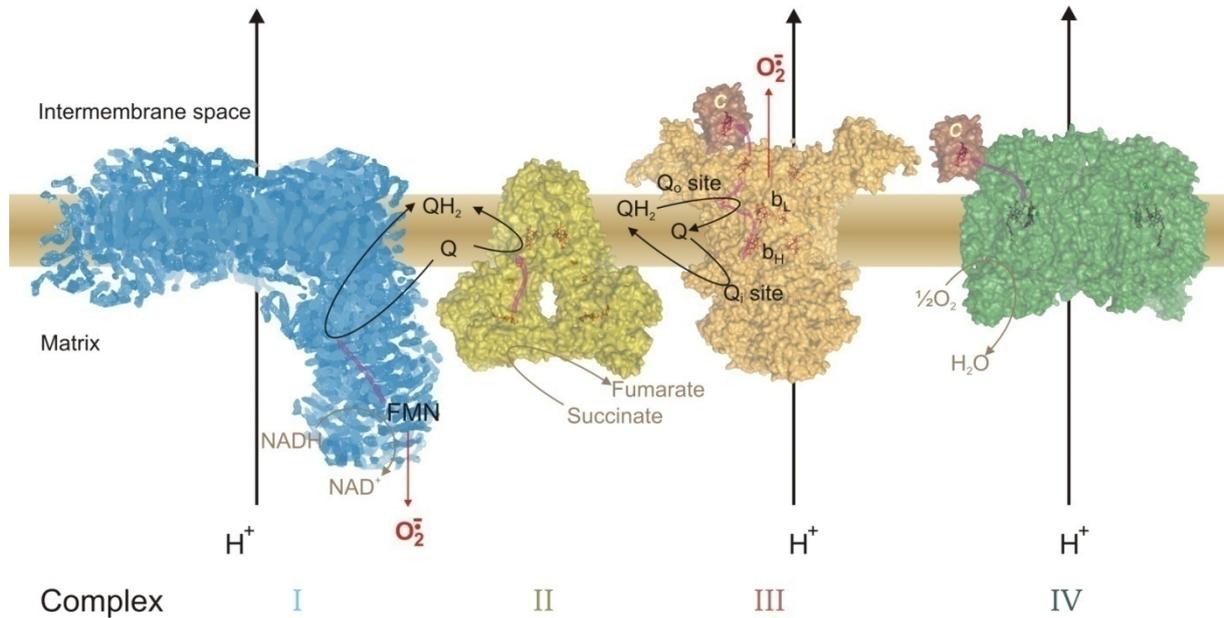
Figure 1. Schematic representation of the mitochondrial respiratory chain. A representation of the three-dimensional structures of respiratory chain complexes I-IV embedded in the inner mitochondrial membrane (IMM) is shown. Substrates and products of the enzymatic reactions are shown in grey. Magenta curved arrows show the electron transfer pathways inside the complexes, whereas black straight arrows indicate proton translocation. The black curved arrows indicate pathways of the quinone accepting electrons from complex I or II and delivering them to complex III. Violet arrows indicate sites of the reactive oxygen species production at complexes I and III. NAD^+ (nicotinamide adenine dinucleotide, oxidized form); NADH (nicotinamide adenine dinucleotide, reduced form); FMN (flavine-mononucleotide); Q (ubiquinone); QH_2 (ubiquinol); b_H (high potential heme b); b_L (low potential heme b); *c* (cytochrome *c*). Figure modified from Dröse, 2011.

The fluid state model of the respiratory chain (Hackenbrock et al., 1986) supposes that each enzyme complex diffuses freely in the lipid bilayer, and that electron transfer occurs during random and transient collisions between the complexes and the small diffusing molecules quinone and cytochrome *c* (Hackenbrock et al., 1986; Höchli and Hackenbrock, 1976). The finding that all individual protein complexes of oxidative phosphorylation system can be purified to homogeneity in an enzymatically active form and lipid dilution experiments (Hatefi et al., 1962; Hackenbrock et al., 1986) support this model.

The solid state model (Chance and Williams, 1955), however, proposes a higher level of organization, in which the individual complexes of the respiratory chain assemble into units called supercomplexes, where electrons may be transferred along well defined routes. Recently, a wide range of experimental findings (reviewed by Wittig and Schägger, 2009a,

and Dudkina et al., 2010) changed the paradigm of how the mitochondrial respiratory chain is organized from the fluid state to the solid state model: (i) Supercomplexes were resolved by blue native polyacrylamide gel electrophoresis (BN-PAGE) (Schägger and Pfeiffer, 2000). (ii) The in-gel activity measurements within blue native gels showed that the supercomplexes exhibited enzymatic activities (Schägger and Pfeiffer, 2000; Eubel et al., 2004). (iii) Supramolecular association between complexes I and III (Hatefi and Rieske, 1967), complexes II and III (Tisdale, 1967; Bruel et al, 1996), complexes III and IV (Berry and Trumpower, 1985; Sone et al., 1987; Iwasaki et al., 1995; Cruciat et al., 2000), and complexes I and IV (Schägger and Pfeiffer, 2000) were observed. (iv) Stoichiometrically assembled respiratory chain complexes of digitonin-solubilized mitochondrial membrane fractions were isolated from the bacterium *P. denitrificans* (Stroh et al., 2004), from plant mitochondria (Eubel et al., 2003, 2004), from the yeasts *S. cerevisiae* (Cruciat et al., 2000; Schägger and Pfeiffer, 2000) and *Y. lipolytica* (Nübel et al., 2009), and from mammalian cells (Schägger and Pfeiffer, 2001). (v) Well defined interactions of OXPHOS complexes within the isolated respiratory supercomplexes were revealed by electron microscopy (Dudkina et al., 2005; Minauro-Sanmiguel et al., 2005; Schäfer et al., 2006; Heinemeyer et al., 2007; Althoff et al., 2011). (vi) Mutations in genes that encode one of the subunits of one OXPHOS complex affect the stability of another complex (Acín-Pérez et al., 2004; Schägger et al., 2004; Diaz et al., 2006). Recently, also a hypothesis for the organization of the respiratory chain combining both the liquid and solid state models has been presented (Genova et al., 2003; Wenz, 2004). It was postulated that supercomplexes physiologically exist in equilibrium with isolated complexes depending on metabolic conditions in the cells.

Respiratory supercomplexes are often called "respirasomes". These are functional and structural units consisting of individual mitochondrial or bacterial respiratory chain enzymes that respire autonomously in the presence of cytochrome *c* and ubiquinone. It has been proposed that the assembly of the individual complexes into respirasomes has the following advantages: substrate channeling, catalytic enhancement, sequestration of reactive intermediates and structural stabilization of individual complexes (Fersht, 1999; Schägger and Pfeiffer, 2000, 2001; Eubel et al., 2003; Genova et al., 2003). Recently, substrate channeling of ubiquinone between complexes I and III in bovine mitochondria was shown by determination of flux control rates (Genova et al., 2003; Bianchi et al., 2004). Catalytic enhancement of supercomplex formation by reduction of cytochrome *c* movement between complex III and complex IV was shown in *S. cerevisiae* and potato mitochondria (Heinemeyer et al., 2007; Lenaz and Genova, 2009). A recent cryo-EM study of bovine heart

mitochondrial supercomplex $I_1III_2IV_1$ suggested that the macromolecular organization of the three electron transport complexes contributes to efficient energy conversion (Althoff et al., 2011). The formation of supercomplexes has been proposed to be necessary for preventing the formation of excess oxygen radicals (Lenaz and Genova, 2009).

Structural roles for supercomplex formation have also been shown in *P. denitrificans* and in human cell lines: supercomplex formation is necessary for complex I assembly and stability (Stroh et al., 2004; Schägger, et al., 2004). Complex I is necessary for fully assembled complex III in human patients (Ugalde et al., 2004) and its absence causes a dramatic loss of complex III in humans (Blakely et al., 2005; Schägger et al., 2004). Moreover the assembly of complex I requires complex IV in mouse fibroblasts (Diaz et al., 2006). Dimeric complex III is vital in the stability of complex I in mouse as well as human cell lines (Acín-Pérez et al., 2004).

It appears that supercomplexes organize further into even larger structures called respiratory strings or patches as shown in Figure 2A (Wittig et al., 2006b; Wittig and Schägger, 2009a; Dudkina et al., 2010). This is seen best with ATP synthase (complex V), which assembles into long oligomeric rows of dimers (Allen et al., 1989; Krause et al., 2005; Dudkina et al., 2006; Strauss et al., 2008; Wittig and Schägger, 2009a; Davies et al., 2011).
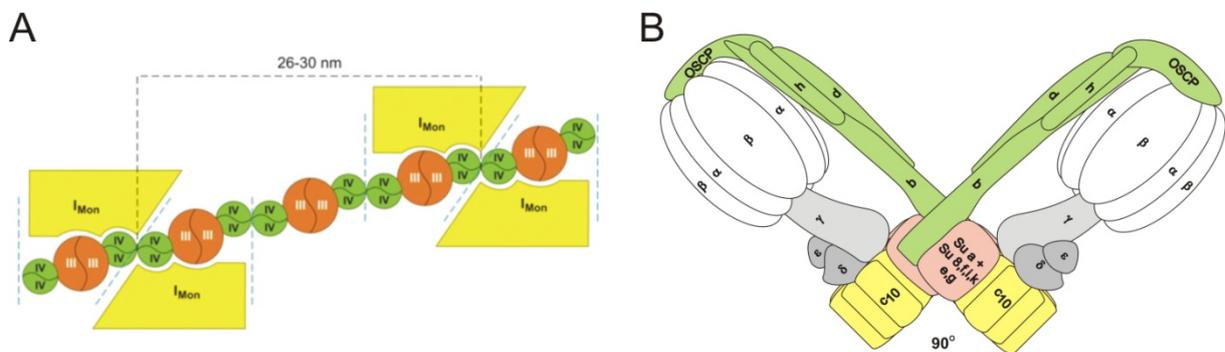
Figure 2. Supramolecular structures of the OXPHOS complexes. (A) Respiratory string model for mammalian mitochondria characterized by tetrameric complex IV linkers. Monomeric complex I (I_{Mon}) is marked yellow. Complex III is marked red. Complex IV is marked green. The building blocks, i.e. the larger and smaller supercomplexes containing and not containing complex I, are separated by dashed blue lines. Taken from Wittig et al., 2006b. (B) Model of dimeric ATP synthase viewed as cross-section through the inner mitochondrial membrane. Taken from Wittig and Schägger, 2009a.

It has been shown that the occurrence of ATP synthase dimers (Fig. 2B) and oligomers stabilize and modulate cristae morphology (Fig. 3, Paumard et al., 2002; Strauss et al., 2008; reviewed by Wittig and Schägger, 2009a).
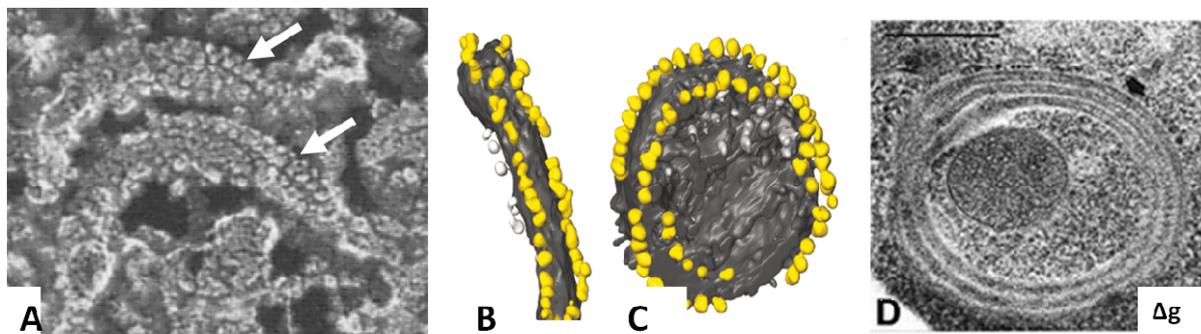
Figure 3. Cristae structure of mitochondria. (A) Mitochondrion from *Paramecium multimicronucleatum* showing tubular cristae curve in a helical pattern. Taken from Allen, 1989. (B, C) Surface views of tomographic volumes of ATP synthase dimer ribbons in a tubular crista vesicle from bovine heart mitochondria. Taken from Strauss et al., 2008. (D) Yeast cells devoid of ATP synthase subunit g have abnormal mitochondria with onion-like appearance. Taken from Paumard et al., 2002.

It has been proposed that supercomplexes may contain previously unknown additional protein components potentially important for stabilizing the supercomplexes and supporting their functional roles (De Coo et al., 1999; Bianchi et al., 2004; Schägger et al., 2004; Acín-Pérez et al., 2004). For example, homo-dimeric yeast ATP synthase contains subunits e and g, which stabilize the dimer (Arnold et al., 1998). These proteins play also a key role in generating cristae morphology (Paumard et al., 2002) and imposing a strong curvature to the membranes (Strauss et al., 2008). Bovine ATP synthase contains two further accessory subunits, AGP and MLQ, with so far unknown functions (Meyer et al., 2007). Respirasomes of *S. cerevisiae* may also contain previously unknown accessory proteins, as suggested by a recent three-way proteomics strategy that identified four candidate proteins potentially associated with complexes III and IV (Helbig et al., 2009).

1.2.   Mitochondrial nucleoids

As mentioned, mitochondria contain their own genetic system, mtDNA. mtDNA found to be remarkably diverse among eukaryotes, although their genetic functions are generally conserved (reviewed by Malka et al., 2006). mtDNAs have sizes between 6 to 400 kb in plants (Burger et al., 2003), 19 to 75 kb in fungi (Williamson, 2002) and 15 to 20 kb in metazoan animals (Boore, 1999). Human mtDNA is a double-stranded, closed and circular molecule of 16.6 kb containing 37 genes (Fig. 4). Thirteen of them encode protein subunits of respiratory complexes I, III, IV, and V. The mtDNA genome also encodes 22 mitochondrial tRNAs and two rRNAs essential for the expression of mitochondrial encoded genes. The transcripts are translated by mitochondrial ribosomes within the mitochondrion. The inheritance of mtDNA does not follow Mendelian rules. Mammalian mtDNA is maternally inherited.
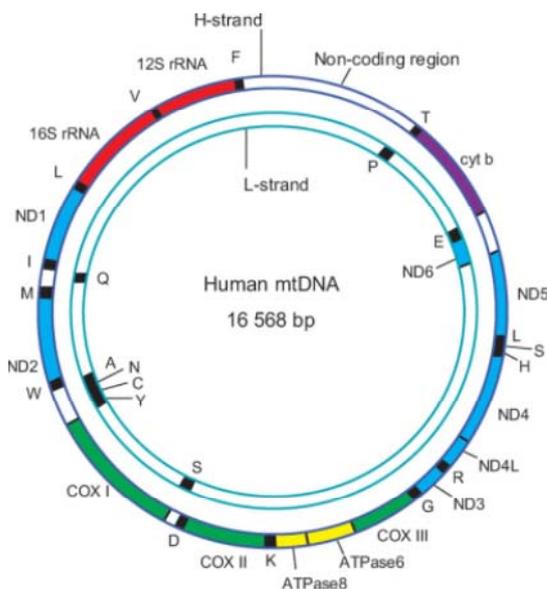
Figure 4. The human mitochondrial DNA gene map. Single letters indicate the positions of the corresponding tRNA genes. ND, NADH dehydrogenase genes; cyt b, cytochrome b gene; COX, cytochrome *c* oxidase genes; A6/8, ATP synthase genes 6 and 8; 12S/16S, ribosomal RNA genes. Taken from Spelbrink, 2010.

Electron microscopic studies of different species such as mammals (Nass, 1966; Albring et al., 1977; Iborra et al., 2004; Prachar, 2010; Brown et al., 2011; Kukat et al., 2011), yeast (Stevens, 1981; Miyakawa et al., 1987) and lower eukaryotes (Kuroiwa, 1982) have revealed the organization of mtDNA in structures named nucleoids. Numerous microscopic studies showed that nucleoids are punctuated structures (450-800 foci in a cell) that spread over the entire mitochondrial network at regular intervals (Satoh and Kuroiwa, 1991; Bereiter-Hahn and Vöth, 1996; Margineantu et al., 2002; Iborra et al., 2004; Legros et al., 2004; Kang and

Hamasaki, 2005). Mitochondrial nucleoids provide a submitochondrial organization of mtDNA, facilitating an efficient maintenance of mtDNA in discrete segregating units. Certain mobility of nucleoids within the matrix has recently been shown by Legros et al., 2004. Nucleoids represent the dynamic and inheritable unit of mtDNA. It is unknown, however, how the mitochondrial fusion and fission machinery interacts with mtDNA maintenance and propagation, and ensures the proper distribution and inheritance of the mitochondrial genome.

It has been shown that mutations of the mtDNA cause a multitude of tissue-specific and systemic diseases with estimated incidence of 1:5000 live births (Thornburn, 2004; Kaufman et al., 2007). Typical mitochondrial diseases, such as myoclonus epilepsy with ragged-red fibers (MERFF), mitochondrial encephalomyopathy, lactic acidosis, stroke-like episodes (MELAS) and Kearns–Sayre syndrome, have been shown to result from high levels of mtDNA mutations and deletions within a certain tissue or cell type (reviewed by DiMauro and Schon, 2003). It has recently been shown that high levels of mtDNA deletions are associated with aging and Parkinson's disease (Bender et al., 2006; Kraytsberg et al., 2006).

Defects in mtDNA maintenance and propagation are caused by mutations in nuclear factors associated with the nucleoids. It seems that defects in both the mitochondrial helicase Twinkle and mitochondrial DNA polymerase γ contribute to the age-dependent accumulation of mtDNA mutations (Spelbrink et al., 2001; Wanrooij et al., 2004; Trifunovic et al., 2004). Furthermore, it has been shown that mutations in polymerase γ cause depletion of mtDNA (Davidzon et al., 2005). In many studies, the loss of TFAM, the mitochondrial transcription factor and principal packaging protein, has been associated with the loss of mtDNA. For example, knockout of TFAM in mice causes mtDNA depletion and mitochondrial dysfunction (Ekstrand et al., 2004), and embryonic lethality (Larsson et al., 1998), while tissue-specific knockout of the TFAM gene generates several models of tissue-specific cell dysfunction (Wang et al., 1999; Silva et al., 2000; Ekstrand et al., 2007).

Multiple genetic variants of mtDNA appear frequently within the same cell and tissue, a phenomenon called heteroplasmy. Cells can usually survive a mtDNA mutation up to a heteroplasmy level of 75%, which can be compensated by the remaining wild-type (WT) mtDNA. However, once the "threshold" (DiMauro and Schon, 2003; Taylor and Turnbull, 2005) is exceeded and sufficient mtDNA-encoded transcripts to adequately produce the necessary OXPHOS proteins are lacking, the remaining WT mtDNAs can no longer maintain membrane potential, respiratory activity and other mitochondrial functions. In short, mutations in mtDNA or nuclear genes that disrupt mitochondrial respiratory function can

have destructive effects on a cell via bioenergetic dysfunction. As the heritable unit of mtDNA, the mitochondrial nucleoid is a fundamental component of bioenergetic homeostasis.

Determining the number of mtDNA molecules per nucleoid would help improve our understanding of the inheritance of mtDNA and the propagation of mutant mtDNA in human disease. Applying fluorescent DNA-binding components such as DAPI (Bereiter-Hahn and Vöth, 1996) it was estimated that one nucleoid contains 2-8 mtDNA molecules in human Hela cells. The studies using antibodies against DNA or the mtDNA-binding protein TFAM to detect nucleoids (Iborra et al., 2004; Legros et al., 2004; Brown et al., 2011) suggested a great variability in mtDNA content ranging from 2.4 to 7.8 copies per nucleoid, depending on the cell type. Very recent studies using super-resolution microscopy found that primary human fibroblasts contained only a single molecule of mitochondrial DNA per nucleoid (Kukat et al., 2011) confirming the estimate by Satoh and Kuroiwa, 1991. It is yet to be determined whether mtDNA copy number per nucleoid remains fixed, or changes among tissues and cell types.

Mitochondrial nucleoid components and nucleoid associated proteins of eukaryotes have been identified by using three different strategies as reviewed by Malka et al., 2006. (i) Identification and purification of proteins with mtDNA. (ii) Biochemical isolation of mitochondrial nucleoids and their analysis. (iii) Genetic screens in yeast. Following are their brief details.

(i) The search for proteins capable of binding mtDNA resulted in the identification of yeast Abf2p protein, which was sufficiently abundant to coat the mtDNA (Diffley and Stillman, 1991). The Abf2p protein contains two high mobility group box (HMG-box) domains, which are characteristic for HMG-proteins, a family of DNA-binding proteins. HMG-proteins resemble HU-proteins involved in bacterial genome condensation, but they are not related to nuclear histones (Bianchi, 1994; Oberto et al., 1994). Homology search of yeast Abf2p led to the identification of a mtDNA-binding protein in mammals (mtTFA/TFAM, Parisi and Clayton, 1991), in *Xenopus* (mtTFA, Antoshechkin and Bogenhagen, 1995), *Drosophila* (mtTFA, Takata et al., 2001) and in *Physarum polycephalum* (Glom, Sasaki et al., 2003). Mammalian TFAM has been reported to contain an additional domain involved in transcription (Parisi and Clayton, 1991; Parisi et al., 1993). It has been proposed that mammalian TFAM is probably the major factor responsible for the packaging of mtDNA within nucleoids (Antoshechkin and Bogenhagen, 1995; Alam et al., 2003; Kaufman et al., 2007). Since a single mtDNA molecule has a contour length of 5 μm, packaging of five to seven mtDNA molecules into a 70 nm structure (Iborra et al., 2004; Legros et al., 2004)

requires a considerable compaction by TFAM. It is interesting to note that different research groups have determined largely different copy numbers of TFAM binding per mtDNA molecule as shown in Table 1.

Table 1. Measurements of the TFAM/mtDNA copy number in mammalian cells. Table modified from Bogenhagen, 2011.

Species	Cell	mtDNA/cell	TFAM/mtDNA	Reference
Human	Hela	1000	1700	Takamatsu et al., 2002
	Hela	5000	50.3	Cotney et al., 2007
	Hek293	nd	35	Maniura-Weber et al., 2004
	Fibroblast	2721	1000	Kukat et al., 2011
Mouse	Kidney	nd	977	Ekstrand et al., 2004
	Liver	nd	1480	Pellegrini et al., 2009

A second mitochondrial protein able to bind DNA is the mitochondrial single-stranded DNA-binding protein (mtSSB). mtSSB binds mtDNA in a salt-resistant manner and has a structure related to bacterial SSB (Curth et al., 1994; Yang et al., 1997). mtSSB has been shown to bind single-stranded DNA (ssDNA) and to coat the ssDNA regions of mtDNA replication intermediates (Van Tuyle and Pavco, 1985). The third protein able to bind to mtDNA, is the human LON protease whose exact role in the function of mtDNA or nucleoids is not yet clear (Fu and Markovitz, 1998; Liu et al., 2004). Recently, mammalian ATAD3 has been reported to bind weakly to supercoiled D-loop sequences (He et al., 2007).

(ii) Nucleoids have been isolated from yeast (Miyakawa et al., 1987, 1995; Newman et al., 1996; Kaufman et al., 2000), human cell lines (Garrido et al., 2003; Wang and Bogenhagen, 2006; Bogenhagen et al., 2008), bovine heart (Hillar et al., 1979), rat liver (Van Tuyle and McPherson, 1979; Van Tuyle and Pavco, 1985), *Xenopus* oocytes (Barat et al., 1985; Bogenhagen et al., 2003) and *P. polycephalum* (Suzuki et al., 1982). Recent studies have identified proteins known to be involved in mtDNA maintenance, such as DNA polymerase γ, T7-like mitochondrial DNA helicase Twinkle, mitochondrial RNA polymerase, TFBM1, TFBM2, Terf1 and mitochondrial topoisomerase I (Bogenhagen et al., 2008). In addition, proteins involved in protein folding and quality control including Hsp60, Hsp70, Hsp40, prohibitins 1 and 2 (Mootha et al., 2003; Bogenhagen et al., 2008) as well as mitochondrial ribosomal proteins (Rorbach et al., 2008; Bogenhagen et al., 2008) have been identified.

Based on these results Bogenhagen suggested that nucleoids have a layered structure with inner and outer cores, involved in the nucleic acid synthesis, and the processing and assembly of nascent polypeptides into respiratory complexes, respectively (Bogenhagen et al., 2008; Fig. 5).
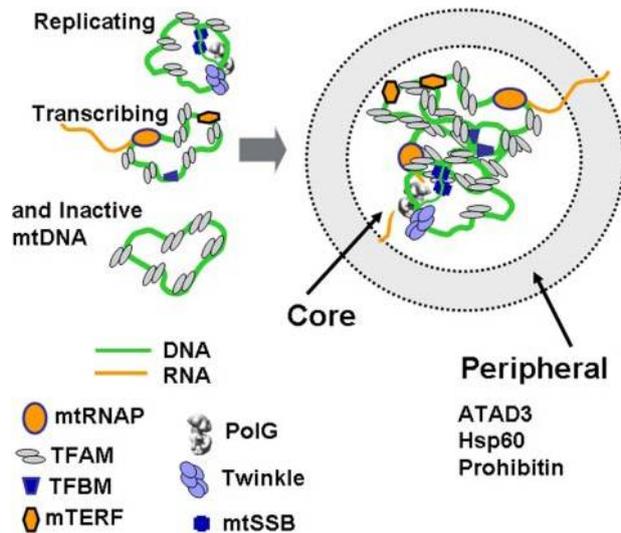
Figure 5. Model for mtDNA nucleoid structure. Proteins involved in transcription, replication and maintanance form the core of the nucleoid. The core is surrounded by a peripheral zone containing proteins involved in protein folding, quality control and mitochondrial translation. Taken from Bogenhagen et al., 2008.

Moreover, proteins involved in lipid metabolism, cytoskeleton structure (reviewed by Bogenhagen, 2011), protein import, mitochondrial biogenesis, citric acid cycle and amino acid metabolism (Chen et al., 2005) have been identified in mammalian and yeast mitochondrial nucleoids. Functional studies have shown that yeast proteins Aco1p (Chen et al., 2007) and Ilv5p (Zelenaya-Troitskaya et al., 1995) are bifunctional. They couple metabolic regulation to nucleoid organization (Chen and Butow, 2005; Chen et al., 2005).

(iii) A series of outer membrane proteins, Mdm10p, Mdm12p and Mmm1p, have been identified by genetic screens in yeast. They form complexes essential in the maintenance of mitochondrial morphology and linkage of mitochondria with the cytoskeleton (Burgess et al., 1994; Sogo and Yaffe, 1994; Berger et al., 1997; Boldogh et al., 2003). The mutation and deletion of these proteins lead to defects in nucleoid morphology, transmission, and to the rapid loss of mtDNA (Hobbs et al., 2001). They seem to assist inner membrane proteins Mdm31p and Mdm32p required for the maintenance of mtDNA and mitochondrial morphology (Dimmer et al., 2005). Chen and Butow, 2005, proposed a model enabling interactions of nucleoids across both mitochondrial membranes (Fig. 6). However, none of

these proteins were identified in nucleoid preparations yet (Kaufman et al., 2000; Chen et al., 2005).
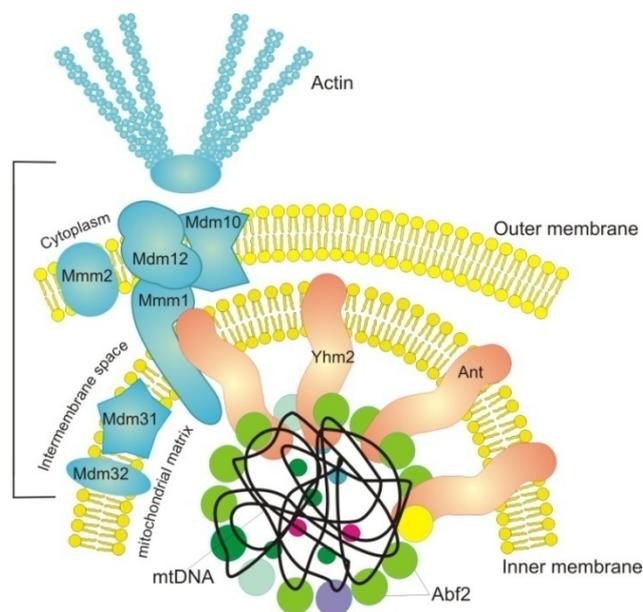
Figure 6. Mitochondrial nucleoid segregation apparatus in yeast according to Chen and Butow, 2005 as modified by Ilka Wittig. Mitochondrial nucleoids are linked to both the inner and outer mitochondrial membranes via the contact sites of the segregation apparatus. The link consists of Mdm10-Mdm12-Mmm1 proteins. The inner membrane proteins Mdm31 and Mdm32 have also been proposed to be part of this apparatus.

Recently, the endoplasmatic reticulum (ER)-mitochondria encounter structure (ERMES) tethering complex composed of Mdm10p, Mdm12p, Mmm1p and Mdm34p has been identified (Kornmann et al., 2009). The ERMES complex has been shown to be involved in regulation of mtDNA replication (Kornmann et al., 2011). Putative homologs of these proteins have not yet been identified in mammals.

Isolation and characterization of nucleoids in the native state is required to identify new components with fundamental nucleoid properties, such as their association with the inner membrane, their distribution throughout mitochondrial network, and their proper segregation and inheritance. Nucleoids containing one copy of the mtDNA genome (16.6 kb in human, 10.7 MDa), and comparable masses of associated protein and RNA (Miyakawa et al., 1987) would have a molecular mass of at least 40 MDa, which is much larger than the one to three MDa of respiratory supercomplexes (Schägger and Pfeiffer, 2000; Schäfer et al., 2007) and even larger than the 10 MDa pyruvate dehydrogenase complex (Zhou et al., 2001), making it the largest structure in a mitochondrion identified so far. Such a huge complex could be isolated here by differential centrifugation and by the newly developed blue native gel electrophoresis on large pore gels (Strecker et al., 2010).

2. Essential techniques for the isolation and analysis of macromolecular complexes

2.1. Native electrophoretic techniques

Native electrophoretic techniques including blue native electrophoresis (BNE, Schägger and von Jagow, 1991; Schägger et al., 1994; Wittig et al., 2006a), clear native electrophoresis (CNE, Schägger et al., 1994; Wittig and Schägger, 2005) and high-resolution clear native electrophoresis (hrCNE, Wittig et al., 2007a, b) are indispensible electrophoretic tools in proteomics studies to separate proteins and protein complexes, especially membrane proteins and membrane protein complexes for biological, biochemical and clinical investigations (Wittig and Schägger, 2008a).

Native gel electrophoresis BNE, CNE and hrCNE differ essentially by the applied cathode buffer, whose variation changes the separation principles and thus affects the resolution considerably (Wittig and Schägger, 2009b).

Samples such as biological membranes or total cell and tissue homogenates are solubilized by mild non-ionic detergents in buffer with low ionic strength at neutral pH. The detergent stability of the protein complexes is the deciding factor in choosing a specific non-ionic detergent (Schägger, 2006). Three types of non-ionic detergents are mainly used. Digitonin, one of the mildest detergents, that has been used to isolate supramolecular associations of multiprotein complexes, identifies physiological protein-protein interactions without using chemical crosslinking. It can even preserve some labile physiological interactions between individual complexes. Thus, respiratory supercomplexes $I_1III_2IV_{0-4}$ containing monomeric complex I, dimeric complex III, and a variable copy number of complex IV (zero to four) can be isolated using digitonin for solubilization of mammalian mitochondria (Schägger and Pfeiffer, 2000). Dodecylmaltoside (DDM) and Triton X-100 are also mild neutral detergents but less mild than digitonin. They are often used to solubilize individual mitochondrial complexes I-V from the inner mitochondrial membrane, since physiological supramolecular structures like oligomeric ATP synthase and supercomplexes of respiratory chain are dissociated by both detergents into their individual components. It has been suggested that these detergents break hydrophobic protein-protein interactions (Pfeiffer et al., 2003) and thus affect the stability of supramolecular structures. Lipids, especially cardiolipin, seem to shield supramolecular structures against the dissociating effect of detergents and preserve

supramolecular structures in native gels (Schägger, 2002; Zhang et al., 2002; Pfeiffer et al., 2003; Brandner et al., 2005; McKenzie et al, 2006; Wittig and Schägger, 2008a; Wenz et al., 2009). The central role of lipid interfaces for the stability of large multiprotein complexes in digitonin-solubilized samples has recently been shown by cryo-EM analysis of bovine respiratory supercomplexes (Althoff et al., 2011).

Following membrane solubilization, the anionic dye Coomassie Brillant Blue G-250 (Coomassie-dye) is added to the supernatant and/or to the cathode buffer for BNE. Coomassie-dye imposes a negative charge shift on proteins upon binding to the protein surface (Schägger et al., 1994). Therefore, all Coomassie binding membrane proteins migrate to the anode in BNE independently from their intrinsic charge. The Coomassie-dye has also some disadvantages: (i) Coomassie combines with neutral detergents used for the initial protein solubilization, producing mixed anionic micelles that can mimic some features of anionic detergents causing partial complex disassembly (Wittig and Schägger, 2008a). Nevertheless this feature can be exploited for controlled disassembly to study protein subcomplexes. (ii) The dye may also interfere with in-gel assays on BN gels. (iii) It quenches fluorescence of protein samples labeled by fluorescent dyes or fused with fluorescent proteins such as green fluorescent protein (GFP).

The experimental setup of CNE is very similar to BNE but separation principles and resolution of CNE and BNE are quite different. Both in BNE and CNE, mild neutral detergents are used for membrane solubilization. In CNE, no Coomassie-dye is added to sample and cathode buffer, thus, in contrast to BNE, proteins migrate according to their intrinsic isoelectric point (pI). As a result, only water soluble acidic proteins migrate to the anode. All proteins with pI > 7 migrate to the cathode, and are lost. Adding to this, many membrane protein complexes migrate as broad bands because of protein aggregation in CNE. For these reasons, CNE is only used in special cases. CNE offers the following advantages: (i) It has been shown to be the best suitable native electrophoretic technique for the analysis of physiological supramolecular structures such as oligomeric ATP synthase from yeast (Pfeiffer et al., 2003; Wittig et al., 2008), mammalian (Wittig and Schägger, 2005; Krause et al., 2005) and human mitochondrial supercomplexes (Wittig et al., 2010b). (ii) Detection of fluorescence-labeled proteins and in-gel assays are enhanced (Wittig and Schägger, 2005; Wittig et al., 2007a).

hrCNE is another non-colored variant of BNE that combines the advantages of BNE and CNE. Mild neutral detergents are also used for membrane solubilization. Instead of

Coomassie-dye, as used in BNE, neutral and anionic detergents forming non-colored mixed micelles are used in the cathode buffer of hrCNE. This induces a charge shift on proteins, which enhances the solubility and anodic migration of membrane proteins. The improved protein solubility makes hrCNE preferable to CNE. However, hrCNE has been found harsher than CNE and even harsher than BNE due to the use of mixed micelles comprising non-ionic and anionic detergents, which may promote dissociation of labile subunits from protein complexes and initiate disassembly of physiological supramolecular structures (Wittig and Schägger, 2009b).

BNE and CNE, together with associated techniques, have widely been applied in the studies of, e.g., protein import, dynamics of proteasomes, biogenesis and assembly of membrane protein complexes, and exploration of mitochondrial alterations in apoptosis, carcinogenesis, neurodegenerative disorders and mitochondrial encephalomyopathies (Wittig and Schägger, 2008a, 2009b).

Recently, a two-dimensional native electrophoretic system (2-D BN/BNE, Schägger and Pfeiffer, 2000, 2001) was introduced as a simple method to identify detergent-labile and non-permanently interacting proteins, as an alternative to *in vivo* cross-linking or to two hybrid system (Fields and Song, 1989). In 2-D BN/BN electrophoresis a mild first dimension BNE is used to separate large supercomplexes. In the second dimension BNE, 0.02% dodecylmaltoside (DDM) is added to the Coomassie-dye containing cathode buffer. This makes the second dimension considerably harsher than the first dimension resulting in dissociation of individual complexes from supercomplexes.

The disadvantage of 2-D BN/BNE is that the cathode buffer for the second dimension still contains Coomassie-dye, which interferes with the detection of fluorescence-labeled proteins and in-gel assays on BN gels. Therefore, a novel two-dimensional native electrophoresis system (2-D BN/hrCNE) was developed in this work and has already been applied successfully for the characterization of low abundant respiratory supercomplexes from *Y. lipolytica* (Nübel et al., 2009).

BNE can also be combined with electroblotting and immunodetection (Schägger and von Jagow, 1991). Gel stripes from 1-D BNE can be used for the second dimension Tricine-SDS-PAGE (Schägger and von Jagow, 1987; Schägger, 2006). Electroblotting of 1-D BN and 2-D BN/SDS gels and immunological detection of proteins by specific antibodies have become popular methods, especially, in the analysis of low abundant proteins. A large variety of epitopes of target proteins identifiable by antibodies can be classified as linear and

conformational (Zickermann et al., 2010). Linear epitopes are characterized by a specific amino acid sequence and are easily detectable by a Western blot after SDS-PAGE, because the protein can be presented to the antibody in denatured form. In contrast, conformational or discontinuous epitopes are more complex and recognized only if the 3-D structure of the protein is sufficiently preserved. Conformation-specific antibodies are attractive tools for different applications in structural biology (Hunte and Michel, 2002) due to their ability to bind to the native enzyme and to discriminate between different functional states, as already shown for the sodium proton antiporter NhaA (Venturi et al., 2002). They play a central role in medicine as diagnostic and therapeutic agents. Although the 3-D structure of the protein is sufficiently preserved after 1-D BNE, the proteins are commonly denatured in subsequent steps for electroblotting, e.g., during the obligatory complete removal of protein bound Coomassie-dye by methanolic solutions. Thus, the Western blot protocols preclude any work with conformation-specific antibodies. Therefore, the standard protocol was modified in this work so that enzymatic activities and full immunological reactivity of native proteins were retained.

2.2. Mass spectrometry

Traditionally, proteins have been identified by *de novo* sequencing, most frequently by using Edman degradation of proteins or isolated peptide fragments (Hewick et al., 1981; Aebersold et al., 1987; Aebersold and Goodlett, 2001). For example, subunit composition of respiratory complexes in plant mitochondria (Jänsch et al., 1996) and choloroplasts (Kügler et al., 1997) were characterized by Edman degradation. Currently mass spectrometry (MS) is one of the most important proteomics tools for the identification of proteins.

A wide variety of samples from cells to entire tissues and body fluids can be investigated by MS-based proteomics (Cox and Mann, 2011). Proteins of these samples can be separated by gel electrophoresis and excised from gels as protein spots for MS analysis. The analysis of isolated proteins is called "top-down" proteomics while the analysis of peptides from a complex mixture of proteins is called "bottom-up" proteomics (McLafferty et al., 2007; Kellie et al., 2010). Peptides are generated by digestion of proteins by sequence-specific enzymes such as trypsin. The first necessary step for the MS analysis of peptides is their ionization and submission to the gas phase. This is achieved mainly by two ionization techniques: liquid phase electrospray ionization (ESI, Fenn et al., 1989) and solid matrix-assisted laser

desorption/ionization (MALDI, Hillenkamp et al., 1991). Both methods can convert the peptide molecules to gas phase ions (Cox and Mann, 2011). ESI used in this study can be coupled on-line with popular chromatographic and electrophoretic separation techniques (Aebersold and Goodlett, 2001) such as high-performance liquid chromatography (HPLC) and capillary electrophoresis (CE). Since peptides can be eluted from the column or the capillary as concentrated peaks, the direct coupling approach increases the sensitivity of the measurement dramatically (Aebersold and Goodlett, 2001). ESI produces multiply charged ions that allows detection of peptides with masses exceeding the nominal mass range of the instrument (Aebersold and Goodlett, 2001), whereas singly charged peptides are dominant in the MALDI process. Moreover, ESI requires very little amount of peptide (femtomol) for a complete and routine sequence characterization making the method very sensitive (Carr and Annan, 1997; Davis et al., 1997; Lazar et al., 1999; Aebersold and Goodlett, 2001).

Following ionization the mass to charge ratios are determined in the mass analyzer. There are many types of mass analyzers including Time-of-flight (TOF, Karas and Hillenkamp, 1988), quandrupole (Yost and Enke, 1979; Loo et al., 1990) mass analyzers and ion traps (Schwartz and Jardine, 1996; Jonscher and Yates, 1997). Ion traps can be classified into three-dimensional quadrupole ion trap, linear quadrupole ion trap and Orbitrap. The novel hybrid linear ion trap Orbitrap instrument (LTQ-Orbitarp, Thermo) used in this study allows to obtain accurate tandem mass spectrometry (MS/MS) information with high sensitivity (Olsen et al., 2007; Frank et al., 2007; Olsen et al., 2009; Pan et al., 2010; Cox and Mann, 2011).

Finally, the obtained fragmentation spectra are evaluated by matching the spectra against a database with known protein sequences (Fasta format), which are derived from genome sequencing of the species. The fragmentation spectra are compared to the theoretical spectra of the peptide generated in silico by softwares such as Mascot and SEQUEST. Scores are calculated depending on how well the obtained spectra match the theoretical spectra. In some cases spectra can be evaluated by *de novo* sequencing if protein databases are not available for the species or the protein sequences are unknown.

2.3. Electron microscopy

Electron microscopy (EM) is a powerful and widely applied technique to study the structure of macromolecular complexes. EM provides higher resolution and magnification than light microscopy (LM). The resolving power of <1 nm of EM is a big advantage compared to the

0.2 µm of a typical LM, making it possible to observe micro objects such as biological macromolecules smaller than 100 nm.

EM is one of the important methods in structural biology along with X-ray crystallography and nuclear magnetic resonance spectroscopy (NMR). Recent improvements of EM allow visualization of macromolecular structures at near atomic resolution (Kühlbrandt and Williams, 1999). Bacteriorhodopsin (Henderson et al., 1990) and Light-harvesting complex II (LHCII) from pea (Kühlbrandt et al., 1994) are the first biological objects whose three-dimensional atomic structures were resolved with the help of EM techniques (Lottspeich and Engels, 2006). The sample preparation procedure is a deciding factor in EM. Negative staining and vitrification are the most common sample preparation methods.

In negative staining (Amos et al., 1982; Slayter and Slayter, 1992; Chen et al., 1998; Ruprecht and Nield, 2001), the contrast is enhanced by embedding biomolecules in a heavy metal salt solution, commonly uranyl acetate (reviewed by Harris and Horne, 1994, and Boekema et al., 2009). The metal salt fills cavities and the space around the molecules on drying without penetrating into the hydrophobic protein interior, achieving a good contrast of protein envelopes (Boekema et al., 2009). Negative staining is simple to perform and provides high contrast. However, negative staining also has some disadvantages: i) possible distortions of the molecules caused by the staining/drying procedure and attachment of molecules to a surface; and ii) restriction of the structural information to topographical features of the molecule surface because of the fact that the image is formed mainly by the stain-protein boundary (Stahlberg and Walz, 2008).

In the vitrification method used for cryo-EM, aqueous solution of specimens on an EM grid are rapidly frozen and thus become embedded in a layer of vitreous (amorphous) ice (Dubochet et al., 1982; Adrian et al., 1984; Dubochet et al., 1988; Baker and Johnson, 1997; Chen et al., 1998). By this method (also called cryo-electron microscopy, cryo-EM), objects are visible without any staining agent. The contrast is only caused by the difference in density between amorphous ice (0.93 g/cm^3) and protein (1.3-1.36 g/cm^3) (Boekema et al., 2009). Thus the contrast is rather low in cryo-EM in comparison to the negative staining. However, in cryo-EM, molecules can be observed in their native aqueous environment and functionally important conformational states can be trapped by rapid freezing (Kühlbrandt and Williams, 1999).

There are three different techniques to determine the structure of biological molecules in cryo-EM: electron crystallography, single-particle EM and electron tomography (Stahlberg and

Walz, 2008). Many identical copies of the same molecule are needed for electron crystallography and single-particle EM because they use averaging (Stahlberg and Walz, 2008) whereas a single object *in situ* is usually sufficient in electron tomography to obtain its 3D density maps (Lucič et al., 2005).

EM has not yet been widely used in the study of the mt-nucleoid structure because tumor-derived human cell lines, which are used most in this field, are too thick for EM. Instead, confocal microscopy was used to obtain information on the location, frequency and dynamics of mt-nucleoids within a living cell. Fluorescence microscopy has a resolution of about 250 nm on the focal plane, and even lower axial resolution of about 600 nm (Bogenhagen, 2011). Recently, super-resolution microscopies such as stimulated emission depletion microscopy (STED, Hell and Wichmann, 1994; Hell, 2009) and two- and three-dimensional photoactivated localization microscopy (PALM, Betzig et al., 2006; iPALM, Huang et al., 2008) have been used to study mammalian mitochondrial nucleoids (Kukat et al., 2011; Brown et al., 2011). These new microscopy techniques enable a resolution well below the diffraction barrier. For example, PALM can locate objects 20 to 50 nm in size (Brown et al., 2011). They involve no tissue sectioning thus allow imaging of all nuceloids of a cell. However, these techniques involve labeling methods, which increase the volume of nucleoids and lead to overestimation of nucleoid size. With a resolution of greater than one nm, EM has a great potential in this field.

There have been rigorous studies to morphologically characterize mt-nucleoids of the lower eukaryote *Physarum polycephalum* using EM (Suzuki et al., 1982; Kuroiwa et al., 2006). However, the nucleoid of *Physarum* is different from the nucleoids of higher eukaryotes in size and shape (Sasaki et al., 2003; Prachar, 2010). One of the EM studies in the yeast *S. cerevisiae* has shown that isolated mt-nucleoid consists of particles 20-50 nm in diameter (Miyakawa et al., 1987). Recent EM studies of mammalian nucleoids revealed that mammalian nucleoids are spheres of 60 to 90 nm in diameter (Iborra et al., 2004; Prachar, 2010).

Both negative staining and cryo-electron tomography techniques were used here to visualize mitochondrial nucleoids from bovine heart prepared by density gradient separation.

3.   Aims

Mitochondrial macromolecular complexes like OXPHOS complexes and mt-nucleoids are associated with a broad spectrum of human diseases, which involve biochemical and genetic pathways. Therefore, they are in the focus of mitochondrial research. The purpose of this work was to develop new techniques, which are required for the isolation and analysis of mitochondrial macromolecular complexes, and to use these novel techniques for a better understanding of these complexes.

A novel two-dimensional native electrophoretic system (2-D BN/hrCNE) comprising BNE for the first dimension and hrCNE for the second dimension was developed in order to increase the sensitivity of detection of fluorescence-labeled supercomplexes. This new system was intended to reduce the complexity of supercomplexes for proteomics and biochemical analysis. 2-D BN/hrCNE should allow for immediate identification and quantification of fluorescence-labeled proteins in 2-D gels.

Then, the Western blot protocol for native gels was modified in such a way that enzymatic activities and full immunological reactivity of native proteins were retained. This novel protocol for native immunoblotting of BN gels should make it possible to monitor the recognition of a protein by conformation-specific antibodies, thus representing a simple alternative method compared to the native ELISA.

As a first biochemical object to apply specific electrophoretic techniques, it was intended to study the protein-protein interaction of a novel protein component (Cox26) of yeast respiratory supercomplex which was found by our group. This hydrophobic protein should be characterized and its interaction partners should be found thus suggesting potential roles of the novel protein. The result should also help to get structural insights into the organization of supercomplexes in the mitochondrial inner membrane of yeast.

A second biochemical object, appling special electrophoretic techniques, was to isolate mitochondrial nucleoids from bovine heart as native and clean as possible. Different approaches including biochemical, biophysical and bioinformatics approaches have to be applied to characterize the native mitochondrial nucleoids. This study provides insights into the organization of mitochondrial DNA in nucleoids from animal tissues and may yield clues for the future therapy of specific mitochondrial dysfunction.

III. Materials and Methods

1. Materials

1.1. Chemicals

Chemicals	Company
6-aminohexanoic acid	Fluka
Acetic acid	J.T. Baker
Acetonitrile	ThGeyer
Acrylamide	Serva
Agarose	Serva
Ammonium hydrogen carbonate	Roth
Ammonium persulfate	Sigma
ATP	Pharmacia
Bisacrylamide	Serva
Bovine serum albumin (BSA)	Biolabs
Calcium chloride	Roth
Coomassie Blue G-250	Serva
Coumarin	Sigma
Cytochrome *c*	Sigma
DeepPurple total protein stain	GE HealthCare
Diaminobenzidine (DAB)	Fluka
Dimethylsulfoxide (DMSO)	Sigma
Dithioerythreitol (DTT)	Roth
DNA ladder	MBI fermantas
EDTA	AppliChem
Ethanol	J.T. Baker
Ethidium bromide	Sigma
Fluorescent monoreactive N-hydroxysuccinimide (NHS) ester dyes (Cy5 and Cy5.5)	GE HealthCare
Formaldehyde solution 36.5%	Riedel-de Haen

Formic acid	Roth
Glucose	Roth
Glycerol	Pharmacia and Fluka
HEPES	Sigma
Hydrogenperoxide 30% solution	Sigma
Imidazole	Fluka
Immobiline Dry Stripes pH 3-10NL, 24cm	GE HealthCare
Iodoacetamide (IAA)	Sigma
IPG buffer pH 3-10 NL	GE HealthCare
Kodak developer, BioMax MR	Sigma
Kodak fixer, BioMax MR	Sigma
Kodak X-ray films, BioMax MR	Sigma
Lead (II) nitrate	Fluka
Luminol	Sigma
Mercaptoethanol	Merck
Methanol	J.T. Baker
Mops	AppliChem
NADH	Sigma
Nitrotetrazoliumblue (NTB)	Sigma
PMSF	AppliChem
Polyethyleneglycol (PEG) 4000	Hampton Research
Polyvinylidendifluoride membranes	Immobilon TMP
Ponceau S	Sigma
Potassium cyanide	Merck
Potassium hydroxide	Roth
Silver nitrate	Fluka AG, Buchs, Swiss
Sodium carbonate	AppliChem
Sodium chloride	Roth
Sodium deoxycholate	Merck
Sodium hydroxide	Roth
Sodium thiosulphate pentahydrate	Merck
Sucrose	Sigma
SyproRuby gel stain solution	Invitrogen
Taq DNA polymerase	Sigma

Tetramethylethylendiamid (TEMED)	Sigma
Thiourea	Sigma
Tricine	Serva
Trifluoroacetic acid	Sigma
Tris (Trizma® Base)	Sigma
Trypsin	Sigma
Urea	Serva

1.2. Kits

Kit	Company
DC protein assay	Bio-Rad
Quant-iT^{TM} PicoGreen®dsDNA reagent and kits	Invitrogen Molecular Probes
Quant-iT^{TM} RiboGreen®RNA assay kits	Invitrogen Molecular Probes
NucleoSpin Extract II	Macherey-Nagel
NucleoSpin Plasmid	Macherey-Nagel
NucleoSpin Blood L kit	Macherey-Nagel
High molecular weight water protein kit	GE HealthCare

1.3. Instruments

Centrifuges	
L8-70TM Ultracentrifuge	Beckman Instruments GmbH
Biofuge	Heraeus

Rotors	
Ti 70 (Ultracentrifuge)	Beckman Instruments GmbH
SW Ti 40 (Swing-out rotor)	Beckman Instruments GmbH

Balances	
AE 160	Mettler
AG 245	Mettler
1204 MP	Sartorius
PB 1502-S	Mettler
PM 400	Mettler

Homogenizers, Mixers, Shakers	
Meat grinder	IKA®-Werke
Motor-driven Potter	Kontess
Electrical Potter homogenizer	IKA®-Werke
Vortex Genie	Scientific industries
Orbital shaker	Edmund Bühler GmbH
Thermomixer comfort	Eppendorf
Ultra Turrax T25	IKA Lab technique

Microplate Readers	
Spectra Max M2	Molecular Devices
Spectra Max PLUS 384	Molecular Devices

PCR-Thermocycler	
PeQSTAR	Biotechnology GmbH Erlangen

Imaging	
Typhon 9400 variable mode imager	Amersham Biosciences
EPSON smart panel	Seiko Epson Corporation
Digital camera D5000	Nikon
Chemi Doc XRS System	Bio-Rad

Electrophoresis instruments	
Ettan IPGphor IEF system	GE HealthCare Life Sciences
Ettan Dalt Twelve electrophoresis system	GE HealthCare Life Sciences
Ettan spot picker	GE HealthCare Life Sciences
Semidry blotter	Fröbel Labortechnik

Semidry blotter	Amersham Biosciences
Electrophoresis chamber, vertical	Custom made
Electrophoresis chamber, horizontal	Shelton Scientific
Power supplies	Fröbel Labortechnik
Peristaltic pump P1	LKB

pH meter	
SevenEasy	Mettler Toledo

1.4. Antibodies

1.4.1. Primary antibodies

Name	Specificity	Origin	Provider (reference)
Y1F5 G2a	NESM (*Y.l.*)	mouse	Dr. Volker Zickermann (Zickermann et al., 2010)
Y30C12 G1	NESM (*Y.l.*)	mouse	Dr. Volker Zickermann (Abdrakhmanova et al., 2004)
Y31A8 G1	NUPM (*Y.l.*)	mouse	Dr. Volker Zickermann (Angerer et al., 2011)
Y35C5 G1	49-kDa (*Y.l.*)	mouse	Dr. Volker Zickermann (Zickermann et al., 2003)
Y40G5 G1	Unknown (*Y.l.*)	mouse	Dr. Volker Zickermann (Zickermann et al., 2010)
Y44G10 G1	Unknown (*Y.l.*)	mouse	Dr. Volker Zickermann (Zickermann et al., 2010)
Cox2	Cox2 (*S.c.*)	mouse	
Cox3	Cox3 (*S.c.*)	mouse	
Cox4	Cox4 (*S.c.*)	mouse	
Cox26	Cox26 (*S.c.*)	rabbit	Prof. Hermann Schägger (Kadeer et al., manuscript in preparation)
TFAM	TFAM (*Bos taurus*)	rabbit	Abcam
Twinkle	Twinkle (*Bos taurus*)	rabbit	Abcam
Es1	Es1 (*Bos taurus*)	rabbit	Sigma

1.4.2. Secondary antibodies

Peroxidase conjugated anti-mouse	Sigma
Peroxidase conjugated anti-rabbit	Sigma

1.5.   **Oligonucleotides (primers)**

Primer	Sequence	Species, accession number and position
ND1-fw	5- TCCTATTGGCCGTAGCATTC-3´	*Bos taurus*, gb/HQ184045.1, nt3139/3158
ND1-rev	5- TATTGCTAGAGGCCATGCTG-3´	*Bos taurus*, gb/HQ184045.1, nt3650/3631
ND5-fw	5- CGGACGAGCAGATGCAAACACA-3´	*Bos taurus*, gb/HQ184045.1, nt12586/12609
ND5-rev	5- GCGGATTTTCCGGTTGCAGCTA-3´	*Bos taurus*, gb/HQ184045.1, nt12783/12762
Cox3-fw	5- CCGAGAAAGCACCTTCCAAGGG-3´	*Bos taurus*, gb/HQ184045.1, nt9156/9176
Cox3-rev	5- GGGGGTTTAGTGGGTGAATGCC-3´	*Bos taurus*, gb/HQ184045.1, nt9349/9328
Lactalbumin-fw	5- CCTGGTAGGCATCCTATTCC-3´	*Bos taurus*, gb/JN258330.1, nt1678/1698
Lactalbumin-rev	5- AGGCTCTCCAACCAATCTCC-3´	*Bos taurus*, gb/JN258330.1, nt2028/2009
Citrate synthase-fw	5-GCAAGACGGTGGTGGGCCAG-3´	*Bos taurus*, gb/NC007303.4, nt61496178/61496197
Citrate synthase-rev	5-TGGGCCCAAAAGCTGAGGGGT-3´	*Bos taurus*, gb/NC007303.4, nt61496458/61496438
TFAM-fw	5-CAGGAGCGGATCTCTGCGCG-3´	*Bos taurus*, gb/NW001494479.1, nt1054059/1054040
TFAM-rev	5-GCAGGGGACAACGAACCCGG-3´	*Bos taurus*, gb/NW001494479.1, nt1053737/1053756
ATP5B-fw	5-GACTCAGCCCTTCAGCGCCG-3´	*Bos taurus*, gb/NC007303.4, nt61233291/61233310
ATP5B-rev	5-TTCGAGAGCGCGAGCAGTGC-3´	*Bos taurus*, gb/NC007303.4, nt61233602/61233583

1.6. Softwares

CorelDRAW® Graphics Suite - Version 12.0 (Corel Corporation)

Microsoft Office 2003 (Microsoft)

Quantity one-4.6.1 (Bio-Rad)

ImageQuant TL (GE Healthcare)

DeCyder™ 2D version 7.0 (GE Healthcare)

1.7. Buffers and solutions

Buffers for isolation of bovine heart mitochondria	
Mitochondria preparation medium	250 mM Sucrose, 10 mM Tris-HCl, 0.5 mM EDTA, pH 7.4
Washing buffer	0.9% KCl, 1 mM EDTA, 5 mM Tris-HCl, pH 7.8
Isolation buffer	0.25 M sucrose, 0.015 M EDTA, 0.01 M Tris-HCl, pH 7.5
Separation buffer	0.25 M sucrose, 0.01 M Tris-HCl, pH 7.8

Buffers and solutions for native gels	
Solubilization buffer	50 mM NaCl, 2 mM 6-aminohexanoic acid, 1 mM EDTA, 50 mM imidazole-HCl, pH 7.0 (4°C).
Gel buffer (3x)	1.5 M 6-aminohexanoic acid, 75 mM imidazole-HCl, pH 7.0
AB mix	49.5% T, 3% C - acrylamide-bisacrylamide mixture (wt/vol)
AB mix for large pore gels	2% T, 20% C - 9% T, 6% C
5% Coomassie-dye stock	5 g Coomassie-dye suspended in 100 ml, 500 mM 6-aminohexanoic acid
Glycerol/Ponceau S stock	50% glycerol (wt/vol), 0.1% Ponceau S
Anode buffer for native gels	25 mM imidazole/HCl, pH 7.0

Cathode buffer for BNE (B)	50 mM Tricine, 7.5 mM imidazole, 0.02% Commassie Blue G-250
Cathode buffer for BNE (B/10)	50 mM Tricine, 7.5 mM imidazole, 0.002% Commassie Blue G-250
Cathode buffer for modified BNE	50 mM Tricine, 7.5 mM imidazole, 0.02% Commassie Blue G-250, 0.02% DDM
Cathode buffer for hrCNE	50 mM Tricine, 7.5 mM imidazole, 0.05% Na-desoxycholate, 0.02% DDM

Buffers and solutions for SDS gels	
SDS gel buffer (3x)	3 M Tris, 1 M HCl, 0.3% SDS (wt/vol)
Anode buffer for Tricine-SDS-PAGE (10x)	1 M Tris, 0.255 M HCl
Cathode buffer for Tricine-SDS-PAGE (10x)	1 M Tris, 1 M Tricine, 1% SDS (wt/vol)
SDS loading buffer, non-reducing (I)	12% SDS (wt/vol), 30% glycerol (wt/vol), 0.05% Coomassie Blue G-250, 50 mM Tris-HCl, pH 7.0
SDS loading buffer, reducing (I+Me)	12% SDS (wt/vol), 6% mercaptoethanol (vol/vol), 30% glycerol (wt/vol), 0.05% Coomassie Blue G-250, 150 mM Tris-HCl, pH 7.0

Buffers and solutions for 2-D IEF/SDS gels	
Thiourea rehydration solution	7 M urea, 2 M thiourea, 2% CHAPS, 0.002% Bromophenol blue, 0.5 % IPG buffer pH 3-10L, 18 mM DTT
DIGE labeling buffer	7 M urea, 2 M thiourea , 4% CHAPS, 30 mM Tris-HCl, pH 8.6
IEF→SDS equilibration buffer A	6 M urea, 2% SDS, 50 mM Tris-HCl, pH 8.8, 0.02% Bromphenolblue, 30% glycerol, 65 mM DTT
IEF→SDS equilibration buffer B	6 M urea, 2% SDS, 50 mM Tris-HCl, pH 8.8, 0.02% Bromphenolblue, 30% glycerol, 135 mM iodoacetamide
Lämmli gel buffer (4x)	1.5 M Tris, 0.4% SDS, 4 M HCl
Lämmli running buffer (10x)	0.25 M Tris, 1.92 M glycine, 1% SDS

Agarose sealing	0.5% agarose, 0.02% Bromphenolblue, 1x Lämmli running buffer

Buffers and solutions for Western blot

Electrode buffer	300 mM Tris-HCl, 100 mM acetic acid, pH 8.6
Staining buffer	25% methanol, 10% acetic acid, 0.02% Coomassie Blue G-250
Destaining buffer	50% methanol, 10% acetic acid
PBS buffer (10x)	80 mM Na_2HPO_4, 20 mM NaH_2PO_4, 100 mM NaCl, pH 7.5
Blocking buffer	1x PBS, 0.5% Tween 20
Washing buffer	1x PBS, 0.1% Tween 20
ECL-1 buffer	0.1 M Tris-HCl pH 8.5, 2.5 mM Luminol, 400 µM Coumarin
ECL-2 buffer	0.1 M Tris-HCl pH 8.5, 0.02% H_2O_2

Buffers and solutions for agarose gels

TAE buffer (10x)	400 mM Tris-acetate, 10 mM EDTA, pH 8.3
TE buffer	10 mM Tris-HCl, 1 mM EDTA, pH 8.0

1.8. Detergents

Detergent	Stock in water (w/v)	Company
Sodium dodecyl sulfate (SDS)	20%	AppliChem
Digitonin	20%	Fluka
Dodecyl-ß-D-maltoside (DDM)	20%	Glycon
Sodium deoxycholate (DOC)	10%	Merck
Triton X-100	10%	Serva
Tween 20	20%	Serva
Brij35	20%	Merck
CHAPS	20%	Sigma

2. Methods

2.1. Isolation of mitochondria

Mitochondria were isolated from bovine heart (*Bos taurus*), *Yarrowia lipolytica* and *Saccharomyces cerevisiae* as detailed in the following.

2.1.1. Isolation of bovine heart mitochondria

Bovine heart mitochondria (BHM) were isolated by two different protocols:

Protocol 1: for the development of electrophoretic techniques with fluorescence-labeled OXPHOS complexes, bovine heart mitochondria were prepared according to Smith, 1967. Bovine hearts were minced with a meat grinder and homogenized in mitochondria preparation medium using a mixer. Mitochondria were isolated using differential centrifugation: nuclei and cell debris were sedimented by 20 min centrifugation at 600g. Mitochondria were then harvested by 10,000g centrifugation for 30 min and washed twice in mitochondrial preparation medium.

Protocol 2: in order to study the protein components of mitochondrial nucleoids, a special preparation protocol (Crane et al., 1956) was required that allows preparation of very pure mitochondria free of other cell organelles, especially nuclei. Briefly, heart tissues were collected fresh, minced and washed several times with washing buffer (0.9% KCl, 1 mM EDTA (protease inhibitor), 5 mM Tris-HCl, pH 7.8). Minced meat was homogenized in ice cold isolation buffer (0.25 M sucrose, 0.015 M EDTA, 0.01 M Tris-HCl, pH 7.5) using the UltraTurrax five times for one min with 30 s break intervals while bubbling with argon. The break intervals were used to check and adjust pH to 7.4 with 1 M Tris base. Nuclei and unbroken cells were removed by centrifugation (13 min at 1600g). Supernatants were filtered through four-layer gaze and mitochondria were sedimented by centrifugation for 15 min at 12,000g. The pellet was re-suspended in separation buffer (0.25 M sucrose, 0.01 M Tris-HCl, pH 7.8) and homogenized using an electrical Potter homogenizer. The mitochondrial heavy and light fractions were separated by centrifugation for 10 min at 17,000g. The obtained pellet was composed of two layers: a lower dark and dense layer representing heavy mitochondria (unbroken and mostly intact) and an upper loose and fluffy layer representing the light mitochondria (mostly broken mitochondria and impurities from reticulum). Mitochondria

were further purified using density gradient centrifugation according to Meisinger et al., 2000, and Wittig and Schägger, 2005. Briefly, mitochondria were loaded onto sucrose density step gradients containing 1 ml each of 15%, 23% and 32% sucrose, 2 ml each of 37%, 47% and 55% sucrose and finally 1 ml of 60% sucrose in 10 mM Na-Mops, 1 mM EDTA, pH 7.2. Density gradient centrifugation was performed using a SW 40Ti swing-out rotor (45 min centrifugation at 130,000g, 4°C). The brownish ring on top of the 47% sucrose step contained heavy mitochondria. This ring was harvested and called super-heavy (SH) fraction. The SH fraction was diluted three-fold with mitochondrial preparation medium, portioned into aliquots containing 20 mg protein, collected by centrifugation at 8,500g for 10 min, shock frozen using liquid nitrogen and stored at -80°C.

2.1.2. Isolation of mitochondria from *Yarrowia lipolytica*

Mitochondria from *Y. lipolytica* were prepared by Andrea Duchene according to Kerscher et al., 1999, and used for the development of native immunoblotting of blue native gels to identify conformation-specific antibodies.

2.1.3. Isolation of mitochondria from *Saccharomyces cerevisiae*

S. cerevisiae mitochondria were prepared by Christian Bach, Andrea Duchene and Gudrun Beyer in our group according to Arnold et al., 1998, and made available for my work. Briefly, yeast cells were harvested by centrifugation at 1,800g and washed with sucrose buffer (250 mM sucrose, 5 mM 6-aminohexanoic acid, 1 mM EDTA, and 10 mM sodium phosphate, pH 7.0). Five grams of sedimented cells, 5 ml of glass beads (0.25-0.5 mm) and 5 ml of sucrose buffer were vortexed in a 50 ml tube 10 times for 1 min with 1 min cooling intervals on ice. After diluting with 10 ml sucrose buffer, the sedimented glass beads were removed and the supernatant was centrifuged for 20 min at 1,250g. Mitochondrial membranes were collected by 30 min centrifugation at 18,000g and stored in sucrose buffer at -80°C.

2.2. Fluorescence labeling of mitochondria

BHM isolated according to protocol 1 (III.2.1.1), were washed twice with 10 mM sodium phosphate buffer to remove primary amines that would hamper labeling of lysines by the monoreactive N-hydroxysuccinimide ester dyes Cy5 and Cy5.5 (NHS-Cy5, NHS-Cy5.5).

Best signal to noise ratios in final multi-dimensional native/denaturing gels were achieved when labeling of mitochondrial complexes was performed directly with native and unsolubilized membranes (Wittig et al., 2007b). Briefly, the dye was dissolved in dimethylformamide (10 µg/µl), 10µl aliquots of the dye (100 µg) were added to 10 mg BHM in 1 ml 250 mM sucrose, 20 mM sodium phosphate, pH 7.5, and gently shaken in the dark for one hour at room temperature. Dye excess was removed by centrifugation of mitochondrial membranes (10 min, 20,000g). Labeled mitochondrial pellets were stored as 400 µg aliquots at -80°C.

2.3. Solubilization of mitochondria

Depending on the detergent stability of the protein complexes of interest, different detergents were chosen for the solubilization (Table 2). The very mild neutral detergent digitonin was used to preserve supramolecular structures. In order to solubilize individual mitochondrial complexes I-V from the inner mitochondrial membrane, the mild neutral detergent dodecylmaltoside (DDM) was used. Different acrylamide gradients were used for the separation of protein complexes of interest by native electrophoresis (NE).

Table 2. Detergent/protein ratios for solubilization of mitochondria

Mitochondria from	Detergent	Protein/ detergent ratio	Centrifugation	Acrylamide gradient for NE
Bovine heart	Digitonin	4 g/g	10 min at 100,000g	3-13%
Yarrowia lipolytica	DDM	1.3 g/g	10 min at 20,000g	4-13%
Saccharomyces cerevisiae	Digitonin	3 g/g	15 min at 20,000g	3-13%

2.4. Protein quantification

Protein concentrations were determined according to a modified Lowry-protocol (Helenius and Simons, 1972) using the commercially available DC protein assay kit (Bio-Rad). Bovine serum albumin (BSA, 0.1 – 2.0 mg/ml) was used for calibration.

2.5.   Estimation of mtDNA by PicoGreen fluorescence assay

To determine the mitochondrial DNA distribution in sucrose gradient fractions, the PicoGreen fluorescence assay (Invitrogen) was applied. The fluorescent dye PicoGreen undergoes a dramatic fluorescence enhancement upon binding to dsDNA that can be measured using a microplate fluorometer (Spectra Max M2, Molecular Devices). The assay was performed as outlined in the protocol supplied with the kit. Briefly, 10 or 20 µl of each sucrose gradient fraction were mixed with 90 or 80 µl nucleoid isolation buffer (500 mM 6-aminohexanoic acid, 25 mM imidazole-HCl, pH 7.0, 1 mM EDTA). Then, 100 µl of diluted PicoGreen (1:200) was added. Samples were mixed and incubated for 5 minutes in the dark in a 96-well plate. The samples were then excited at 488 nm and the emission was measured at 525 nm (cutoff 515 nm). A standard curve was generated using 3.125–200 ng/ml Lambda DNA standard supplied with the kit.

2.6.   Electrophoretic techniques

2.6.1.   Blue native electrophoresis (BNE)

BNE (Schägger and von Jagow, 1991; Schägger et al., 1994; Wittig et al., 2006a) was used to separate mitochondrial membrane protein complexes in the first dimension.

2.6.2.   Blue native electrophoresis on large pore gels

Large pore gels were developed by us to isolate and characterize mega complexes with sizes up to 50 MDa. In order to repurify native mitochondrial nucleoids, blue native electrophoresis on 2-9% acrylamide gels was applied as described by Strecker et al., 2010.

2.6.3.   High-resolution clear native electrophoresis (hrCNE)

High-resolution clear native electrophoresis is a non-coloured version of BNE. hrCNE-1 was performed as detailed in Wittig et al., 2007a, b.

2.6.4. Two-dimensional blue native electrophoresis (2-D BN/BNE)

In order to dissociate supercomplexes from first dimension BN gels into the individual complexes and to separate loosely attached proteins, the modified cathode buffer (50 mM Tricine, 7.5 mM imidazole, 0.02% Commassie Blue G-250, 0.02% DDM) was applied for second dimensional native separation as described by Schägger and Pfeiffer, 2000, 2001.

2.6.5. SDS-polyacrylamide gel electrophoresis (SDS-PAGE)

Glycine-SDS-PAGE, also known as Laemmli-SDS-PAGE (Laemmli, 1970), and Tricine-SDS-PAGE (Schägger and von Jagow, 1987; Schägger, 2006), based on Glycine-Tris and Tricine-Tris buffer systems, respectively, are the commonly used SDS polyacrylamide gel electrophoretic techniques to separate individual denatured proteins. Tricine-SDS-PAGE is used preferentially for the optimal separation of proteins smaller than 30 kDa whereas Glycine-SDS-PAGE is used for proteins larger than 30 kDa. The lower acrylamide concentration required for Tricine-SDS-PAGE compared to Glycine-SDS-PAGE facilitates electroblotting, which is particularly important for hydrophobic proteins. For SDS separation of mitochondrial nucleoids, samples were concentrated by centrifugation (10 min, 100,000g) after dilution with at least 6-fold volumes of water. Based on the Lowry assay, the protein pellets were resuspended to a concentration of 10 mg/ml. 10 µg of each sample was applied to the gel wells of a 10 % acrylamide gel.

2.6.6. Doubled SDS-polyacrylamide gel electrophoresis (dSDS-PAGE)

Tricine-SDS-PAGE is also used preferentially for dSDS-PAGE (composed of two orthogonal SDS gels), which is a proteomic tool to isolate extremely hydrophobic proteins for mass spectrometric identification. The gels were performed as described by Rais et al., 2004.

2.6.7. Two-dimensional blue native/SDS polyacrylamide gel electrophoresis (2-D BN/SDS-PAGE)

Gel stripes from BNE were prepared for second dimension Tricine-SDS-PAGE as described by Schägger, 2006, to analyze the subunit composition of native complexes.

2.6.8. Processing of 2-D native gels by dSDS-PAGE

Gel pieces from 2-D BN/BNE or 2-D BN/hrCNE were processed further by doubled SDS-PAGE (Rais et al., 2004) to resolve the subunits of the native protein complexes. This 4-D system comprised two orthogonal native electrophoreses followed by two orthogonal SDS-PAGEs (Meyer et al., 2007). Briefly, gel pieces from the 2-D native gels were incubated for 30 min with 1% SDS, and then processed by 3-D Tricine-SDS-PAGE using 9%, 10% or 12% acrylamide gels with or without 6 M urea. Lanes from 3-D gels were then incubated for 30 min in acidic solution containing 100 mM Tris, 150 mM HCl, pH 2, and separated by an orthogonal 4-D SDS-PAGE on 16% acrylamide gels with or without urea. The 4-D gels were stained with Coomassie Blue G-250 or silver.

2.6.9. 2-D IEF/SDS electrophoresis

2-D IEF/SDS electrophoresis was performed essentially as described by Görg et al., 1988. Two-dimensional electrophoresis separates proteins by their isoelectric points (pI) in the first dimension and then by their molecular masses in the second dimension. Separation in the first dimension was achieved by focusing the solubilized proteins in a gel containing an immobilized pH gradient (IPG stripes). Following the first dimension, the IPG stripe was equilibrated in buffer containing SDS. The equilibrated IPG stripe was placed on top of an SDS gel. Electrophoresis was then performed to separate the proteins by molecular mass in this second dimension. The gels were fluorescence-stained either by DeepPurple or by SyproRuby. Fluorescence-intensities were quantified using a Typhoon scanner and the program DeCyder™ 2-D Differential Analysis Software v7.0 (GE HealthCare). 100-150 protein spots were picked for MS analysis using an Ettan Spot Picker (GE HealthCare).

2.7. Protein staining techniques

2.7.1. Coomassie staining

Coomassie stain is a classic organic dye stain. The organic dye Coomassie Brillant Blue binds to basic and hydrophobic parts of proteins. Proteins are visible as blue bands. Detection limit is around 100 ng protein/band. Coomassie staining was carried out as described by Schägger, 2006.

2.7.2. Silver staining

Proteins bind silver ions (Ag+) that can be reduced under appropriate conditions to build up a visible image of finely distributed silver metal. Silver staining is more sensitive than Coomassie staining (<10 ng protein/band). Silver staining was performed as described by Rais et al., 2004.

2.7.3. SyproRuby and DeepPurple stain

SyproRuby (Invitrogen) and DeepPurple stains (GE HealthCare) are fluorescence based protein staining methods. SyproRuby is a fluorescent metal chelate, which builds an organic complex that interacts non-covalently with proteins. DeepPurple total protein stain is based on epicocconone, a naturally occurring biodegradable fluorescent compound extracted from a fungus. Epicocconone is a water soluble fluorophore that spontaneously and covalently binds to primary amines to yield fluorescent products. Both dyes can be efficiently excited by a green laser at 532 nm and detected by a Typhoon scanner. The sensitivity of the SyproRuby and DeepPurple protein gel stain is superior to colloidal Coomassie Brilliant Blue stain or silver stain.

2-D IEF/SDS gels were stained with SyproRuby or DeepPurple according to the manufacture's instructions. Briefly, for SyproRuby detection, gels were fixed for one hour in 10% methanol, 7% acetic acid. Gels were then placed in SyproRuby solution (Invitrogen). Staining was carried out for two hours. For DeepPurple staining, gels were fixed for one hour in 30% methanol 7.5% acetic acid. The gels were then rinsed with water and placed for two hours into staining solution (1:200 dilution of DeepPurple in 100 mM sodium borate, pH 10.5). The gels were then rinsed for 30 min in 30% methanol, acidified for 30 min in 30% methanol, 7.5% acetic acid, and again rinsed for 30 min in 70% methanol. Finally, in both stains, the gels were reequilibrated in water for 10 min prior to imaging.

2.8. In-gel assays

In-gel assays were applied in this work to identify and quantify mitochondrial complexes from bovine heart and from *Y. lipolytica* on BN gels. Complex I in-gel activity assay, also called NADH:NTB oxidoreductase assay, complex II in-gel activity assay (in-gel succinate:NTB oxidoreductase assay), complex III/IV in-gel assay (native heme stain assay)

and the complex V in-gel activity assay (ATP hydrolysis assay) were performed according to Zerbetto et al., 1997, with minor modifications as described by Wittig et al., 2007b. Buffers, reagents and solutions to stop the reactions are summarized in Table 3.

Table 3. In-gel assays

Complex	Buffer	Reagent	Stop solution
Complex I	5 mM Tris-HCl, pH 7.4	3 mM NTB, 150 µM NADH	50% methanol, 10% acetic acid
Complex II	5 mM Tris-HCl, pH 7.4	20 mM Na-succinate, 0.2 mM PMS	50% methanol, 10% acetic acid
Complex III/IV	50 mM NaPO$_4$, pH 7.4	2.3 mM DAB, 50 µM Cyt *c*	50% methanol, 10% acetic acid
Complex V	35 mM Tris, 270 mM glycin, pH 8.3 (25°C)	14 mM MgSO$_4$ 0.2% Pb(NO$_3$)$_2$, 8 mM ATP	50% methanol

2.9. Western blot analysis

2.9.1. Western blotting of proteins from SDS gels

In order to transfer also hydrophobic proteins from high percentage acrylamide Tricine-SDS gels, the semidry electroblotting technique of Schägger, 2006, was used. Immunodetection was performed as described in Carrozzo et al., 2006. For Western blot analysis of mitochondrial nucleoids, the PVDF membranes were blocked in PBS buffer containing 0.1 % Tween 20 and 3 % bovine serum albumin (BSA).

2.9.2. Western blotting of native proteins from BN gels

Native immunoblotting of proteins from BN gels (NIBN) was developed in this work. The new method will be presented in more detail in section 2 (chapter IV, Results). The blotting conditions are compared and shortly summarized below (Table 4).

Table 4. Blotting conditions for SDS and native gels

		Tricine-SDS gels	BN gels
Protein transfer onto PVDF membranes	Voltage	15 V	20 V
	Current	0.4 mA/cm2 gel area	0.8 mA/cm2 gel area
	Time	16-24 h	1.5 h
Staining for documentation		25% methanol, 10% acetic acid, 0.02% Coomassie-dye	25% methanol, 10% acetic acid, 0.02% Coomassie-dye
Destaining for immunodetection		100% methanol	2x2 h 0.2% Tween 20, 10 mM imidazole/HCl pH 7.0

2.10. Characterization of the binding specificity of antibodies by Western blot and LC-MS/MS

We used a three-dimensional electrophoresis technique (BNE followed by dSDS-PAGE) to separate the protein subunits of *Y. lipolytica* complex I (CI) and to characterize the binding specificity of monoclonal antibody 31A8. To prepare CI for BN-PAGE, 3 µl dodecylmaltoside (10%) was first added to 1 mg (20 µl) of chromatographically purified CI, followed by dilution with 400 µl solubilization buffer (50 mM NaCl /50 mM imidazole pH 7.0), addition of 80 µl of 50% glycerol, 0.1% Ponceau S and supplementation with 1 µl of a 5% Coomassie Blue G-250 stock. The diluted complex I was then repurified using a preparative BN gel (14 cm width of the sample well). Following BN-PAGE the visible blue stained complex I band was excised and separated by SDS-PAGE in a second dimension. Several gel stripes from the 2-D SDS gel were then used for 3-D resolution by further orthogonal SDS gels (dSDS-PAGE, Rais et al., 2004). Following electroblotting of the dSDS gels on PVDF membranes according to a recently described protocol (Schägger, 2006), monoclonal antibody 31A8 was used for immunological detection. The Western blot signal was compared with the original gel and a gel piece corresponding to the signal was cut out for LC-MS/MS analysis from a duplicate Coomassie-stained gel. LC-MS/MS analysis was performed by Dr. Heinrich Heide and Dipl.-Ing. Mirco Steger from our group.

2.11. Mass spectrometric analysis by LC-MS/MS

2.11.1. Tryptic proteolysis

Tryptic proteolysis was carried out essentially according to the protocols of Shevchenko et al., 2006, and Collins et al., 2008. Briefly, destaining of Coomassie, SyproRuby and DeepPurple-stained spots in perforated 96-well plates (Proxeon, Denmark) was achieved by incubation with 50% methanol, 50 mM ammonium hydrogen carbonate for 45 or 15 min at room temparature on a shaker while silver-stained gels were washed twice with 30 mM potassium ferricyanide and 100 mM sodium thiosulfate for 10 min, and at least three times with 150 µl water (LC-MS-grade) and 50 µl 50 mM ammonium hydrogen carbonate until the spots were clear. Subsequently, disulfide bonds were reduced by incubation with 5 mM DTT in ammonium hydrogen carbonate for 60 min and the newly generated free sulfhydryl groups were blocked by 15 mM iodoacetamide (IAA) in ammonium hydrogen carbonate for another 45 min. For dehydration, 100 µl or 65 µl acetonitrile were added for 10 min and then the solution was removed by centrifugation. For trypsin digestion of Coomassie-stained spots, 20 µl of 2.5 ng/µl trypsin solution in ammonium hydrogen carbonate, 10% acetonitrile and 0.5 mM $CaCl_2$ were placed in each well of the micro test plate, while 10 µl of the same solution was used for selected spots, which were picked by a spot picker (Ettan). The spot solutions were incubated for 10 min at 4°C. Then, 30 µl and 10 µl of ammonium hydrogen carbonate were added in the case of Coomassie and silver-stained spots, respectively, to completely cover the gel pieces. The well plates were sealed with a plastic film or aluminium foil to prevent the solution from evaporation. After overnight digestion at 37°C, the peptide containing supernatants were collected into a new 96-well micro plate by centrifugation. In order to enhance the peptide extraction, an additional extraction step was performed using 20-50 µl 50% acetonitrile/1% trifluoroacetic acid and incubation for 60 min at room temperature. The combined extracts were dried in a SpeedVac centrifuge at 40°C. Finally, the peptides were redissolved for mass spectrometry in 20 µl 5% acetonitrile, 0.5% trifluoroacetic acid.

2.11.2. Mass spectrometry

Mass spectrometric analysis were performed by Dr. Heinrich Heide and Dipl.-Ing. Mirco Steger from our group. The tryptic peptides obtained from gel pieces were subjected to LC-MS/MS analysis on an Orbitrap XL mass spectrometer (Thermo) with an Agilent1200 nano-HPLC on the front end. Peptides were separated on 3 µm C18 reversed phase silica beads

filled into a 75 μm ID PicoTip emitter column (New Objectives) in 90 min HPLC runs using 60 min gradients of 5% to 50% acetonitrile with 0.1% formic acid, followed by a 15 min column wash with 90% acetonitrile and 15 min re-equilibration with 5% acetonitrile after each run. Eluted peptides were analyzed in positive mode by a MS method programmed to fragment the top ten most abundant ions using dynamic exclusion for 3 min with a resolution of 30000 at 400Th. Single charged precursor ions were rejected and peptide ions were fragmented in the linear ion trap by CID at 35% collision energy. For accurate mass measurements the lock mass option was enabled at m/z 445.120025 (Olsen et al., 2005).

2.11.3. Database search

The validation of RAW spectra was done using the Mascot server 2.2 search engine. The search parameters were set as follows: 10 ppm deviation on the precursor and 0.8 Da on fragment masses, fixed carbamidomethylation of cysteine, variable oxidation of methionine and two missed cleavages. Spectra were matched against the organism specific protein database (*Bos taurus*) downloaded from Uniprot. Only significant peptide hits indicating identity or extensive homology (p<0.05) were taken into account. Database search was performed by Dr. Heinrich Heide and Dipl.-Ing. Mirco Steger from our group.

2.12. Electron microscopy

Electron microscopy analysis of nucleoids was performed by Dr. Karen Davies from the Max-Planck-Institute of Biophysics, Department of Structural Biology, Frankfurt.

2.12.1. Sample preparation for electron microscopy

For electron microscopy of nucleoids from sucrose gradient fractions, three protocols were applied: (i) The main sucrose gradient fraction was analyzed directly. (ii) Buffer exchange and concentration by ultrafiltration were performed by centrifugation (20 min, 4,500g) through ultrafiltration membranes with a cutoff value of 300 kDa. (iii) After diluting the sample with six volumes of buffer (25 mM NaCl/25 mM imidazole/HCl, pH 7.4, 0.05% dodecylmaltoside), the mt-nucleoids were pelleted by centrifugation (60 min, 100,000g) and resuspended in a small volume of the same buffer.

2.12.2. Negative stain electron microscopy

3 µl of sample was applied to a glow-discharged 400 mesh copper EM grid containing a continuous carbon support film. Grids were washed with 50 µl H_2O and stained with 3µl 1% (w/v) uranyl acetate. Micrographs were collected with a 2 x 2K Gatan CCD camera on a Tecani Spirit electron microscope (FEI, Eindhoven, the Netherlands).

2.12.3. Electron cryo-tomography

Nucleoid samples mixed 1:1 with 6 nm Protein-A gold fiducials (AURION) were applied to carbon-coated Quantifoil grids containing 1.2 µm holes and vitrified in liquid-ethane using a home-made plunge-freezing device. Tomograms were collected on a 2k x 2k CCD camera at 300 kV in a FEI Polara electron microscope equipped with a post-column energy filter (GIF Tridiem 863 Gatan), at a slit size of 20 eV for zero loss energy filtering. Single axis tomograms were collected between +/- 60°, with a step size of 1.5° and a defocus of 7 µm at a magnification of 24.6K. Tomograms were collected at 82K under low-dose conditions using the FEI automatic tomogram collection software. Tomographic volumes were reconstructed with IMOD (Kremer et al., 1996). Contrast was enhanced by non-linear anisotropic diffusion (Frangakis and Hegerl, 2001) and segmentation was performed using the isosurface option in IMOD (Kremer et al., 1996).

2.13.   Molecular biology methods

2.13.1. Polymerase chain reaction

For polymerase chain reaction (PCR) analysis of sucrose gradient fractions, 1 µl of each fraction was applied directly as template. As positive control, mtDNA was isolated from a very pure super heavy (SH, III.2.1.1) mitochondrial fraction prepared using the NucleoSpin Blood L kit (Macherey-Nagel). The same kit was used for the isolation of DNA from crude mitochondria (p), which contained significant nuclear DNA contaminations. No template was added for the negative control. The PCR reaction mixture contained 1 µl template, 2 µl 10x PCR buffer, 2 µl dNTP (2 mM), 0.5 µl of each primer (10 mM), 0.3 µl Taq polymerase and 13.7 µl water. The reaction was started by adding Taq DNA polymerase (manual hot start). PCR conditions were set as follows:

- Initial denaturation: 30 sec at 94°C

- Denaturation: 30 sec at 94°C

- Annealing: 30 sec at 60°C

- Extension: 30 sec at 72°C

- 25 cycles

- Final extension: 5 min at 72°C

PCR products were stored at -80°C

2.13.2. Agarose gel electrophoresis of DNA

The PCR product was separated on 1.5% agarose gels according to Sambrook et al., 1989. Agarose gels were prepared with TAE buffer (0.4 M Tris/acetate, 10 mM EDTA, pH 8.3) and contained 0.5 µg/ml ethidium bromide. The GeneRuler™ 1kb and 100bp plus DNA ladders (both from MBI Fermentas) were used as DNA size markers. Electrophoresis was performed at 120 V and 90 mA. Gels were documented by Chemi DOC XRS System (Bio-Rad).

IV. Results

1. Fluorescent and functional analysis of bovine heart mitochondrial complexes separated by two-dimensional native electrophoresis

The complexity of the superamolecular structures, which are separated by BNE, can be reduced by subsequent second dimensional native separation, as exemplified by 2-D BN/BN electrophoresis (Schägger and Pfeiffer, 2000). However, since Coomassie-dye interferes with the detection of fluorescence-labeled proteins and with in-gel assays, the non-colored high-resolution clear native electrophoresis (hrCNE, Wittig et al., 2007a, b) was introduced for the second dimension electrophoresis. To take advantage of their special properties, BNE and hrCNE were used sequentially for the first and second dimensional native separations. In order to preserve supramolecular structures, bovine heart mitochondria were solubilized by digitonin and the (super)complexes were separated first by BNE. Next, hrCNE was used for the second dimensional resolution for the following reasons: hrCNE offers high-resolution comparable to BNE and has the potential to release individual complexes from supercomplexes similar to modified BNE (i.e. BNE with detergent added to the cathode buffer). Most importantly, with hrCNE no background Coomassie stain can hamper the visualization of in-gel assays. The individual steps of the 2-D BN/hrCNE protocol are summarized in Figure 7.
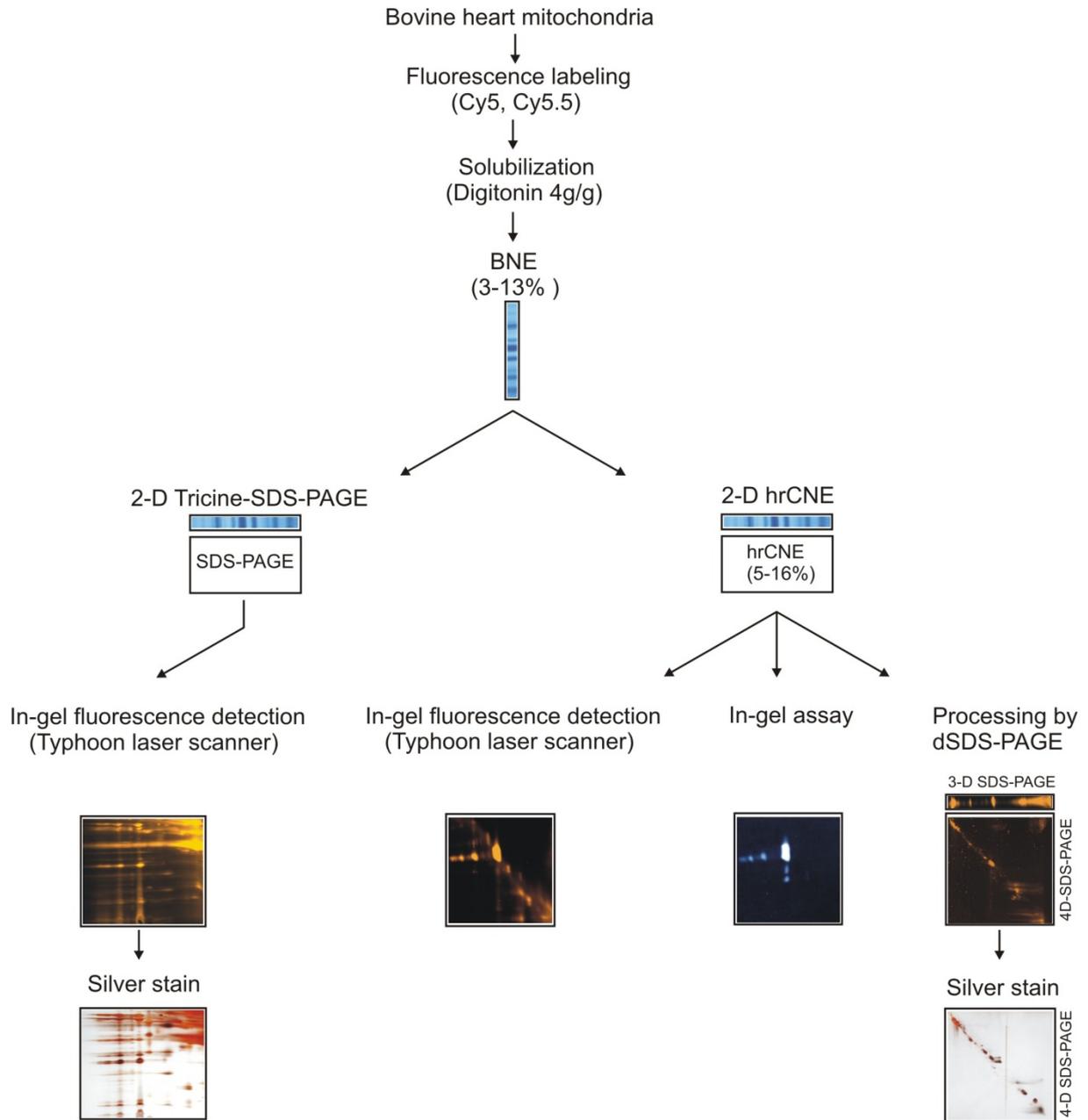
Figure 7. Steps in the fluorescent and functional analysis of bovine heart mitochondrial complexes using two-dimensional native electrophoresis (right side) compared to a conventional protocol (left side).

1.1. Setup for two-dimensional native electrophoresis (2-D BN/hrCNE)

First dimension BNE was performed as described by Wittig et al., 2006a. Gel stripes from BNE were incubated for a few seconds in water and placed on glass plates at the position of the sample gel. An acrylamide gradient gel (5-16% acrylamide) that was slightly thinner than the 1-D gel was cast below the BNE gel stripe. Following polymerization, more water was added on top to remove any air bubbles between both gels and the 1-D stripe was then gently pushed down to get into direct contact to the separating gel. Anode buffer and special cathode buffer for hrCNE-variant 1 (50 mM Tricine, 7.5 mM imidazole, 0.05% Na-desoxycholate, 0.02% DDM) were then supplied and electrophoresis was performed under the same gel and electrophoresis conditions as described for 2-D BN/BN electrophoresis (Wittig et al., 2006b). Electrophoresis was stopped when Coomassie-dye from 1-D BNE, running at the front, started to leave the gel.

1.2. In-gel fluorescent analysis of mitochondrial complexes using 2-D BN/hrCNE

Fluorescence-labeled bovine heart mitochondria were solubilized by digitonin and the (super)complexes were separated by 2-D BN/hrCNE as described above using 5-16% acrylamide gradient gels for the second dimension. Following 2-D BN/hrCNE, the 2-D gel shielded by the glass plates was inspected for fluorescence-labeled proteins using a Typhoon laser scanner (Fig. 8B). Under the labeling conditions used (mitochondria were labeled by Cy5), the monomeric (M), dimeric (D), tetrameric (T), and hexameric (H) forms of complex V were preferentially labeled and converted to the monomeric forms in second dimension hrCNE (Fig. 8B). Following the documentation of the 2-D gels, the same gel was reused for Coomassie staining to obtain a survey of the individual mitochondrial complexes that were dissociated by hrCNE from the larger supercomplexes (Fig. 8C). After that it was possible to assign the strongest band in the high mass region (marked 1 in Fig. 8A, C) to respiratory supercomplex $I_1III_2IV_1$ containing monomeric complex I, dimeric complex III, and one copy of complex IV. Band 1 overlapped with some comigrating dimeric complex V. All complexes that had not been part of supramolecular structures during first dimension BNE, i.e. the individual complexes I, II, III, IV and M were found on a diagonal of spots in the 2-D gels (Fig. 8).
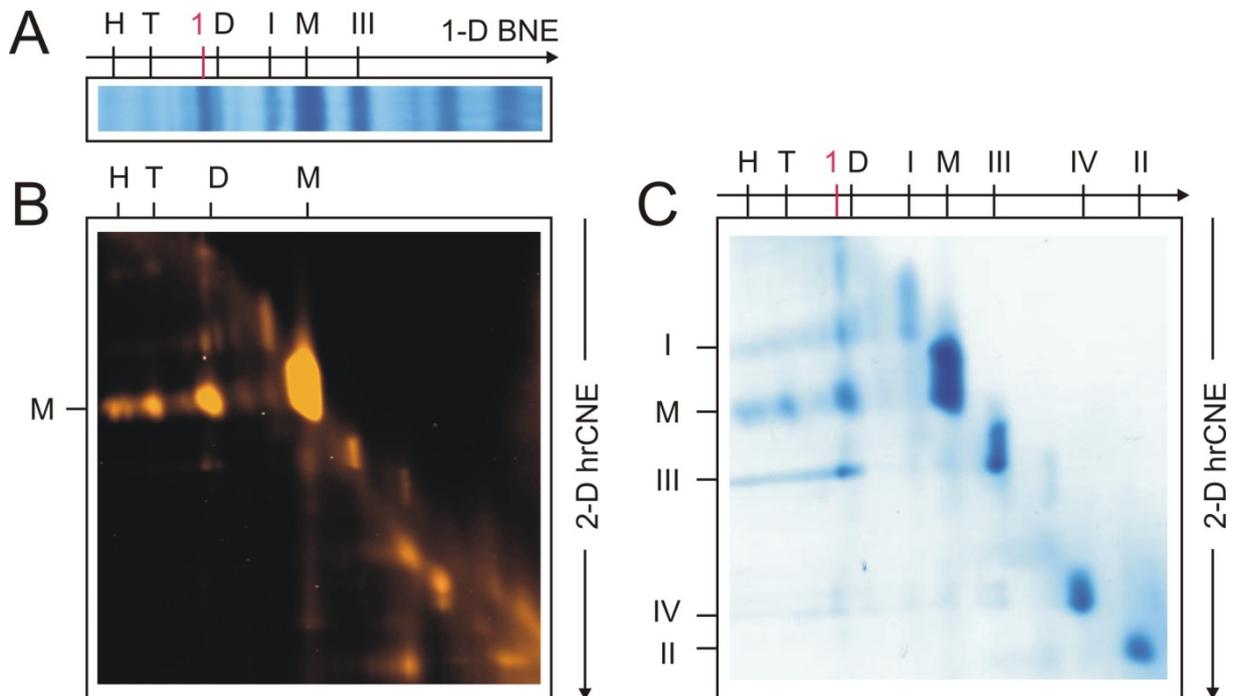
Figure 8. 2-D BN/hrCNE separation of mitochondrial complexes. (A) 1-D BN electrophoresis. Respiratory complexes I and III (I, III) and the monomeric (M), dimeric (D), tetrameric (T) and hexameric (H) forms of ATP synthase are assigned. Supercomplex $I_1III_2IV_1$ (marked 1) comigrated with dimeric ATP synthase (marked D). (B) The 1-D BN gel stripe was processed by second dimension hrCNE using a 5-16% acrylamide gradient gel and the fluorescence-labeled (Cy5) proteins were identified by a Typhoon laser scanner. (C) Gel B was reused for Coomassie staining. Complex II (II) could also be detected.

Additional minor bands of further supercomplexes (marked 0-3 in Fig. 9) could be detected when the mitochondria were labeled with Cy5.5. The resolution in the high mass range was improved in this experiment so that supercomplexes $I_1III_2IV_{0-3}$ (marked 0-3 in Fig. 9) migrating close to dimeric complex V could be detected and assigned. These complexes were also characterized by in-gel assays (see below).

Both major supercomplexes (marked 1 and 0 in 1-D BNE, Fig. 9A) dissociated partially as indicated by the characteristic pairs of spots of complexes I and III (marked I and III on the left side of Fig. 9B). A similar protein pattern was also obtained by Coomassie staining (Fig. 9C). From the Coomassie-stained gel it became apparent that some proteins dissociated from the complexes and migrated close to the dark blue electrophoretic front (ragged blue bottom area). The area above (ellipsoid) was expected to contain detergent-labile proteins or potentially novel accessory proteins of supercomplexes. A mass spectrometric survey of the dissociated proteins and complexes could be obtained by excising 1 cm gel stripes from

unfixed fluorescence-labeled gels (vertically boxed area in Fig. 11B) and separating the proteins by 3-D SDS-PAGE (Fig. 11D, E).
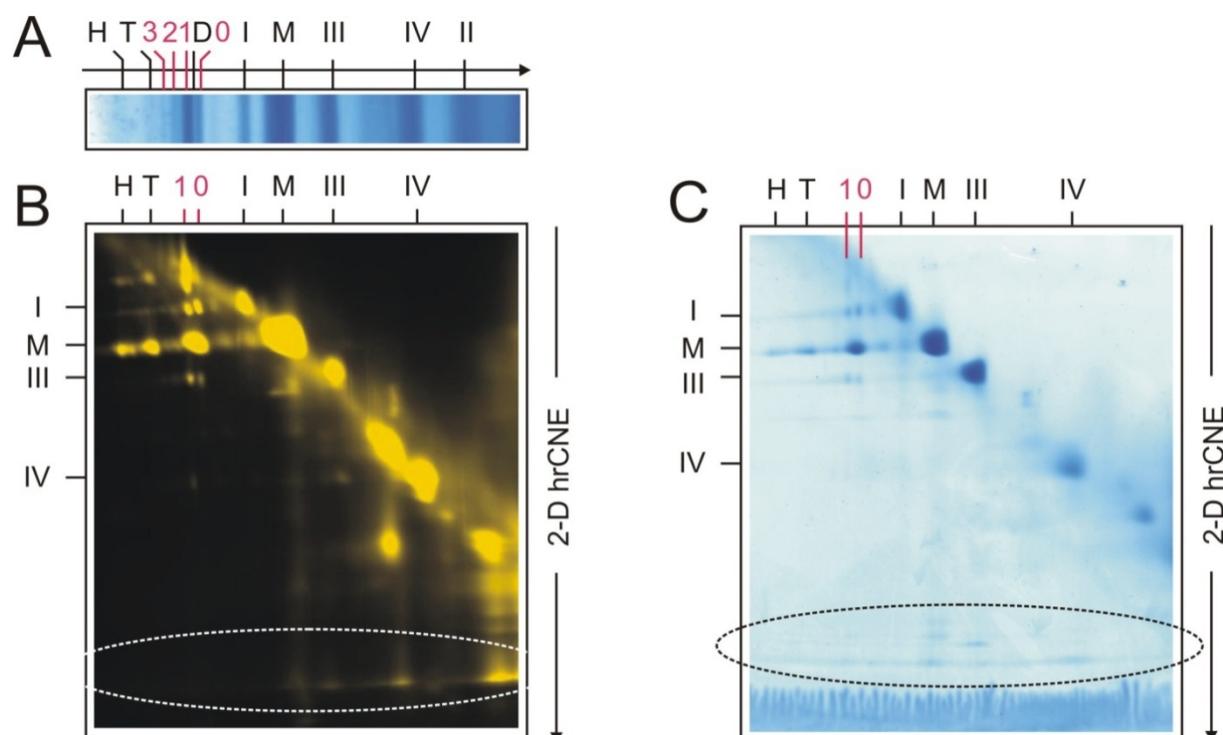
Figure 9. 2-D BN/hrCNE separation of mitochondrial supercomplexes. (A) 1-D BN electrophoresis. Respiratory complexes and ATP synthase forms (M, D, T, H) were assigned as in Figure 8. Additionally assigned were supercomplexes $I_1III_2IV_{0-3}$ containing monomeric complex I, dimeric complex III, and zero to three copies of complex IV (marked 0-3). (B) Detection of fluorescence-labeled (Cy5.5) complexes following 2-D separation by 1-D BNE and 2-D hrCNE. Labile subunits and potentially novel accessory proteins of supercomplexes can be expected in the marked gel area (ellipsoid). (C) A gel comparable to Figure part B was stained with Coomassie.

1.3. In-gel assays on 2-D BN/hrCN gels

To perform functional analysis of mitochondrial complexes, 2-D native gels similar to Figure 9 were applied for in-gel assays of complexes I, II, IV and V.
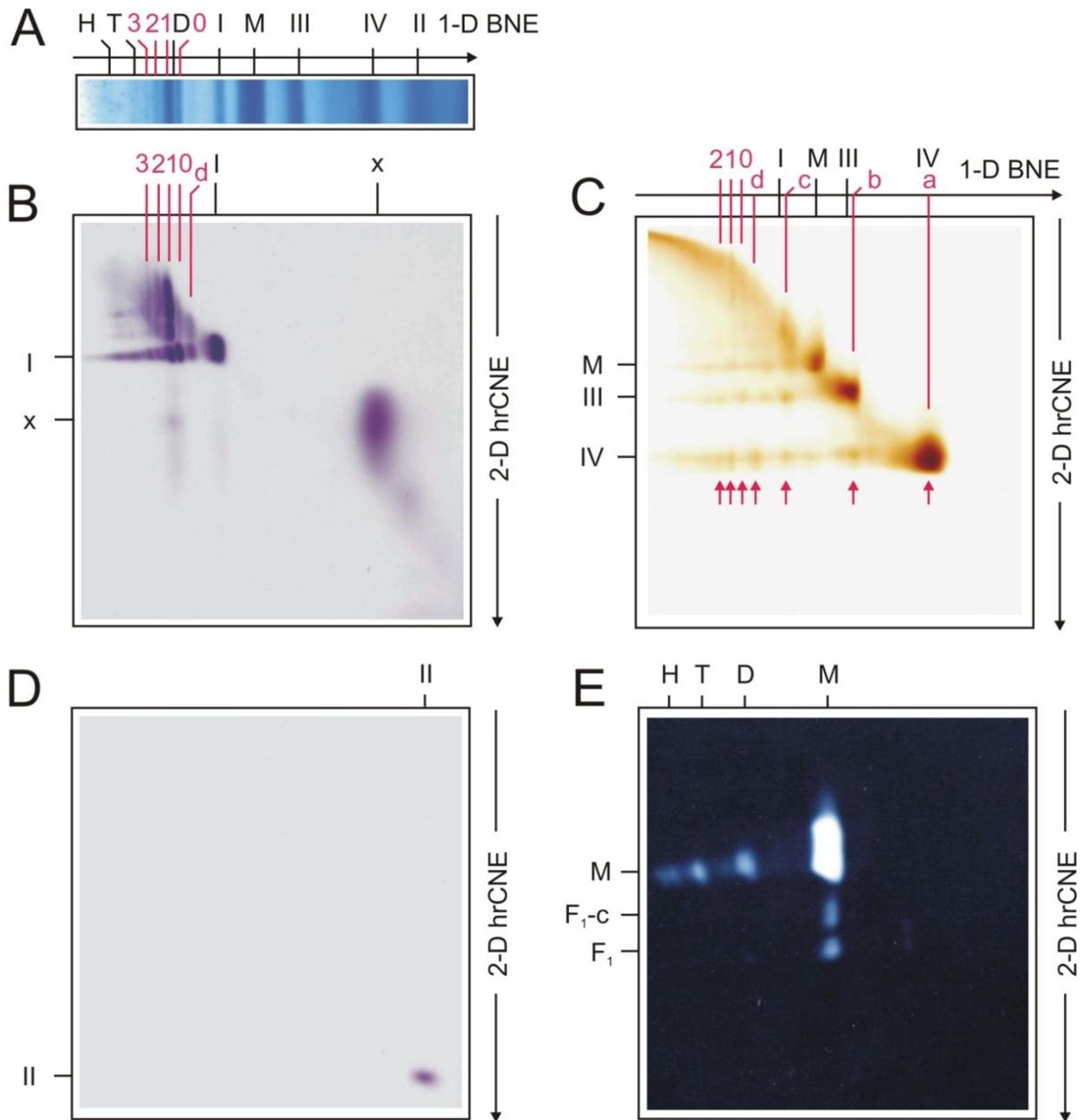
Figure 10. In-gel assays on 2-D BN/hrCN gels. (A) 1-D BNE similar to Figure 9A. (B) NADH:NTB oxidoreductase assay identified respiratory complex I (marked I), a supercomplex (marked d) containing complexes I and IV, supercomplexes $I_1III_2IV_{0-3}$ (marked 0-3), and a presumed flavoprotein subcomplex of complex I (marked x). (C) A native heme stain assay identified a horizontal line of spots of complex IV (arrows) that were derived from complexes a, b, c, d, and supercomplexes 0-2. The assay identified also complex III and for unknown reasons some monomeric complex V as well. Tentative assignments of further complexes: band a, monomeric complex IV; band b, dimeric complex IV; band c, supercomplex III_2IV_2, and band d, supercomplex I_1IV_1. (D) Complex II was identified by in-gel succinate:NTB oxidoreductase assay. (E) ATP hydrolysis assay identified various forms of ATP synthase (M, D, T, H), the catalytically active F_1 subcomplex, and the F_1 subcomplex associated with a ring of c-subunits (F_1-c).

The complex I in-gel activity assay, also called in-gel NADH:NTB oxidoreductase assay (Fig. 10B), identified complex I (marked I), a number of respiratory supercomplexes (marked 0-3), a supercomplex containing complexes I and IV but no complex III (marked d), and a much smaller compound (marked x) that presumably represented the flavoprotein part of complex I with a mass around 200 kDa.

Complex II was identified in Figure 10D by the succinate:NTB oxidoreductase activity assay. Its position in the 1-D BN gel indicated that complex II was clearly smaller than complex IV (200 kDa) and therefore suggested that it was present in a monomeric state (calculated mass 130 kDa).

In-gel heme stain (designed to track complex IV on native gels) identified complexes IV and III with comparable signal intensities (Fig. 10C), and for unknown reasons marked also some complex V (M) that does not possess a heme group of its own. Complexes and supercomplexes resolved by 1-D BNE could be aligned with the columns of dissociated complexes (marked by arrows). Band a with the lowest mass in 1-D BNE was assigned to monomeric complex IV. The complex remained essentially unchanged after 2-D hrCNE. Complex b migrating close to complex III (480 kDa) in the 1-D BN gel, was most likely dimeric complex IV (2 x 200 kDa). It was dissociated into the monomers by 2-D hrCNE. Complex c comigrating with complex I (1 MDa) was dissociated into the individual complexes III and IV and presumably represented a III_2IV_2 supercomplex (calculated mass 980 kDa). Band d was interpreted as a I_1IV-supercomplex because dissociated complexes I and IV were identified but no free complex III (Fig. 10B, C). Complex 0 was interpreted as core supercomplex I_1III_2 not containing complex IV, because hrCNE did not dissociate any complex IV, i.e. the corresponding arrow pointed to a gap in the horizontal line of spots of complex IV. Band 1 (supercomplex $I_1III_2IV_1$) was dissociated by hrCNE into individual complexes I (Fig. 10B), IV (Fig. 10D), and III (best detected in Fig. 9B, C).

The ATP hydrolysis activity of complex V (CV in-gel activity assay) was measured as the intensity of white lead phosphate precipitates that appeared upon release of phosphate from ATP during the catalytic cycle (Fig. 10E). In addition to the oligomeric forms of ATP synthase that were already identified by their fluorescence-labels (Fig. 8B, 9B) two further protein complexes with ATP hydrolysis activity were detected below monomeric complex V (M). This position in the 2-D gel indicated that both additional complexes were smaller than monomeric complex V, and that they dissociated during 2-D hrCNE from monomeric complex V. Most likely these spots represented F_1 and F_1-c subcomplexes that had been

identified as stable subcomplexes in a different context resulting from human mitochondrial biosynthesis disorders (Carrozzo et al., 2006).

1.4. Resolution of complexes from 2-D BN/hrCN gels by Tricine-SDS-PAGE

In order to analyze fluorescence-labeled protein subunits, the 2-D native gels were processed further by Tricine-SDS-PAGE for 3-D or 4-D analysis. First, spots of complexes in the 2-D native gels were identified using a laser scanner. Second, the positions of the spots were marked on both covering glass plates. Following removal of one glass plate, a one cm wide gel stripe (boxed in Fig. 11B) containing all proteins and complexes dissociated from supercomplexes (marked 1 and 0) was excised for 3-D SDS-PAGE as illustrated in Figure 11B.

Following the resolution by 3-D SDS-PAGE, fluorescence-labeled (Cy5.5) subunits of supercomplex 0, of complexes I, V, III and IV, and dissociated individual proteins (located on the right half of the 3-D gel) were detected by their fluorescence (Fig. 11D) or after silver staining (Fig. 11E).

Conditions and detergents used for fluorescence-labeling seem critical. Under the labeling conditions used here, we observed considerable specificity of fluorescence-labeling. For example, an intensely labeled 30 kDa protein (marked by arrow head) was hardly identified in silver stain. Another protein (marked by *), however, was detected only in silver stain. The dissociated individual proteins are mostly detergent-labile subunits of the supercomplexes and constituent complexes, but may also comprise novel proteins associated with supercomplexes that previously escaped detection (more detailed in Results part 3).

After 2-D native isolation of multiprotein complexes a gel piece containing monomeric ATP synthase (boxed in Fig. 12B) was excised, resolved by dSDS-PAGE, and fluorescence was detected (Fig. 12C, D). After fluorescence detection the same gel was reused for Coomassie or silver staining (Fig. 12E, F).
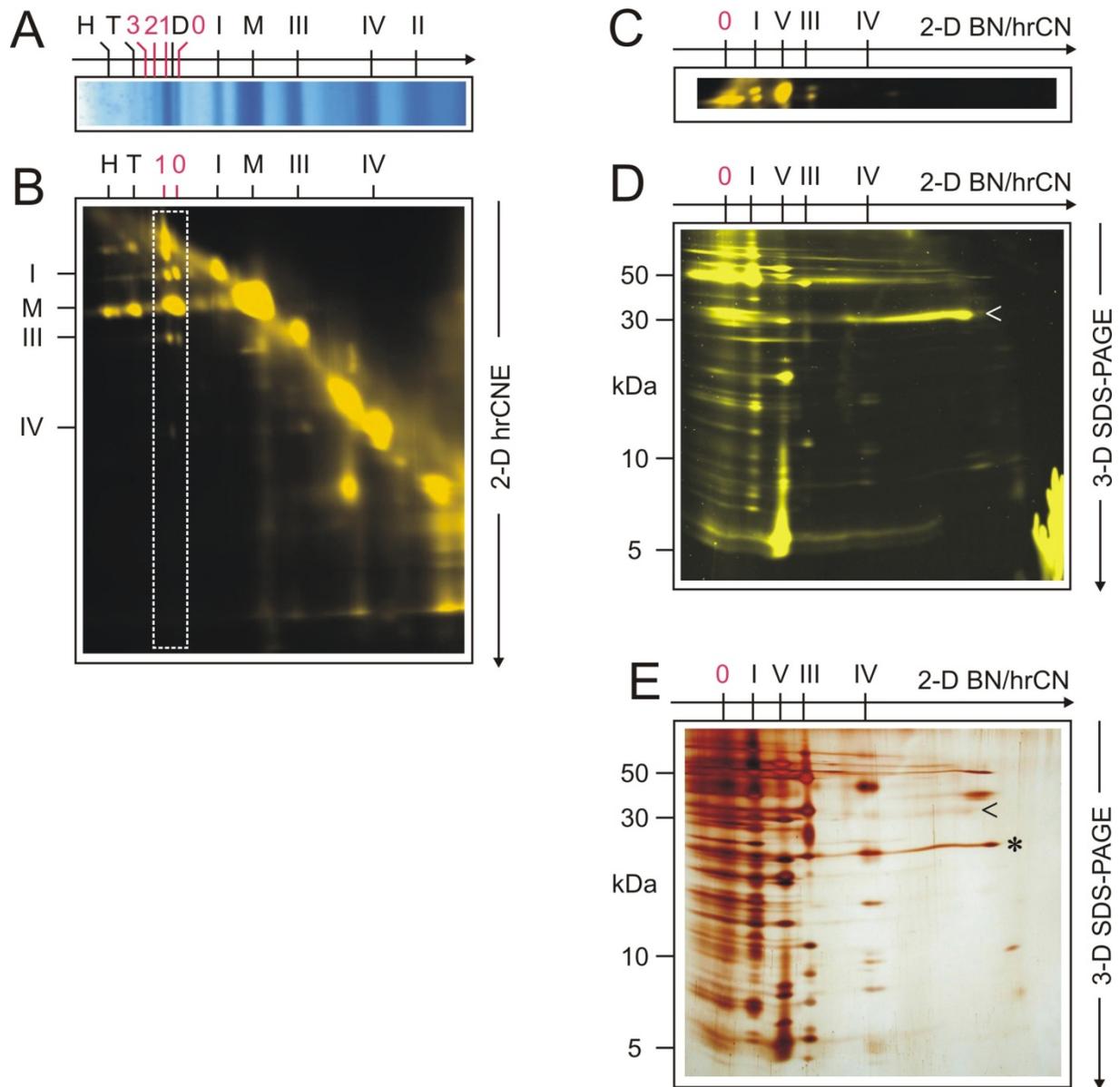
Figure 11. Separation of subunits of complexes by 3-D SDS-PAGE. (A) 1-D BN electrophoresis, and (B) detection of fluorescence-labeled complexes following 2-D separation by 1-D BNE and 2-D hrCNE were similar to Figure 9. (C) A vertical gel stripe (boxed in Fig. 5B) containing all fragments that had dissociated from supercomplexes by second dimension hrCNE, was used for 3-D SDS-PAGE. (D) Detection of fluorescence-labeled (Cy5.5) protein subunits following 3-D Tricine-SDS-PAGE using a 16% acrylamide gel. (E) Gel D was reused for silver staining. Note the strongly differing fluorescence- and silver-stain intensities of two selected proteins (< and *). Labile subunits and potential novel accessory proteins are generally located on the right half of 3-D gels.
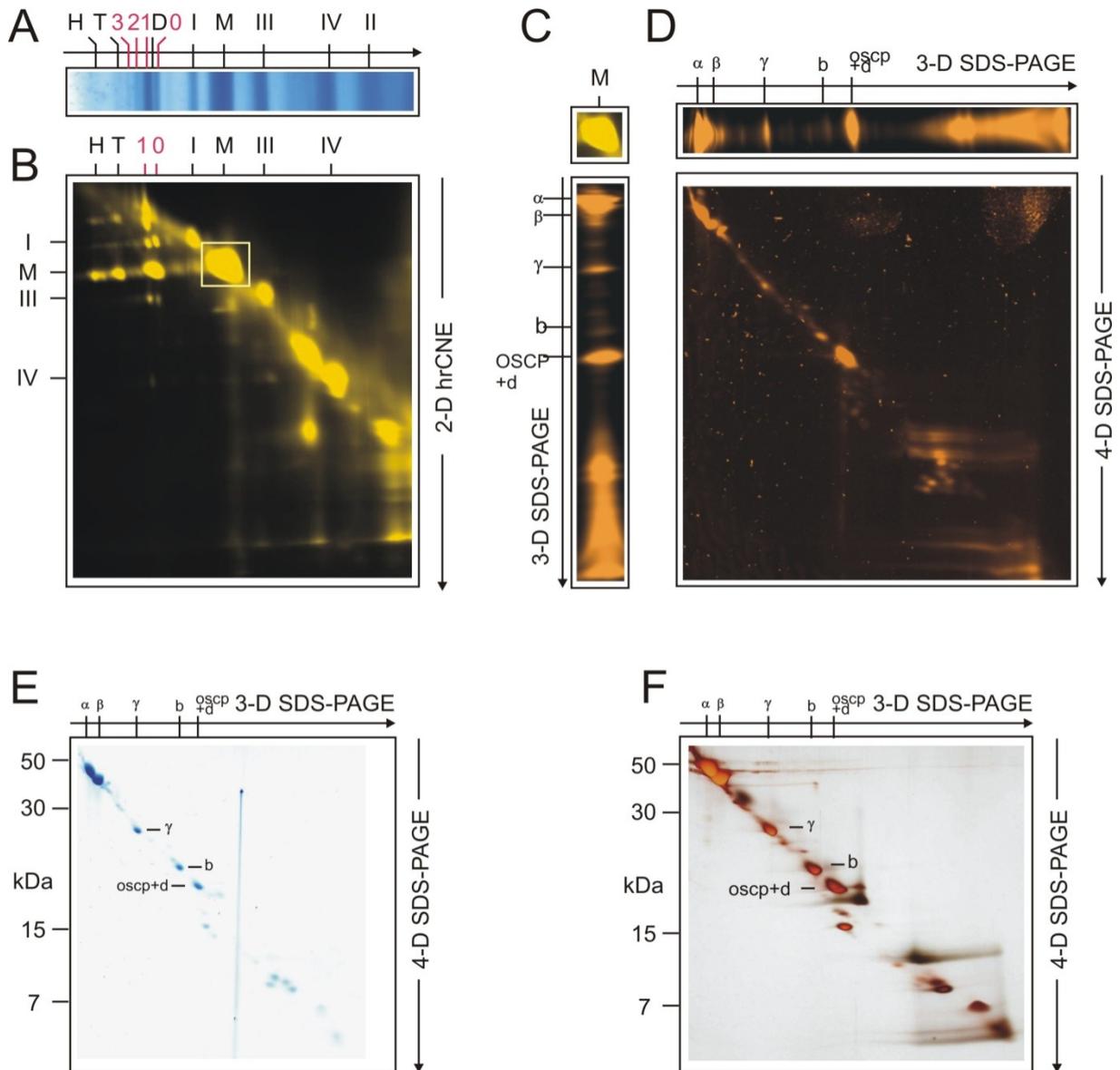
Figure 12. Separation of subunits of complexes by 4-D SDS-PAGE. (A) 1-D BN and (B) 2-D BN/hrCN gels (same as in Fig. 11AB) were used here to illustrate the 4-D electrophoresis system. (C) Monomeric ATP synthase (boxed in B) was excised and resolved by 3-D Tricine-SDS-PAGE using a 12% acrylamide, 6 M urea gel. (D) A gel stripe from 3-D Tricine-SDS-PAGE was resolved by 4-D Tricine-SDS-PAGE using a 16% acrylamide gel and the labeled protein subunits were detected by their fluorescence. Gel D was reused for (E) Coomassie or (F) silver staining.

This 4-D system separates hydrophobic subunits from the diagonal of the hydrophilic subunits. Thus hydrophobic subunits can be excised from the gel without major contamination by hydrophilic proteins and therefore have a better chance to be detected by mass spectrometry.

1.5.   Comparison of 2-D BN/hrCNE with conventional 2-D BN/SDS-PAGE

Bovine heart mitochondria were labeled with fluorescent dye as described in 2.2. In order to preserve the supercomplexes, a very mild neutral detergent digitonin was used for the solubilization. The solubilized complexes and supercomplexes were then separated by blue native electrophoresis in the first dimension (1-D BNE). The gel was fixed and stained with Coomassie (Fig. 13A). Bands of separated complexes I, III, IV, and the monomeric (M), dimeric (D), tetrameric (T) and hexameric (H) forms of compex V, the mitochondrial ATP synthase, were detected. However, no fluorescent band was detected in the 1-D BN gel, due to around 95% fluorescence quenching by Coomassie-dye (Wittig et al., 2007a).
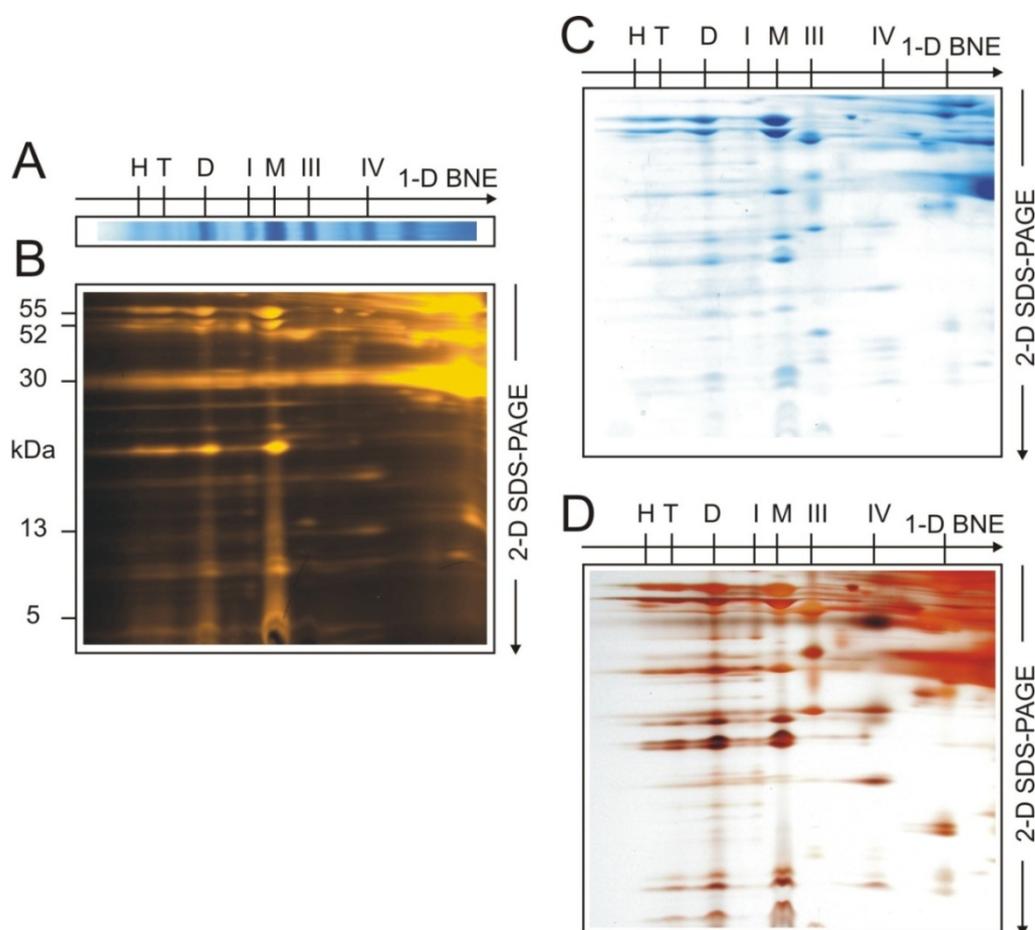
Figure 13. 2-D BN/SDS-PAGE of mitochondrial complexes. M, D, T, H, monomeric, dimeric, tetrameric and hexameric ATP synthase. I, II, III, IV, respiratory complexes I, III and IV. (A) Bovine heart mitochondria were solubilized by digitonin and the solubilized complexes were separated by 1-D BNE. (B) Detection of Cy5-labeled protein subunits following 2-D SDS-PAGE. Gel B was reused for (C) Coomassie and (D) silver staining.

To visualize the fluorescence-labeled protein subunits, a BN gel stripe (Fig. 13A) was subjected to Tricine-SDS-PAGE for second dimensional resolution, which removed protein bound Coomassie-dye. The protein subunits were detected using a Typhoon laser scanner (Fig. 13B). Compared with the Coomassie-stained gel (Fig. 13C) it seemed that a few proteins were clearly fluorescence-labeled. This can be explained by selective fluorescence-labeling of the readily accessible protein surfaces, e.g., of the 55 kDa and 52 kDa subunits α and β of complex V. Silver staining of the same gel revealed more proteins and characteristic subunit patterns of complexes (Fig. 13D).

2. Native immunoblotting of blue native gels (NIBN) to identify conformation-specific antibodies

Proteins from a vast variety of quite different samples can be separated or isolated using gel electrophoresis. Depending on the treatment of the sample and the electrophoresis system used, proteins can be separated in their native state, i.e. retaining their 3-D structure (e.g., blue native gel electrophoresis, BNE, Schägger and von Jagow, 1991) or in denatured state, i.e. the polypeptide is unfolded (e.g., Tricine-SDS-gel electrophoresis, Schägger, 2006). Analytical techniques like Western blotting can be used to detect specific proteins. For this, the proteins are transferred to inert membranes (e.g., nitrocellulose or PVDF), where they are detected using antibodies specific to the target protein. The effectiveness of the protein transfer from the gel to the membrane is checked by staining the membrane, for example with Coomassie-dye, which has to be removed from the membrane by organic solvents like methanol prior to immunological analysis. However, methanol destroys the native structure of the protein complexes.

Therefore, such Western blot protocols can only be applied when retention of the native state of proteins is not important. However, to detect native protein complexes by conformation-specific antibodies or to screen for conformation-specific antibodies, preserving the 3D structure of the protein is necessary. Therefore, a native immunoblotting method seemed desirable.

2.1. Complex I of *Yarrowia lipolytica* as a model system for the development of a native electroblotting technique

Complex I of *Y. lipolytica* has been well characterized by our group (Kerscher et al., 2002) and a variety of monoclonal and polyclonal antibodies are available (Zickermann et al., 2003). This made complex I a convenient model system for the development of a native immunoblotting method.

Mitochondrial membranes of *Y. lipolytica* were solubilized using the mild neutral detergent dodecylmaltoside (DDM). DDM was used, because separation of the individual mitochondrial complexes was desired. The solubilized mitochondrial complexes were then separated by blue native gel electrophoresis (BNE) as outlined in Wittig et al., 2006a. The gel was stained with

Coomassie and the individual mitochondrial oxidative phosphorylation complexes complex I (I), complex V (V), complex III (III), subcomplex of complex V (F) and complex IV were assigned according to their typical migration properties. In order to confirm that complex I was native after BN separation, a so-called complex I in-gel activity assay (Fig. 14, lane 2) was performed using a duplicate BN gel, which was not stained.
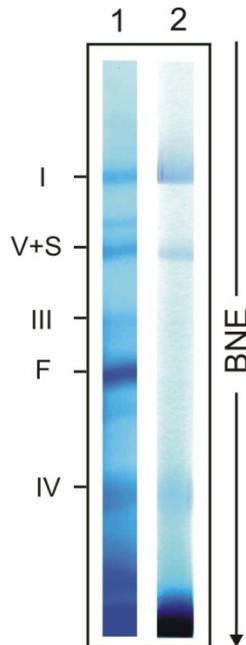
Figure 14. Separation of *Y. lipolytica* mitochondrial complexes by BNE. 200 μg total mitochondrial protein was solubilized by DDM using a detergent to protein ratio of 1.3 g/g. Mitochondrial complexes were separated by BNE on 4-13% acrylamide gradient gels. (Lane 1) BN gel was stained with Coomassie. (Lane 2) NADH:NTB oxidoreductase staining of complex I on the BN gel. I, III, IV, V, mitochondrial complexes I, III, IV and V of oxidative phosphorylation; S, subcomplex of complex I; F, subcomplex of complex V.

Complex I in-gel activity assay on the BN gel (Fig. 14, lane 2) showed that the NADH oxidation domain of complex I was functional at this stage. Interestingly, this assay detected also a second band below the main complex I band, which comigrated with complex V (monomer, mass ~600 kDa). Recent progress in X-ray structural analysis of complex I confirmed that the electron entry site resides in hydrophilic arm domain, where the reaction responsible for the activity staining takes place. Thus this band is likely to represent a subcomplex of complex I comprising its hydrophilic arm. Protein complexes can be assigned based on their known subunit pattern. In order to assign this unknown complex, a second dimension SDS gel electrophoresis was therefore performed.

2.2. Identification of a subcomplex of complex I by two-dimensional gel electrophoresis (2-D BN/SDS-PAGE)

Complex I activity assay on the BN gel (Fig. 14, lane 2) showed a second band, which migrated together with complex V monomer at around 600 kDa. In order to analyse the subunit composition of this complex, a BN gel stripe was subjected to second dimensional resolution by Tricine-SDS-PAGE.
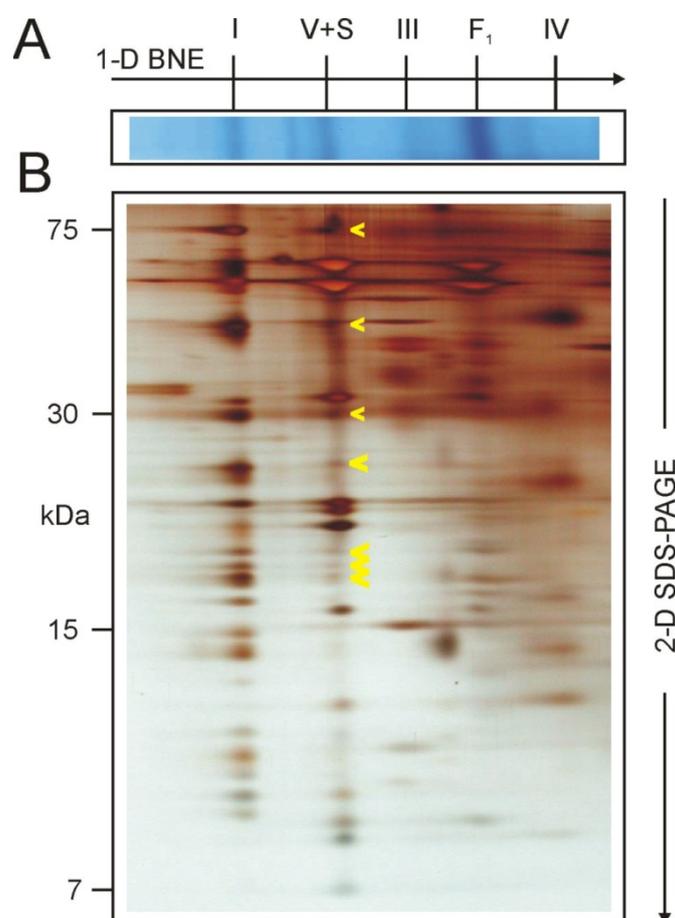
Figure 15. Identification of a subcomplex of complex I from *Y. lipolytica* mitochondria. (A) Mitochondria were solubilized by dodecylmaltoside and enzyme complexes were separated by BNE in the first dimension (1-D BNE). (B) 2-D BN/SDS-PAGE. Yellow arrows mark subunits of a subcomplex of complex I that comigrated with complex V. I, III, IV, V mitochondrial complexes of oxidative phosphorylation; S, subcomplex of complex I; F_1, subcomplex of complex V.

After silver staining of the second dimension SDS gels, some characteristic protein subunits of complex I such as the 75 kDa subunit and the 30 kDa subunit and several small subunits in

the range of 20 kDa could be detected in the same position as subunits of complex V (Fig. 15).

2.3.   Preserving the native state of protein complexes after destaining of electroblots

The native protein complexes isolated by BN were transferred onto PVDF membranes essentially as described by Schägger, 2006. Voltage and current were limited to 20 Volt and 0.8 mA/cm^2 gel area, respectively. The gels were electroblotted for 1.5, 2.5 and 4 hours at room temperature using 50 mM Tricine, 7.5 mM imidazole, pH 7.0 buffer. Following electroblotting the gels were stained with Coomassie and compared with duplicate non-blotted BN gels (not shown). Following electroblotting for 1.5 hours, almost no protein bands were detectable on the BN gel by staining with Coomassie, indicating that 1.5 hours of electroblotting under these conditions were sufficient for complete transfer of the protein complexes onto the PVDF membrane. The complex I in-gel activity assay on the blot membrane after 1.5 hours transfer confirmed that complex I retained its catalytic activity (not shown). Usually, the electroblotted protein spots were visualized for documentation, e.g., by staining with Coomassie and destained prior to any kind of immunological assay. However, destaining by methanol resulted in complete loss of complex I activity on the blot membrane indicating significant denaturation. For the development of native immunoblotting technique, the obligatory Coomassie removing step by methanol seemed to be critical due to the denaturing effect of the organic solvent.

In order to destain the membranes, we thus used mild non-ionic detergents Tween 20 (Fig. 16, lane 2), digitonin (Fig. 16, lane 3) and Brij 35 (Fig. 16, lane 4) instead of methanol. Coomassie could be removed completely by washing the Coomassie-stained membrane twice for two-hours with 0.2% of any of the mild non-ionic detergents in 10 mM imidazole/HCl buffer with pH 7.0. The detection of holo-complex I and its subcomplex by activity staining demonstrated that all three non-ionic detergents preserved the native state of complex I (Fig. 16, lanes 2, 3, 4). Tween 20 was preferably used in later experiments since it is widely used in many laboratories.
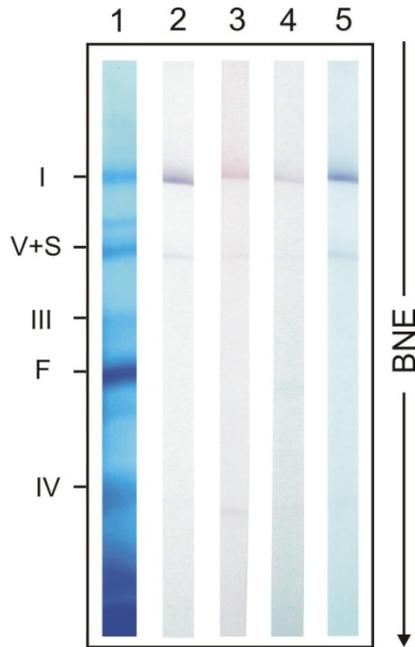
Figure 16. Native electroblotting of blue native gels. Lane 1, Coomassie stained BN gel strip of *Y. lipolytica* mitochondria; lanes 2–4, NADH:NTB oxidoreductase staining on the blot membrane following washing with 0.2% Tween 20 (lane 2), 0.2% Brij 35 (lane 3), 0.2% digitonin (lane 4), and after storage at -80°C (lane 5). Mitochondrial complexes were assigned as in Figure 14.

2.4.   Detection of complex I with conformation-specific monoclonal antibodies

The activity assay of complex I on membranes, which had been destained with Tween 20, digitonin or Brij 35, showed that NADH oxidation site of complex I was still functional after Coomassie removal. The native state of the enzyme on the membrane treated with mild detergents was tested further with conformation-specific antibodies. Monoclonal antibodies 31A8 and 40G5 had been previously characterized to recognize exclusively native complex I (Zickermann at al., 2010). Antibody 1F5, which was characterized to bind complex I subunit NESM under denaturing condition, was used as a control. Again, mitochondrial complexes were solubilized using DDM and complexes were separated by BNE, electroblotted onto PVDF membrane, and destaining was performed either using methanol (Fig. 17, panel B) or Tween 20 (Fig. 17, panel C).

Destaining of the blot membrane with methanol allowed for protein detection by antibody 1F5 recognizing a linear epitope (Fig. 17B, lane 1). However, methanol destroyed the native protein conformation and precluded binding of antibodies 40G5 and 31A8 (Fig. 17B, lanes 2 and 3). In contrast, a blot that was destained with Tween 20 and kept in aqueous solution until use showed immunological reactivity towards all three antibodies (Fig. 17C). Recognition of the NESM subunit by antibody 1F5 on the native blot indicated that this subunit is located on the surface of the native enzyme. Panel D shows membranes, which were first destained with

Tween 20 but dried for storage prior to immunodetection. No signal was then detected by the monoclonal antibody 40G5 (Fig. 17D, lane 2) suggesting that complex I was at least partially denatured, although antibody 31A8 showed some residual affinity (Fig. 17D, lane 3).
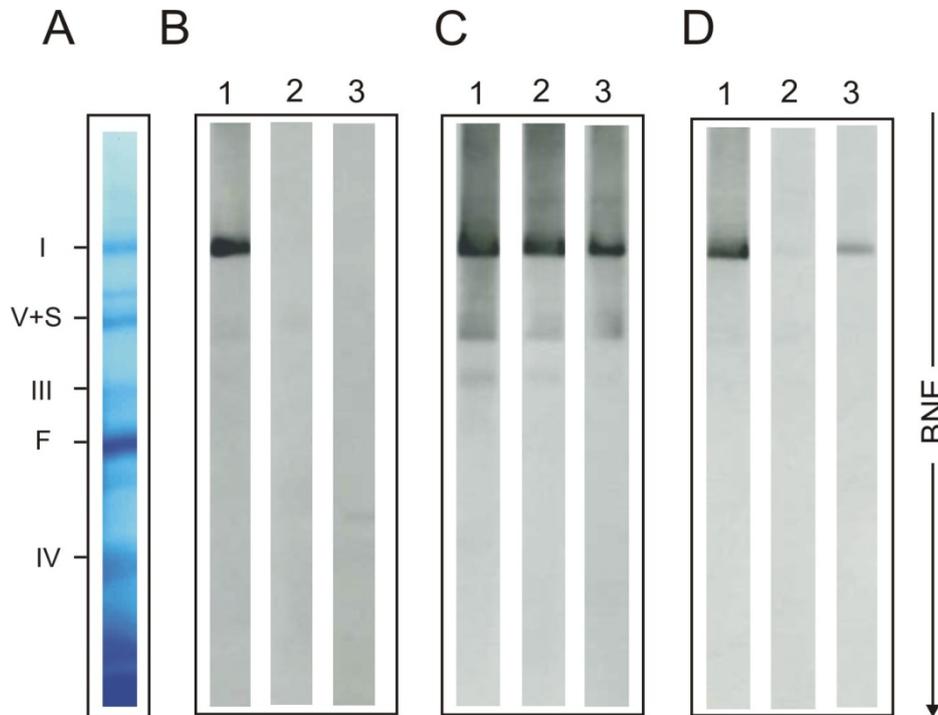
Figure 17. Native immunoblotting of blue native gels (NIBN). (A) Coomassie-stained BN gel of *Y. lipolytica* mitochondria. (B-D) Immunological reactivity of complex I with antibody 1F5 (lanes 1) recognizing a linear epitope and conformation-specific antibodies 40G5 (lanes 2) and 31A8 (lanes 3). Blot membranes were destained by methanol (B), or destained by Tween 20 and kept wet (C), or destained by Tween 20 and dried prior to immunodetection (D).

For long term storage the membranes were incubated for 10 min in 15% glycerol, 10 mM imidazole/HCl, pH 7.0, frozen, shrink-wrapped and stored at -80°C. Complex I activity assays on these membrane revealed that the catalytic activity of the enzyme was retained under these conditions even after several weeks (Fig. 16, lane 5).

Taken together, the protocol for native immunoblotting of blue native gels (NIBN) includes the following steps:

mitochondria

↓

BNE
(4-13 % acrylamide
gradient gel)

↓

storage   ◀··   electroblotting to
-80 C°   PVDF membrane

⋮   ↓

native processing of blot membrane:
destain 2 x 2 h with 0.2 % Tween
in 10 mM imidazole/HCl pH 7.0

↓

analysis,
activity staining,
immunodetection
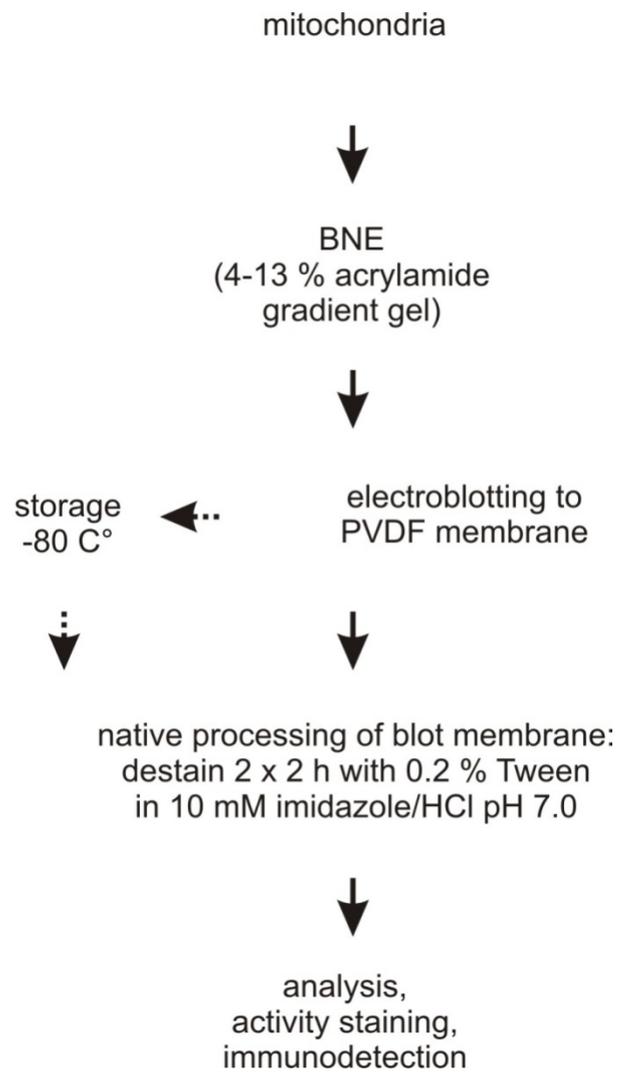
Figure 18. Flow chart for native immunoblotting of blue native gels (NIBN).

2.5. Comparison of native immunoblotting of blue native gels (NIBN) with conventional Western blot

We compared the new immunoblotting technique with a conventional Western blot procedure by testing the immunological reactivity of complex I under two conditions. Condition 1: following solubilization of mitochondrial membranes by DDM, the solubilized complexes were separated by BNE and electroblotted using the new NIBN technique (Fig. 19A). Condition 2: the mitochondrial membranes were directly resolved by 10% acrylamide Tricine-SDS gels, followed by standard Western blotting (Fig. 19B). In order to assign the subunits of complex I, chromatographically purified complex I (Kashani-Poor et al., 2001) was used as marker and loaded on the same gel. Six different antibodies were applied for the detection of complex I. Antibodies 31A8, 40G5 and 44G10 have been characterized previously by native ELISA. They bind to the enzyme under native conditions (Zickermann et al., 2010). Antibody 35C5 was known to bind a 49 kDa subunit of complex I on SDS denatured blot (Zickermann et al., 2003) whereas antibodies 1F5 and 30C12 recognize the NESM subunit under denaturing condition (Abdrakhmanova et al., 2004; Zickermann et al., 2010).

Antibodies 1F5, 30C12 and 35C5 bind to complex I processed under native and SDS denaturing conditions (Fig. 19A, B, lanes 2, 3, 5). Accessibility of the linear epitopes without denaturation indicated that they are located on the surface of the native enzyme complex. Clearly different patterns of immunological reactivity between the Western blot after SDS-PAGE and NIBN were observed for conformation-specific antibodies 31A8, 40G5, and 44G10 (Fig. 19A, B, lanes 4, 6, 7). No signals were visible when complex I was processed under denaturing conditions (Fig. 19B, lanes 4, 6, 7). In contrast, all antibodies including 31A8, 40G5, and 44G10 recognized complex I on the native immunoblot developed in this work (Fig. 19A).
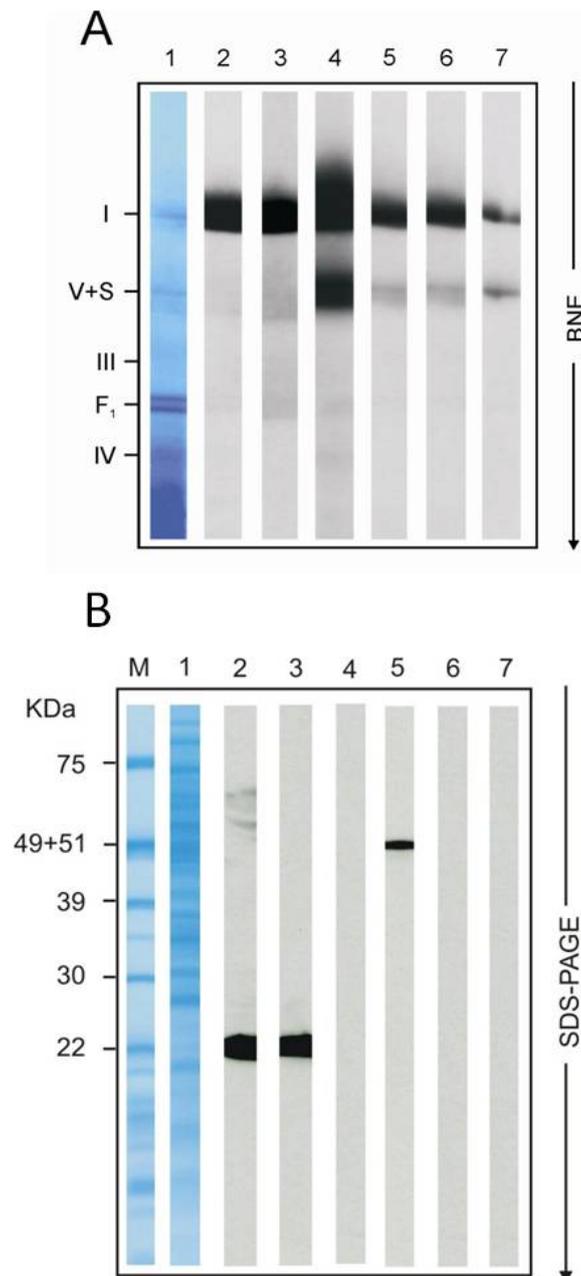
Figure 19. Immunodetection of complex I from *Y. lipolytica* mitochondria. (A) Immunodetection of complex I after native immunoblotting of blue native gels. Mitochondrial complexes (total protein 400 µg/cm lane) were separated by BNE, transferred to PVDF membrane by a native blot protocol, and Coomassie-stain was removed by Tween 20 before antibodies were added. (B). *Y. lipolytica* mitochondria were resolved by 1-D SDS-PAGE, and electroblotted using a Western blotting protocol. Lane 1, Coomassie-stained blot; lanes 2-7, detection by antibodies; lane 2, Y1F5; lane 3, Y30C12; lane 4, Y31A8; lane 5, Y35C5; lane 6, Y40G5; lane 7, Y44G10. ; M, purified complex I used as marker; subunit assignment is based on molecular masses.

2.6. Estimation of the detection limit of NIBN

The detection limit of the NIBN assay was estimated by appling varing amounts of mitochondrial protein (200, 100, 50, and 25 µg) to 0.5 cm gel lanes for BNE (Fig. 20, lanes 1-4). The proteins were then transferred to the PVDF membrane and processed using the novel destaining protocol. Immunological reactivity of the protein complex was monitored using the antibody 1F5. Applying extracts from 25 µg mitochondrial protein was sufficient for unambiguous detection of antibody 1F5 binding to complex I (Fig. 20, lane 4).
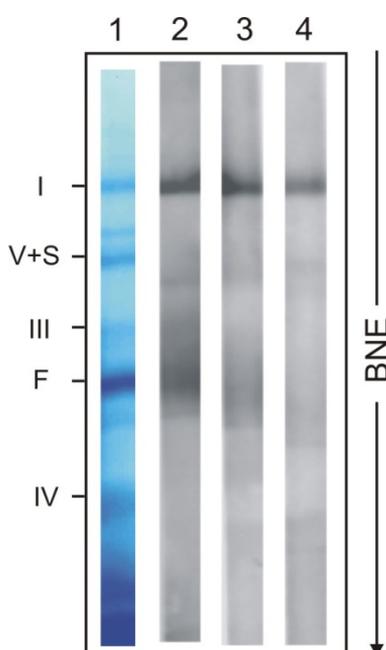
Figure 20. Detection limit of the NIBN. Lane 1, mitochondrial complexes (total protein 200 µg/0.5 cm lane) were separated by BNE and Coomassie stained. Extracts from 100, 50, and 25 µg of total mitochondrial protein were loaded onto 0.5 cm gel wells for lanes 2, 3, and 4, respectively, transferred to PVDF membrane by a native blot protocol, and Coomassie-stain was removed by Tween 20 before antibodies were added and immunoblotted. Antibody 1F5 was used for the detection.

Based on catalytic activity, the fraction of complex I was estimated to be 1.5% of the total mitochondrial protein (Kashani-Poor et al., 2001). With a molecular mass of almost 1 MDa for complex I (Morgner et al., 2008) it follows that in the case of antibody 1F5 less than 0.5 pMol of a polypeptide can be detected by NIBN.

2.7. Identification of the subunit detected by monoclonal antibody 31A8 by three-dimensional gel electrophoresis and LC-MS/MS analysis

The monoclonal antibody 31A8 is known to be Western blot negative (Zickermann et al., 2010) and this could also be confirmed by comparing complex I reactivity on native and

denatured blots (Fig. 19A, B, lane 4). However, the antibody also gave rise to a signal when a NIBN blot was dried prior to immunodetection (Fig. 17D). Although drying of the membrane seems to have a denaturing effect, the observed signal suggested that the epitope of the monoclonal antibody was still intact under this condition. In order to follow-up on this, we isolated mitochondrial complexes under the same conditions as used for Figure 19A, the complex I band was excised from the unfixed BN gel and the subunits were resolved by SDS-PAGE in the second dimension. The gel was electroblotted using the conventional Western blot protocol. The same six antibodies were applied for the detection.
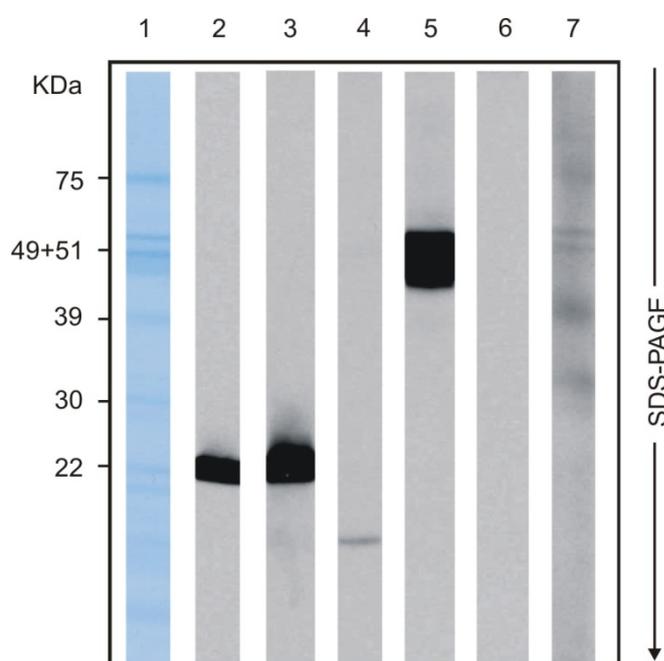
Figure 21. Immunodetection of *Y. lipolytica* complex I on the blot of a 2-D BN/SDS gel. Complex I was excised from a BN gel, resolved by 2-D SDS-PAGE, and electroblotted using a Western blotting protocol. Lane 1, Coomassie-stained blot; lane 2-7, detection by antibodies; lane 2, Y1F5; lane 3, Y30C12; lane 4, Y31A8; lane 5, Y35C5; lane 6, Y40G5; lane 7, Y44G10.

Again, antibodies 1F5, 30C12 and 35C5 recognized their epitopes as expected. Monoclonal antibody 40G5 gave no signal (Fig. 21, lane 6). The weak signals on lane 7 may be explained by unspecific binding of the antibody to the membrane, because antibody 44G10 is known to bind to the native enzyme complex (Zickermann et al., 2010) and it does not give rise to a signal after SDS denaturation (Fig. 19B). Surprisingly, the antibody 31A8, which is known to be Western blot negative, produced a binding signal when complex I was excised from a BN gel and processed by SDS-PAGE (Fig. 21, lane 4). In order to find out the target protein of this, we used a three-dimensional electrophoresis technique (BNE followed by dSDS-PAGE). Chromatographically purified complex I (CI) (Kashani-Poor et al., 2001) was repurified by BNE. The repurified CI band was then excised and the subunits were separated using doubled

SDS-PAGE (Fig. 22A). Following electroblotting of the dSDS gels on PVDF membranes monoclonal antibody 31A8 was used for immunological detection according to the Western blot protocol given in Schägger, 2006. A strong signal was observed as shown in Figure 22B. Following comparison of the Western blot signal with the original Coomassie-stained PVDF membrane as illustrated in Figure 22C, a gel piece from a duplicate Coomassie-stained gel (circled yellow in the silver-stained gel in Fig. 22A) was cut out for LC-MS/MS analysis. LC-MS/MS analysis was performed by Dr. Heinrich Heide and Dipl.-Ing. Mirco Steger. The MS analysis revealed the binding of monoclonal antibody 31A8 to subunit NUPM (Angerer et al., 2011). The MS data are listed in Appendix I (Fig. 50).
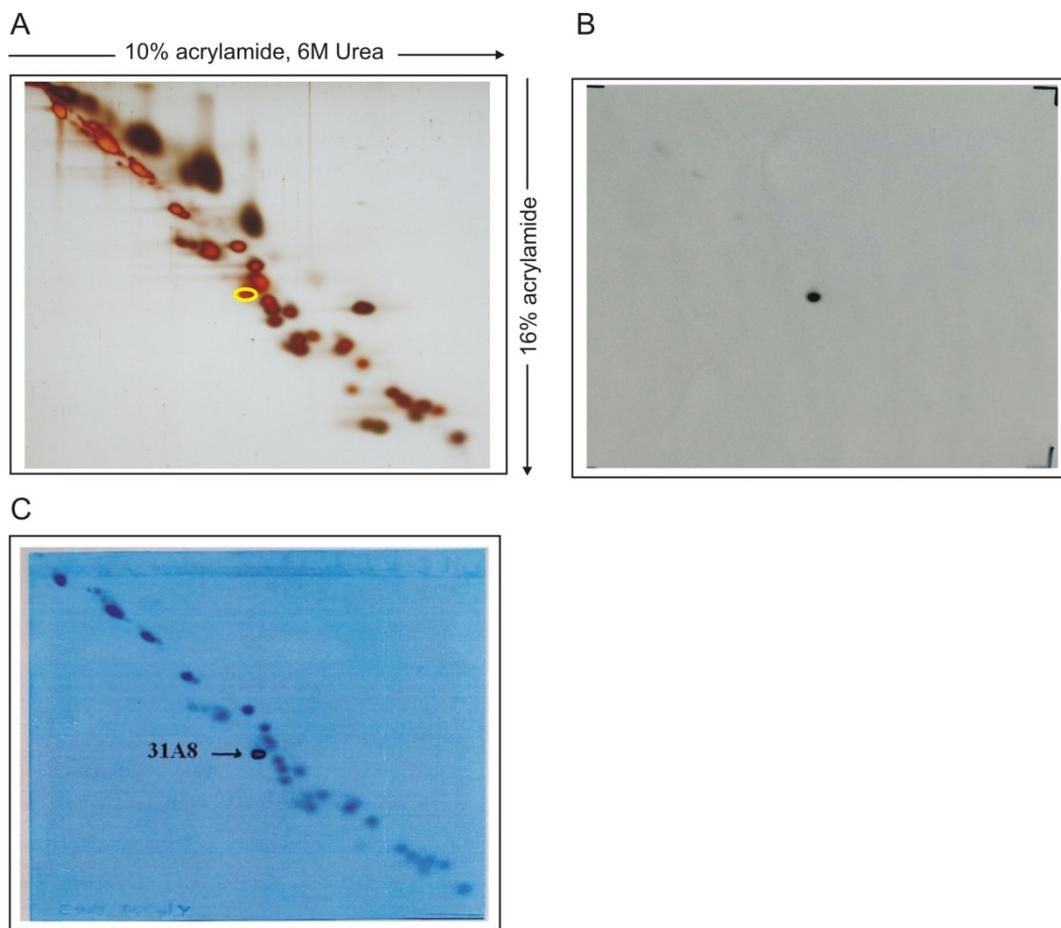
Figure 22. Identification of the NUPM subunit by monoclonal antibody 31A8. Chromatographically purified CI was repurified by BNE. The CI to DDM ratio was 0.3 g/g. CI band was then excised for dSDS-PAGE. (A) Silver staining of 3-D BN/dSDS gel. (B) dSDS gel was electroblotted using Western blot protocol. Monoclonal antibody 31A8 was used for immunodetection. (C) Coomassie-stained PVDF blot membrane prior to immunodetection. The spot corresponding to the Western blot signal was circled and marked with an arrow.

3. Respirasome-associated Cox26 protein binds to cytochrome *c* oxidase subunit Cox2.

The yeast respiratory supercomplex from *S. cerevisiae* (Schägger and Pfeiffer, 2000) contains a minimum of 21 subunits, i.e. ten subunits of complex III (Brandt et al., 1994) and eleven subunits of complex IV (Geier et al., 1995). The respirasome may also contain additional, previously unknown accessory proteins, which are potentially important in stabilizing supercomplexes or supporting functional roles of supercomplexes (De Coo et al., 1999; Schägger et al., 2004; Bianchi et al., 2004; Acín-Pérez et al., 2004) as suggested by a recent three-way proteomics strategy that identified four candidate proteins potentially associated with complexes III and IV (Helbig et al., 2009). By a protein-chemical study of yeast supercomplex, Schägger and colleagues identified a previously unkown protein component of the respiratory supercomplex composed of complexes III and IV. This protein was later annotated in data bank as Cox26 protein and listed as one of the four candidate proteins associated with the respirasome (Helbig et al., 2009). One of the biochemical aims of this work was to characterize the Cox26 protein and to identify its interaction partners.

3.1. Identification of Cox26 as a component of yeast mitochondrial respirasomes composed of respiratory complexes III and IV

We identified Cox26, a hydrophobic 6.4 kDa protein as a component of yeast mitochondrial respirasomes consisting of respiratory complexes III and IV (Fig. 23).

Digitonin-solubilized mitochondrial (super)complexes from *S. cerevisiae* were separated by BNE. A gel stripe from 1-D BNE (Fig. 23A) was then used to dissociate supercomplexes into individual complexes for the second dimensional resolution by modified BNE (Fig. 23B). After 2-D native isolation of complexes, a gel stripe as marked in Figure 23B (pink box) was then used to separate subunits of complexes and loosely associated detergent-labile components of supercomplexes for the third dimensional resolution by Tricine-SDS-PAGE (Fig. 23C). The 3-D gel was then electroblotted onto PVDF membrane. The subunits of complexes were assigned according to detection by specific antibodies and according to Geier et al., 1995.
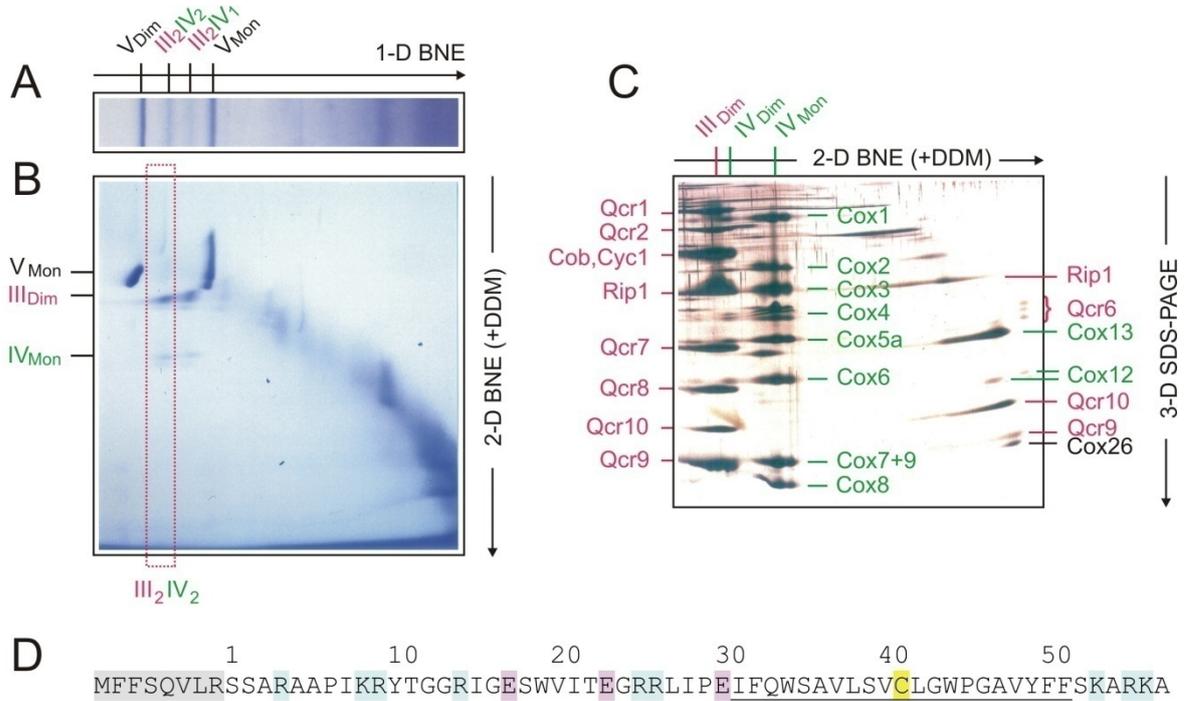
Figure 23. Identification of Cox26 by three-dimensional gel electrophoresis. Assignment of complexes: III_2IV_2, III_2IV_1, respiratory supercomplexes containing dimeric complex III and two or one copy of complex IV, respectively. V_{Dim}, V_{Mon}, IV_{Dim}, IV_{Mon}, III_{Dim}, dimeric and monomeric complexes V, IV, and III. (A) Yeast mitochondria were solubilized by digitonin and the mitochondrial complexes were separated by BNE. (B) A gel stripe from 1-D BNE was used for second dimensional resolution by modified BNE. (C) A gel stripe from 2-D BNE was used for third dimension SDS-PAGE. Subunits of dimeric complex III (III_{Dim}) and the detergent-labile subunits (labeled on the right side) were marked purple. Subunits of dimeric and monomeric complex IV (IV_{Dim} and IV_{Mon}) and the detergent-labile subunits were marked green. Cox26 (black) was detectable only after 3-D electrophoretic separation. (D) Sequence and features of Cox26 protein. Based on Edman sequencing the mature protein starts with the sequence SSARAA⋯. The presequence containing eight amino acids (shaded grey) was deduced from the DNA data base. Basic and acidic residues are marked light blue and pink, respectively. A cysteine residue (C41 marked yellow) is located at the center of a predicted transmembrane helix (underlined; TMpred; Hofmann and Stoffel, 1993).

Hermann Schägger and Kathy Pfeiffer could show by Western blot analysis of 2-D BN/SDS gels from wild-type yeast (Fig. 24) and from null mutants of subunits of complex III (Δ*qcr6, 8, 9, 10*) and of complex IV (Δ*cox8, 12, 13*) that Cox26 binds always to complex IV and/or to respiratory supercomplexes and is not detectable as free protein in significant amounts.
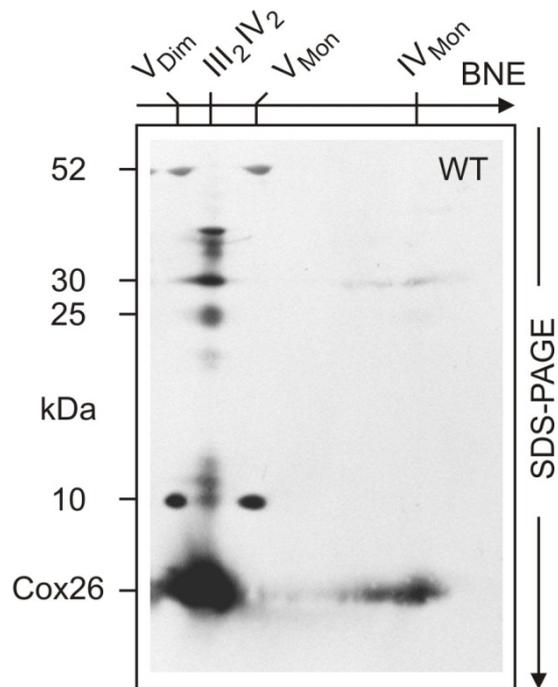
Figure 24. Cox26 protein is associated with complex IV. Complexes are labeled as in Figure 23. Digitonin-solubilized mitochondrial complexes from wild-type yeast were separated by BNE, followed by Tricine-SDS-PAGE in the second dimension using 13% acrylamide gels and electroblotted onto PVDF membranes. Anti-Cox26 antibody identified Cox26 (6.4 kDa) in the column of subunits of the III_2IV_2-supercomplex and in monomeric complex IV.
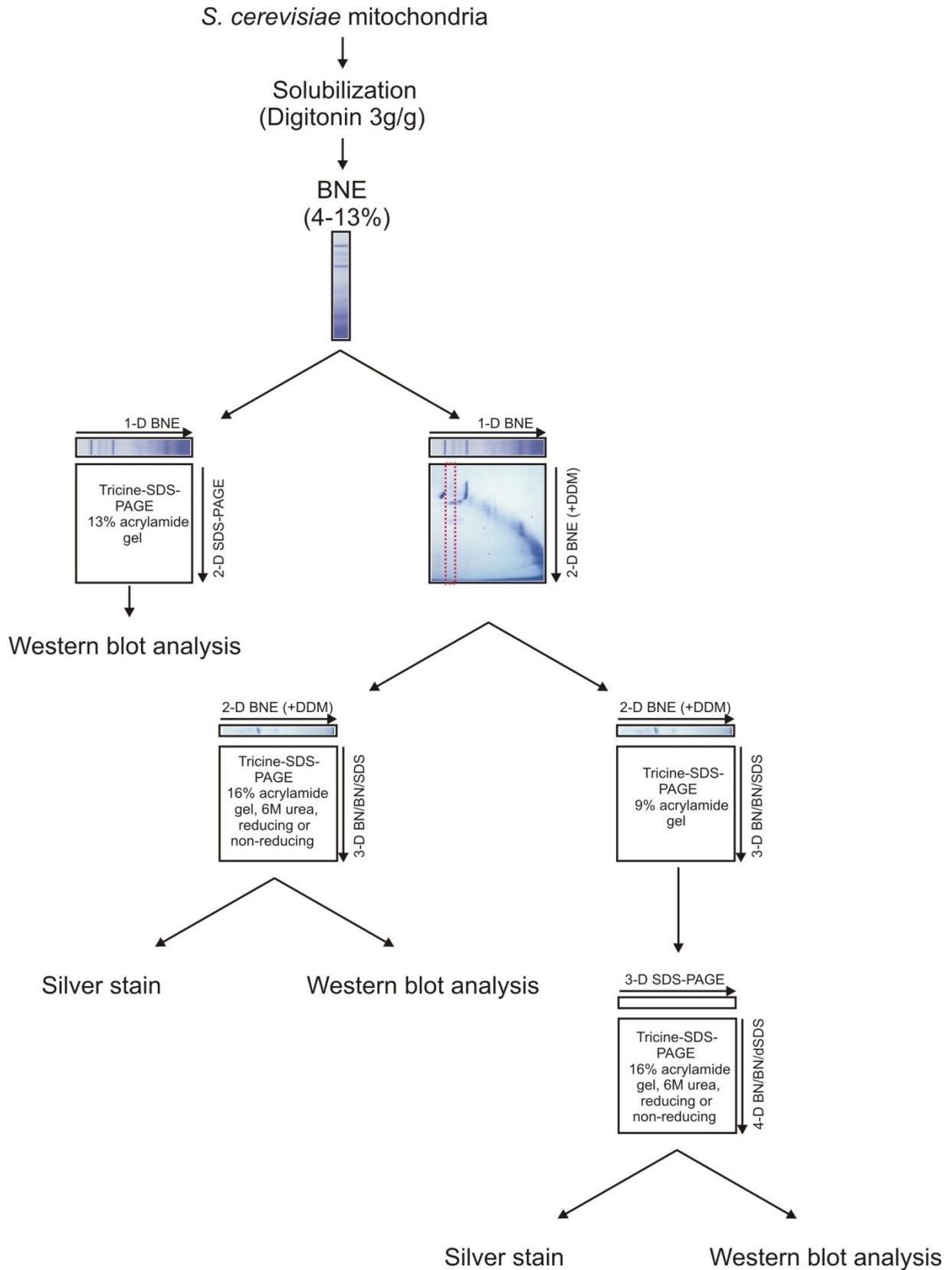
Figure 25. Steps to identify association of Cox26 with complex IV and to find interaction partners of Cox26.

3.2.   Analysing the association of Cox26 with complex IV

To further characterize Cox26 and identify possible interactions with other proteins we subjected mitochondrial membranes from wild-type yeast and the Cox26 deletion strain Δ*cox26* that was generated by cooperation of the groups of Hermann Schägger and Rosemary Stuart to multi-dimensional gel electrophoresis. The gels for wild-type and null mutant strain were always run in parallel. In order to test whether any of the bands that cross reacted with the anti-Cox26 antibody on the 2-D BN/SDS gel (Fig. 24) contained Cox26 covalently bound via a disulfide bond with cys41, a 3-D electrophoretic system was used under special conditions (Fig. 26): digitonin-solubilized mitochondrial complexes from wild-type and null mutant strain were separated by BNE in the first dimension. The modified BNE with DDM in the cathode buffer was applied for second dimensional resolution to dissociate supercomplexes into individual complexes and to separate loosely associated proteins. Finally Tricine-SDS-PAGE was used for third dimensional separation of the protein subunits under reducing (Fig. 26A, B, D, E) and non-reducing conditions (Fig. 26C, F). Mercaptoethanol served here as a reducing agent. Assuming that Cox26 binds covalently via a disulfide bond to CIV, Cox26 should be released upon incubation with mercaptoethanol. If there is a non-covalent association of Cox26 with CIV, Cox26 should be released also under non-reducing conditions. The 3-D gels were electroblotted on to PVDF membranes. Cox26 antibody, which was generated by the groups of Schägger and Stuart, was used for the Western blot analysis.

Cox26 protein was identified as the smallest of all detergent-labile proteins that were removed from respirasomes (assigned on the right side of the silver-stained gel, Fig. 26A). While other cross reacting bands were observed in the wild-type and Δ*cox26* strains (Fig. 26B, C, E, F), two bands denoted L and S at about 30 and 25 kDa (Fig. 26C) that were labeled by the anti-Cox26 antibody were absent in the membranes of the deletion strain like Cox26 itself (Fig. 26F).

Anti-Cox26 antibody identified Cox26 protein at three positions in 3-D Western blots of the wild-type membranes (bottom of Fig. 26B, C). The intensity of the spots suggested that most of the Cox26 protein was released from respirasomes during modified 2-D BNE under native and non-reducing conditions already in the conditions of the second dimension BNE. Smaller amounts of Cox 26 protein were obviously retained by the monomeric and dimeric complex IV under these conditions and came off only in the third dimension SDS-PAGE. The fact that this occurred already under non-reducing conditions suggested that this Cox26 fraction was bound more tightly, but still non-covalently. However, detection of bands L and S under non-

reducing conditions (Fig. 26C) and loss of these signals by mercaptoethanol (Fig. 26B) suggested that a very small fraction of Cox26 protein was associated with complex IV monomer covalently via a disulfide bridge.
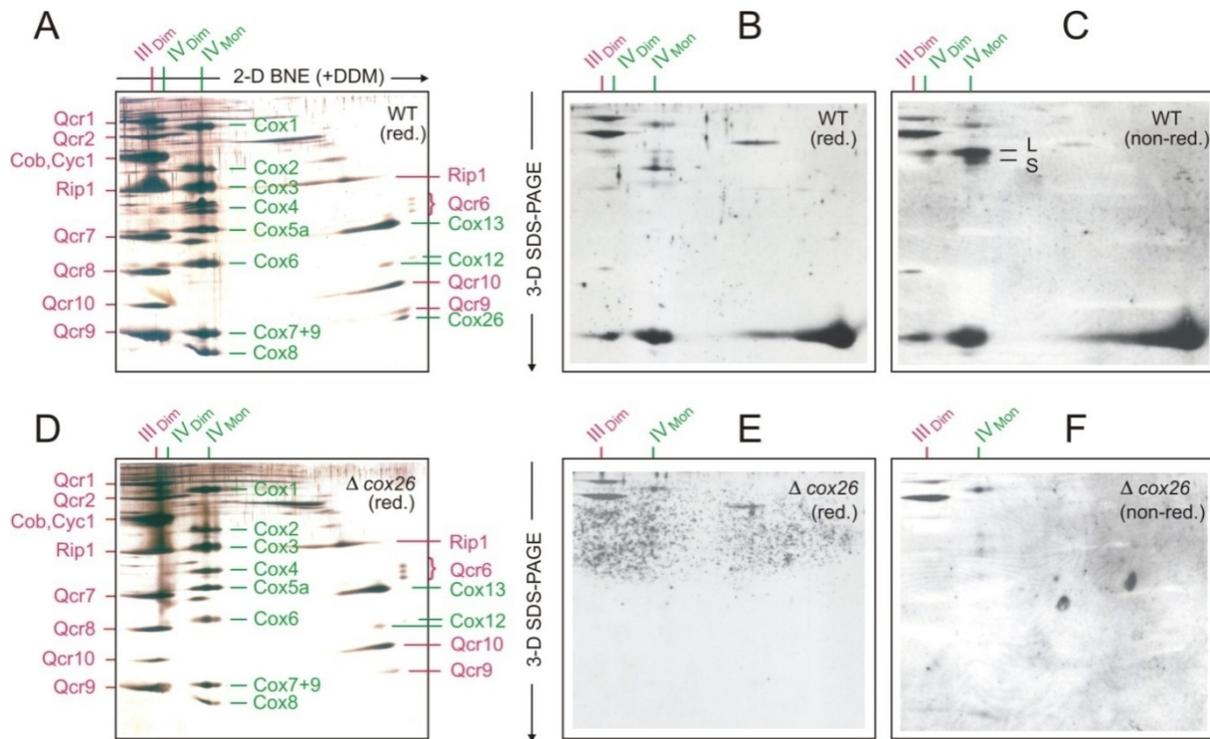
Figure 26. Evidence of hydrophobic and covalent interactions of Cox26 and complex IV. Assignment of complexes and subunits in (A) and (D) was done as in Figure 23. Respiratory supercomplexes from wild-type (WT) strain and $\Delta cox26$ strain were isolated by 1-D BNE of mitochondrial membranes (not shown). The individual complexes and detergent-labile subunits were then released by second dimension modified BNE (+DDM) and resolved by third dimension Tricine-SDS-PAGE using 16% acrylamide gels containing 6 M urea. Silver-stained gels from wild-type (A) and $\Delta cox26$ (D) strains and Western blots for wild-type (B, C) and $\Delta cox26$ strains (E, F) are shown. Reducing conditions (incubation of the gel stripe with 1% mercaptoethanol) were applied for third dimensional SDS-PAGE except for C and F that were run under non-reducing conditions. Anti-Cox26 antibody was applied for the Western blot analysis.

Knowing that a minor fraction of Cox26 protein binds to complex IV covalently, we wanted to find the specific binding partner of Cox26. Since the apparent masses of bands L and S were around 30 and 25 kDa, respectively, subunits Cox2, Cox3, and Cox4 of complex IV were potential candidates to bind the 6.4 kDa Cox26 protein covalently.

3.3.   Search for interaction partners of Cox26

We used an even more complex 4-D electrophoretic technique to identify the Cox26 binding partners in bands L and S. Again, 1-D BNE was applied first to isolate the respirasomes from wild-type strain and Δ*cox26* strain membranes. Complex IV was then released and isolated from the respirasomes by 2-D modified BNE (Fig. 23B). Gel pieces from the 2-D BNE containing complex IV and associated L and S were analyzed by two orthogonal SDS gels (3-D and 4-D SDS separations shown in Fig. 27).

All 1-D, 2-D and 3-D gels were performed under non-reducing conditions. Both non-reducing (Fig. 27A-E upper panels for the wild-type and F-J upper panels for the deletion strain) and reducing conditions (Fig. 27A-E lower panels for the wild-type and F-J lower panels for the deletion strain) were used for the final fourth dimension SDS-PAGE. Silver-stained 3-D/4-D separations of complex IV from the wild-type strain and the Δ*cox26* strain are shown in Figure 27A and F, respectively. A few contaminations were observed (unmarked spots). In corresponding Western blots (Fig. 27 B-E and G-J) polyclonal anti-Cox26 rabbit antibody was applied first, followed consecutively by monoclonal mouse anti-Cox4, anti-Cox3, and anti-Cox2 antibodies on the same blot membrane. Note that in the upper panel of Figure 27B a local defect of the PVDF membrane (marked X) gave a smear with all antibodies.

Polyclonal anti-Cox26 antibody identified individual Cox26 protein and two bands (L and S) under non-reducing conditions (Fig. 27B, upper panel), and two Cox26 protein spots that were dissociated from bands L and S under reducing conditions (Fig. 27B, lower panel). It also showed a weak reaction at the position of Cox1 (Fig. 27B, upper panel). Such presumably non-specific signals are sometimes observed when high local protein concentrations generate a hydrophilic environment on the hydrophobic PVDF membrane and thus facilitate access of antibodies to the membrane. Circles in Figure 27 mark the actual or expected positions of bands L and S. Anti-Cox4 and anti-Cox3 antibodies identified individual Cox4 and Cox3 proteins but no bands L and S (Fig. 27 C, D, H, and J). Since Cox4 and Cox3 proteins were not released from bands L and S under reducing conditions, we concluded that neither Cox4 nor Cox3 is a component of bands L and S.

Reusing the same blots, an anti-Cox2 antibody finally recognized Cox2 protein at two positions in wild-type (Fig. 27E, upper panel) and in Δ*cox26* (Fig. 27J, upper panel) under non-reducing conditions. Interestingly, it also recognized band L in the wild-type under non reducing conditions. However, under reducing conditions (Fig. 27E, lower panel), band L was no longer detected but a third Cox2 spot below the expected position of band L appeared (Fig.

27E, lower panel, marked by a red arrow), as expected, if this form of Cox2 had dissociated from band L. This suggested that band L comprises Cox2 and Cox26.
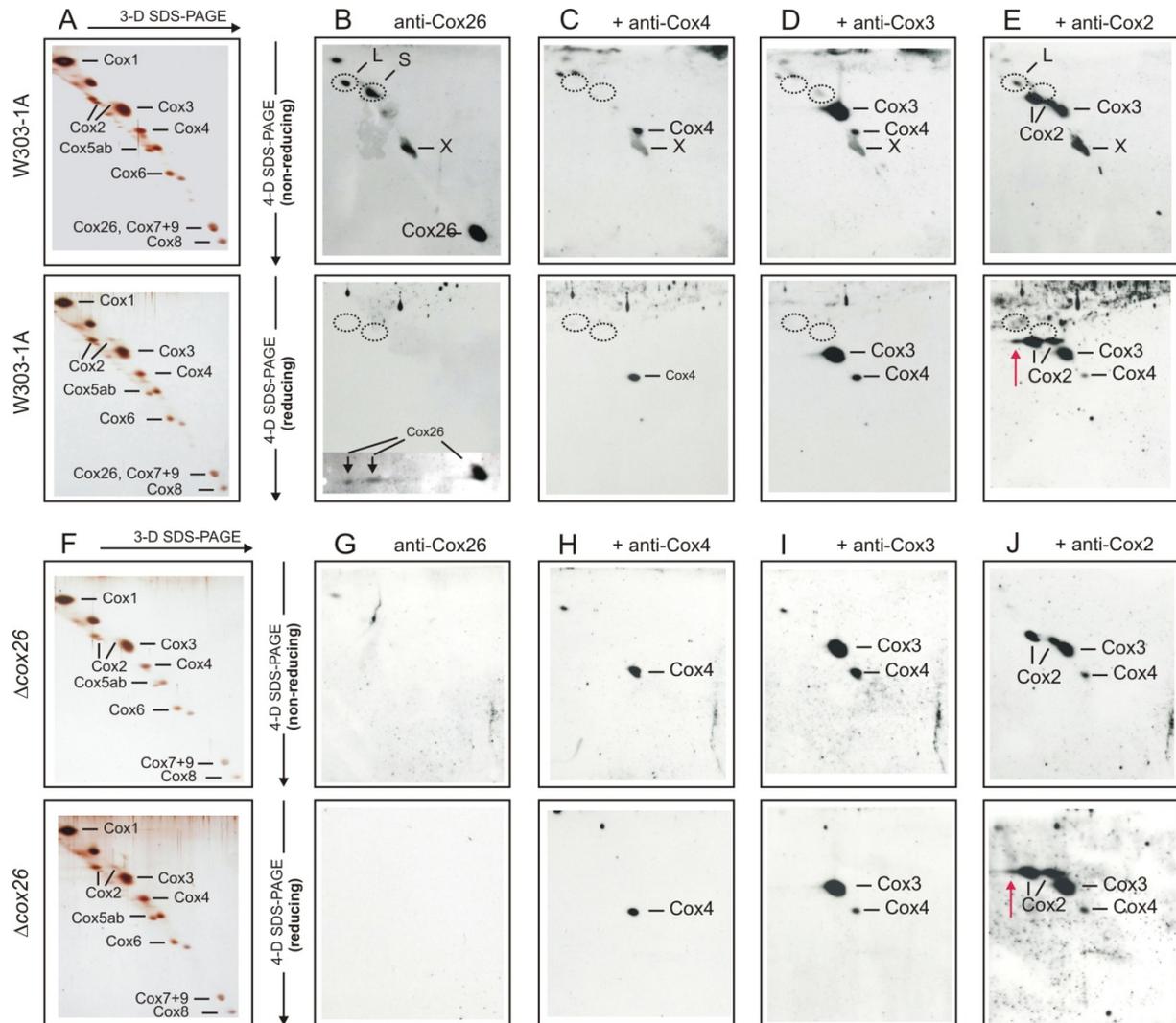
Figure 27. Evidence for covalent interaction of Cox26 with Cox2 in complex IV. (A-E) Analysis of W303-1A wild-type strain. (F-J) Analysis of Δ*cox26* strain. Gel pieces from 2-D BN/BNE (not shown) containing complex IV were resolved under non-reducing conditions by third dimension Tricine-SDS-PAGE using 9% acrylamide gels. 3-D gel stripes were then incubated under non-reducing (upper panels) or reducing conditions (1% mercaptoethanol, lower panels) followed by fourth dimension Tricine-SDS-PAGE using 16% acrylamide gels containing 6 M urea. The 4-D gels were silver stained (A and F) or blotted onto PVDF membranes (B-E and G-J). Polyclonal anti-Cox26 antibody and monoclonal antibodies against Cox 4, 3 and 2 were applied as indicated consecutively for Western blot analysis without using stripping protocols. Circles mark the actual or expected positions of bands L and S. X marks a local defect of the PVDF membrane (B, lower panel). Since detection of Cox 26 was low with short film exposition, a second film with prolonged exposition was inserted as the bottom part of the Figure B.

Although this extra signal presumably corresponded partially or largely to Cox2 that was released from band L under reducing conditions, it should be noted that minor signal intensity was also detected in the Δ*cox26* control lacking band L (Fig. 27J, lower panel, red arrow).

In short, all evidences point to the association of Cox26 and Cox2 via a disulfide-bridge in band L. The identity of the second component in band S remains obscure. However Cox2, Cox3, and Cox4 can be excluded as potential binding partners for Cox26 protein, because they were not detected by specific antibodies in band S.

4.   Structure and composition of native nucleoids from bovine heart mitochondria

One of the aims of this thesis was to isolate and characterize native mitochondrial nucleoids (mt-nucleoids). For this purpose, it was essential to isolate highly pure mitochondria from bovine heart (III.2.1.1). Initial attempts to isolate nucleoids with the help of common cell disruption methods, like French-press or sonication, were not found useful, since nucleoids turned out to be structurally labile under these conditions. An alternative strategy was to solubilize all mitochondrial membrane protein complexes and to fractionate the mitochondrial nucleoids by sucrose density centrifugation. Dodecylmaltoside (DDM) was used, because it solubilized the five oxidative phosphorylation (OXPHOS) complexes completely as individual complexes, in contrast to e.g., Triton X-100 or Nonidet NP-40. Thus supramolecular structures of ATP synthase and of respiratory complexes were eliminated. These structures might have similar sedimentation properties as mt-nucleoids and therefore would have been difficult to remove by this approach.

4.1.   Development of a protocol to isolate native mitochondrial nucleoids

Mitochondrial nucleoids were isolated from bovine heart super-heavy (SH) mitochondria (III.2.1.1). SH mitochondria (~226 μl, 20 mg) were suspended in 141 μl water and 333 μl triple concentrated solubilization buffer (1.5 M 6-aminohexanoic acid, 3 mM EDTA, 75 mM imidazole/HCl, pH 7.4), and solubilized by adding 300 μl dodecylmaltoside (20% w/v) to set a detergent/protein ratio of 3 g/g. The final protein concentration was 20 mg/ml. After 5 minutes of incubation on ice, the sample was loaded on top of a 10 ml linear 32-50% sucrose gradient containing 500 mM 6-aminocaproic acid, 25 mM imidazole/HCl, pH 7.4, 1 mM EDTA and 0.1% DDM. Centrifugation was performed for 3 hours at 4°C, using a SW40 Ti swing-out rotor (27,000 rpm corresponding to 60,000g and 130,000g at the minimal (r_{min}) and maximal radius (r_{max}), respectively). Following centrifugation, 0.5 or 1.0 ml fractions were collected from the bottom using a long thin cannula and a peristaltic pump. The fractions were shock frozen and stored at -80°C or immediately used for further purification by BN-PAGE on large pore gels.
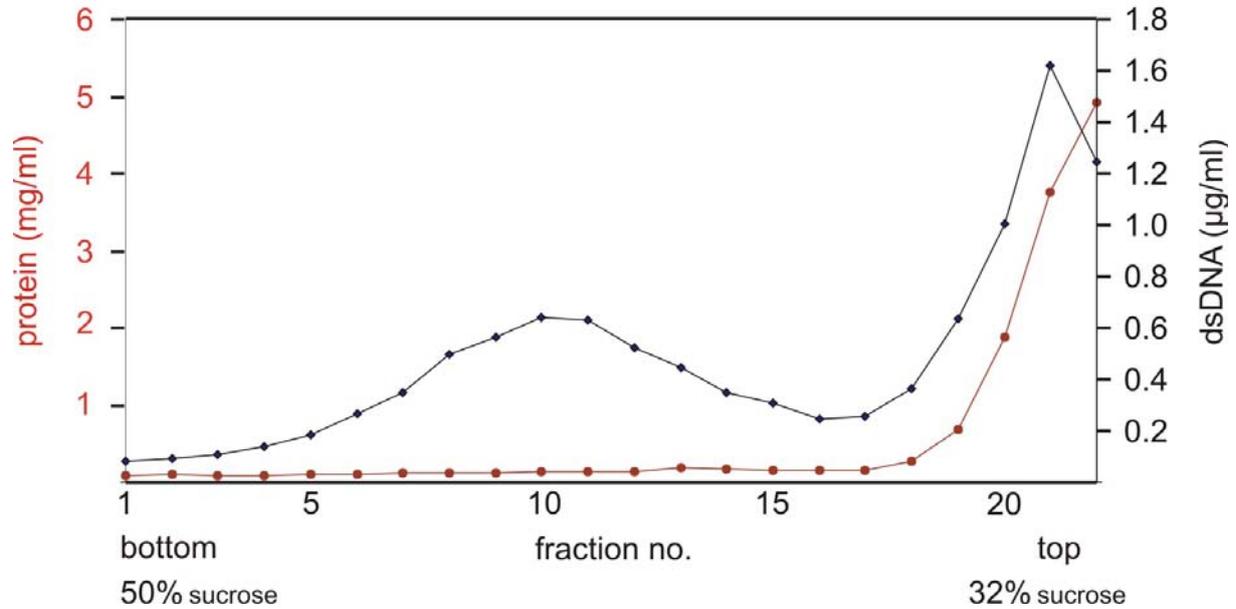
Figure 28. mtDNA and protein determination in the fractions of the sucrose density gradient. Solubilized BHM (1 ml) were loaded on a 10 ml linear sucrose gradient (32-50% sucrose) containing 0.1% DDM. 500 µl fractions were collected. mtDNA containing fractions were identified using the PicoGreen assay (black spots). Protein concentration (red spots) was determined according to a modified Lowry protocol.

Fluoresence of PicoGreen that binds only to double-stranded DNA was detected in the central fractions 6-15 and in the top fractions 20-22 (Fig. 28). The high PicoGreen signal in fractions 20-22 on top of the gradient correlated with a very high detergent content (3 g DDM/g protein) that seemed to interfere with the assay. The central peak fractions 6-15 contained double-stranded DNA and had a protein concentration of about 0.1 mg/ml (Fig. 28) and were tentatively assigned as the fractions containing mitochondrial nucleoids (termed in the following mt-nucleoids or just nucleoids).

4.1.1. Protein composition analysis of sucrose density gradient fractions by 1-D Tricine-SDS-PAGE

For the SDS gel analysis of the sucrose gradient fractions, the samples (fractions 1-15, Fig. 29) were precipitated by dilution with an at least 6-fold volume of water and subsequent centrifugation (10 min 100,000g). Based on the Lowry assay, the protein pellets were solubilized to adjust approximately equal protein concentrations. Samples were treated for 1-

D Tricine-SDS-PAGE as described by Schägger, 2006. 10 µg protein of each fraction was applied to the gel wells of a 10 % acrylamide gel.
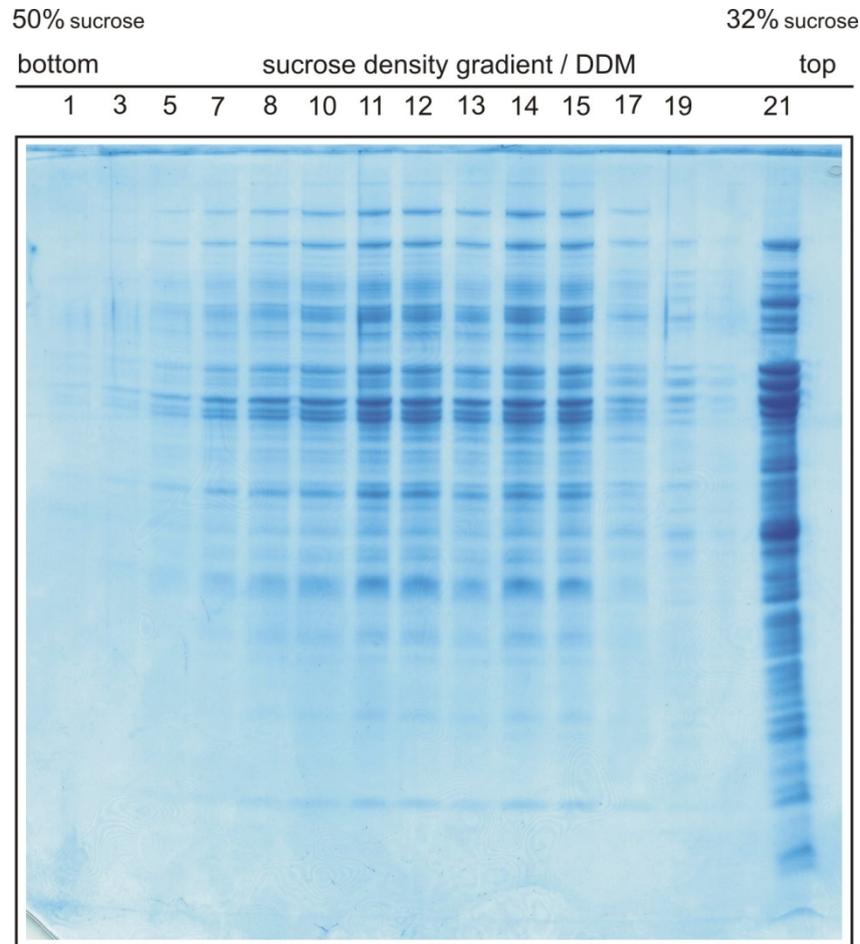
Figure 29. 1-D Tricine-SDS-PAGE of sucrose density gradient fractions. See legend to Figure 28 for details. Approximately 10µg protein of the central fractions was loaded per gel well. The gel was stained with Coomassie.

All fractions showed almost identical protein patterns except the high density fractions 19 and 21 (Fig. 29). Although it was attempted to load the same amount of protein from each fraction, the low density fractions (1-6) showed much lower stain intensity compared to the central fractions (7-15, Fig. 29). This might be due to an increased error of the Lowry assay when assaying very low protein concentrations or by incomplete protein sedimentation of very dilute protein solutions by the dilution/centrifugation step.

4.1.2. PCR analysis to search for mtDNA containing nucleoid fractions

To test whether the central sucrose gradient fractions contained mtDNA, a PCR analysis was performed (Fig. 30). Another batch of very pure bovine heart mitochondria was solubilized by dodecylmaltoside under low ionic strength conditions and separated by sucrose density gradient centrifugation. Following centrifugation eleven 1 ml fractions were collected. DNA content and protein concentration of these fractions were determined by PicoGreen and Lowry assay, respectively. The PicoGreen assay showed an enrichment of DNA in central fractions 3-8 (not shown). The protein concentration in these fractions was 0.1 mg/ml.
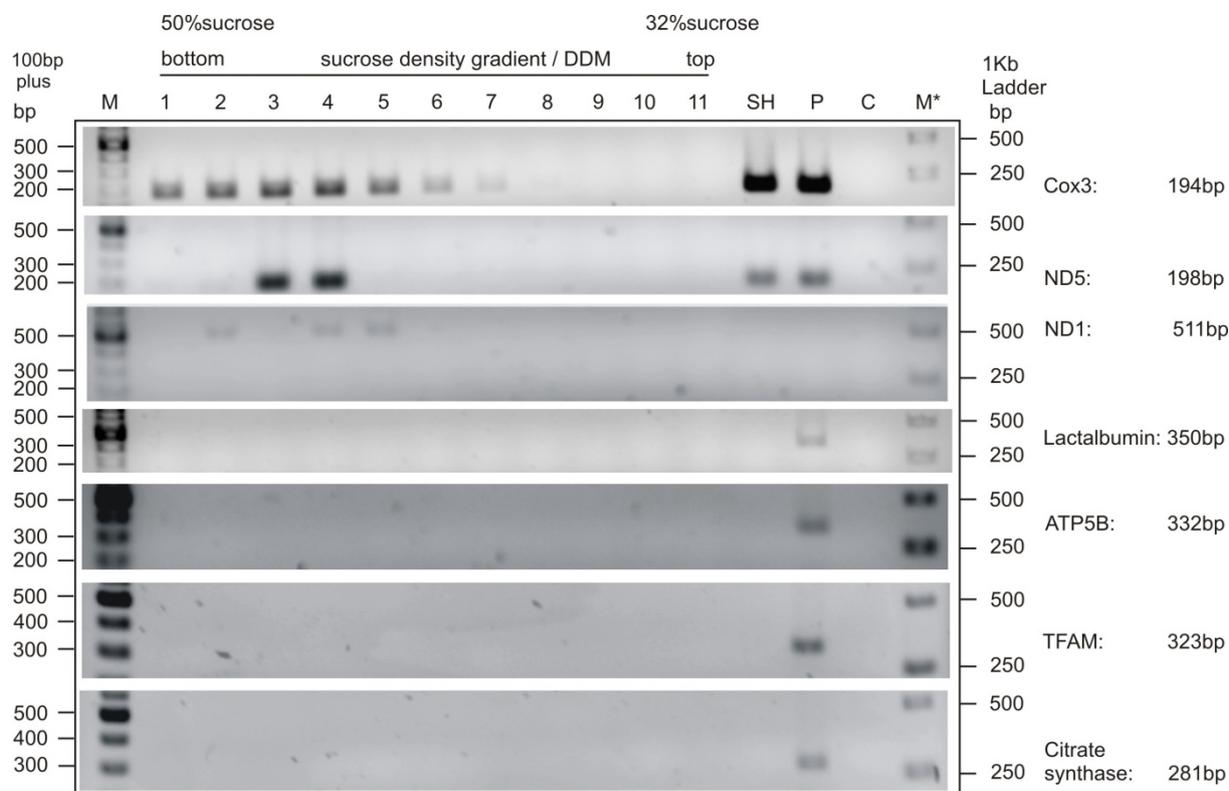
Figure 30. PCR analysis of the sucrose density gradient fractions of bovine heart mitochondria. Bovine heart mitochondria were solubilized by DDM and separated by sucrose density gradient centrifugation. Eleven 1000 μl fractions were collected from bottom to top. PCR analysis was performed with primer pairs detecting genes encoded by mtDNA (Cox3, ND5, ND1) and nuclear DNA (lactalbumin, ATP5B, TFAM, citrate synthase). The size of the PCR products as determined by appropriate markers (M, 100bp plus; M*, 1kb ladder) is indicated on the left and right side of the 1.5% agarose gel. The size of the expected PCR products is indicated on the very right side in base pairs (bp). SH (super heavy mitochondria) and P (crude mitochondria) DNA were applied as positive controls. C: control for PCR primers without a template.

For PCR analysis of the sucrose density gradient fractions, 1 µl of each fraction was directly applied as template. As positive control, DNA was isolated from the very pure super heavy (SH) mitochondria and from crude mitochondria (P). Crude mitochondria were found to be contaminated with nuclear DNA. Fractions 1 to 7 contained mtDNA as shown by the Cox3 gene, a marker of mitochondrial DNA. Presence of other mitochondrial genes, the ND5 and ND1 genes for respiratory complex I subunits in central fractions 3 and 4 or 5, suggested that these are indeed the main nucleoid fractions. Primer pairs against genomic DNA, i.e. lactalbumin, mitochondrial transcription factor (TFAM), citrate synthase, and ATP synthase subunit 5 (ATP5B) produced no PCR product in the fractions of the sucrose gradient and in the starting material applied to the gradient (SH) whereas crude mitochondria gave a product demonstrating that sucrose fractions are free of nuclear DNA (Fig. 30).

In short, it could be shown that the central fractions of the sucrose gradient contained mtDNA and protein. The symmetry of the central PicoGreen peak (Fig. 28), the almost identical protein patterns of the central fractions (Fig. 29), the presence of mtDNA in central fractions and the absence of nuclear DNA from all fractions (Fig. 30) suggested that a rather homogeneous pool of nucleoid particles had been isolated.

4.2.   Repurification of nucleoids by BNE on large pore gels

Sucrose density gradient fractions were analysed by blue native electrophoresis on a 2-9% large pore acrylamide gel, a new electrophoretic technique to isolate extremely large protein complexes with sizes up to around 50 MDa (Strecker et al., 2010). 20 µl of each fraction was directly applied for the analysis. Fractions 3-7 in Figure 31 showed defined bands in the high mass range, which were tentatively assigned as nucleoid bands (N). They showed minor differences in migration distance and particle size. Fractions 8-10, near the top of the density gradient, contained known large mitochondrial complexes, e.g., pyruvate dehydrogenase complex (P), oxoglutarate dehydrogenase complex (O), monomeric ATP synthase (M), and respiratory complexes I, III, and IV. The top fraction 11 contained monomeric ATP synthase (M) and respiratory complexes I, III, and IV (Fig. 31).

Analysis of sucrose gradient fractions by BNE on large pore gel suggested a fairly homogeneous pool of nucleoid particles in all peak fractions (3-7).
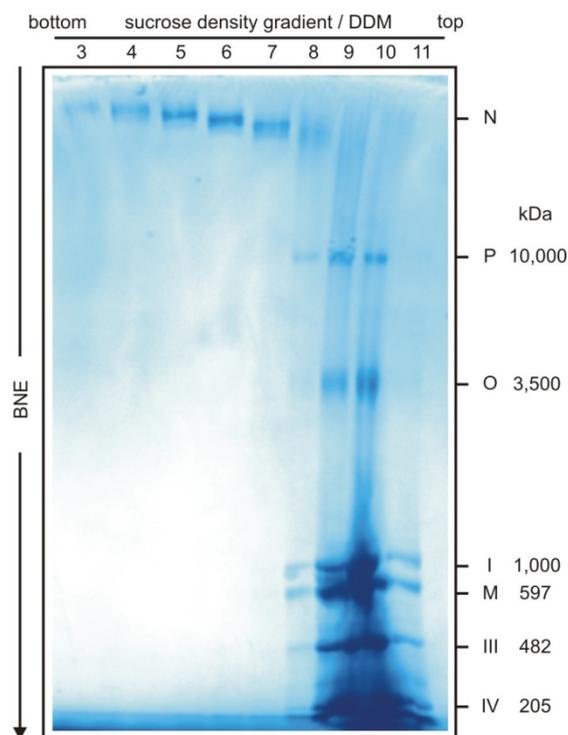
Figure 31. Purification of mitochondrial nucleoids by BNE on large pore gel. Very pure bovine heart mitochondria were solubilized using a DDM/protein ratio of 3 g/g and separated by sucrose density gradient centrifugation. Following centrifugation eleven fractions were collected. All fractions (fractions 3-11) were analyzed by BNE on a 2–9% acrylamide gel. Assignment of complexes was based on the results of Wittig et al., 2010a. The gel was fixed and stained with Coomassie.

4.3. Mass estimation of nucleoids

For the mass determination of nucleoids, another batch of very pure mitochondria was solubilized and separated by sucrose density gradient centrifugation. Following centrifugation, fractions were collected and analyzed by BN electrophoresis, which is an established technique for mass estimation of native membrane proteins. Known large mitochodrial complexes served as markers for mass calibration on the large pore gel (Fig. 32A). Additionaly, crude bovine heart mitochondria (Fig. 32B) and a commercially available high molecular weight marker kit of water soluble protein complexes (HMW) (Fig. 32C) was used for mass calibration on the same gel. An aliquot of 400 µg crude mitochondria was solubilized by digitonin (5 g/g protein), centrifuged for 10 min at 20,000g and the supernatant was applied to the gel. Digitonin was used for membrane solubilization in order to preserve mitochondrial supramolecular complexes and different forms of ATP synthase. Separation of

these complexes on the same gel together with the mitochondrial nucleoids enhanced the reliability of the mass estimation.
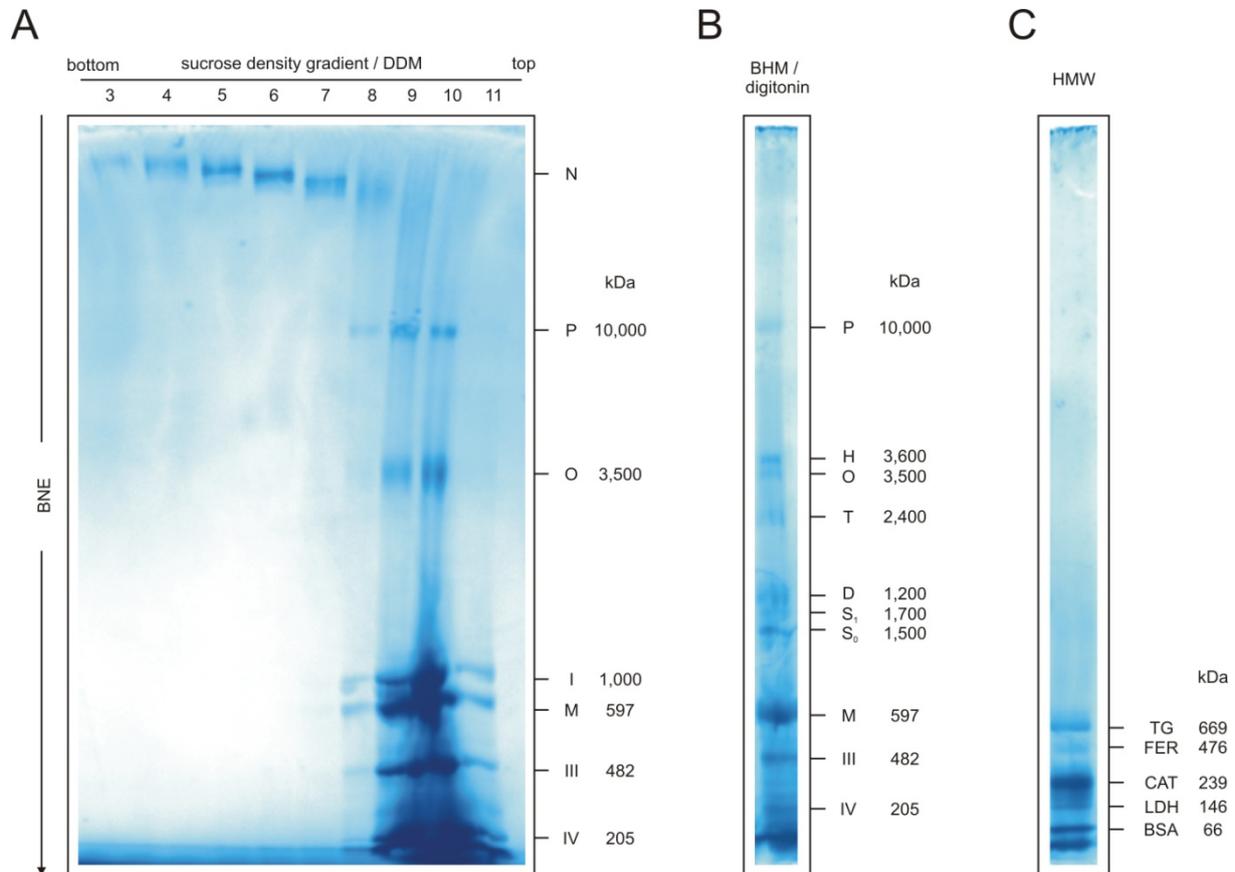
Figure 32. Mass estimation of mitochondrial nucleoids. (A) Purification of mitochondrial nucleoids by BNE on large pore gel. See legend to Figure 31 for details. (B) Crude bovine heart mitochondria were solubilized using a digitonin/protein ratio of 5 g/g and separated by BNE on a 2–9% acrylamide gradient gel. (C) High molecular weight protein marker kit (HMW) was also used for mass calibration on the same gel. 3-11, sucrose gradient fractions 3-11; N, mitochondrial nucleoid; P, pyruvate dehydrogenase complex; H, T, D, M, hexameric, tetrameric, dimeric, and monomeric ATP synthase; O, oxoglutarate dehydrogenase complex; I, III, IV, respiratory complexes I, III, and IV; S_1, respiratory supercomplex comprising monomeric complex I, dimeric complex III, and one copy of complex IV; S_0, respiratory supercomplex comprising monomeric complex I and dimeric complex III. TG, thyroglobulin dimer; FER, ferritin; CAT, catalase; LDH, lactate dehydrogenase; BSA, bovine serum albumin.

Table 5. Migration behaviour of DDM-solubilized mitochondrial complexes on a large pore gel.

Protein complex	Migration distance (mm)	Apparent mass (kDa)
Nucleoid from fraction 3 (F3)	7	36000
Nucleoid from fraction 5 (F5)	10	33000
Nucleoid from fraction 7 (F7)	12	30000
Puryvate dehydrogenase complex (P)	42	10000
Oxogluturate dehydrogenase complex (O)	72	3500
Complex I (I)	114	1000
Complex V (V)	120.5	597
Complex III (III)	133	482
Complex IV (IV)	147	205

Table 6. Migration behaviour of digitonin-solubilized mitochondrial complexes on a large pore gel.

Protein complex	Migration distance (mm)	Apparent mass (kDa)
Nucleoid from fraction 3 (F3)	7	36000
Nucleoid from fraction 5 (F5)	10	33000
Nucleoid from fraction 7 (F7)	12	30000
Puryvate dehydrogenase complex (P)	42	10000
Hexameric ATP synthase (H)	68.5	3600
Oxogluturate dehydrogenase complex (O)	72	3500
Tetrameric ATP synthase (T)	81	2400
Dimeric ATP synthase (D)	96.5	1200
Supercomplex I III$_2$IV (S$_1$)	100	1700
Supercomplex I III$_2$ (S$_0$)	103.5	1500
Complex V (V)	121.5	597
Complex III (III)	130	482
Complex IV (IV)	140.5	205

Table 7. Migration behaviour of high molecular weight kit protein markers on large pore gel.

High molecular weight kit	Migration distance (mm)	MW (kDa)
Thyroglobulin dimer (TG)	124	669
Ferritin (FER)	135	476
Catalase (CAT)	137	239
Lactate dehydrogenase (LDH)	141	146
Bovine serum albumin (BSA)	145	66

A high molecular weight marker kit of water soluble protein complexes was also tried for mass calibration. However, it seemed that the water soluble proteins were too small and not ideally suited as marker for the mass estimation of mitochondrial nucleoids (Fig. 32C, Wittig et al., 2010a).
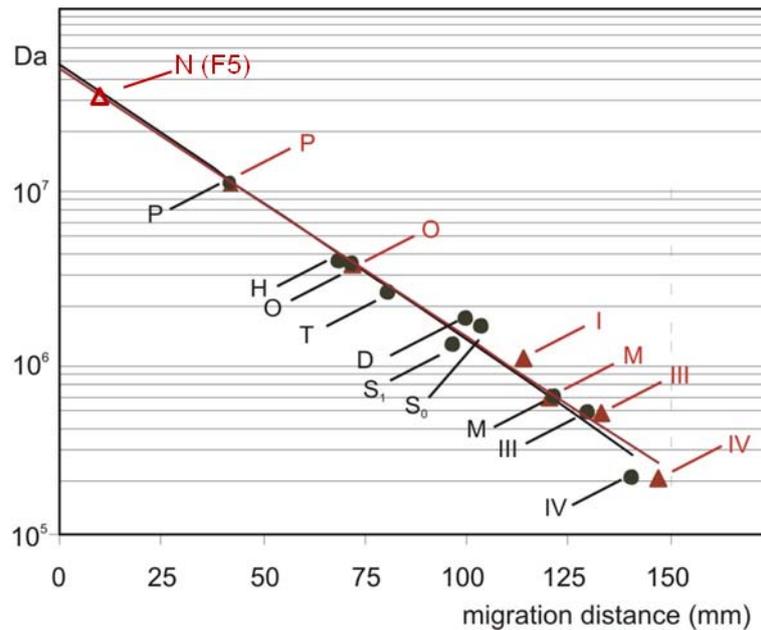
Figure 33. Mass calibration for BNE on large pore gels. Dodecylmaltoside- (red triangles) and digitonin- (black dots) solubilized mitochondrial protein complexes were separated by BNE using a 2-9% acrylamide gradient gel. Migration distances of the dodecylmaltoside- or digitonin-solubilized complexes were plotted versus the logarithmic protein mass.

Using the DDM-solubilized mitochondrial complexes (Fig. 32A; Table 5) and the digitonin-solubilized mitochondrial complexes (Fig. 32B; Table 6) for calibration, an apparent mass around 33 MDa was estimated for the nucleoid bands of fractions 5 and 6. Smaller and larger apparent masses around 30 MDa and 36 MDa were estimated for the nucleoids of fractions 7 and 3, respectively (Fig. 33, Tables 5 and 6). These apparent masses should be regarded as minimal masses (see chapter V, Discussion).

4.4. Electron microscopic analysis of mt-nucleoids

Mammalian mitochondrial nucleoid structure has been studied by applying different microscopic methods either in cell culture (Satoh and Kuroiwa, 1991; Bereiter-Hahn and Vöth, 1996) or in isolated mitochondria (Navratil et al., 2007; Poe et al., 2010). These studies were performed mainly to determine the number of mtDNA copies that may be localized within a single nucleoid or in clusters of nucleoids. There are only a few electron microscopic studies on isolated mitochondrial nucleoids. Little is known about the structure of mitochondrial nucleoids from animal tissues since the isolation of morphologically intact nucleoids is quite challenging. The electron microscopic analysis of isolated bovine heart mitochondrial nucleoids was performed by Dr. Karen Davies from the Max-Planck-Institute of Biophysics, Department of Structural Biology, Frankfurt.

4.4.1. Preparation of mitochondrial nucleoids for electron microscopic analysis

Nucleoids from sucrose gradient fractions were either analyzed directly by electron microscopy (Fig. 34A, C, D, 35A) or after buffer exchange and concentration by ultrafiltration (Fig. 34B, 35B), or after concentration by dilution/precipitation (Fig. 35C) (III.2.12.1).

4.4.2. Overview of nucleoid particles by electron microscopy

Mitochodrial nucleoids were analyzed by electron microscopy with two different methods: negative stain and cryo-electron tomography. In both methods, nucleoids that had been separated by sucrose density gradient centrifugation were applied directly to grids as described in methods (III.2.12). Upper panels (A, B) and lower panels (C, D) of Figure 34 show the negative stain images and the cryo images of the nucleoids, respectively. As evident from panels A and C, the nucleoid particles indicated a quite homogenous and native preparation. Panels B and D with higher magnification showed that nucleoids appeared as closely packed particles with a size around 85 x 115 nm for negative stained samples (Fig. 34B) and a size around 100 x 150 nm for cryo-preserved samples (Fig. 34D). Some of the nucleoids showed dumbbell-shape indicating dimerization of nucleoids (Fig. 34B).
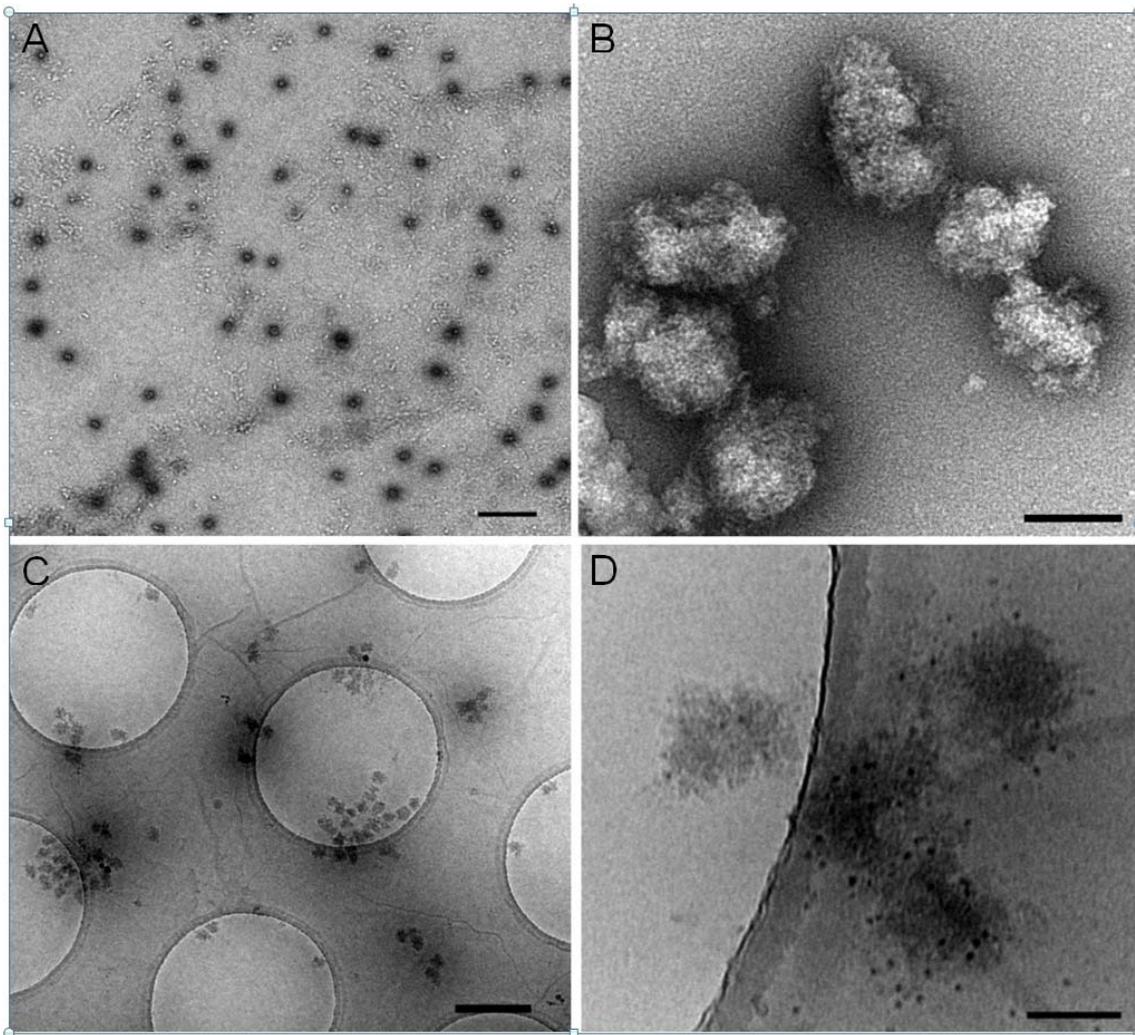
Figure 34. Electron microscopy images of nucleoids. (A) Low magnification image of nucleoids in negative stain. (B) Magnified image of nucleoids in negative stain. (C) Low magnification cryo-image of nucleoids on holey carbon support film. Each hole is 1.2 microns (D) magnified cryo-image of native nucleoids. Scale bar (A) and (C) = 500 nm, (B) and (D) = 100 nm. Electron microscopy was performed by Dr. Karen Davies, Max-Planck-Institute of Biophysics, Department of Structural Biology, Frankfurt.

4.4.3.   Cryo-electron tomography analysis of mt-nucleoids

For the detailed cryo-EM tomography of nucleoids, samples were prepared as described above (IV.4.4.1). Nucleoids appeared as compact electron dense particles of heterogenous appearance. The overall shape is irregular with an approximate length of 150 nm and diameter 100 nm (Fig. 35A). The nucleoids appear to consist of closely packed spheres of approximately 70 nm in diameter (Fig. 35D; movie 1 in Appendix II on CD). This assembly is more apparent after buffer exchange when the tight packing of the nucleoids has been disrupted resulting in the slight separation of one or more of these spheres (Fig. 35B). Large-

scale disruption of the nucleoids resulted in complete unfolding and the appearance of filamentous structures (Fig. 35C). Nucleoids turned out to be extremely sensitive to the electron beam indicating high protein content.
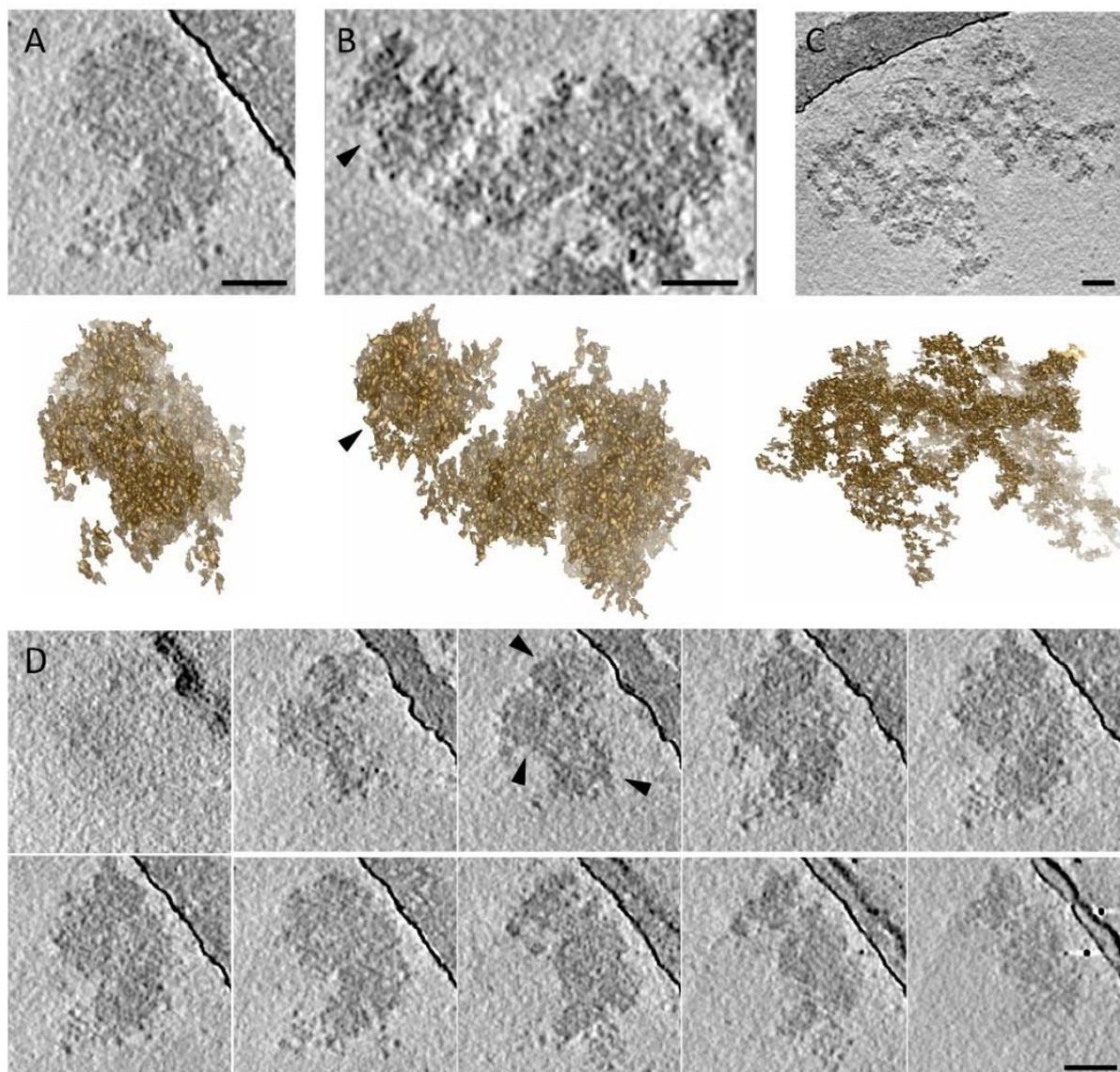
Figure 35. Electron cryo-tomographic images of nucleoids. Tomographic slice and isosurface of a compact (A), a partially disrupted (B), and a completely disrupted (C) nucleoid. (D) Successive tomographic slices through the nucleoid depicted in (A). The edge of the carbon support film is visible in the top right corner of the images (A), (C) and (D). Nucleoids have irregular shape with length 150 nm and diameter 100 nm. They appear to consist of closely packed spheres with diameter 70 nm. Three such spheres are indicated by arrowheads in (D). The spheres are best observed in partially disrupted nucleoids as shown by arrowheads in (B). Scale bar is 50 nm. Electron microscopy was performed by Dr. Karen Davies, Max-Planck-Institute of Biophysics, Department of Structural Biology, Frankfurt.

4.5. Protein composition of bovine heart mitochondrial nucleoids

For the detailed analysis of proteins associated with the mitochondrial DNA and to follow the further purification of the crude nucleoids isolated by sucrose density centrifugations, three different types of samples were analyzed by LC-MS/MS. The LC-MS/MS analysis was performed by Dr. Heinrich Heide and Dipl.-Ing. Mirco Steger.

(i) The band from large pore BNE containing nucleoids with mass around 33 MDa.

(ii) The central fractions of the sucrose density gradient containing crude nucleoids.

(iii) Proteins running at the front of the large pore BN gel.

4.5.1. Protein composition of the 33 MDa mitochondrial nucleoids

The 33 MDa band containing mt-nucleoids was excised from the large pore BN gel (Fig. 32, fraction 5), prepared for Tricine SDS-PAGE (Fig. 36, left panel) and analyzed by LC-MS/MS. Counting only proteins that were characterized by at least two non-redundant peptides, a total number of 448 proteins was identified by mass spectrometry, as summarized in Table 10 in Appendix I. The 448 mt-nucleoid components were ranked according to Mascot scores, and grouped according to functional properties (Fig. 36, right panel; Table 11 in Appendix I). Functional information of the MS-identified proteins was obtained automatically or manually from the Uniprot data base.

Thirty proteins (6.7% of 448 proteins) were assigned to the group of nucleic acid binding or modifying proteins. This group included DNA and RNA binding proteins, factors involved in replication and transcription, and especially several certified mt-nucleoid components like mitochondrial transcription factor A (TFAM, rank 145), mitochondrial dimethyladenosine transferase 2 (TFB2M, rank 219), mitochondrial dimethyladenosine transferase 1 (TFB1M, rank 229), mitochondrial DNA polymerase subunit gamma-2 (POLG2, rank 231), mitochondrial single-stranded DNA-binding protein (SSBP1, rank 257), and C26H10ORF2 protein (Twinkle, rank 287). The most prominent protein in this group, however, was bovine homologue of human ES1 protein (Es1, rank 5) that was recognized here for the first time in a nucleoid fraction.
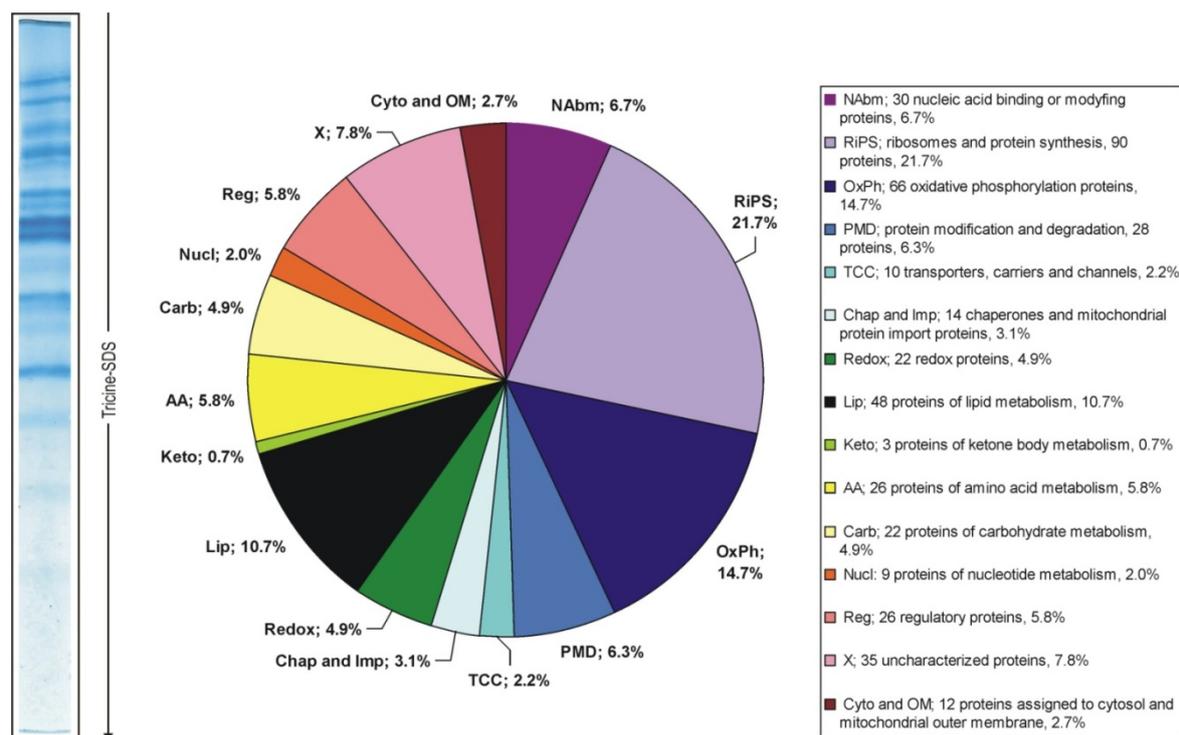
Figure 36. Protein composition analysis of BNE-repurified mitochondrial nucleoids. Left panel: nucleoids were solubilized by DDM and separated by sucrose density gradient centrifugation. For the protein component analysis, central gradient fractions were pooled and repurified by BNE on large pore gel. The nucleoid band was excised and resolved for protein component analysis by Tricine-SDS-PAGE using a 10% acrylamide gel. The gel was stained with Coomassie and 59 slices were excised and subjected to LC-MS/MS analysis after tryptic in-gel digestion. Original Mascot-search results of the slices are shown in Appendix II on CD. Right panel: The 448 identified protein components of BNE purified nucleoids were grouped according to their presumed functional properties.

The very large "ribosomes and protein synthesis group (RiPS)" (97 proteins; 21.7%) comprised an almost complete set of subunits of mitochondrial ribosomes, e.g., 28S ribosomal proteins S22 and S25 (ranks 71 and 89, respectively), many proteins involved in the translational process like aminoacyl-tRNA synthases (e.g., ranks 101 and 108) and elongation factors, e.g., elongation factors Tu and Ts (ranks 2 and 8, respectively). This suggested that the nucleoid fraction contained significant amounts of mitochondrial ribosomes.

Sixty-six proteins (14.7%) could be assigned to the system of oxidative phosphorylation comprising at least 100 individual components. The most prominent identified proteins were ATP synthase subunits alpha and beta (ranks 9 and 12) and complex I subunits NDUFS1 and NDUFA 10 (ranks 11 and 43).

101

Twenty-eight proteins (6.3%) were assigned to the protein modification and degradation group, including deacetylases, kinases, transferases, hydrolases, proteases and proteasomal components. Further ten proteins (2.2%) were classified as carriers, transporters and channels; fourteen proteins (3.1%) as chaperones and mitochondrial import proteins; twenty-two proteins (4.9%) as redox proteins other than those involved in oxidative phosphorylation, and 26 proteins (5.8%) as regulatory proteins involved in signal transduction and further regulatory processes. Fourty-eight proteins (10.7%) were members of lipid metabolism pathways including enzymes of fatty acid biosynthesis and degradation, steroid hormone and ubiquinone biosynthesis. Three proteins (0.7%) were involved in ketone body biosynthesis and utilization; 26 proteins (5.8%) in amino acid synthesis, modification and degradation; 22 proteins (4.9%) in carbohydrate metabolism including glycolysis, pyruvate dehydrogenase, and tricarboxylic acid cyle, and 9 proteins (2.0%) in the nucleotide metabolism. Thirty-five previously hypothetical and mostly uncharacterized proteins (7.8 %) could not be assigned to the above protein classes. Only twelve proteins (2.7%) had an extra-mitochondrial localization, e.g., the L23 subunit of the cytosolic ribosome (rank 393) and 8 cytoskeletal and intercellular adhesion proteins (ranks 153, 201, 313, 357, 409 etc.), or could be assigned to the outer mitochondrial membrane, e.g., the voltage dependent anion carriers VDAC 1 and 2 (ranks 369 and 258) and the mitochondrial outer membrane import complex protein 2 (Metaxin-2, rank 193). Overall, the identification of many highly abundant mitochondrial proteins like those of the complexes of the oxidative phosphorylation system and the fatty acid metabolism demonstrated that even the purest nucleoid fractions contained significant contaminations by these highly abundant mitochondrial complexes.

4.5.2. Protein composition of crude mitochondrial nucleoids

Crude mt-nucleoids were analyzed by a different approach avoiding repurification by BNE in order to retain also weakly bound proteins that might dissociate during BNE. Briefly, central fractions from sucrose gradients were concentrated more than 20-fold by dilution/centrifugation, as described in IV.4.1.1. The proteins of pelleted crude nucleoids were then separated by 1-D Tricine SDS-PAGE (Fig. 37) and analyzed by LC-MS/MS (Table 10 in Appendix I, columns 8 and 9).
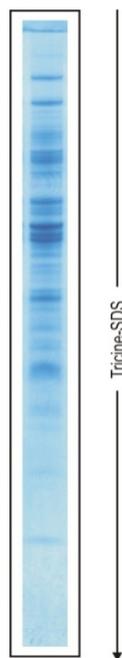
Figure 37. Protein composition analysis of crude mitochondrial nucleoids. Nucleoids were solubilized by DDM and separated by sucrose density centrifugation. Protein composition analysis of a central gradient fraction was performed. 10 µg of a central gradient fraction was separated by Tricine-SDS-PAGE using a 10% acrylamide gel. The gel was Coomassie stained and 103 slices were cut for LC-MS/MS analysis (Table 10 in Appendix I, columns 8 and 9). Original Mascot-search results of the slices are shown in Appendix II on CD.

365 of the 448 proteins identified in BNE-repurified nucleoids were also identified in crude nucleoids. The lower number of identified proteins is explained by the use of less protein. However, sixty additional proteins were identified in spite of using less protein (presented at the bottom of Table 10 in Appendix I, columns 8 and 9). Specific roles seem excluded for proteins like serum albumin, lysozyme C, and hemoglobin subunit beta (ranks 41, 190, and 232). 2-D BN/SDS-PAGE (Fig. 38) showed that minor amounts of mitochondrial oxidative phosphorylation complexes I-V, pyruvate and oxoglutatate dehydrogenase complexes, and several smaller mitochondrial proteins dissociated from the nucleoids during BNE and therefore must be regarded as contaminants. However, it seems important to note that significant amounts of the mentioned mitochondrial complexes were still found in the BNE-repurified nucleoid fractions. Even conditions that favour dissociation like adding 100 mM NaCl for membrane solubilization, for sucrose gradient centrifugation and before application to the BN gel, did not substantially alter the composition of mt-nucleoid fractions as analyzed by LC-MS/MS (these control experiments are summarized in Appendix II on CD).

4.5.3. Proteins running at the front of the large pore BN gel

Identification of loosely associated nucleoid proteins can help to distingish between central and peripheral or possibly contaminating components. Complementing the analysis of the crude nucleoids, we thus analyzed also the proteins running at the front of the BN gels used in

further purifying the crude nucleoid fractions obtained by sucrose density centrifugation. The crude nucleoid fractions from the linear sucrose gradient were pooled (2 ml) and loaded on top of large pore gels for purification by BNE (Strecker et al., 2010). The anionic Coomassie-dye in the cathode buffer for BNE and residual detergent, which was used for membrane solubilization (3 g protein/g detergent), can bind to the surface of nucleoids and induce a charge shift. Thus, loosely bound protein components may be stripped off from the tightly bound core components during native gel electrophoresis. The dissociated Coomassie binding proteins and contaminants (hydrophobic and also most hydrophilic proteins) will migrate to the anode due to the negative charge of the Coomassie-dye. Water soluble acidic proteins (pI <7.5) will also migrate during the BNE to the anode (even without binding Coomassie). Water soluble basic proteins will show anodic migration if they bind enough Coomassie-dye that imposes a charge shift. However, water soluble basic proteins (pI > 7.5) without or with too little bound Coomassie-dye will migrate towards the cathode and will be lost for the protein analysis (Wittig and Schägger, 2005). Following BNE purification, a gel stripe can be used to separate dissociated protein complexes from BNE into individual subunits by second dimension Tricine-SDS-PAGE and to analyze them further, e.g., by peptide mass spectrometry.

As evident from Figure 38, the major amount of protein was concentrated in the nucleoid band (N) but also a significant amount of protein complexes and individual proteins had dissociated from the larger particles during BNE. Most of the larger complexes could be assigned just by comparison with previous analysis of heart mitochondria (Wittig et al., 2010a). Further spots from a 2-D BN/SDS gel (Fig. 38, circled) were analyzed by LC-MS/MS. The identified proteins are summarized in Table 8.
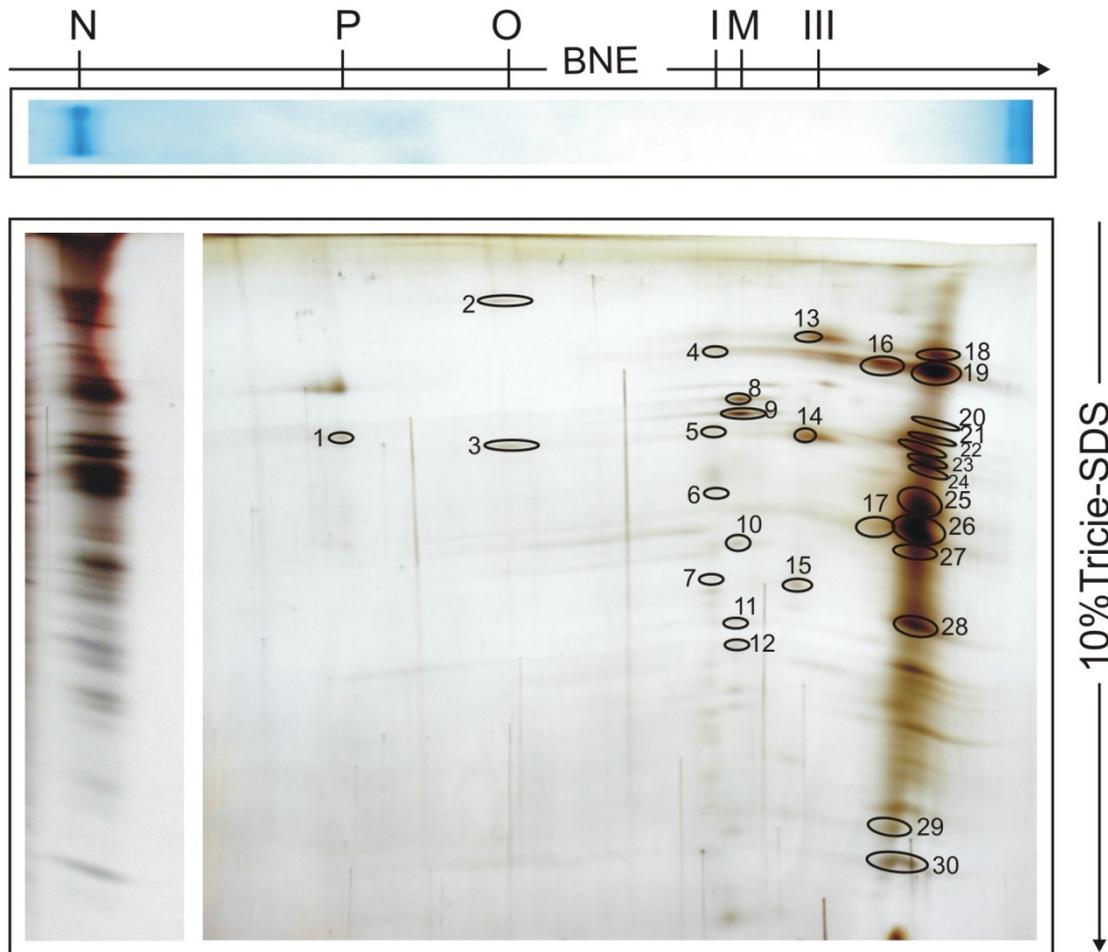
Figure 38. 2-D BN/SDS separation of the crude nucleoid fraction and identification of dissociated proteins. 1-D BNE of pooled central gradient fractions separated the presumed nucleoid band (N). Following BNE a gel stripe was processed by 2-D Tricine-SDS-PAGE using a 10 % acrylamide gel. The gel was fixed and silver stained. Besides subunits of pyruvate dehydrogenase complex (P), oxoglutarate dehydrogenase complex (O), monomeric ATP synthase (M), and respiratory complexes I, III, and IV, 30 further spots (circled) were cut out of the silver-stained gel and analyzed by LC-MS/MS.

Mass spectrometric analysis of 30 protein spots that were removed from nucleoids during BNE revealed that the tentatively assigned nucleoids from sucrose density gradient contained bound mitochondrial complexes like pyruvate dehydrogenase complex (P), oxoglutarate dehydrogenase complex (O), monomeric ATP synthase (M), and respiratory complexes I, III, and IV, as identified by several characteristic subunits (Table 8).

Table 8. Identification of proteins and complexes separated from the nucleoid fraction by BNE on large pore gel.

Spot no.	UniProt	Protein; Gene	Precursor mass	Non-redundant peptides	Mascot score
1	P22439	Pyruvate dehydrogenase protein X component; PDHX	53852	6	202
	B0JYQ0	ALB protein; ALB	69248	2	87
2	P11179	Dihydrolipoyllysine-residue succinyltransferase component of 2-oxoglutarate dehydrogenase complex; DLST	48942	9	523
	Q148N0	2-oxoglutarate dehydrogenase; OGDH	115734	9	328
3	P11179	Dihydrolipoyllysine-residue succinyltransferase component of 2-oxoglutarate dehydrogenase complex; DLST	48942	9	502
	B0JYQ0	ALB protein; ALB	69248	2	88
4	Q3ZCH0	Stress-70 protein; HSPA9	73696	9	527
	P15690	NADH-ubiquinone oxidoreductase 75 kDa subunit; NDUFS1	79391	8	411
5	O46629	Mitochondrial trifunctional protein; HADHB	53670	7	289
	P17694	NADH dehydrogenase [ubiquinone] iron-sulfur protein 2; NDUFS2	52522	3	92
	A7MB35	Pyruvate dehydrogenase E1 component subunit alpha; PDHA1	43360	2	89
	P34943	NADH dehydrogenase (Ubiquinone) 1 alpha subcomplex, 9, 39kDa; NDUFA9	41634	2	72
6	A7MB35	Pyruvate dehydrogenase E1 component subunit alpha, somatic form; PDHA1	43360	2	105
	P34943	NADH dehydrogenase (Ubiquinone) 1 alpha subcomplex, 9, 39kDa; NDUFA9	41634	2	69
7	P23709	NADH dehydrogenase [ubiquinone] iron-sulfur protein 3; NDUFS3	30266	2	135
8	P19483	ATP synthase subunit alpha; ATP5A1	59683	12	562
9	P00829	ATP synthase subunit beta; ATP5B	56249	24	987
	P19483	ATP synthase subunit alpha; ATP5A1	59683	2	77
10	P05631	ATP synthase subunit gamma; ATP5C1	33051	5	254
11	P13619	ATP synthase subunit b; ATP5F1	28803	4	113
	Q02369	NADH dehydrogenase [ubiquinone] 1 beta subcomplex subunit 9; NDUFB9	21775	2	89
12	P13620	ATP synthase subunit d; ATP5H	18681	6	237

	P13621	ATP synthase subunit O; ATP5O	23305	3	173
13	Q3SZ00	HADHA protein; HADHA	83196	16	607
	Q3ZCH0	Stress-70 protein; HSPA9	73696	7	380
14	P23004	Cytochrome bc_1 complex subunit 2; UQCRC2	48119	14	660
	A5D9E7	Mitochondrial trifunctional protein, beta subunit; HADHB	53670	10	367
	Q3MI02	UQCRC1 protein; UQCRC1	52487	6	220
15	P00125	Cytochrome c_1, heme protein; CYC1	35274	2	67
16	Q3ZCH0	Stress-70 protein; HSPA9	73696	26	1462
	P11966	Pyruvate dehydrogenase E1 component subunit beta; PDHB	39101	2	77
17	P11966	Pyruvate dehydrogenase E1 component subunit beta; PDHB	39101	8	315
	A7MB35	Pyruvate dehydrogenase E1 component subunit alpha; PDHA1	43360	2	87
18	Q3ZCH0	Stress-70 protein; HSPA9	73696	21	1103
	P11966	Pyruvate dehydrogenase E1 component subunit beta; PDHB	39101	12	536
	A7MB35	Pyruvate dehydrogenase E1 component subunit alpha; PDHA1	43360	10	413
19	Q3ZCH0	Stress-70 protein; HSPA9	73696	38	1924
	P11966	Pyruvate dehydrogenase E1 component subunit beta; PDHB	39101	10	502
	Q2TBI4	Heat shock protein 75 kDa; TRAP1	79331	6	377
	A7MB35	Pyruvate dehydrogenase E1 component subunit alpha; PDHA1	43360	8	371
	P21839	2-oxoisovalerate dehydrogenase subunit beta; BCKDHB	42908	2	119
	Q2TBT9	BCKDHA protein; BCKDHA	51401	2	92
20	Q3ZCH0	Stress-70 protein; HSPA9	73696	5	216
	P19483	ATP synthase subunit alpha; ATP5A1	59683	3	141
	B0JYQ0	ALB protein; ALB	69248	3	133
	P11966	Pyruvate dehydrogenase E1 component subunit beta; PDHB	39101	3	105
	A7MB35	Pyruvate dehydrogenase E1 component subunit alpha; PDHA1	43360	2	44
21	P00829	ATP synthase subunit beta; ATP5B	56249	24	1091
	Q3ZCH0	Stress-70 protein; HSPA9	73696	5	260
	P35816	[Pyruvate dehydrogenase [acetyl-transferring]]-phosphatase 1; PDP1	61146	4	163
	P11966	Pyruvate dehydrogenase E1 component subunit beta; PDHB	39101	3	93

22	Q3ZCH0	Stress-70 protein; HSPA9	73696	3	168
	A7MB35	Pyruvate dehydrogenase E1 component subunit alpha; PDHA1	43360	2	88
23	P11178	2-oxoisovalerate dehydrogenase subunit alpha; BCKDHA	51646	12	530
	Q3ZCH0	Stress-70 protein; HSPA9	73696	9	402
	Q04467	Isocitrate dehydrogenase [NADP]; IDH2	50707	5	225
	Q29RK1	Citrate synthase; CS	51739	3	106
	A7MB35	Pyruvate dehydrogenase E1 component subunit alpha; PDHA1	43360	2	88
	P11966	Pyruvate dehydrogenase E1 component subunit beta; PDHB	39101	2	68
24	P11178	2-oxoisovalerate dehydrogenase subunit alpha; BCKDHA	51646	9	435
	Q3ZCH0	Stress-70 protein; HSPA9	73696	8	400
	A7MB35	Pyruvate dehydrogenase E1 component subunit alpha; PDHA1	43360	4	175
	Q29RZ0	Acetyl-CoA acetyltransferase; ACAT1	44860	2	140
	Q04467	Isocitrate dehydrogenase [NADP]; IDH2	50707	3	113
	P11966	Pyruvate dehydrogenase E1 component subunit beta; PDHB	39101	2	99
	Q8SPJ1	Junction plakoglobin; JUP	81769	3	82
	Q3MHX5	Succinyl-CoA ligase [GDP-forming] subunit beta; SUCLG2	46662	2	75
25	A7MB35	Pyruvate dehydrogenase E1 component subunit alpha; PDHA1	43360	26	1093
	P11966	Pyruvate dehydrogenase E1 component subunit beta; PDHB	39101	5	244
	P35705	Thioredoxin-dependent peroxide reductase; PRDX3	28177	4	196
	P00829	ATP synthase subunit beta; ATP5B	56249	3	186
	Q3ZCH0	Stress-70 protein; HSPA9	73696	3	130
	P21839	2-oxoisovalerate dehydrogenase subunit beta; BCKDHB	42908	2	97
26	P11966	Pyruvate dehydrogenase E1 component subunit beta; PDHB	39101	22	1048
	A7MB35	Pyruvate dehydrogenase E1 component subunit alpha; PDHA1	43360	20	860
	P21839	2-oxoisovalerate dehydrogenase subunit beta; BCKDHB	42908	3	120
	Q148J8	Isocitrate dehydrogenase 3 (NAD+) alpha; IDH3A	39672	2	93
	Q2KJ64	Arginase-1; ARG1	34987	2	66
	Q0IIB7	C13H20ORF7 protein (Fragment); C13H20ORF7	39096	2	55
27	P11966	Pyruvate dehydrogenase E1 component subunit beta; PDHB	39101	12	435
	Q32LG3	Malate dehydrogenase; MDH2	35646	9	385
	Q0P5A2	Ubiquinone biosynthesis methyltransferase COQ5; COQ5	37567	4	265
	A7MB35	Pyruvate dehydrogenase E1 component subunit alpha; PDHA1	43360	3	128
	Q2NL34	Ubiquinone biosynthesis protein COQ9; COQ9	35756	2	100

28	Q3T0B6	Complement component 1 Q subcomponent-binding protein; C1QBP	30587	7	298
	Q0II87	Transcription factor A; TFAM	28888	5	129
	Q3T0J3	39S ribosomal protein L16; MRPL16	28555	3	117
29	P00829	ATP synthase subunit beta; ATP5B	56249	2	95
30	Q01321	NADH dehydrogenase [ubiquinone] 1 alpha subcomplex subunit 4; NDUFA4	9319	6	260

4.6.   Quantification of the most abundant proteins from mitochondrial nucleoids

The protein constituents of the nucleoids from the central gradient fractions were separated by 2-D IEF/SDS-PAGE. The gels were fluorescence-stained by DeepPurple (Fig. 39) and SyproRuby (Fig. 40). Fluorescent staining with DeepPurple (Fig. 39) and SyproRuby (Fig. 40, shown after spot-picking and restaining with silver) allowed to quantify the relative amounts of more than 250 protein spots, and to identify about 90 of the most abundant nucleoid proteins by LC-MS/MS as summarized in Table 9. The LC-MS/MS analysis was performed by Dr. Heinrich Heide and Dipl.-Ing. Mirco Steger.

4.6.1. Quantification of the 53 most abundant nucleoid proteins according to DeepPurple staining

DeepPurple staining was used here to detect around 155 individual protein spots on a 2-D IEF/SDS gel (Fig. 39). Quantification based on the assumption that DeepPurple stain and protein amount are proportional. 53 different proteins were identified according to LC-MS/MS as summarized in Table 9. Proteins were considered as identified if at least two non-redundant peptides were characterized and Mascot scores were larger than 25 for each of the two peptides. The proteins were ranked according to their abundance relative to the most abundant protein Es1 (100%), which is based on the stain/mass ratio (311.4 in DeepPurple-stained gel, Fig. 39). For the ranking of proteins according to their abundance (stain/mass ratio) in Table 9, following points were considered: stain intensity values of individual spots were fully assigned only to the protein identified with highest score thus neglecting any contributions of all further less abundant proteins. Since individual proteins were often present at more than one place, the intensities of all relevant spots for an individual protein were summed up and listed as total stain intensity values in Table 9. Intensity values were not used for calculation (i) if no or only one single peptide was available to characterize a protein and (ii) if dust particles were removed from the spotmap by filtering spots with slopes <1.5 by DeCyder 7.0 DIA module. The total stain intensity of a specific protein was marked as non-reliable (NR) in Table 9 when only a single non-reliable intensity value was available. Total stain intensity values of some proteins were marked with the prefix (>) to indicate that several reliable intensity values have been summed up to give the indicated value and at least one non-reliable value was also present.
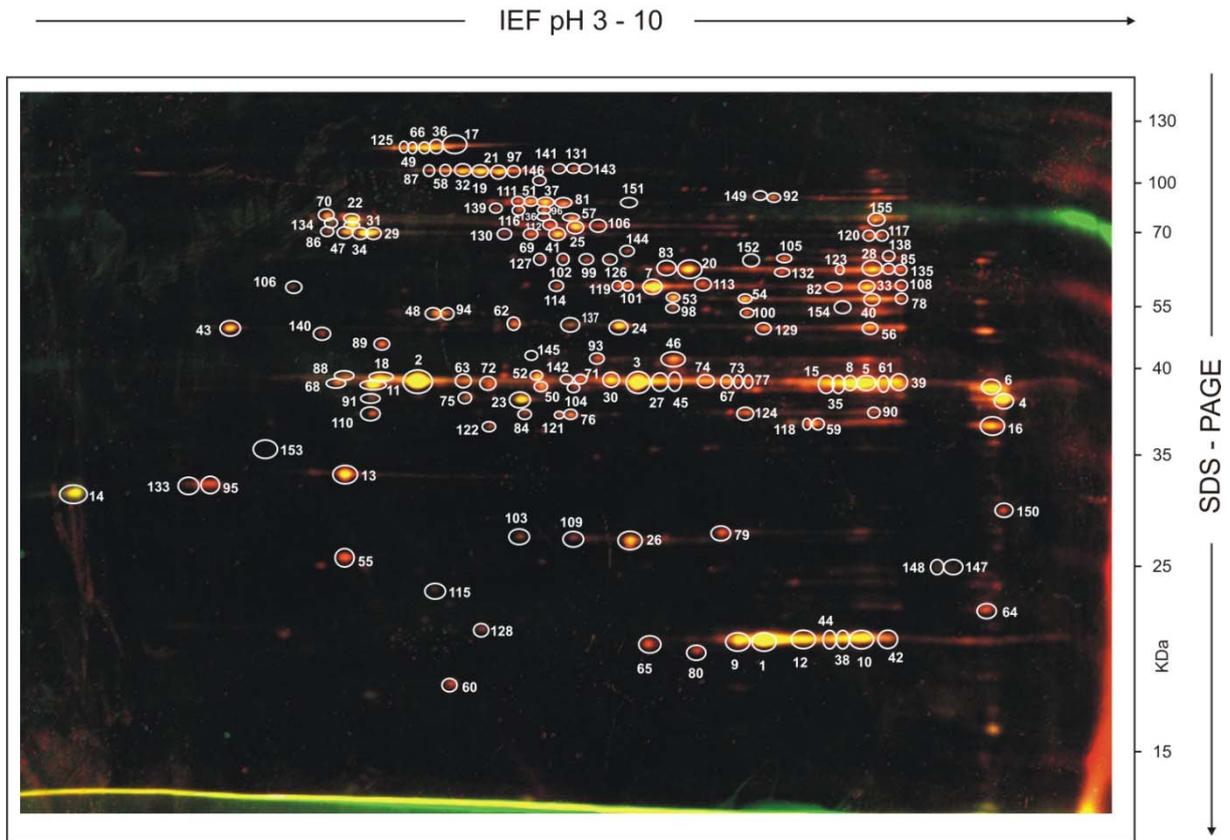
Figure 39. Detection of highly abundant nucleoid proteins by DeepPurple staining. A central gradient fraction (160 μg protein) was analyzed by IEF/Glycine-SDS polyacrylamide gel electrophoresis. The DeepPurple-stained 2-D gel was scanned with Typhoon 9400 scanner (GE HealthCare) and analyzed by DIA modul (Differential In-Gel Analysis) of the DeCyder^TM 2D 7.0 software (GE HealthCare) for densitometric quantification of fluorescence intensities of selected 155 clearly visible protein spots. The numbers indicate the spots picked for the analysis by LC-MS/MS after tryptic in-gel digestion.

The most abundant nucleoid proteins were the Es1 protein, a protein of the nucleic acid binding and modifying group, followed by elongation factor Tu, a protein of the ribosome/protein synthesis group (RiPS), three succinyl-CoA ligases and NADP-dependent isocitrate dehydrogenase involved in the carbohydrate metabolism (Table 9). None of these proteins, except elongation factor Tu, has been identified before as a component of mammalian mitochondrial nucleoids.

4.6.2. Quantification of further 40 highly abundant nucleoid proteins by SyproRuby staining

Since well known mitochondrial nucleoid components like mitochondrial transcripton factor (TFAM), single-stranded DNA-binding protein (mtSSB), DNA polymerase gamma were not identified in the DeepPurple-stained gel (Fig. 39), further protein spots were analyzed from a SyproRuby-stained 2-D IEF/SDS gel (Fig. 40).
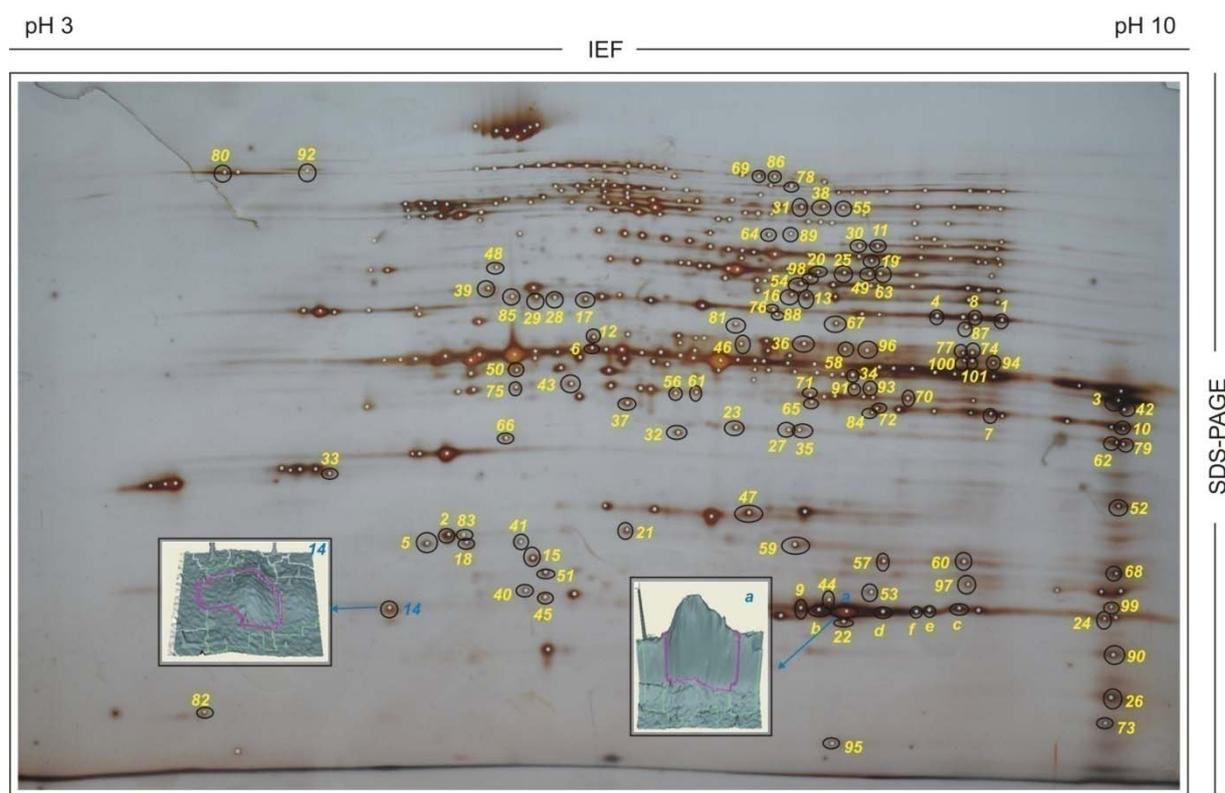
Figure 40. Detection of highly abundant nucleoid proteins by SyproRuby staining. A central gradient fraction (160 µg protein) was analyzed by 2-D IEF/glycine-SDS polyacrylamide gel electrophoresis. The SyproRuby-stained 2-D gel was scanned with Typhoon 9400 scanner (GE HealthCare) and analyzed by DIA modul (Differential In-Gel Analysis) of the DeCyder™ 2D 7.0 software (GE HealthCare) for densitometric quantification of fluorescence intensities of selected clearly visible protein spots. 101 protein spots, which were not detected by DeepPurple staining were picked and analyzed by LC-MS/MS. Spots *a-f* were picked as control for Es1 protein. Following the spot picking the gel was restained with silver. Examples of the peak images from the DeCyder analysis are shown for spots *a* (Es1) (Spot No: 4077; position: 1991, 1199; Volume: 1.354e+007; peak height: 12816; Area: 1441) and *14* (TFAM and NADH dehydrogenase [ubiquinone] iron-sulfur protein 8) (Spot No: 4127; position: 912, 1213; Volume: 1.326e+006; peak height: 2177; Area: 2087), respectively.

113

Based on the assumption that SyproRuby stain and protein amount are proportional, further 101 protein spots (Fig. 40, numbers in *italics*) that were not detected as individual spots in DeepPurple stain were analyzed on a SyproRuby-stained gel (Fig. 40, shown after spot picking and restaining with silver). Around 40 additional proteins (designated 54*-92* in Table 9) were identified by LC-MS/MS. Spots *a-f* were picked as a control for the Es1 protein. Aound 40 MS-identified proteins were ranked according to their abundance relative to the most abundant protein Es1 (100%), which is based on the stain/mass ratio (26064 in SyproRuby-stained gel, Fig. 40). For the ranking of the SyproRuby-stained gels, the same criteria were taken into account as described for the DeepPurple-stained gel (see above). Transcription factor A (93**) and DNA polymerase subunit gamma-2 (94**) were identified with 7 and 2 non-redundant peptides and Mascot scores of 252 and 110, respectively, together with NADH dehydrogenase [ubiquinone] iron-sulfur protein 8 (55*, Score 340) and NADH dehydrogenase [ubiquinone] flavoprotein 1 (69*, score 962). The mass spectra of Es1 and TFAM are shown in Figures 42 and 43, respectively. The Mascot-search results of all spots picked are shown in Appendix II on CD.
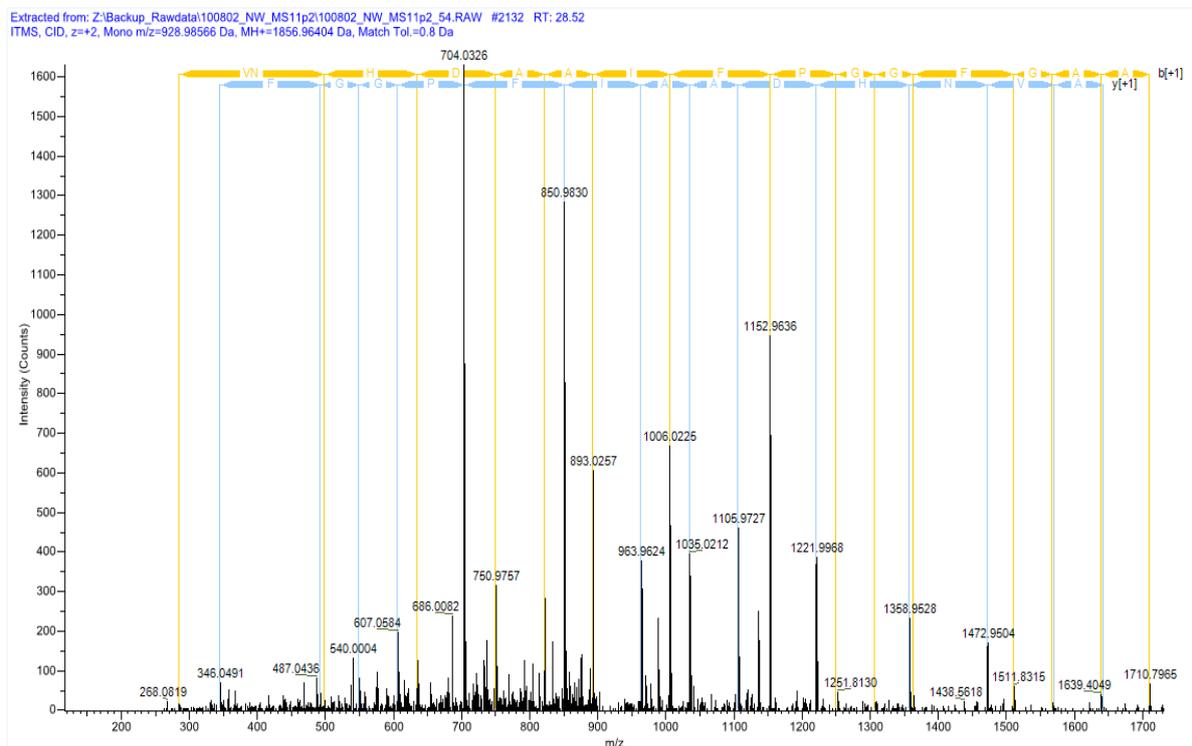
Figure 41. LC-MS/MS spectrum of Es1 protein. Spot number 1 from the DeepPurple-stained gel (Fig. 40) was picked for LC-MS/MS analysis as described in methods. 21 non-redundant peptides were found, which could be assigned to the Es1 protein. A spectrum of one of these peptides is exemplified here. This peptide was identified

11 times. The found sequence is: LTAVNHDAAIFPGGFGAAK; Charge: +2, Monoisotopic m/z: 928.98566 Da (-0.77 ppm), MH+: 1856.96404 Da, RT: 28.52 min, IonScore: 92, Fragment Match Tolerance: 0.8 Da; Es1 protein OS=*Bos taurus* GN=ES1 PE=2 SV=1 - [Q3T0U3_BOVIN].
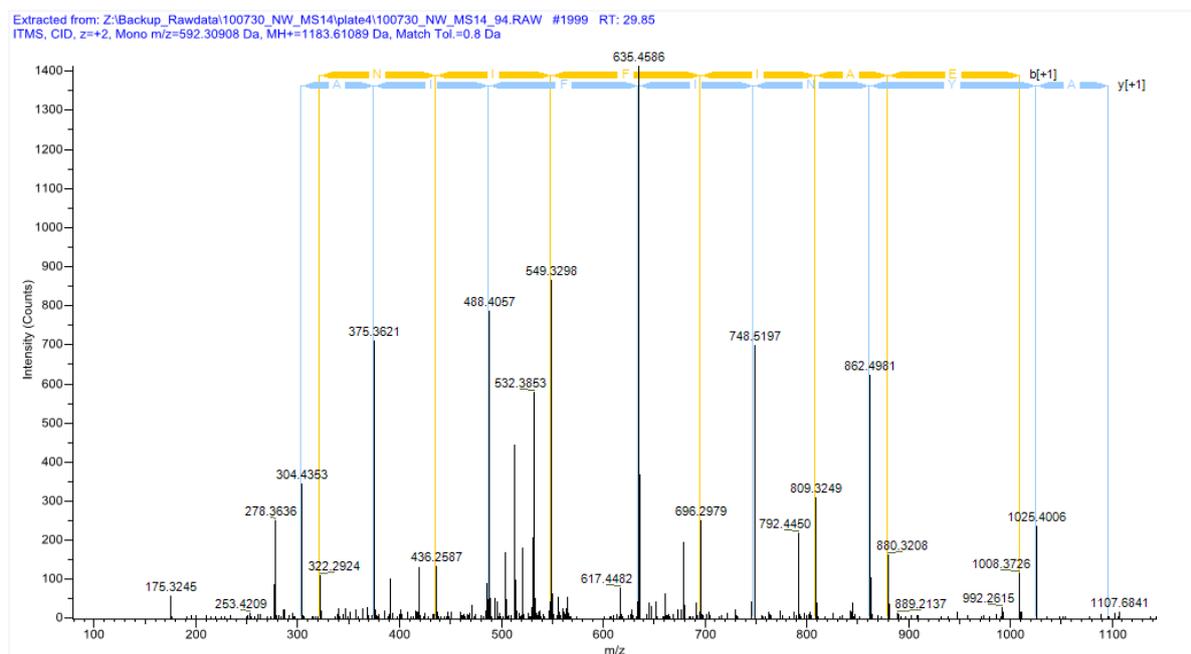
Figure 42. LC-MS/MS spectrum of TFAM. Spot number 14 from the SyproRuby-stained gel (Fig. 41) was picked for LC-MS/MS analysis. 7 non-redundant peptides were identified. One of them is shown here. The sequence of this peptide is: SAYNIFIAER; Charge: +2, Monoisotopic m/z: 592.30908 Da (+0.21 ppm), MH+: 1183.61089 Da, RT: 29.85 min,

IonScore: 69, Fragment Match Tolerance: 0.8 Da; Transcription factor A, mitochondrial OS=*Bos taurus* GN=TFAM PE=2 SV=1 - [TFAM_BOVIN]

Table 9. The most abundant proteins found in crude native nucleoids from bovine heart mitochondria. **Red**: Human homologues of the bovine mitochondrial proteins have been identified as nucleoid components before (Bogenhagen et al. 2008). **Mr**, precursor mass. **IP**, isoelectric point. Proteins were assigned to functional groups: **NAbm**, nucleic acid binding or modifying; **RiPS**, ribosomes and protein synthesis; **Carb**, carbohydrate metabolism; **OxPh**, oxidative phosphorylation; **Reg**, regulatory processes; **Pmd**, protein modification and degradation; **Lip**, lipid metabolism; **AA**, amino acid metabolism; **Keto**, ketone body metabolism; **Redox**, redox proteins; **X**, unknown function; **Chap**, chaperone; **Imp**, mitochondrial protein import.

No.	Protein; Gene	UniProt accession	Group	Mr (kDa)	IP	Protein spot numbers	Total stain	Stain/ mass	% of Es1
1	Es1 protein; ES1	Q3T0U3|Q3T0U3_BOVIN	NAbm	29.0	8.76	1, 9, 10, 12, 38, 44	9039	311.4	100
2	Elongation factor Tu, mitochondrial; TUFM	P49410|EFTU_BOVIN	RiPS	49.7	6.72	3, 5, 8, 15, 27, 30, 35, 39, 45, 61, 64, 67, 71, 73, 74, 77	>9838	>197.9	>63
3	Succinyl-CoA ligase [ADP-forming] subunit beta, mitochondrial; SUCLA2	Q148D5|SUCB1_BOVIN	Carb	50.4	6.73	2, 18, 23 68, 88, 142	6922	137.2	44
4	Succinyl-CoA ligase [GDP-forming] subunit alpha, mitochondrial; SUCLG1	Q58DR8|SUCA_BOVIN	Carb	36.5	9.41	4, 150	>2100	>57.5	>18
5	Isocitrate dehydrogenase [NADP], mito; IDH2	Q04467|IDHP_BOVIN	Carb	51.2	8.88	6	1727	33.8	10.9
6	Chaperone activity of bc1 complex-like, mitochondrial; CABC1	Q29RI0|ADCK3_BOVIN	OxPh	72.5	5.86	7, 33, 82, 89, 101, 108, 119, 144	2213	30.5	9.8
7	Succinyl-CoA ligase [GDP-forming] subunit beta, mitochondrial; SUCLG2	Q3MHX5|SUCB2_BOVIN	Carb	47.0	7.51	11, 63, 75, 90, 91	1384	29.4	9.4
8	Complement component 1 Q subcomponent-binding protein, mitochondrial; C1QBP	Q3T0B6|C1QBP_BOVIN	Reg	31.0	4.75	14	670	21.6	6.9
9	Stress-70 protein, mitochondrial; HSPA9	Q3ZCH0|GRP75_BOVIN	Chap	74.0	5.97	29, 31, 34, 47, 86	1524	20.6	6.6
10	Lon protease homolog, mitochondrial; LONP1	Q59HJ6|LONM_BOVIN	Pmd	107.2	6.22	19, 21, 32, 58, 87, 97, 125, 146	1992	18.6	6.0
11	Acyl-CoA synthetase family member 2, mitochondrial; ACSF2	Q17QJ1|ACSF2_BOVIN	Lip	68.9	7.88	20, 28, 83, 85, 123, 135, 152	>1189	>17.2	>5.5
12	Pyruvate dehydrogenase E1 component subunit beta, mitochondrial; PDHB	P11966|ODPB_BOVIN	Carb	39.4	6.21	13, 153	>678	>17.2	>5.5

117

#	Protein	Accession	Cat						
13	Lipoamide acyltransferase component of branched-chain alpha-keto acid dehydrogenase complex; DBT	P11181|ODB2_BOVIN	AA	53.8	8.45	24, 56, 62, 137	>817	>15.2	>4.9
14	3-oxoacid CoA transferase 1; OXCT1	Q24JZ7|Q24JZ7_BOVIN	Keto	56.9	8.57	40, 53, 54, 78, 154	>828	>14.6	>4.7
15	Isocitrate dehydrogenase [NAD] subunit gamma; IDH3G	Q58CP0|IDH3G_BOVIN	Carb	43.2	9.06	16, 118	>628	>14.5	>4.7
16	Elongation factor Ts, mitochondrial; TSFM	P43896|EFTS_BOVIN	RiPS	37.0	7.13	26	421	11.4	3.7
17	Glutathione S-transferase kappa 1; GSTK1	Q2KIW8|Q2KIW8_BOVIN	Redox	25.8		65, 80	280	10.9	3.5
18	Heat shock protein 75 kDa, mitochondrial; TRAP1	Q2TBI4|TRAP1_BOVIN	Chap	79.6	6.66	41, 69, 117, 120, 130	662	8.3	2.7
19	NADH-ubiquinone oxidoreductase 75 kDa subunit, mitochondrial; NDUFS1	P15690|NDUS1_BOVIN	OxPh	80.4	5.82	22, 70	657	8.2	2.6
20	Acyl-CoA synthetase short-chain family member 1; ACSS1	A4FUC5|A4FUC5_BOVIN	Lip	75.0	6.49	25, 107, 112	614	8.2	2.6
21	Isovaleryl-CoA dehydrogenase, mito; IVD	Q3SZI8|IVD_BOVIN	AA	47.0	7.1	50, 72, 104	>381	>8.1	>2.6
22	Pyruvate dehydrogenase E1 component subunit alpha, somatic form; PDHA1	A7MB35|ODPA_BOVIN	Carb	44.1	8.32	46, 93	357	8.1	2.6
23	Chromosome 1 open reading frame 93 ortholog; C16H1orf93	A4FUH8|A4FUH8_BOVIN	X	21.8		60	170	7.8	2.5
24	Inner membrane protein, Mitofilin; IMMT	A7E3V3|A7E3V3_BOVIN	X	83.4	6.37	37, 51, 111	>589	>7.1	>2.3
25	Prohibitin; PHB	Q3T165|PHB_BOVIN	Reg	29.8		55	192	6.4	2.1
26	Glutaminase; GLS	A0JN67|A0JN67_BOVIN	AA	67.0		99, 102, 114, 126, 127, 128	382	5.7	1.8
27	NDUFA10 protein (Fragment); NDUFA10	Q3SZE6|Q3SZE6_BOVIN	OxPh	38.0		84, 121	189	5.0	1.6
28	ATP synthase subunit beta; ATP5B	P00829|ATPB_BOVIN	OxPh	56.2	5.5	43	272	4.8	1.5
29	Ubiquinone biosynthesis methyltransferase COQ5; COQ5	Q0P5A2|COQ5_BOVIN	Lip	37.8		103, 109	175	4.6	1.5
30	Ubiquinone biosynthesis protein COQ9; COQ9	Q2NL34|COQ9_BOVIN	Lip	35.9		95, 133	166	4.6	1.5
31	Pyruvate dehydrogenase protein X component; PDHX	P22439|ODPX_BOVIN	Carb	54.1	8.64	48, 94	>242	>4.5	>1.4
32	NADH dehydrogenase [ubiquinone] iron-sulfur protein 2, mitochondrial; NDUFS2	P17694|NDUS2_BOVIN	OxPh	52.9		52	213	4.0	1.3
33	NAD-dependent deacetylase sirtuin-5; SIRT5	Q3ZBQ0|SIRT5_BOVIN	Pmd	34.6		79, 147, 148	>125	>3.6	>1.2
34	Methylmalonyl Coenzyme A mutase; MUT	Q0III1|Q0III1_BOVIN	AA	83.7		57, 136, 155	>240	>2.9	0.9
35	NADH dehydrogenase [ubiquinone] iron-sulfur protein 3, mitochondrial; NDUFS3	P23709|NDUS3_BOVIN	OxPh	30.4		115	81	2.7	0.9
36	Cytochrome bc_1 complex subunit 1; UQCRC1	P31800|QCR1_BOVIN	OxPh	53.4		89	108	2.0	0.6
37	Sorting and assembly machinery component 50 homolog; SAMM50	Q2HJ55|SAM50_BOVIN	Imp	52.3		98	97	1.9	0.6
38	Isocitrate dehydrogenase 3 (NAD+) alpha; IDH3A	Q148J8|Q148J8_BOVIN	Carb	40.1		122	75	1.9	0.6
39	28S ribosomal protein S22; MRPS22	P82649|RT22_BOVIN	RiPS	40.9		110, 134	>64	>1.6	>0.5
40	Ribosome-releasing factor 2, mitochondrial; GFM2	A6QNM2|RRF2M_BOVIN	RiPS	86.7		96, 116, 139	>134	>1.5	>0.5

118

No.	Protein	Accession	Cat	MW	pI	Peptides	Score		
41	2-oxoglutarate dehydrogenase; OGDH	Q148N0|ODO1_BOVIN	Carb	116.9		131, 141, 143	164	1.4	0.4
42	60 kDa heat shock protein, HSP60; HSPD1	P31081|CH60_BOVIN	Chap	61.2		106	87	1.4	0.4
43	Aconitate hydratase, mitochondrial; ACO2	P20004|ACON_BOVIN	Carb	86.0		92, 149	>106	>1.2	>0.4
44	Acyl-CoA synthetase family member 3; ACSF3	Q58DN7|ACSF3_BOVIN	Lip	65.5		113	81	1.2	0.4
45	ATP synthase subunit alpha; ATP5A1	P19483|ATPA_BOVIN	OxPh	59.8		129	68	1.1	0.4
46	G-rich RNA sequence binding factor 1; GRSF1	A0JNI7|A0JNI7_BOVIN	NAbm	53.5		140	52	1.0	0.3
47	Carnitine acetyltransferase; MGC142781	Q08DN5|Q08DN5_BOVIN	Lip	71.4		132	66	0.9	0.3
48	Carnitine O-palmitoyltransferase 2; CPT2	Q2KJB7|CPT2_BOVIN	Lip	75.0		105, 138	>54	>0.7	>0.2
49	5-lipoxygenase (Fragment); ALOX5AP	Q9BEG3|Q9BEG3_BOVIN	Reg	50.6		59	NR	NR	NR
50	Pyruvate dehydrogenase phosphatase regulatory subunit, mitochondrial; PDPR	O46504|PDPR_BOVIN	Carb	99.8		81, 151	NR	NR	
51	Methylmalonate-semialdehyde dehydrogenase [acylating], mitochondrial; ALDH6A1	Q07536|MMSA_BOVIN	AA	58.5		100	NR	NR	NR
52	Isocitrate dehydrogenase [NAD] subunit beta; IDH3B	O77784|IDH3B_BOVIN	Carb	42.8		124	NR	NR	NR
53	BCKDHA protein (Fragment); BCKDHA	Q2TBT9|Q2TBT9_BOVIN	AA	51.7		145	NR	NR	NR
1*	Es1 protein; ES1	Q3T0U3|Q3T0U3_BOVIN	NAbm	29.0	8.76	*a, b, c, d, e, f*	26064	899	100
54*	Abhydrolase domain-containing protein 11; ABHD11	Q3SZ73|ABHDB_BOVIN	Pmd	33.5		*57, 60, 68*	2069	61.8	6.9
55*	NADH dehydrogenase [ubiquinone] iron-sulfur protein 8; NDUFS8	P42028|NDUS8_BOVIN	OxPh	23.9		*14*	1326	55.5	6.6
56*	DNA polymerase delta interacting protein 2; POLDIP2	A5D9H9|A5D9H9_BOVIN	NAbm	41.9		*27, 35*	1864	44.5	4.9
57*	28S ribosomal protein S26; MRPS26	Q3SZ86|RT26_BOVIN	RiPS	23.8		*24*	999	42.0	4.7
58*	Uncharacterized protein C2orf47 homolog; C2orf47	A3KN05|CB047_BOVIN	X	32.9		*15*	1324	40.2	4.5
59*	Fumarate hydratase; FH	Q148D3|Q148D3_BOVIN	Carb	54.6		*58, 73, 77, 96*	2077	38.0	4.2
60*	Coenzyme Q10 homolog A (S. cerevisiae); COQ10A	Q1RMM6|Q1RMM6_BOVIN	Lip	27.1		*26*	967	35.7	4.0
61*	NADH dehydrogenase [ubiquinone] flavoprotein 2; NDUFV2	P04394|NDUV2_BOVIN	OxPh	27.3		*45*	810	29.7	3.3
62*	Peptide methionine sulfoxide reductase; MSRA	P54149|MSRA_BOVIN	Redox	25.8		*53*	775	30.0	3.3
63*	Ornithine aminotransferase; OAT	Q3ZCF5|OAT_BOVIN	AA	48.0		*12*	1374	28.6	3.2
64*	Dihydrolipoyllysine-residue succinyltransferase component of 2-oxoglutarate dehydrogenase complex; DLST	P11179|ODO2_BOVIN	Carb	48.9		*17*	1292	26.4	2.9
65*	Quinone oxidoreductase-like protein 2	A6QQF5|QORL2_BOVIN	Redox	37.6		*32*	931	24.8	2.8
66*	Peptidyl-prolyl cis-trans isomerase F; PPIF	P30404|PPIF_BOVIN	RiPS	22.2		*73*	556	25.0	2.8
67*	28S ribosomal protein S31; MRPS31	P82925|RT31_BOVIN	RiPS	43.6		*23*	1041	23.9	2.7
68*	ECH1 protein (Fragment); ECH1	Q3T172|Q3T172_BOVIN	Lip	37.5		*47*	788	21.0	2.3
69*	NADH dehydrogenase [ubiquinone] flavoprotein 1; NDUFV1	P25708|NDUV1_BOVIN	OxPh	50.6		*67, 87*	975	19.3	2.2

70*	Citrate synthase; CS	Q29RK1|CISY_BOVIN	Carb	51.7	34	929	18.0	2.0
71*	Ferrochelatase; FECH	P22600|HEMH_BOVIN	OxPh	46.9	42	840	17.9	2.0
72*	Glycerate kinase; GLYCTK	Q2KJF7|GLCTK_BOVIN	Carb	54.7	29	944	17.3	1.9
73*	Isobutyryl-CoA dehydrogenase; ACAD8	Q0NXR6|ACAD8_BOVIN	AA	45.3	56	772	17.0	1.9
74*	NADH dehydrogenase [ubiquinone] 1 alpha subcomplex subunit 10; NDUFA10	P34942|NDUAA_BOVIN	OxPh	39.2	61	684	17.4	1.9
75*	Isochorismatase domain-containing protein 2; ISOC2	Q32KX0|ISOC2_BOVIN	AA	22.4	90	359	16.0	1.8
76*	2-oxoisovalerate dehydrogenase subunit alpha; BCKDHA	P11178|ODBA_BOVIN	AA	51.6	46	807	15.6	1.7
77*	Aminomethyltransferase; AMT	P25285|GCST_BOVIN	AA	42.8	91, 93	673	15.7	1.7
78*	Cat eye syndrome chromosome region, candidate 5 isoform 2; CECR5	Q58D58|Q58D58_BOVIN	X	42.5	65	613	14.4	1.6
79*	[Pyruvate dehydrogenase [acetyl-transferring]]-phosphatase 1; PDP1	P35816|PDP1_BOVIN	Carb	61.1	48	785	12.8	1.4
80*	28S ribosomal protein S10; MRPS10	P82670|RT10_BOVIN	RiPS	23.0	95	277	12.0	1.3
81*	Ubiquinone biosynthesis monooxygenase COQ6; COQ6	Q2KIL4|COQ6_BOVIN	Lip	51.1	81	464	9.1	1.0
82*	Coiled-coil-helix-coiled-coil-helix domain-containing protein 3; CHCHD3	Q5E9D3|CHCH3_BOVIN	X	26.1	97	214	8.2	0.9
83*	Cob(I)yrinic acid a,c-diamide adenosyltransferase; MMAB	Q58D49|MMAB_BOVIN	Pmd	26.6	99	202	7.6	0.8
84*	Serine hydroxymethyltransferase; SHMT2	Q3SZ20|GLYM_BOVIN	AA	55.6	88	366	6.6	0.7
85*	IARS2 protein (Fragment); IARS2	Q3SZJ1|Q3SZJ1_BOVIN	RiPS	56.1	92	338	6.0	0.7
86*	3-ketoacyl-CoA thiolase; ACAA2	Q3T0R7|THIM_BOVIN	Lip	42.1	94, 100, 101	>248	5.9	0.7
87*	SDHA protein; SDHA	Q2HJI1|Q2HJI1_BOVIN	OxPh	74.4	64, 89	>363	4.9	>0.5
88*	39S ribosomal protein L46; MRPL46	Q3SZ22|RM46_BOVIN	RiPS	31.7	21	NR	-	-
89*	GrpE protein homolog 1; GRPEL1	Q3SZC1|GRPE1_BOVIN	Imp	24.3	40	NR	-	-
90*	Prohibitin-2; PHB2	Q2HJ97|PHB2_BOVIN	Reg	33.3	52	NR	-	-
91*	Reticulon-4-interacting protein 1; RTN4IP1	Q0VC50|RT4I1_BOVIN	Redox	43.6	62, 79	NR	-	-
92*	Short-chain specific acyl-CoA dehydrogenase; ACADS	Q3ZBF6|ACADS_BOVIN	Lip	44.4	84	NR	-	-
							-	-
93**	Transcription factor A; TFAM	Q0II87|TFAM_BOVIN	NAbm	28.9	14	nd	-	-
94**	DNA polymerase subunit gamma-2; POLG2	Q0VC30|DPOG2_BOVIN	NAbm	54.6	67, 87	nd	-	-

The MS-identified proteins from both gels were assigned to functional groups (Table 9, Fig. 43): NAbm, nucleic acid binding or modifying; RiPS, ribosomes and protein synthesis; Carb, carbohydrate metabolism; OxPh, oxidative phosphorylation; Reg, regulatory processes; Pmd, protein modification and degradation; Lip, lipid metabolism; AA, amino acid metabolism; Keto, ketone body metabolism; Redox, redox proteins; X, unknown function; Chap, chaperone; Imp, mitochondrial protein import.
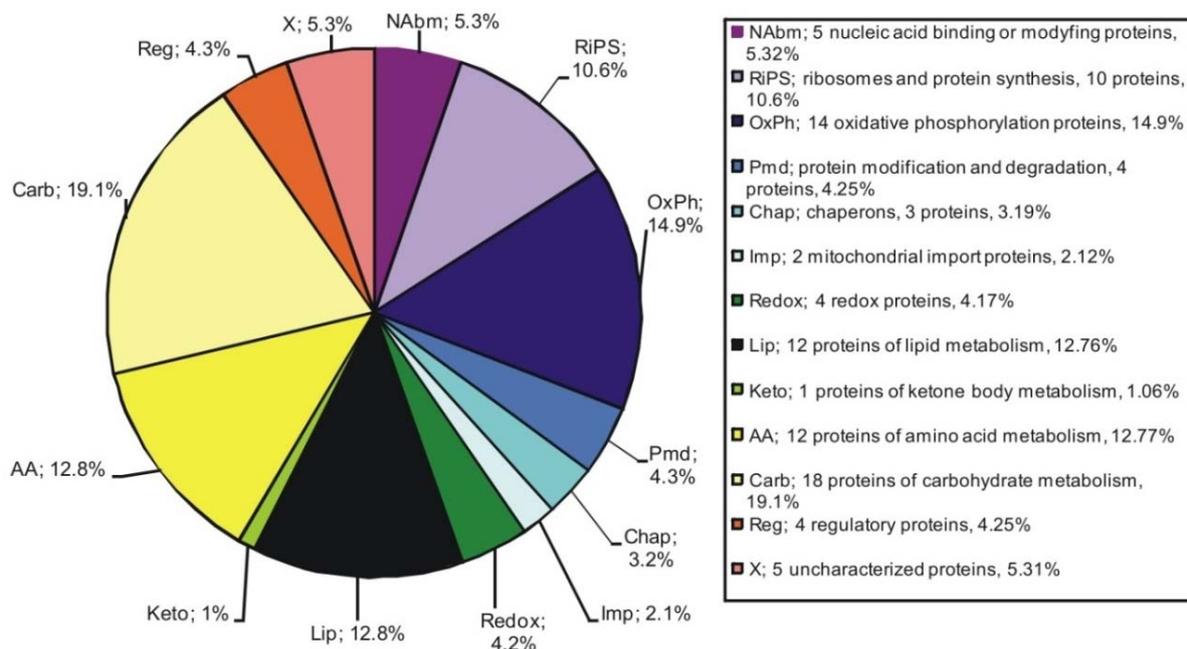
Figure 43. Sortiment of most abundant nucleoid proteins. The MS-identified 94 nucleoid proteins from 2-D IEF/SDS gels (Fig. 39, 40) were sorted in groups according to their presumed functional properties.

Five proteins (5.3% of 94 proteins) were assigned to the group of nucleic acid binding or modifying proteins. This group included DNA and RNA binding proteins, factors involved in replication and transcription, and especially several certified mt-nucleoid components like mitochondrial transcription factor A (TFAM, rank 93**), mitochondrial DNA polymerase subunit gamma-2 (POLG2, rank 94**). The most prominent protein in this group, however, was bovine homologue of human ES1 protein (Es1, rank 5) that was recognized here for the first time in a nucleoid fraction.

The very large carbohydrate metabolism group (18 proteins; 19.1%) included proteins of glycolysis, pyruvate dehydrogenase and tricarboxylic acid cyle.

The ribosome/protein synthesis group (10 proteins; 10.6%) comprised mitochondrial ribosomes, e.g., 28S ribosomal proteins S22 and S25 (ranks 39 and 89, respectively) and elongation factors, e.g., elongation factors Tu and Ts (ranks 2 and 8, respectively).

Fourteen proteins (14.9%) could be assigned to the system of oxidative phosphorylation. The most prominent identified proteins were ATP synthase subunits alpha and beta (ranks 45 and 28) and complex I subunits NDUFS1 and NDUFA 10 (ranks 19 and 27).

Four proteins (4.25%) were assigned to the protein modification and degradation group; three proteins (3.1%) as chaperones and two proteins (2.12%) as mitochondrial import proteins; further four proteins (4.17%) as redox proteins, and four proteins (4.25%) as regulatory proteins involved in signal transduction and further regulatory processes. Twelve proteins (12.76%) were assigned to the lipid metabolic group including enzymes of fatty acid biosynthesis and degradation, steroid hormone and ubiquinone biosynthesis. One protein (1%) was involved in ketone body biosynthesis and utilization; twelve proteins (12.77%) in amino acid synthesis, modification and degradation; five uncharacterized proteins (5.31 %) could not be assigned to the above protein classes.

4.7.   Confirmation of selected proteins as nucleoid components

Quantification of the nucleoid proteins seemed to suggest that the mitochondrial transcription factor A (TFAM) was not an abundant protein in nucleoids. Instead, the uncharacterized mitochondrial protein Es1 (Fig. 39, 40, Table 9) appeared as a major component. In order to follow up on this unexpected result, Western blot analysis of nucleoids on SDS gel was performed with polyclonal antibodies against TFAM and Es1, respectively (Fig. 44). For the separation of nucleoid proteins by SDS-PAGE, samples were concentrated as described in IV.4.1.1.

The antibody against TFAM detected two proteins with apparent masses around 42 kDa in fractions 4-7 and 52 kDa in low density fractions 9-11, respectively (Fig. 44, left panel). In the starting material (BHM) only the 52 kDa protein was detected. The detection of two proteins with different sizes by the antibody suggested that the smaller one might be a splice variant. A smaller isoform of human mitochondrial transcription factor has been reported where the exon 5 was missing (Tominaga et al., 1993). Virgilio et al., 2011, experimentally validated the presence of a 22 kDa TFAM isoform in a human cell line. It seemed that this isoform was enriched in central nucleoid fractions. Moreover, bovine mitochondrial

transcription factor (TFAM) is composed of 246 amino acids (UniProt), the precursor protein is 28.9 kDa and the mature protein is 24.3 kDa (ExPASy). There is a discrepancy between the molecular mass of TFAM and the molecular mass of the detected protein. This could only be explained by assuming that TFAM migrated as dimer in SDS gel, which is roughly double of the single protein size of 24 kDa and the presumed bovine 22 kDa isoform, respectively. Dimerization of proteins in SDS is very rare but the dimeric state of TFAM was also observed by others (see chapter V, Discussion).
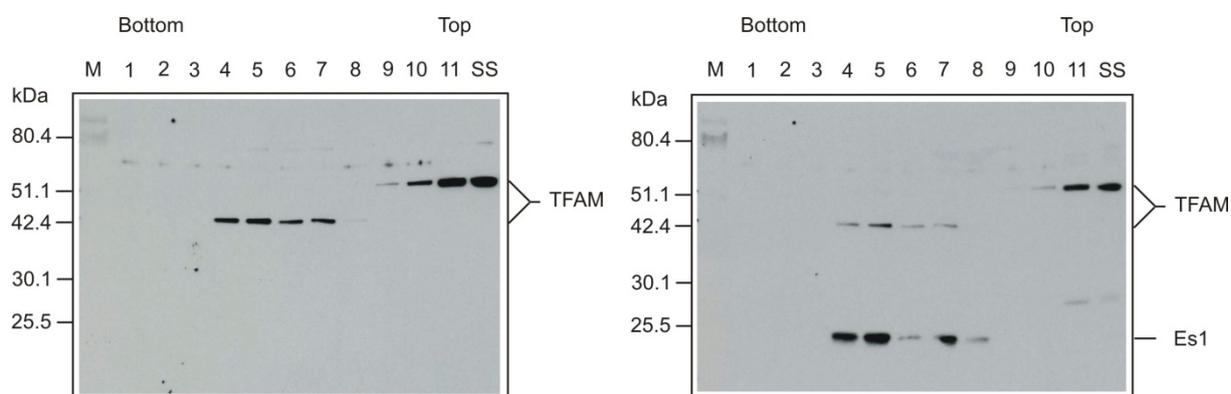
Figure 44. Western blot analysis of mitochondrial nucleoids using TFAM and Es1 antibodies. DDM-solubilized mitochondria were separated by sucrose density centrifugation. The eleven fractions were concentrated as described in Methods. 5 μg of each sample was applied per gel well of a 10 % acrylamide gel for Tricine SDS-PAGE. Polyclonal antibodies against TFAM (applied first, left panel) and Es1 (applied subsequently, right panel) were sequentially used for the detection. Peroxidase conjugated anti rabbit antibody was used as secondary antibody in 1:20000 dilution. M: PageRuler[TM] Prestained Protein Ladder (Fermentas); 1-11: gradient fractions 1-11; SS: start sample for the nucleoid separation.

Appling the antibody against Es1 on the same blot gave an additional signal in fractions 4-8 with an apparent mass around 24 kDa (Fig. 44, right panel). Bovine Es1 protein is composed of 274 amino acids (UniProt). It is proposed to be a mitochondrial protein (UniProt). However, mitochondrial targeting sequence of this protein was not shown. The first 47 amino acid sequences (labeled green in Fig. 46) could be assigned to the mitochondrial import sequence of bovine Es1 protein by sequence alignment of ES1 protein homologue from different organisms (Fig. 46). Known mitochondrial import sequences are labeled red and similar last three sequences are labeled blue. The molecular mass of the mature bovine Es1 (23.9 kDa) could be predicted by the program ExPASy, which is in full agreement with the detected band (Fig. 44). However, no protein was detectable by the anti-Es1 antibody in

starting material even by increasing protein amounts (30 μg or 60 μg protein per lane, not shown). Interestingly, Es1 seemed to be enriched in central nucleoid fractions 4 and 5, which corresponded to the PicoGreen profile of nucleoids (Fig. 28).

In order to exclude the possibility that TFAM was not released from mtDNA under the applied condition and thus the TFAM antibody detected the protein in the high molecular mass region, samples were treated under harsh conditions using a different protocol (Ekstrand et al., 2004). Briefly, samples were boiled at 95°C for 10 minutes and sonicated for 5 seconds before they were loaded on SDS gels. After transfer onto PVDF membranes, polyclonal antibodies against TFAM and Es1 were sequentially used on the same blot (Fig. 45).
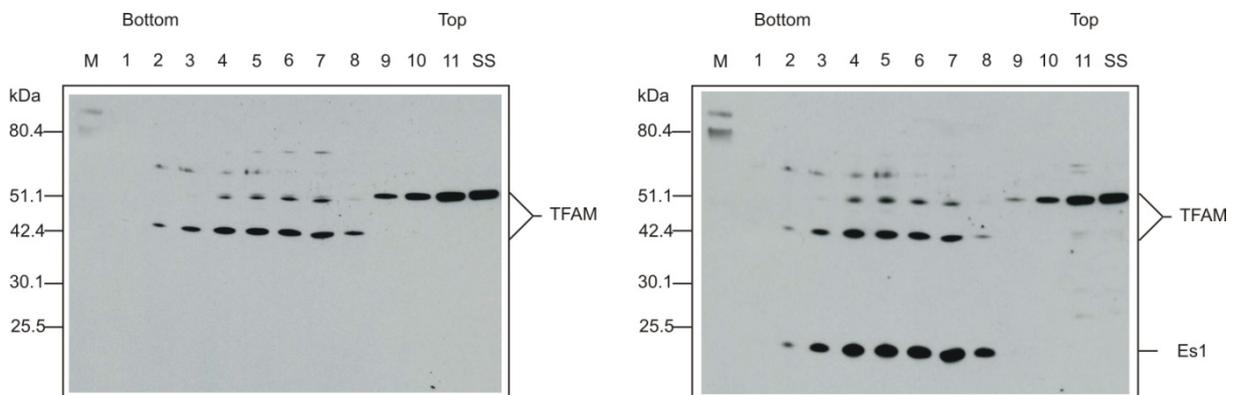
Figure 45. Western blot analysis of TFAM and Es1 from mitochondrial nucleoids under harsh condition. Sample preparation is the same as in Figure 44 except that samples were boiled and sonicated here before they were loaded on SDS gels. Polyclonal antibodies against TFAM (left panel) and Es1 (right panel) were sequentially used on the same blot for the detection. Peroxidase conjugated anti rabbit antibody was used as secondary antibody at 1:20000 dilution. M: PageRuler[TM] Prestained Protein Ladder (Fermentas). 1-11: gradient fractions 1-11; SS: start sample for the nucleoid separation.

After boiling and sonification, additional signals could be detected in fractions 4-7 with an apparent mass around 52 kDa (Fig. 45, right panel) suggesting that these nucleoid fractions contained not only the assumed TFAM isoform but also the full TFAM. However, the putative isoform of TFAM seemed to be more concentrated in nucleoid fractions.

```
R.norvegicus   MAAVRVLVSPRLA--------SALLPLSGRHRTTSQRAAIHSSAPRPRAR  42
M.musculus     MAAVRVLVAPRLA--------SALLPLSRYHRAPSQRAALHSSAPRPGAR  42
H.sapiens      MAAVRVLVASRLAAA------SAFTSLSPGGRTPSQRAALHLSVPRPAAR  44
B.taurus       MAAFRALAAARLAVTPGFAPRPGLWPLPFGGPAPSSRAAFHASAPRPGPR  50
               ***.*.*.:.***        ..: .*.    :.*.***:* *.*** .*


R.norvegicus   VALVLSGCGVYDGTEIHEASAILVHLSRGGAEVHIFAPDVPQMHVIDHTK  92
M.musculus     VALVLSGCGVYDGTEIHEASAILVHLSRGGAEVQIFAPDVPQMHVIDHTK  92
H.sapiens      VALVLSGCGVYDGTEIHEASAILVHLSRGGAEVQIFAPDVPQMHVIDHTK  94
B.taurus       VAVVLSGCGVYDGTELHEASSILVHLSRGGAEVQIFAPDVPQMHVIDHIK 100
               **:************:****:************:************** *


R.norvegicus   GEPSEKESRNVLAESARIARGKITNLAQLSAANHDAAIFPGGFGAAKNLS 142
M.musculus     GEPSERESRNVLAESARIARGKITSLAQLNAANHDAAIFPGGFGAAKNLS 142
H.sapiens      GQPSEGESRNVLTESARIARGKITDLANLSAANHDAAIFPGGFGAAKNLS 144
B.taurus       GQPSEGETRNVLTESARIARGKITDLAKLTAVNHDAAIFPGGFGAAKNLS 150
               *:*** *:****:************.**:*.*.*****************


R.norvegicus   TFAVDGKDCKVNKEVERVLKEFHGAKKPIGLCCIAPVLAAKVIKGVEVTV 192
M.musculus     TFAVDGKDCKVNKEVERVLKEFHGAKKPIGLCCIAPVLAAKVIKGVEVTV 192
H.sapiens      TFAVDGKDCKVNKEVERVLKEFHQAGKPIGLCCIAPVLAAKVLRGVEVTV 194
B.taurus       TFAVDGGTCKVNRDVERVLKEFHQAGKPIGLCCIAPVLAAKVLRGVEVTV 200
               ******  ****::********* * ****************::******


R.norvegicus   GHEQEEGGKWPYAGTAEAVKALGAKHCVKGVTEAHVDQKNKVVTTPAFMC 242
M.musculus     GHEQEEGGKWPYAGTAEAIKALGAKHCVKGVTEAHVDQKNKVVTTPAFMC 242
H.sapiens      GHEQEEGGKWPYAGTAEAIKALGAKHCVKEVVEAHVDQKNKVVTTPAFMC 244
B.taurus       GHEQEEGGKWPHAGTAEVIKALGAKHCVMGVTEAHVDQKNKVVTTPAFMC 250
               ***********:*****.:*********  *.******************


R.norvegicus   ETELHHIHDGIGAMVKKVLELTGK 266
M.musculus     ETALHHIHDGIGAMVKNVLELTGK 266
H.sapiens      ETALHYIHDGIGAMVRKVLELTGK 268
B.taurus       DTALHHIHDGIGAMVRKVLELAGR 274
               :* **:*********::****:*:
```

Figure 46. Amino acid sequence alignment of the ES1 protein homologue from various organisms. The UniProt sequences of *R.norvegicus* (Rat, Accession: P56571), *M.musculus* (Mouse, Accession: Q9D172), *H.sapiens* (Human, Accession: P30042) and *B.taurus* (Bovine, Accession: Q3T0U3) were aligned by the multiple sequence alignment program ClustalW. Invariant (*), highly (:) and weakly similar (.) positions are labeled. Mitochondrial protein import sequence for bovine Es1 protein was predicted (green) by comparing the known protein import sequences (red) from other organisms. The last common 3 amino acid sequences were labeled blue.

125

V.   Discussion

1.   Two-dimensional native electrophoresis

A classical straightforward approach to analyze the subunit composition of complexes is the separation of native complexes by BNE in the first dimension followed by resolution of the subunits by Tricine-SDS-PAGE for the second dimension. However, higher order structures like respiratory chain supercomplexes or oligomeric ATP synthase are often too complex for this two-step approach and introducing a further step for the initial separation of proteins in the native state seemed advisable.

The complexity of the supramolecular structures can be reduced by a two-dimensional blue native electrophoresis (2-D BNE/modified BNE or 2-D BN/BNE, Schägger and Pfeifer, 2000, 2001). Since modified BNE (DDM was added to the cathode buffer) is less mild than BNE, supercomplexes dissociate into the individual complexes during the second dimension modified BNE (Schägger and Pfeifer, 2000, 2001). The big disadvantage of this BNE/modified BNE system is that the cathode buffer for the second dimension contains 0.02% DDM and Coomassie-dye, which interferes with the detection of fluorescence-labeled proteins and with in-gel assays on native gels. The cathode buffer for hrCNE, however, contains mixed micelles from 0.05% sodium desoxycholate (DOC) and 0.02% dodecylmaltoside (DDM) and no Coomassie-dye could bind to substrates in the activity assay, as observed with the binding of Coomassie-dye to cytochrome c in the complex IV assay. Therefore, two already existing native electrophoresis systems (BNE and hrCNE) were combined here to a two-dimensional native electrophoresis (2-D BN/hrCNE) with special advantages for the first or second dimensional separation of biological membrane complexes.

The two systems (2-D BN/BNE and 2-D BN/hrCNE) are similar in some aspects. Firstly, both of the second dimensional resolutions of modified BNE and hrCNE are less mild than first dimension BNE. Supercomplexes therefore dissociate into the individual complexes. Secondly, these 2-D gels comprising two orthogonal native dimensions are useful in determining the stoichiometry of complexes in supercomplexes (Schägger and Pfeiffer, 2000). The essential advantage of the 2-D BN/hrCNE system, however, lies in the Coomassie-free 2-D native gel, which enhances detection of fluorescence-labeled proteins considerably and provides optimal conditions for in-gel assays.

Stripes from these 2-D native gels can be used for 3-D SDS-PAGE to identify known and novel accessory subunits of supercomplexes. For example, one previously unknown subunit of *S. cerevisiae* supercomplex, Cox26, was identified by using 3-D BN/BN/SDS-PAGE (Kadeer et al., manuscript in preparation). 2-D native gels comprising two orthogonal native dimensions can also be followed by doubled SDS-PAGE (dSDS-PAGE, Rais et al., 2004) comprising two orthogonal SDS gels to generate a 4-D system, as exemplified in this work (Fig. 12) to uncover the subunit composition of supercomplexes or individual membrane protein complexes. The two orthogonal SDS gels separate the hydrophobic subunits from the diagonal of the hydrophilic subunits. This additional purification step improves the separation of hydrophobic from hydrophilic proteins and therefore improves the identification of hydrophobic proteins by mass spectrometry (Rais et al., 2004). This 4-D system was used here to identify protein interaction partners of Cox26 within complexes (Kadeer et al., manuscript in preparation) and it was also successfully used recently to identify two novel accessory proteins of mammalian ATP synthase (Meyer et al., 2007).

In conclusion, the development of the two-dimensional native electrophoresis system (2-D BN/hrCNE), which is native in both dimensions, turned out to be very useful for the proteomic analysis and component analysis of membrane protein complexes either for the detection of fluorescence-labeled proteins or by allowing for catalytic activity assays of complexes in native gels. Using these methods, new mitochondrial supercomplexes could be identified and characterized in the aerobic yeast *Y. lipolytica* (Nübel et al., 2009). Since individual complexes can be released from the supercomplexes thus reducing complexity, this two-dimensional native gel electrophoresis simplifies the analysis of the components of supercomplexes.

2.   Native immunoblotting of blue native gels (NIBN)

Protein complexes can be solubilized from biological membranes using mild detergents. Depending on the detergent, even fragile membrane supramoclecular structures like respiratory supercomplexes or respirasomes can be mobilized from mitochondrial membranes of eukaryotic cells (Schägger and von Jagow, 1991; Schägger et al., 1994; Wittig et al., 2006b). The solubilized mitochondrial complexes can then be purified by blue native gel electrophoresis (BNE). For the analytical study of the protein complexes the proteins isolated by BNE can be transferred from the native gel onto a suitable membrane where they can be

detected by specific antibodies. Although protein complexes are still active after transfer to the membrane, the subsequent removal of Coomassie-dye from the membrane, which is an obligatory step before immunological detection, destroys the native state of many proteins. Thus the current Western blot protocols do not allow for screening for conformation-specific antibodies, which play an important role in structural biology because of their ability to bind to native protein complexes. In this study we aimed at modifying the protocol in such a way that protein complexes retain their 3-D structure after transfer from gel to membrane. We selected complex I, the largest and most complicated enzyme of the respiratory chain of mitochondria from the yeast *Y. lipolytica* as a test model for the development of a native immunoblotting method.

Following the separation of individual mitochondrial complexes and native electroblotting, the essential step in the native immunoblotting of blue native gels (NIBN) followed: the processing of the blot membrane for immune-reactivity analysis. This step was substantially modified. The mild detergents Tween 20, digitonin and Brij 35 (Fig. 16) were applied instead of methanol for the obligatory removal of Coomassie-dye. Retention of the native state of complex I could be shown by in-gel assay (Fig. 16) and by immuno-reactivity of complex I on the membrane with the help of conformation-specific antibodies (Fig. 17).

Antibody 31A8 has been characterized by native ELISA (Zickermann et al., 2010) to bind exclusively to the native complex I. We could identify the epitope of the monoclonal antibody 31A8 by using a three-dimensional gel electrophoresis (BN/SDS/SDS-PAGE) and LC-MS/MS (Fig. 22, Fig. 50 in Appendix I). The gel electrophoretic/Western blot analysis and LC-MS/MS finding contributed to the determination of the subunit position by 2D average electron microscopic analysis of complex I/mab co-complexes and to the determination of the topological arrangement of the accessory subunits in the membrane arm of the huge complex I (Angerer et al., 2011).

Monoclonal antibody 31A8 seems to be sensitive to the way how denaturation was achieved. For example, the antibody could not identify the NUPM subunit of complex I (CI) when the commonly used harsh protocols to denature CI by SDS were applied (Fig. 19B). But it clearly recognized the NUPM subunit when CI was isolated by BN-PAGE and then resolved by SDS-PAGE in the second dimension (Fig. 21), or by dSDS-PAGE (Fig. 22). It seems that the constituent subunits of the big CI in dSDS-PAGE separate from each other differently if the complex is transferred from BN-PAGE to the SDS-PAGE in the second dimension. This discrepancy might be explained by some attenuation of the denaturing properties of SDS

following BN-PAGE, since (i) lipids bound to membrane proteins after BN-PAGE (Wittig et al., 2010b) may exert a shielding effect against SDS, and (ii) the SDS concentration reaching the proteins during 2-D separation after BN-PAGE (0.1% SDS in the cathode buffers of Glycine-SDS-PAGE (Laemmli, 1970) and Tricine-SDS-PAGE (Schägger, 2006) are low compared to the 1.5% SDS concentrations of common SDS incubation protocols. This view is also supported by the recovery of non-covalently linked complexes of hydrophobic proteins, like a ring of 10 c-subunits associated with the a-subunit following BN-PAGE and 2-D SDS-PAGE or dSDS-PAGE (Wittig et al., 2008). The availability of the epitope of the monoclonal antibody after blue native gel electrophoresis followed by doubled SDS gel electrophoresis might also be explained as follows: sequence based analysis revealed that the NUPM subunit contains cysteine motives, which are characteristic of proteins imported into the intermembrane space of mitochondria via the Mia40 pathway (Herrmann and Koehl, 2007). Complex I was incubated with 130 mM DTT (dithiothreitol) prior to dSDS-PAGE. It can not be excluded that the reduction of the cysteine residues makes the antibody accessible to its binding site.

In conclusion, using a set of monoclonal antibodies against respiratory complex I, we showed that the new technique of native immunoblotting of blue native gels (NIBN) preserves the native state of complex I. This was demonstrated by the conservation of NADH:NTB oxidoreductase activity (complex I activity, Fig. 16) and binding of three different conformation-specific antibodies 31A8, 40G5 and 44G10 (Fig. 17). Therefore the new technique can be used as a straightforward extension of the repertoire of blue native electrophoresis and gives us a simple alternative method to monitor the conformation-specific recognition of a protein by antibodies. Unlike the time consuming native ELISA, which is also used to screen for conformation-specific antibodies, it is not necessary to introduce appropriate affinity tags and to purify the target protein by chromatography. As BNE is well suited to deal with complex samples (Wittig et al., 2006a) this NIBN technique is especially useful for projects requiring a microscale approach and for proteins that are not easily accessible to genetic manipulation.

3.   Multi-dimensional gel electrophoresis for protein interaction studies

Here it is demonstrated how multi-dimensional electrophoretic techniques are used to identify non-covalent and covalent protein-protein interactions. Two native dimensions (1-D BNE and 2-D modified BNE) were used here to isolate native membrane protein complexes directly from biological membranes. This simple two-step native electrophoresis, performed on a micro-scale, can replace multi-step chromatographic isolation protocols that otherwise have to be established in time consuming optimization trials and have to be carried out on a much larger preparative scale. We also show that three-dimensional BN/BN/SDS-PAGE offers great advantages to the component analysis of multiprotein complexes and facilitates the identification of novel components, as exemplified with Cox26 (Fig. 23). Furthermore, 3-D BN/BN/SDS gels give valuable qualitative and quantitative information on covalent and non-covalent interactions of protein components, as exemplified with the interaction of Cox26 and subunits of cytochrome *c* oxidase (Fig. 26). Four-dimensional BN/BN/SDS/SDS-PAGE applying reducing and non-reducing conditions for the final 4-D SDS-PAGE was found to be a valuable means to identify inter-protein disulfide bridges, like a disulfide linkage between Cox26 and Cox2 (Fig. 27).

We show that most of the Cox26 protein was non-covalently bound to the complex IV moiety of the respirasomes and minor amounts of it used the single cysteine residue in the center of a predicted transmembrane helix (Fig. 23D) to form a disulfide bond with the Cox2 subunit of complex IV. It seems that Cox26 plays a specific role for CIV. Concerning the function of Cox26 for CIV a lot of functional studies were performed by our group. However, no pronounced phenotype for Cox26 deficiency was observed. In this respect Cox26 resembles several of the proteins found in respiratory chain complexes with unknown functions. The 6.4 kDa subunit of bovine complex III, for example, can be removed from the complex without affecting ubiquinol:cytochrome *c* reductase activity (Schägger et al., 1990). Similarly, deletion strains of subunits e, g, and k of yeast ATP synthase do not reveal a specific phenotype. Growth and catalytic activity of the null mutants are unchanged (Arnold et al., 1998). For subunits e and g, at least a structural role for the dimerization of ATP synthase has been established.

Similarly, based on the structural models (Fig. 47, 48) and knowing that Cox2 is an interaction partner of Cox26, we postulate a structural role of Cox26 protein for the

assembly/stability of respiratory strings or patches, i.e. the assembly of respirasomes into even larger structures. Evidence for the existence of respiratory strings or patches has been presented before (Wittig et al., 2006b; Nübel et al., 2009; Bultema et al., 2009; Dudkina et al., 2010).

A model for the association of complexes III and IV in respirasomes (Fig. 47) and the binding of Cox26 protein (Fig. 48) was made by Dr. Heike Angerer from our group.
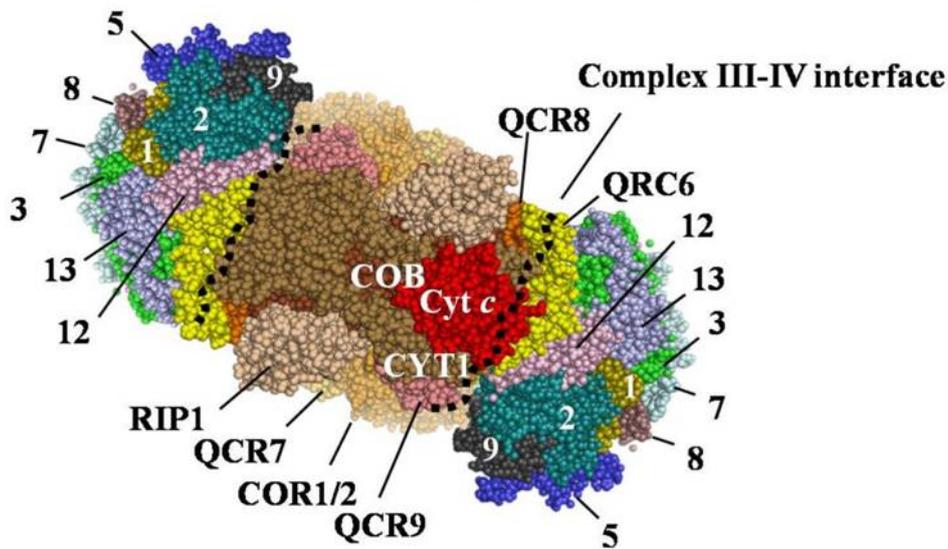
Figure 47. Model for the association of yeast complexes III and IV in respirasomes. The interface of complexes (dotted black line) comprises cytochrome c_1 (CYT1), hidden transmembrane parts of cytochrome b (COB), and all three hydrophobic subunits of complex IV, Cox1 (1), Cox2 (2), and Cox3 (3). QCR6 and cytochrome c (Cyt c) cover the transmembraneous complex III-IV interface. RIP1, Rieske iron-sulfur protein. Core proteins 1 and 2 (COR1/2) and QCR6-9 of complex III, and the subunits Cox5 (5), Cox7-9 (7-9), Cox12 (12), and Cox13 (13) of complex IV. The model was generated based on structural information of yeast complex III (Solmaz and Hunte, 2008) and bovine complex IV (Tsukihara et al., 1996) using the software PyMOL Molecular Graphics System, Version 1.2, Schrödinger, LLC. This model was prepared by Dr. Heike Angerer from our group.
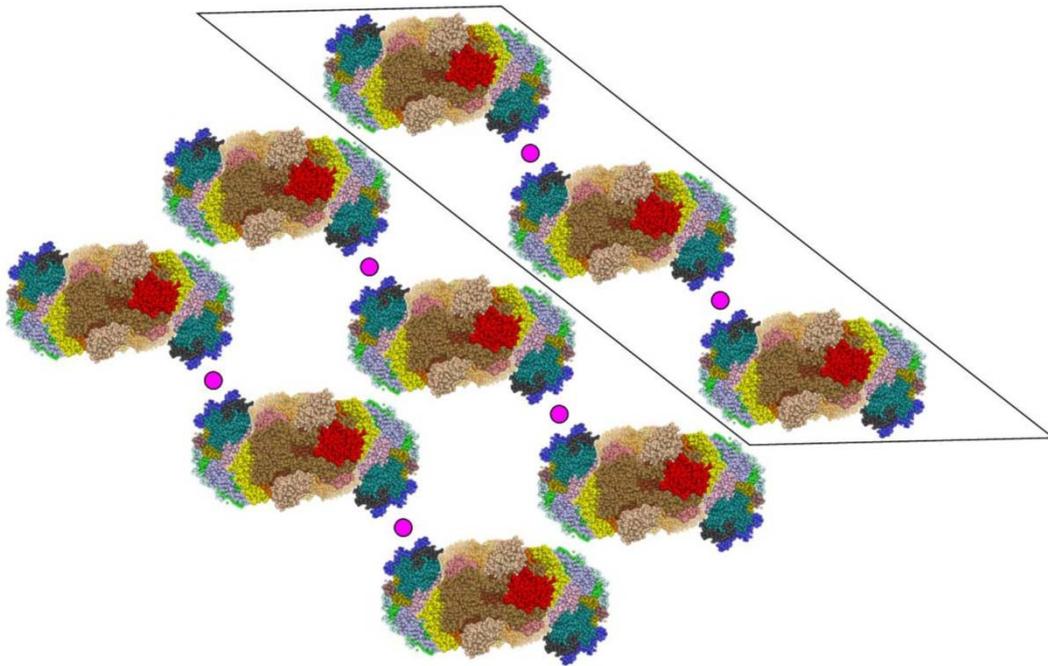
Figure 48. Model for the association of respirasomes into respiratory strings (boxed) or patches. Association of respirasomes into respiratory strings may involve the hydrophobic transmembrane helix of Cox26 protein (red dot), which is involved in disulfide bonding with Cox2. Further association of respiratory strings into respiratory patches may involve interactions of subunits of complex IV, especially Cox3, Cox7, and Cox13. This model was prepared by Dr. Heike Angerer from our group.

Experimental verification of this model for the association of respirasomes into respiratory strings (boxed) or patches is difficult at present, since a protocol to isolate respiratory strings or patches from yeast mitochondria, which is prerequisite to such studies, is not yet available. However, it seems promising to modify a recent protocol for the isolation of putative respiratory strings or patches from bovine mitochondria (Strecker et al., 2010).

4. Structure and composition of native nucleoids from bovine heart mitochondria

It is not easy to achieve the purification of nucleoids in their native state. This is one of the main reasons why so little is known about the composition and structure of nucleoids so far. Furthermore, purification of mammalian mt-nucleoids has mainly been attempted using only one type of cells, the rapidly growing tumor derived cell lines. Since nucleoid organization may differ between postmitotic, fully differentiated animal tissues such as heart and cells from rapidly growing human cell lines, we isolated nucleoids from bovine heart mitochondria. It was also of considerable advantage that protocols to isolate large amounts of highly pure mitochondria were available.

In this work, much emphasis was put on the elaboration of gentle approaches that were developed to isolate nucleoids in their native state. In order to preserve non-covalent DNA-protein and transient protein-protein interactions and to retain native structure of nucleoids, mitochondria were solubilized at very low ionic strength (IV.4.1). Since nucleoids are anchored to the inner mitochondrial membrane (Albring et al., 1977) and we intended to remove contaminating components of the mitochondrial membrane as completely as possible, we used the non-ionic detergent dodecylmaltoside (DDM) for the solubilization of mitochondria and not the commonly used detergents Triton X-100 and Nonidet NP-40. In contrast to Triton X-100 and Nonidet NP-40, DDM does not preserve supercomplexes and oligomeric forms of ATP synthase, which would later be difficult to remove from nucleoids by differential centrifugation because of their similar sedimentation properties. Following solubilization, nucleoids were separated by differential centrifugation on sucrose density gradients and by the newly developed blue native electrophoresis on large pore gels, which offers considerably higher resolution compared to density gradient centrifugation.

4.1. Native nucleoids show moderate differences in size

Blue native gel electrophoresis on large pore gels has been shown to separate protein complexes with sizes up to around 50 MDa (Strecker et al., 2010). Applying the new gel system to purify mt-nucleoids revealed distinct bands of mt-nucleoid particles on the BN gel and thus indicated that the pores of large pore gels were sufficiently large to separate even extremely large complexes such as nucleoids. These particles showed minor differences in

migration distance/particle size (Fig. 31). Mass estimation of nucleoids on the native gels revealed apparent masses of 30-36 MDa indicating that the prepared nucleoids differed moderately in size (Fig. 32, Tables 5 and 6). This is in agreement with the microscopical observation of nucleoids in living cells (Legros et al., 2004; Holt et al., 2007; Brown et al., 2011). Electron microscopy of isolated nucleoids from yeast also showed size variations (Miyakawa et al., 1987).

The observed size differences may be explained by differential binding of loosely attached proteins and complexes such as pyruvate dehydrogenase complex (P), oxoglutarate dehydrogenase complex (O), monomeric ATP synthase (M), and respiratory complexes I, III, and IV. These complexes and other proteins were identified as loosely attached components of nucleoids, since these components were released from nucleoids during blue native gel electrophoresis and identified by MS (Fig. 38, Table 8). Loose attachment of mitochondrial complexes to nucleoids means that smaller or larger amounts of mitochondrial complexes can be dissociated from the mt-nucleoids during BNE thereby reducing the amounts of mitochondrial complexes relative to the central mt-nucleoid components. However, complete removal of the loosely attached components under conditions preserving the native state of nucleoids has never been achieved. Major amounts of associated components or contaminations always remained bound to the nucleoids (see Appendix II on CD).

4.2.   mtDNA copy number per mt-nucleoid

It has been reported that nucleoids in the human cell system contain one to ten copies of mtDNA (Satoh and Kuroiwa, 1991; Bereiter-Hahn and Vöth, 1996; Legros et al., 2004; Iborra et al., 2004; Gilkerson et al., 2008). Most of these estimations were generated by quantification of the mtDNA copy number per cell and dividing by the number of nucleoids per cell. The disadvantage of this estimation is that, depending on the resolution of the microscope used in counting the number of nucleoids per cell, small nucleoids might be easily overlooked whereas closely spaced two or three nucleoids might be miscounted as one, thus ending up in different results.

The copy number of mtDNA within a nucleoid from bovine heart mitochondria can be deduced from the estimated mass of nucleoids on native gels. Using 325 Da for the average mass of one nucleotide and 650 Da for one base pair, the 16.6 kb mammalian mtDNA has a mass of 10.79 MDa. Assuming that bovine mitochondrial nucleoids comprise equal amounts of DNA, RNA and protein, as shown for yeast (Miyakawa et al., 1987), the 33 MDa bovine

heart mt-nucleoid should not contain more than one complete 16.6 kb double-stranded mt-DNA. This result is in agreement with a recent report of the group of Larsson, who applied high-resolution microscopy to determine the mtDNA number (Kukat et al., 2011). Our results also support the so called faithful nucleoid model (Jacobs et al., 2000; Gilkerson et al., 2008), in which nucleoids, as a general rule, do not exchange genomes with each other, suggesting that the inheritable unit of mtDNA in animal tissue is one. However, it is worth to mention that the estimation of the mtDNA copy number per nucleoid is based on the very preliminary mass estimation of mt-nucleoids on native gels. The mass estimation of mt-nucleoids must be regarded as crude approximation because of following reasons: (i) The acrylamide gradient in the upper area of the large pore gel is not linear, since a uniform 2% acrylamide gel layer was layered of top of the gradient gel for stability reasons (Strecker et al., 2010). Therefore, it is highly probable that the true mass is bigger than estimated. (ii) Although the soluble pyruvate dehydrogenase complex of mitochondria (10 MDa), the largest complex that we used for the mass calibration, fits the regression line almost ideally and gives the impression that the calibration is essentially linear up to 10 MDa or even beyond, the proposed linearity over the whole mass range cannot be verified experimentally due to the absence of well-defined membrane protein markers for the 10-50 MDa mass range (Strecker et al., 2010). (iii) Since bound Coomassie-dye can equal or even exceed the mass of a membrane protein moiety (Heuberger et al., 2002; Wittig and Schägger, 2008a; Wittig et al., 2010a) it seems likely that nucleoids also bind large amounts of Coomassie-dye and the total nucleoid mass including bound dye may be considerably larger than the apparent mass. In conclusion, the 33 MDa just sets the minimal value for the nucleoid mass and the deduced mtDNA copy number, one mtDNA per nucleoid, has to be regarded with caution.

4.3.   Structural analysis of bovine heart mt-nucleoids

Only a few reports have been published on the size of mitochondrial nucleoids in mammals. Confocal microscopy studies suggest a size of 0.1 to 0.3 μm for cells transfected with Twinkle-GFP or imaged with antibodies against TFAM or mtSSB (Garrido et al., 2003) and a size of 0.4 to 0.9 μm for cells imaged with PicoGreen and antibodies against DNA (Holt et al., 2007).

Recent studies (Iborra et al., 2004) involving anti-DNA immunogold electron microscopy (EM) reported sizes of 70 nm of single nucleoids. EM analysis of mouse and human cells showed that nucleoids have a size of 60-90 nm (Prachar, 2010). Recent studies based on

super-resolution microscopy reported that mammalian nucleoids are ovoid or ellipsoidal structures with average diameter of 70 nm (Kukat et al., 2011; Brown et al., 2011).

Our EM analysis of bovine heart mt-nucleoids from sucrose gradient fractions showed surprisingly homogenous particles with a size around 85 x 115 nm as observed in negative stain (Fig. 34B), and a size of 100 x 150 nm as observed in the cryo-EM images (Fig. 34D). The different sizes of nucleoids observed for the two sample preparations are expected, since the sample is dehydrated during the process of negative staining and thus shrinks in size. This is particularly severe for DNA samples, which are highly hydrated molecules. The sizes measured by the cryo-preservation method are thus more accurate as the DNA remains in a hydrated state. In spite of the apparent homogeneity of nucleoids in negative stain and in cryo-EM images, moderate molecular mass differences of individual nucleoids, as observed on native gels, seem possible (Fig. 31).

Further cryo-tomographic analysis of nucleoids showed that nucleoids consist of closely packed spheres of approximately 70 nm in diameter (Fig. 35B). This is in good agreement with published nucleoid sizes from both EM and high-resolution microscopy, if we assume that native nucleoids had been dissociated during purification. Our approach has following advantages compared to other structural analysis of mt-nucleoids. (i) Electron microscopy enabled resolution well below the diffraction barrier of confocal microscopy and the so called high-resolution microscopies. (ii) Isolated nucleoids have the advantage that they involve no cell sectioning technique, which makes determination of nucleoid size difficult since the analyzed ultra thin sections often contain part of the nucleoid (Prachar, 2010).

4.4.   Protein composition analysis of nucleoids

The protein composition of bovine heart mt-nucleoids was analyzed by a number of complementary approaches to identify core nucleoid components, peripheral nucleoid components and easily dissociating proteins. Native and/or denaturing gel electrophoresis (BN-large pore/Tricine-SDS-PAGE) was coupled to high sensitivity mass spectrometry (LC-MS/MS) to carry out a comprehensive protein component analysis.

Protein component analysis of BNE-repurified nucleoid (33 MDa band from BNE on large pore gels, Fig. 36) revealed the presence of several proteins with known roles in mtDNA replication and transcription such as mitochondrial transcription factor A (TFAM), mitochondrial dimethyladenosine transferase 2 (TFB2M), mitochondrial dimethyladenosine transferase 1 (TFB1M), mitochondrial DNA polymerase subunit gamma-2 (POLG2),

mitochondrial single-stranded DNA-binding protein (SSBP1), and C26H10ORF2 protein (Twinkle). These proteins have been identified as core nucleoid components from mammalian mt-nucleoids in several biochemically isolated nucleoid preparations (Garrido et al., 2003; Tyynismaa et al., 2004; Wang and Bogenhagen, 2006; Kasashima et al., 2008; Bogenhagen et al., 2008) and served as a positive control.

Assigning the MS-identified proteins to their potential functional properties (Fig. 36, right panel) revealed that more than 20% of the identified proteins belong to the ribosome/protein synthesis group, which contained an almost complete set of subunits of mitochondrial ribosomes, suggesting that the nucleoids contained significant amounts of mitochondrial ribosomes. Despite the fact that mitochondria have a relatively low content of ribosomes (Attardi and Schatz, 1988) association of a quite large number of mitochondrial ribosomal proteins and mitochondrial ribosomal recycling factors with nucleoids have also been reported by several other groups (Wang and Bogenhagen, 2006; Rorbach et al., 2008; Bogenhagen et al., 2008). This indicates that there might be a significant physical association between nucleoids and ribosomes. The identification of an almost complete set of mitochondrial ribosomal proteins that copurified with native nucleoids can be explained by a so called transertion model. The term transertion originated from a model of bacteria where transcription, translation, and membrane insertion of nascent proteins are coupled (Lynch and Wang, 1993; Woldringh, 2002). Possible occurrence of this coupling has been shown in yeast mitochondria (Bryan et al., 2002). Recently, it has been reported that mitochondrial ribosomal protein L12 (MRPL12) acted as a transcription-translation coupling factor in human mitochondria (Wang et al., 2007). This protein was identified here as a nucleoid component. This supports the idea that mammalian nucleoids may be held near the inner membrane by a coupled transcription-translation process analogous to bacterial and yeast transertion as noted by Bogenhagen, 2011.

Almost 15% of MS-identified proteins were assigned to the oxidative phosphorylation system. Remarkably, almost half of the identified proteins in this group were the subunits of complex I, despite the fact that this is the least abundant respiratory complex (Hatefi, 1985; Schwerzmann et al., 1986). This can be explained by the fact that complex I contains more mtDNA-encoded subunits than any other complex. Although subunits of oxidative phosphorylation complexes were often found by analysis of mt-nucleoids, they have generally been suspected as contaminants of mt-nucleoids. However, their abundance (confirmed by protein quantification, Table 9) suggested that proteins of mitochondrial complexes I-V are also associated with mt-nucleoids. Recently, Bogenhagen et al., 2008, proposed a layered

structural model of nucleoid organization (Fig. 5) suggesting that respiratory complexes might be assembled on the periphery of nucleoids. This layered model can help explain why subunits of oxidative phosphorylation complexes are copurified with mt-nucleoids.

A pioneering work by the Attardi group (Albring et al., 1977) showed the association of mtDNA with the mitochondrial inner membrane. Several studies postulated the presence of an mtDNA "tether" protein, which would link the nucleoid with the mitochondrial inner membrane (Iborra et al., 2004; Legros et al., 2004; Prachar, 2010; Brown et al., 2011). The identification of subunits of mitochondrial complexes I-V and other mitochondrial inner membrane components such as the ATAD3 and the adenine nucleotide translocase (ANT) with high amounts (Table 10 in Appendix I) in native nucleoids, however, favours an unspecific attachment of mt-nucleoides to the inner mitochondrial membrane and makes a tether protein very unlikely. The suggested unspecific association of nucleoids to the entire membrane via multiple binding sites may potentially contribute to the stability of nucleoids as suggested by electron microscopy: the native 100x150 nm nucleoid particles (Fig. 34D) are relatively stable but coisolated with many membrane proteins. Further purification of the native nucleoids induced dissociation into 70 nm structures (Fig. 35B), which might constitute the nucleoid core. Isolation of these 70 nm particles will be difficult because of their instability. Potentially, this instability is related to the removal of those mitochondrial membrane components that were classified here as loosely associated or contaminating proteins.

Several other membrane proteins such as the inner membrane protein Mitofilin and the outer membrane assembly factor Sam 50 could also be identified in nucleoid fractions. The human homologue of Mitofilin has already been identified as a nucleoid component (Wang and Bogenhagen, 2006), whereas Sam 50 was recognized here in a nucleoid fraction. Regarding the identification of these proteins in nucleoid fractions, some functional similarities between mammals and yeast could be drawn: In yeast, the outer membrane protein Mmm1 has been shown to be involved in the assembly of beta-barrel proteins in the outer mitochondrial membrane (Meisinger et al., 2007). In mammals, Sam 50 is a beta-barrel protein and crucial in sorting and assembly of the outer membrane machinery (Xie et al., 2007). Moreover, the yeast protein Mmm1 has been reported to be important to maintain both normal mitochondria and nucleoid shape (Burgess et al., 1994; Hobbs et al., 2001). Interestingly, in mammals Mitofilin has been proposed to be involved in cristae morphology (John et al., 2005) and its association with Sam 50 in mitochondria has recently be confirmed (Xie et al., 2007). This would suggest that Sam 50 might be involved in maintenance of nucleoid structure. Mmm1

seems to play a role in mtDNA segregation (Hobbs et al., 2001). Our results suggested that Sam 50 might have an important functional role in mammalian mt-nucleoids. It is possible that Sam 50 enables interactions of nucleoids across both mitochondrial membranes as shown for Mmm1 in yeast (Hobbs et al., 2001).

Mmm1 is a member of the endoplasmatic reticulum (ER)-mitochondria encounter structure (ERMES) tethering complex, which has recently been identified in yeast (Kornmann et al., 2009). It has been proposed that ERMES is involved in the regulation of mtDNA replication (Kornmann et al., 2011). It is possible that mammalian nucleoids are involved in such an ER-mitochondria junction structure, in which nucleoids associate with inner membrane proteins such as Mitofilin, ANT and the outer membrane proteins Sam50, VDAC 1 and 2, which were abundantly identified in our nucleoid preparation.

Protein composition analysis of nucleoids also identified some cytoskeletal proteins as nucleoid components, which might be regarded as contaminants. On the other hand cytoskeletal proteins have frequently been identified from mitochondrial proteomics research (Taylor et al., 2003; Mootha et al., 2003; Ponamarev et al., 2005) suggesting their localization in mitochondria. It is known that mitochondria can be transported within cells through cytoskeletal elements (reviewed by Boldogh and Pon, 2007; Liesa et al., 2009). The identification of a number of cytoskeletal associated proteins from bovine heart mt-nucleoids in this study, from Hela cells (Bogenhagen et al., 2008) and from rat liver even by high salt lysis method (Reyes et al., 2011) would suggest that these cytoskeletal elements might enter the mitochondria to form direct contacts with nucleoids as proposed by Reyes et al., 2011.

Other proteins contained in the native nucleoid were classified as carriers, transporters, channels, and mitochondrial import proteins. The identification of these proteins can be explained by a model proposed by Iborra et al., 2004. According to this model, nascent mitochondrial proteins synthesized on cytoplasmic ribosomes are imported into mitochondria through import channels located in the vicinity of nucleoids as a means to coordinate respiratory complex assembly. It is interesting to note that this model has similarities with the above mentioned ERMES complex. This model is also similar to the proposal that nucleoids associate with both mitochondrial membranes. These models together suggest a coordination of mtDNA maintenance with mitochondrial translation, cytoplasmic translation, protein import and assembly of respiratory complexes.

A number of chaperones were also identified in our nucleoid preparation. This group included proteins with mtDNA-binding ability such as HSP60 (Kaufman et al., 2003), proteins

involved in mtDNA stability such as the yeast homologue of DNAJ (Duchniewicz et al., 1999), and proteins involved in nucleoid stability (Kasashima et al., 2008), mitochondrial structure (Merkwirth et al., 2008), and a wide variety of cellular functions, including apoptosis, cell cycle regulation, signal transduction, and lifespan regulation (Czarnecka et al., 2006) such as the chaperon prohibitin. Identification of these proteins in nucleoid fractions implies that nucleoids participate in essential cellular processes beyond mitochondria.

Even lower abundant proteins (reviewed by Bogenhagen, 2011) known to function in mtDNA maintenance and repair, including ribonuclease H1 (RNASEH1) and several DNA damage-specific glycosylases were identified in our nucleoid preparation, highlighting the sensitivity of our approach.

Protein composition of crude mt-nucleoids (sucrose gradient fraction) showed high similarity with that of BNE-repurified nucleoids. One might expect that, in crude mt-nucleoids, the amount of mitochondrial complexes (loosely attached) relative to central mt-nucleoid components is considerably higher than after repurification by BNE on large pore gels. However, large differences were not identified by MS although some removal of mitochondrial complexes during BNE was detected. MS analysis of crude nucleoids identified additional proteins, which presumably are best regarded as contaminants. However, identification of the protein NIPSNAP1 that has been found to associate with mt-nucleoids from rat liver (He et al., 2007; Reyes et al., 2011) only in crude nucleoid fraction (Table 10) indicated the importance of protein component analysis of the crude mt-nucleoids.

In short, our approach of using mitochondria enriched tissue for the detection of low abundant proteins and applying high sensitivity MS techniques enabled us to find a wide array of proteins together with mt-nucleoids. Our gentle approach to purify nucleoids doesn't allow us to distinguish whether the identified proteins are intrinsic or peripheral components or simply contaminants in case they are just stoichiometrically abundant or sticky. Proteomics results have to be combined with functional studies to verify the bona fide components.

4.5. Quantification of the most abundant nucleoid proteins

In order to identify low and high abundant nucleoid proteins, and to give a ranking of the most abundant mt-nucleoid proteins, fluorescence based quantification analysis was applied on 2-D IEF/SDS gels (Fig. 39, 40). It was expected that the fluorescent staining of all proteins separated on 2-D gels were proportional to the amount of the respective proteins. Therefore we quantified proteins according to their staining intensity. It seems that SyproRuby showed

higher sensitivity because more protein spots (4682) were detected compared to staining with DeepPurple (2420). Although TFAM and mitochondrial DNA polymerase gamma subunit 2 (POLG2) were identified they were not included in the list of the 90 most abundant proteins. This suggested that there are major differences between species or tissues especially concerning the amount of TFAM.

4.6. TFAM is not a major component of bovine heart mt-nucleoids

Although it is well known that TFAM is an important factor for mtDNA transcription its role in nucleoid as mtDNA packaging factor is quite contradictory. Several studies reported a correlation of TFAM levels with mtDNA copy number, for example, in patients (Larsson et al., 1994), in transgenic mice (Ekstrand et al., 2004), and in cell culture (Pohjoismäki et al., 2006). Others reported varying ratios of TFAM per mtDNA (Table 1) like 1700 TFAM/mtDNA (Takamatsu et al., 2002) to 35 TFAM/mtDNA (Maniura-Weber et al., 2004). It was argued that variation among methods used in the determination of the stoichiometry between TFAM and mtDNA may cause these differences. However, it seems also possible that the TFAM amount varies between species, tissues and cells. Our results from protein quantification clearly indicated that bovine heart mt-nucleoids contained quite low amount of TFAM excluding the possibility that TFAM functioned as an mtDNA packaging factor in the fully differentiated heart tissue.

Western blot analysis of TFAM on SDS gels showed that TFAM was isolated as a dimer (Fig. 44). Dimerization of proteins under SDS conditions has so far been observed only in very hydrophobic c-ring of ATP synthase. Dimerization of such a basic protein as TFAM under the quite stringent conditions used (boiling and sonification, Fig. 45) cannot be explained yet. TFAM was thought to act as a monomer (Fisher and Clayton, 1988). However, Kaufman et al., 2007, showed that TFAM functions as a homodimer (47.78 kDa) using Western blot analysis and size exclusion chromatography. Our results are in full agreement with the latter. Kaufman et al., 2007, observed TFAM monomer (24 kDa) only when it was purified in high salt buffers (500 mM NaCl) for the size exclusion chromatography. They argued that the difference between their results and the original work describing TFAM as a monomer (Fisher and Clayton, 1988) was caused by the fact that TFAM lost its DNA-binding activity and was unstable under the conditions used by Fischer and Clayton. Interestingly, the Western blot analysis of TFAM in this work (Fig. 44, 45) showed a smaller isoform that was enriched in the nucleoid fraction but hardly detectable in isolated mitochondria. Tominaga et al., 1993,

reported that the part corresponding to the helix 1 of HMG-box domain 2 (HMG2) is missing in human TFAM splice variant (Fig. 49; Rubio-Cosials et al., 2011). It has been proposed that TFAM organizes mtDNA into nucleoid structure via bending DNA upon binding to U-form thus fulfilling its architectural function in packaging of mtDNA. It could be shown that strong bending of the DNA is dependent on HMG box2 (Hallberg and Larsson, 2011; Ngo et al., 2012). Amino acid sequence alignment of human TFAM and its isoform with bovine TFAM showed high sequence similarity (Fig. 49). Database search could not clarify whether the detected putative bovine TFAM splice variant also contains part of HMG box2. It seemed that the TFAM splice variant does not act as mtDNA packaging protein. Further investigations are required to characterize the isoform in more detail.

```
HUMAN           MAFLRSMWGVLSALGRSGAELCTGCGSRLRSPFSFVYLPRWFSSVLASC PKKPVSSYLRF  60
HUMAN_ISOFORM   MAFLRSMWGVLSALGRSGAELCTGCGSRLRSPFSFVYLPRWFSSVLASCPKKPVSSYLRF  60
BOVIN           MALLRGVWGVLNALGKSGADLCAGCGSRLRYPFSFAYVPKWFSSSLSGY PKKPMTSYVRF  60
                **:**.:****.***:***:**:******* ****.*:*:**** *:. ****::**:**

HUMAN           SKEQLPIFKAQNPDAKTTELIRRIAQRWRELPDSKKKIYQDAYRAEWQVYKEEISRFK EQ 120
HUMAN_ISOFORM   SKEQLPIFKAQNPDAKTTELIRRIAQRWRELPDSKKKIYQDAYRAEWQVYKEEISRFKEQ 120
BOVIN           SKEQLPIFKAQNPDAKNSELIKKIAKLWRELPDSEKKIYEDAYRADWQVYKEEINRIQ EQ 120
                ***************.:***::**: ******:****:*****:******** .*::**

HUMAN           LTPSQIMSLEKEIMDKHLKRKAMTKKKELTLLGK PKRPRSAYNVYVAERFQE AKGDSPQE 180
HUMAN_ISOFORM   LTPSQIMSLEKEIMDKHLKRKAMTKKKELTLL-------------------------E 153
BOVIN           LTPSQMVSLEKEIMQKRLKKKALIKKRELTMLGK PKRPRSAYNIFIAERFQEARDGTSQV 180
                *****::********:*:**:**: **:***:*

HUMAN           KLKTVKENWKNLSDSEKELYIQHAKEDETRYHNEMKSWE EQMIEVGRKDLLRRTIKKQRK 240
HUMAN_ISOFORM   KLKTVKENWKNLSDSEKELYIQHAKEDETRYHNEMKSWEEQMIEVGRKDLLRRTIKKQRK 213
BOVIN           KLKAINENWKNLSNSQKQVYIQLAKDDKIRYYNEMKSWE EQMMEVGREDLIRRSIKYPAK 240
                ***::********:*:*::*** **:*: **:**********:****:**:**:**   *

HUMAN           YGAEEC 246
HUMAN_ISOFORM   YGAEEC 219
BOVIN           NDPEKF 246
                 ..*:
```

Figure 49. Amino acid sequence alignment of human and bovine TFAM. The UniProt sequences of bovine TFAM (Accession: Q0II87), human TFAM (Accession: Q00059), and human TFAM isoform (Tominaga et al., 1993) were aligned by the multiple sequence alignment program ClustalW. Invariant (*), highly (:) and weakly similar (.) positions are labeled. Sequnces for HMG1 are boxed in orange for human, yellow for bovine, whereas sequences for HMG2 are boxed in blue for human and green for bovine. Sequences for helix1 within HMG2 are marked red.

Detection of full length TFAM in nucleoid fractions only under a harsher treatment clearly demonstrated that more TFAM was released from mtDNA under the harsher conditions. It seemed that less DNA-binding proteins such as TFAM were detected on 2-D IEF/SDS gels, which were used to quantify proteins since these samples were prepared under milder conditions.

4.7.   Es1 is the most abundant bovine heart mitochondrial nucleoid protein

Both qualitative and quantitative analysis of the protein composition of mt-nucleoids revealed that the uncharacterized mitochondrial protein Es1 (UniProt, same as HES1/KNP-I) was the most abundant protein in mt-nucleoids from bovine heart. ES1 protein (note that ES1 and Es1 denote mitochondrial proteins of human and bovine, respectively) was first identified in zebra fish (Chang and Gilbert, 1997). Mitochondrial localization of bovine Es1 was shown by Ponamarev et al., 2005, where Es1 was identified as a potential RNA-binding protein. The human homologue of Es1 (ES1 protein homolog) has been shown to be involved in pathogenesis of the brain deficit in Down syndrome (Shin et al., 2004). We identified bovine Es1 not only as a nucleoid component but also as the most abundant nucleoid protein, highlighting an important functional role in nucleoids. The detection of Es1 in Western blots only in nucleoid fractions but not in mitochondria (Fig. 44, 45, right panels) suggested that Es1 is highly enriched in bovine heart nucleoids.

It is interesting to compare the DNA-binding proteins from bacteria with those from eukaryotes. In *E. coli*, HU and INT are histone-like proteins. In yeast and mammals, DNA is wrapped by the HMG-box proteins Abf2p and TFAM, respectively. It has been shown that expression of Abf2 in *E. coli* can compensate for a deficiency in HU protein (Megraw and Chae, 1993) while in the yeast *S. cerevisiae* deficiency of abf2p can be complemented by two metabolic proteins, ILv5 (Zelenaya-Troitskaya et al., 1995) and Aco1p (Chen et al., 2007). It is not yet known that any proteins can compensate for a TFAM deficiency in mammals. Analysis of nucleoids in *E.coli* identified a set of 12 major DNA-binding proteins. Some of the proteins in growing cells are replaced by others as cells enter stationary phase (Azam and Ishihama et al., 1999; Azam et al., 1999; Dillon and Dorman, 2010).

In eukaryotes mitochondrial nucleoids have been isolated mainly from yeast, Xenopus oocytes and in mammals from rapidly growing tumor derived cell lines. In that respect, the set of proteins associated with mitochondrial DNA reflects a composition required for continuous mtDNA replication and expression. Nucleoid organization may differ in differentiated and

postmitotic animal tissues such as heart compared to rapidly growing cancer cell lines or cells. Interestingly, it has recently been reported that the mRNA levels of ES1 increased during differentiation of the murine myoblast cell line C2C12, and that the detectable protein level was found only in fully differentiated myotubes (Kislinger et al., 2005). We assume that Es1 is a DNA wrapping protein and it replaces TFAM in mammals in postmitotic tissues like heart. However, detailed characterizations and further investigations of Es1 are required to clarify its role in mammalian nucleoids.

VI. References

1. Abrahams, J. P., Leslie, A. G. W., Lutter, R., and Walker, J. E. (1994) Structure at 2.8 Å resolution of F_1-ATPase from bovine heart mitochondria. *Nature* **370,** 621-628

2. Abdrakhmanova, A., Zickermann, V., Bostina, M., Radermacher, M., Schägger, H., Kerscher, S., and Brandt, U. (2004) Subunit composition of mitochondrial complex I from the yeast *Yarrowia lipolytica*. *Biochim. Biophys. Acta* **1658**, 148-156

3. Acín-Pérez, R., Bayona-Bafaluy, M. P., Fernandez-Silva, P., Moreno-Loshuertos, R., Pérez-Martos, A., Bruno, C., Moraes, C. T., and Enríquez, J. A. (2004) Respiratory complex III is required to maintain complex I in mammalian mitochondria. *Mol. Cell* **13**, 805-815

4. Adrian, M., Dubochet, J., Lepault, J., and McDowall, A. W. (1984) Cryo-electron microscopy of viruses. *Nature* **308**, 32-36

5. Aebersold, R. H., Leavitt, J., Saavedra, R. A., Hood, L. E., and Kent, S. B. (1987) Internal amino acid sequence analysis of proteins separated by one- or two-dimensional gel electrophoresis after in situ protease digestion on nitrocellulose. *Proc. Natl. Acad. Sci. U. S. A.* **84**, 6970-6974

6. Aebersold, R., and Goodlett, D. R. (2001) Mass Spectrometry in Proteomics. *Chem. Rev.* **101**, 269-295

7. Alam, T. I., Kanki, T., Muta, T., Ukaji, K., Abe, Y., Nakayama, H., Takio, K., Hamasaki, N., and Kang, D. (2003) Human mitochondrial DNA is packaged with TFAM. *Nucl. Acids Res.* **31**, 1640-1645

8. Albring, M., Griffith, J., and Attardi, G. (1977) Association of a protein structure of probable membrane derivation with HeLa cell mitochondrial DNA near its origin of replication. *Proc. Natl. Acad. Sci. U. S. A.* **74**, 1348-52

9. Allen, R. D., Schroeder, C. C., and Fok, A. K. (1989) An investigation of mitochondrial inner membranes by rapid-freeze deep-etch techniques. *J. Cell Biol.* **108**, 2233-2240

References

10. Althoff, T., Mills, D. J., Popot, J. L., and Kühlbrandt, W. (2011) Arrangement of electron transport chain components in bovine mitochondrial supercomplex $I_1III_2IV_1$. *EMBO J.* **30**, 4652-4664

11. Altmann, R. (1890) Die Elementarorganismen und ihre Beziehungen zu den Zellen. *Veit, Leipzig*

12. Amos, L. A., Henderson, R., and Unwin, P. N. (1982) Three-dimensional structure determination by electron microscopy of two-dimensional crystals. *Prog. Biophys. Mol. Biol.* **39**, 183-231

13. Andersson, S. G., and Kurland, C. G. (1999) Origins of mitochondria and hydrogenosomes. *Curr. Opin. Microbiol.* **2**, 535-541

14. Angerer, H., Zwicker, K., Wumaier, Z., Sokolova, L., Heide, H., Steger, M., Kaiser, S., Nübel, E., Brutschy, B., Radermacher, M., Brandt, U., and Zickermann, V. (2011) A scaffold of accessory subunits links the peripheral arm and the distal proton pumping module of mitochondrial complex I. *Biochem. J.* **437**, 279-288

15. Antoshechkin, I., and Bogenhagen, D. F. (1995) Distinct roles for two purified factors in transcription of *Xenopus* mitochondrial DNA. *Mol. Cell. Biol.* **15**,7032-7042

16. Arnold, I., Pfeiffer, K., Neupert, W., Stuart, R. A., and Schägger, H. (1998) Yeast mitochondrial F_1F_0-ATP synthase exists as a dimer: identification of three dimer-specific subunits. *EMBO J.* **17**, 7170-7178

17. Attardi, G., and Schatz, G. (1988) Biogenesis of mitochondria. *Annu. Rev. Cell Biol.* **4**, 289-333

18. Azam, T. A., and Ishihama, A. (1999) Twelve species of the nucleoid-associated protein from *Escherichia coli*. *J. Biol. Chem.* **274**, 33105-33113

19. Azam, T. A., Iwata, A., Nishimura, A., Ueda, S., and Ishihama, A. (1999) Growth phase-dependent variation in protein composition of the *Escherichia coli* nucleoid. *J. Bacteriol.* **181**, 6361-6370

20. Baker, T. S., and Johnson, J. E. (1997) Principles of virus structure determination. In: *Structural Biology of Viruses*. Oxford University Press, Oxford 38-55

21. Barat, M., Rickwood, D., Dufresne, C., and Mounolou, J. C. (1985) Characterization of DNA–protein complexes from the mitochondria of *Xenopus* laevis oocytes. *Exp. Cell Res.* **157**, 207-217

22. Bell, E. L., Klimova, T. A., Eisenbart, J., Moraes, C. T., Murphy, M. P., Budinger, G. S., and Chandel, N. S. (2007) The Q_o site of the mitochondrial complex III is required for the transduction of hypoxic signaling via reactive oxygen species production. *J. Cell Biol.* **177**, 1029-1036

23. Benda, C. (1898) Über die Spermatogenese der Vertebraten und höherer Evertebraten, II. Teil: Die Histiogenese der Spermien. *Arch. Anat. Physiol.* **73**, 393-398

24. Bender, A., Krishnan, K. J., Morris, C. M., Taylor, G. A., Reeve, A. K., Perry, R. H., Jaros, E., Hersheson, J. S., Betts, J., and Klopstock, T. (2006) High levels of mitochondrial DNA deletions in substantia nigra neurons in aging and Parkinson disease. *Nat. Genet.* **38**, 515-517

25. Benzi, G., and Moretti, A. (1995) Are reactive oxygen species involved in Alzheimer's disease? *Neurobiol. Aging* **16**, 661-674

26. Bereiter-Hahn, J., and Vöth, M. (1994) Dynamics of mitochondria in living cells: shape changes, dislocations, fusion, and fission of mitochondria. *Microsc. Res. Tech.* **27**, 198-219

27. Bereiter-Hahn, J., and Vöth, M. (1996) Distribution and dynamics of mitochondrial nucleoids in animal cells in culture. *Exp. Biol. Online* **1**, 4

28. Berger, K. H., Sogo, L. F., and Yaffe, M. P. (1997) Mdm12p, a component required for mitochondrial inheritance that is conserved between budding and fission yeast. *J. Cell Biol.* **136**, 545-553

29. Berry, E. A., and Trumpower, B. L. (1985) Isolation of ubiquinol oxidase from *Paracoccus denitrificans* and resolution into cytochrome bc_1 and cytochrome c-aa$_3$ complexes. *J. Biol. Chem.* **260**, 2458-2467

30. Betzig, E., Patterson, G. H., Sougrat, R., Lindwasser, O. W., Olenych, S., Bonifacino, J. S., Davidson, M. W., Lippincott-Schwartz, J., and Hess, H. F. (2006) Imaging intracellular fluorescent proteins at nanometer resolution. *Science* **313**, 1642-1645

31. Bianchi, C., Genova, M. L., Parenti Castelli, G., and Lenaz, G. (2004) The mitochondrial respiratory chain is partially organized in a supercomplex assembly: kinetic evidence using flux control analysis. *J. Biol. Chem.* **279**, 36562-36569

32. Bianchi, M. E. (1994) Prokaryotic HU and eukaryotic HMG1: a linked relationship. *Mol. Microbiol.* **14**, 1-5

33. Blakely, E. L., Mitchell, A. L., Fisher, N., Meunier, B., Nijtmans, L. G., Schaefer, A. M., Jackson, M. J., Turnbull, D. M., and Taylor, R. W. (2005) A mitochondrial cytochrome *b* mutation causing severe respiration chain enzyme deficiency in humans and yeast. *FEBS J.* **14**, 3583-3592

34. Boekema, E. J., Folea, M., and Kouřil, R. (2009) Single particle electron microscopy. *Photosynth. Res.* **102**, 189-196

35. Bogenhagen, D. F. (2011) Mitochondrial DNA nucleoid structure. *Biochim. Biophys. Acta* **1819**, 914-920

36. Bogenhagen, D. F., Rousseau, D., and Burke, S. (2008) The layered structure of human mtDNA nucleoids. *J. Biol. Chem.* **283**, 3665-3675

37. Bogenhagen, D. F., Wang, Y., Shen, E. L., and Kobayashi, R. (2003) Protein components of mitochondrial DNA nucleoids in higher eukaryotes. *Mol. Cell. Proteomics* **2**, 1205-1216

38. Boldogh, I. R., and Pon, L. A. (2007) Mitochondria on the move. *Trends Cell Biol.* **17**, 502-510

39. Boldogh, I. R., Nowakowski, D. W., Yang, H. C., Chung, H., Karmon, S., Royes, P., and Pon L. A. (2003) A protein complex containing Mdm10p, Mdm12p, and Mmm1p links mitochondrial membranes and DNA to the cytoskeleton-based segregation machinery. *Mol. Biol. Cell* **14**, 4618-4627

40. Bolender, N., Sickmann, A., Wagner, R., Meisinger, C., and Pfanner, N. (2008) Multiple pathways for sorting mitochondrial precursor proteins. *EMBO J.* **9**, 42-49

41. Boore, J. L. (1999) Animal mitochondrial genomes. *Nucl. Acids Res.* **27**, 1767-1780

42. Borek, A., Sarewicz, M., and Osyczka, A. (2008) Movement of the iron-sulfur head domain of cytochrome bc_1 transiently opens the catalytic Q_o site for reaction with oxygen. *Biochemistry* **47**, 12365-12370

43. Boveris, A., Cadenas, E., and Stoppani, A. O. (1976) Role of ubiquinone in the mitochondrial generation of hydrogen peroxide. *Biochem. J.* **156**, 435-444

44. Brandner K., Mick, D. U., Frazier, A. E., Taylor, R. D., Meisinger, C., and Rehling, P. (2005) Taz1, an outer mitochondrial membrane protein, affects stability and assembly of inner membrane protein complexes: implications for Barth Syndrome. *Mol. Biol. Cell* **16**, 5202-5214

45. Brandt, U. (1996) Energy conservation by bifurcated electron-transfer in the cytochrome bc_1 complex. *Biochim. Biophys. Acta* **1275**, 41-46

46. Brandt, U. (2006) Energy converting NADH: quinone oxidoreductase (complex I). *Annu. Rev. Biochem.* **75**, 69-92

47. Brandt, U. (2011) A two-state stabilization-changem mechanism for proton-pumping complex I. *Biochim. Biophys. Acta* **1807**, 1364-1369

48. Brandt, U., Uribe, S., Schägger, H., and Trumpower, B. L. (1994) Isolation and characterization of QCR10, the nuclear gene encoding the 8.5-kDa subunit 10 of the S*accharomyces cerevisiae* cytochrome bc_1 complex. *J. Biol. Chem.* **269**, 12947-12953

49. Brown, T. A., Tkachuk, A. N., Shtengel, G., Kopek, B. G., Bogenhagen, D. F., Hess, H. F., and Clayton, D. A. (2011) Super-resolution fluorescence imaging of mammalian mitochondrial nucleoids. *Mol. Cell. Biol.* **31**, 4994-5010

50. Bruel, C., Brasseur, R., and Trumpower, B. L. (1996) Subunit 8 of the *Saccharomyces cerevisiae* cytochrome bc_1 commplex interacts with succinate-ubiquinone reductase complex. *J. Bioenerg. Biomembr.* **28**, 59-68

51. Bruggen, V. E., Borst, P., Ruttenberg, G., Gruber, M., and Kroon, A. (1966) Circular mitochondrial DNA. *Biochim. Biophys. Acta* **119**, 437-439

52. Bryan, A. C., Rodeheffer, M. S., Wearn, C. M., and Shadel, G. S. (2002) Sls1p is a membrane-bound regulator of transcription-coupled processes involved in *Saccharomyces cerevisiae* mitochondrial gene expression. *Genetics* **160**, 75-82

References

53. Bultema, J. B., Braun, H. P., Boekema, E. J., and Kouřil, R. (2009) Megacomplex organization of the oxidative phosphorylation system by structural analysis of respiratory supercomplexes from potato. *Biochim. Biophys. Acta* **1787**, 60-67

54. Burger, G., Gray, M. W., and Lang, B. F. (2003) Mitochondrial genomes: anything goes. *Trends Genet.* **19**, 709-716

55. Burgess, S. M., Delannoy, M., and Jensen, R.E. (1994) Mmm1 encodes a mitochondrial outer membrane protein essential for establishing and maintaining the structure of yeast mitochondria. *J. Cell Biol.* **126**, 1375-1391

56. Cadenas, E., Boveris, A., Ragan, C. I., and Stoppani, A. O. (1977) Production of superoxide radicals and hydrogen peroxide by NADH-ubiquinone reductase and ubiquinol-cytochrome *c* reductase from beef-heart mitochondria. *Arch. Biochem. Biophys.* **180**, 248-257

57. Carr, S. A., and Annan, R. S. (1997) Overview of peptide and protein analysis by mass spectrometry. *Curr. Protoc. Mol. Biol*. John Wiley and Sons: New York, unit **10.21**, 10.21.1-10.21.27

58. Carrozzo, R., Wittig, I., Santorelli, F. M., Bertini, E., Hofmann, S., Brandt, U., and Schägger, H. (2006) Subcomplexes of human ATP synthase mark mitochondrial biosynthesis disorders. *Ann. Neurol*. **59**, 265-275

59. Chan, N. C., and Lithgow, T. (2008) The peripheral membrane subunits of the SAM complex function codependently in mitochondrial outer membrane biogenesis. *Mol. Biol. Cell* **19**, 126-136

60. Chance, B., and Williams. G. R. (1955) Respiratory enzymes in oxidative phosphorylation. III. The steady state. *J. Biol. Chem.* **217**, 409-427

61. Chang, H., and Gilbert, W. (1997) A novel zebrafish gene expressed specifically in the photoreceptor cells of the retina. *Biochem. Biophys. Res. Commun.* **237**, 84-89

62. Chen, S., Roseman, A. M., and Saibil, H. R. (1998) Electron Microscopy of Chaperonins. In: *Methods Enzymol*. Lorimer, G.H., and Baldwin, T.O. (Eds.). Molecular Chaperones, Academic Press, San Diego. **290**, 242-253

63. Chen, X. J., and Butow, R. A. (2005) The organization and inheritance of the mitochondrial genome. *Nat. Rev. Genet.* **6**, 815-825

64. Chen, X. J., Wang, X., and Butow, R. A. (2007) Yeast aconitase binds and provides metabolically coupled protection to mitochondrial DNA. *Proc. Natl. Acad. Sci. U. S. A.* **104**, 13738-13743

65. Chen, X. J., Wang, X., Kaufman, B. A., and Butow, R. A. (2005) Aconitase couples metabolic regulation to mitochondrial DNA maintenance. *Science* **307**, 714-717

66. Collins, M. O., Yu, L., and Choudhary, J. S. (2008) Analysis of protein complexes by 1-D SDS-PAGE and tandem mass spectrometry. *Protocol Exchange* doi:10.1038/nprot.2008.123

67. Cotney, J., Wang, Z., and Shadel, G. S. (2007) Relative abundance of the human mitochondrial transcription system and distinct roles for h-mtTFB1 and h-mtTFB2 in mitochondrial biogenesis and gene expression. *Nucl. Acids Res.* **35**, 4042-4054

68. Cox, J., and Mann, M. (2011) Quantitative, high-resolution proteomics for data-driven systems biology. *Annu. Rev. Biochem.* **80**, 273-299

69. Crane, F.L., Glenn, J. L., Green, D. E. (1956) Studies on the electron transfer system: IV. The electron transfer particles. *Biochim. Biophys. Acta* **22**, 475-487

70. Cruciat, C. M., Brunner, S., Baumann, F., Neupert, W., and Stuart, R. A. (2000) The cytochrome bc_1 and cytochrome c oxidase complexes associate to form a single supracomplex in yeast mitochondria. *J. Biol. Chem.* **275**, 18093-18098

71. Curth, U., Urbanke, C., Greipel, J., Gerberding, H., Tiranti, V., and Zeviani, M. (1994) Single-stranded-DNA-binding proteins from human mitochondria and *Escherichia coli* have analogous physicochemical properties. *Eur. J. Biochem.* **221**, 435-445

72. Czarnecka, A. M., Campanella, C., Zummo, G., and Cappello, F. (2006) Mitochondrial chaperones in cancer: from molecular biology to clinical diagnostics. *Cancer Biol. Ther.* **5**, 714-720

73. Davidzon, G., Mancuso, M., Ferraris, S., Quinzii, C., Hirano, M., Peters, H. L., Kirby, D., Thorburn, D. R., and DiMauro, S. (2005) POLG mutations and Alpers syndrome. *Ann. Neurol.* **57**, 921-923

74. Davies, K. M., Strauss, M., Daum, B., Kief, J. H., Osiewacz, H. D., Rycovska, A., Zickermann, V., and Kühlbrandt, W. (2011) Macromolecular organization of ATP synthase and complex I in whole mitochondria. *Proc. Natl. Acad. Sci. U. S. A.* **108**, 14121-14126

75. Davis, M. T., and Lee, T. D. (1997) Rapid protein identification using a microscale electrospray LC/MS system on an ion trap mass spectrometer. *J. Am. Soc. Mass Spectrom.* **8**, 1059

76. De Coo, I. F., Renier, W. O., Ruitenbeek, W., Ter Laak, H. J., Bakker, M., Schägger, H., Van Oost, B. A., and Smeets, H. J. (1999) A 4 bp deletion in mitochondrial cytochrome *b* gene associated with Parkinsonism/MELAS overlap syndrome. *Ann. Neurol.* **45**, 130-133

77. De Vries, S., and Marres, C. A. (1987) The mitochondrial respiratory chain of yeast: Structure and biosynthesis and the role in cellular metabolism. *Biochim. Biophys. Acta* **895**, 205-239

78. Diaz, F., Fukui, H., Garcia, S., and Moraes, C. T. (2006) Cytochrome *c* oxidase is required for the assembly/stability of respiratory complex I in mouse fibroblasts. *Mol. Cell. Biol.* **26**, 4872-4881

79. Diffley, J. F., and Stillman, B. (1991) A close relative of the nuclear, chromosomal high-mobility group protein HMG1 in yeast mitochondria. *Proc. Natl. Acad. Sci. U. S. A.* **88**, 7864-7868

80. Dillon, S. C., and Dorman, C. J. (2010) Bacterial nucleoid-associated proteins, nucleoid structure and gene expression. *Nat. Rev. Microbiol.* **8**, 185-195

81. DiMauro, S., and Schon, E. A. (2003). Mitochondrial respiratory-chain diseases. *N. Engl. J. Med.* **348**, 2656-2668

82. Dimmer, K. S., Jakobs, S., Vogel, F., Altmann, K., and Westermann, B. (2005) Mdm31 and Mdm32 are inner membrane proteins required for maintenance of mitochondrial shape and stability of mitochondrial DNA nucleoids in yeast. *J. Cell Biol.* **168**, 103-115

83. Dröse, S. (2011) Kumulative Habilitationsschrift: Untersuchungen zum Mechanismus von mitochondrialen Atmungsketten Komplexe: Protonenpumpen und Superoxid-Generatoren.

84. Dröse, S., and Brandt, U. (2008) The mechanism of mitochondrial superoxide production by the cytochrome bc_1 complex. *J. Biol. Chem.* **283**, 21649-21654

85. Dröse, S., Bleier, L., and Brandt, U. (2011) A common mechanism links differently acting complex II inhibitors to cardioprotection: modulation of mitochondrial reactive oxygen species production. *Mol. Pharmacol.* **79**, 814-822

86. Dubochet, J., Adrian, M., Chang, J. J., Homo, J. C., Lepault, J., Mc-Dowall, A. W., and Schultz, P. (1988) Cryo-electron microscopy of vitrified specimens. *Q. Rev. Biophys.* **21**, 129-228

87. Dubochet, J., Lepault, J., Freeman, R., Berriman, J. A., Homo, J. C. (1982) Electron microscopy of frozen water and aqueous solutions. *J. Microsc.* **128**, 219-237

88. Duchniewicz, M., Germaniuk, A., Westermann, B., Neupert, W., Schwarz, E., and Marszalek, J. (1999) Dual role of the mitochondrial chaperone Mdj1p in inheritance of mitochondrial DNA in yeast. *Mol. Cell. Biol.* **19**, 8201-8210

89. Dudkina, V. N., Kouřil, R., Peters, K., Braun, H. P., and Boekema, J. E. (2010) Structure and function of mitochondrial supercomplexes. *Biochim. Biophys. Acta* **1797**, 664-670

90. Dudkina, N. V., Eubel, H., Keegstra, W., Boekema, E. J., and Braun, H. P. (2005) Structure of a mitochondrial supercomplex formed by respiratory-chain complexes I and III. *Proc. Natl. Acad. Sci. U. S. A.* **102**, 3225-3229

91. Dudkina, N. V., Sunderhaus, S., Braun, H. P., and Boekema, E. J. (2006) Characterization of dimeric ATP synthase and cristae membrane ultrastructure from Saccharomyces and Polytomella mitochondria. *FEBS Lett*. **580**, 3427-3432

92. Efremov, R. G., Baradaran, R., and Sazanov, L. A. (2010) The architecture of respiratory complex I. *Nature* **465**, 441-445

93. Efremov R. G., and Sazanov, L. A. (2011) Structure of the membrane domain of respiratory complex I. *Nature* **476**, 414-420

References

94. Ekstrand, M. I., Falkenberg, M., Rantanen, A., Park, C. B., Gaspari, M., Hultenby, K., Rustin, P., Gustafsson, C. M., and Larsson, N. G. (2004) Mitochondrial transcription factor A regulates mtDNA copy number in mammals. *Hum. Mol. Genet*. **13**, 935-944

95. Ekstrand, M. I., Terzioglu, M., Galter, D., Zhu, S., Hofstetter, C., Lindqvist, E., Thams, S., Bergstrand, A., Hansson, F. S., Trifunovic, A., Hoffer, B., Cullheim, S., Mohammed, A. H., Olson, L., and Larsson, N. G. (2007) Progressive parkinsonism in mice with respiratory-chain-deficient dopamine neurons. *Proc. Natl. Acad. Sci*. **104**, 1325-1330

96. Embley, T. M., van der Giezen, M., Horner, D. S., Dyal, P. L., and Foster, P. (2003) Mitochondria and hydrogenosomes are two forms of the same fundamental organelle. *Philos. Trans. R. Soc. Lond. B. Biol. Sci.* **358**, 191-204

97. Emerit, J., Edeas, M., and Bricaire, F. (2004) Neurodegenerative diseases and oxidative stress. *Biomed. Pharmacother.* **58**, 39-46

98. Ernster, L., and Schatz, G. (1981) Mitochondria: a historical review. *J. Cell Biol.* **91**, 227-255

99. Eubel, H., Heinemeyer, J., and Braun, H. P. (2004) Identification and characterization of respirasomes in potato mitochondria. *Plant Physiol.* **134**, 1450-1459

100. Eubel, H., Jänsch, L., and Braun, H. P. (2003) New insights into the respiratory chain of plant mitochondria supercomplexes and a unique compositions of complex II. *Plant Physiol.* **133**, 274-286

101. Fenn, J. B., Mann, M., Meng, C. K., Wong, S. F., and Whitehouse, C. M. (1989) Electrospray ionization for mass spectrometry of large biomolecules. *Science* **246**, 64-71

102. Fersht, A. (1999) Structure and mechanism in protein science: guide to enzyme catalysis and protein folding. WH Freeman & Co, New York 540-614

103. Fields, S., and Song, O. (1989) A novel genetic system to detect protein-protein interactions. *Nature* **340**, 245-246

104. Finkel, T., and Holbrook, N. J. (2000) Oxidants, oxidative stress and the biology of ageing. *Nature* **408**, 239-247

105. Fisher, R. P., and Clayton, D. A. (1988) Purification and characterization of human mitochondrial transcription factor 1. *Mol. Cell. Biol.* **8**, 3496-3509

106. Frangakis, A. S., and Hegerl, R. (2001) Noise reduction in electron tomographic reconstructions using nonlinear anisotropic diffusion. *J. Struct. Biol.* **135**, 239-250

107. Frank, A. M., Savitski, M. M., Nielsen, M. L., Zubarev, R. A., Pevzner, P. A. (2007) *De novo* peptide sequencing and identification with precision mass spectrometry. *J. Proteome Res.* **6**, 114-123

108. Fridovich, I. (1978) The biology of oxygen radicals. *Science* **201**, 875-880

109. Fu, G. K., and Markovitz, D. M. (1998) The human LON protease binds to mitochondrial promoters in a single stranded, site-specific, strand-specific manner. *Biochemistry* **37**, 1905-1909

110. Galkin, A. S., Grivennikova, V. G., and Vinogradov, A. D. (1999) --> H+/2e-stoichiometry in NADH-quinone reductase reactions catalyzed by bovine heart submitochondrial particles. *FEBS Lett.* **451**, 157-161

111. Galkin, A., and Brandt, U. (2005) Superoxide radical formation by pure complex I (NADH:ubiquinone oxidoreductase). *Yarrowia lipolytica*. *J. Biol. Chem.* **280**, 30129-30135

112. Garrido, N., Griparic, L., Jokitalo, E., Wartiovaara, J., van der Bliek, A. M., and Spelbrink, J. N. (2003) Composition and dynamics of human mitochondrial nucleoids. *Mol. Biol. Cell* **14**, 1583–1596

113. Geier, B. M., Schägger, H., Ortwein, C., Link, T. A., Hagen, W. R., and Brandt, U. (1995) Kinetic properties and ligand binding of the eleven subunit cytochrome *c* oxidase from *Saccharomyces cerevisiae* isolated with a novel large scale purification method. *Eur. J. Biochem.* **227**, 296-302

114. Genova, M., Bianchi, C., and Lenaz, G. (2003) Structural organization of the mitochondrial respiratory chain. *Ital. J. Biochem.* **52**, 58-61

115. Gilkerson, R. W., Schon, E. A., Hernandez, E., and Davidson, M. M. (2008) Mitochondrial nucleoids maintain genetic autonomy but allow for functional complementation. *J. Cell Biol.* **181**, 1117-1128

116. Görg, A., Postel, W., and Günther, S. (1988) Two-dimensional electrophoresis of proteins in an immobilized pH 4-12 gradient. *Electrophoresis* **9**, 531-546

117. Hackenbrock, C. R., Chazotte, B., and Gupte, S. S. (1986) The random collision model and a critical assessment of diffusion and collision in mitochondrial electron transport. *J. Bioenerg. Biomembr.* **18**, 331-368

118. Hallberg, B. M., and Larsson, N. G. (2011) TFAM forces mtDNA to make a U-turn. *Nat. Struct. Mol. Biol.* **18**, 1179-1181

119. Harris, J. R., and Horne, R. W. (1994) Negative staining: a brief assessment of current technical benefits, limitations and future possibilities. *Micron* **25**, 5-13

120. Hatefi, Y. (1985) The mitochondrial electron transport and oxidative phosphorylation system. *Annu. Rev. Biochem.* **54**, 1015-1069

121. Hatefi, Y., and Rieske, J. S. (1967) The preparation and properties of DPNH-cytochrome *c* reductase (complex I-II of respiratory chain). *Methods Enzymol.* **10**, 225-231

122. Hatefi, Y., Haavik, A. G., and Rieske, J. S. (1962) Studies on the electron transfer system. Preparation and properties of mitochondrial DPNH-Coenzyme Q reductase. *J. Biol. Chem.* **237**, 1676-1680

123. He, J., Mao, C. C., Reyes, A., Sembongi, H., Re, Di. M., Granycome, C., Clippingdale, A. B., Fearnley, I. M., Harbour, M., Robinson, A. J., Reichelt, S., Spelbrink, J. N., Walker, J. E., and Holt, I. J. (2007) The AAA$^+$ protein ATAD3 has displacement loop binding properties and is involved in mitochondrial nucleoid organization. *J. Cell Biol.* **176**, 141–146

124. Heinemeyer, J., Braun, H. P., Boekema, E. J., and Kouřil, R. (2007) A structural model of the cytochrome *c* reductase/oxidase supercomplex from yeast mitochondria. *J. Biol. Chem.* **282**, 12240-12248

125. Helbig, A. O., de Groot, M. J., van Gestel, R. A., Mohammed, S. de Hulster, E. A., Luttik, M. A., Daran-Lapujade, P., Pronk, J. T., Heck, A. J., and Slijper, M. (2009) A three-way proteomics strategy allows differential analysis of yeast mitochondrial

membrane protein complexes under anaerobic and aerobic conditions. *Proteomics* **9**, 4787-4798

126. Helenius, A., and Simons, K. (1972) The binding of detergents to lipophilic and hydrophilic proteins. *J. Biol. Chem*. **247**, 3656-3661

127. Hell, S. W, and Wichmann, J. (1994) Breaking the diffraction resolution limit by stimulated emission: Stimulated-emission-depletion fluorescence microscopy. *Opt. Lett.* **19**, 780-782

128. Hell, S. W (2009) Far-field optical nanoscopy in *Single Molecule Spectroscopy in Chemistry, Physics and Biology (Springer, Berlin)* 365-398

129. Henderson, R., Baldwin, J. M., Ceska, T. A., Zemlin, F., Beckmann, E., and Downing, K. H. (1990) Model for the structure of bacteriorhodopsin based on high-resolution electron cryo-microscopy. *J. Mol. Biol.* **213**, 899-920

130. Herrmann, J. M., and Koehl, R. (2007) Catch me if you can! Oxidative protein trapping in the intermembrane space of mitochondria. *J. Cell Biol*. **176**, 559-563

131. Herrmann, J. M. (2003) Converting bacteria to organelles: evolution of mitochondrial protein sorting. *Trends Microbiol.* **11**, 74-79

132. Heuberger, E. H., Veenhoff, L. M., Duurkens, R. H., Friesen, R. H, and Poolman, B. (2002) Oligomeric state of membrane transport proteins analyzed with blue native electrophoresis and analytical ultracentrifugation. *J. Mol. Biol.* **317**, 591-600

133. Hewick, R. M., Hunkapiller, M. W., Hood, L. E., and Dreyer, W. J. (1981) A gas-liquid solid phase peptide and protein sequenator. *J. Biol. Chem.* **256**, 7990-7997

134. Hillar, M., Rangayya, V., Jafar, B. B., Chambers, D., Vitzu, M., and Wyborny, L. E. (1979) Membrane-bound mitochondrial DNA: isolation, transcription and protein composition. *Arch. Int. Physiol. Biochim.* **87**, 29-49

135. Hillenkamp, F., Karas, M., Beavis, R. C., and Chait, B. T. (1991) Matrix-assisted laser desorption/ionization mass spectrometry of biopolymers. *Anal. Chem.* **63**, 193-203

136. Hobbs, A. E., Srinivasan, M., McCaffery, J. M., and Jensen, R. E. (2001) Mmm1p, a mitochondrial outer membrane protein, is connected to mitochondrial DNA (mtDNA) nucleoids and required for mtDNA stability. *J. Cell Biol.* **152**, 401-410

137. Höchli, M., and Hackenbrock, C. R. (1976) Lateral translational diffusion of cytochrome *c* oxidase in the mitochondirla energy-transducing membrane. *Proc. Natl. Acad. Sci.U. S. A* **73**, 1636-1640

138. Hofmann, K., and Stoffel, W. (1993) TMbase - a database of membrane spanning protein segments. *Biol. Chem. Hoppe-Seyler*. **374**, 166

139. Holt, I. J., He, J., Mao, C. C., Boyd-Kirkup, J. D., Martinsson, P., Sembongi, H., Reyes, A., and Spelbrink, J. N. (2007) Mammalian mitochondrial nucleoids: Organizing an independently minded genome. *Mitochondrion* **7**, 311-321

140. Huang, B., Wang, W. Q., Bates, M., and Zhuang, X. W. (2008) Three-dimensional super-resolution imaging by stochastic optical reconstruction microscopy. *Science* **319**, 810-813

141. Huang, L. S., Cobessi, D., Tung, E. Y., and Berry, E. A. (2005) Binding of the respiratory chain inhibitor antimycin to the mitochondrial bc_1 complex: a new crystal structure reveals an altered intramolecular hydrogen-bonding pattern. *J. Mol. Biol*. **351**, 573-597

142. Hunte, C., and Michel, H. (2002) Crystallisation of membrane proteins mediated by antibody fragments. *Curr. Opin. Struct. Biol.* **12**, 503-508

143. Hunte, C., Zickermann, V., and Brandt, U. (2010) Functional modules and structural basis of conformational coupling in mitochondrial complex I. *Science* **329**, 448-451

144. Iborra, F. J., Kimura, H., and Cook, P. R. (2004) The functional organization of mitochondrial genomes in human cells. *BMC Biol*. **2**, 9-23

145. Iwasaki, T., Matsuura, K., and Oshima, T. (1995) Resolution of the aerobic respiratory system of the thermoacidophilic archaeon, Sulfolobus sp. strain 7. I. The archaeal terminal oxidase supercomplex is a functional fusion of respiratory complexes III and IV with no *c*-type cytochromes. *J. Biol. Chem.* **270**, 30881-30892

146. Iwata, S., Lee, J. W., Okada, K., Lee, J. K., Iwata, M., Rasmussen, B., Link, T. A., Ramaswamy, S., and Jap, B. K. (1998) Complete structure of the 11-subunit bovine mitochondrial cytochrome bc_1 complex. *Science* **281**, 64-71

147. Jacobs, H. T., Lehtinen, S. K., and Spelbrink, J. N. (2000) No sex please, we're mitochondria: a hypothesis on the somatic unit of inheritance of mammalian mtDNA. *BioEssays* **22**, 564-572

148. Jänsch, L., Kruft, V., Schmitz, U. K., and Braun, H. P. (1996) New insights into the composition, molecular mass and stoichiometry of the protein complexes of plant mitochondria. *Plant J.* **9**, 357-368

149. John, G. B., Shang, Y., Li, L., Renken, C., Mannella, C. A., Selker, J. M., Rangell, L., Bennett, M. J., and Zha, J. (2005) The mitochondrial inner membrane protein mitofilin controls cristae morphology. *Mol. Biol. Cell* **16**, 1543-1554

150. Jonscher, K. R., and Yates, J. R., III. (1997) The quadrupole ion trap mass spectrometer-a small solution to a big challenge. *Anal. Biochem.* **244**, 1-15

151. Joseph-Horne, T., Holloman, D. W., and Wood, P. M. (2001) Fungal respiration: a fusion of standard and alternative components. *Biochim. Biophys. Acta* **1504**, 179-195

152. Kadeer, Z., Cruciat, M., Strecker, V., Angerer, H., Pfeiffer, K., Schägger, H., Stuart, R. A., and Wittig, I. (2012) Respirasome-associated Cox26 protein binds to cytochrome *c* oxidase subunit Cox2. *Manuscript in preparation*

153. Kang, D., and Hamasaki, N. (2005) Mitochondrial transcription factor A in the maintenance of mitochondrial DNA: overview of its multiple roles. *Ann. N. Y. Acad. Sci.* **1042**, 101-108

154. Karas, M., and Hillenkamp, F. (1988) Laser desorption ionization of proteins with molecular masses exceeding 10,000 daltons. *Anal. Chem.* **60**, 2299-2301

155. Kasashima, K., Sumitani, M., Satoh, M., and Endo, H. (2008) Human prohibitin 1 maintains the organization and stability of the mitochondrial nucleoids. *Exp. Cell Res.* **314**, 988-996

156. Kashani-Poor, N., Kerscher, S., Zickermann, V., and Brandt, U. (2001) Efficient large scale   purification   of   his-tagged   proton   translocating   NADH:ubiquinone

oxidoreductase (complex I) from the strictly aerobic yeast *Yarrowia lipolytica. Biochim. Biophys. Acta* **1504**, 363-370

157. Kaufman, B. A., Durisic, N., Mativetsky, J. M., Costantino, S., Hancock, M. A., Grutter, P., and Shoubridge, E. A. (2007) The mitochondrial transcription factor TFAM coordinates the assembly of multiple DNA molecules into nucleoid-like structures. *Mol. Biol. Cell* **18**, 3225-3236

158. Kaufman, B. A., Kolesar, J. E., Perlman, P. S., and Butow, R. A. (2003) A function for the mitochondrial chaperonin Hsp60 in the structure and transmission of mitochondrial DNA nucleoids in *Saccharomyces cerevisiae. J. Cell Biol.* **163**, 457-461

159. Kaufman, B. A., Newman, S. M., Hallberg, R. L., Slaughter, C. A., Perlman, P. S., and Butow, R. A. (2000) In organello formaldehyde crosslinking of proteins to mtDNA: identification of bifunctional proteins. *Proc. Natl. Acad. Sci. U. S. A.* **97**, 7772-7777

160. Kellie, J. F., Tran, J. C., Lee, J. E., Ahlf, D. R., and Thomas, H. M., Ntai, I., Catherman, A. D., Durbin, K. R., Zamdborg, L., Vellaichamy, A., Thomas, P. M, and Kelleher, N. L. (2010) The emerging process of top down mass spectrometry for protein analysis: biomarkers, protein-therapeutics, and achieving high throughput. *Mol. Biosyst.* **6**, 1532-1539

161. Kerscher, S., Dröse, S., Zwicker, K., Zickermann, V., and Brandt, U. (2002) *Yarrowia lipolytica*, a yeast genetic system to study mitochondrial complex I. *Biochim. Biophys. Acta* **1555**, 83-91

162. Kerscher, S., Okun, J. G., and Brandt, U. (1999) A single external enzyme confers alternative NADH:ubiquinone oxidoreductase activity in *Yarrowia lipolytica. J. Cell Sci.* **112**, 2347-2354

163. Kislinger, T., Gramolini, A. O., Pan, Y., Rahman, K., MacLennan, D. H., and Emili, A. (2005) Proteome dynamics during C2C12 myoblast differentiation. *Mol. Cell. Proteomics* **4**, 887-901

164. Kornmann, B., Currie, E., Collins, S. R., Schuldiner, M., Nunnari, J., Weissman, J. S., and Walter, P. (2009) An ER-mitochondria tethering complex revealed by a synthetic biology screen. *Science* **325**, 477-481

165. Kornmann, B., Osman, C., and Walter, P. (2011) The conserved GTPase Gem1 regulates endoplasmic reticulum–mitochondria connections. *Proc. Natl. Acad. Sci*. **108**, 14151-14156

166. Krause, F., Reifschneider, N. H., Goto, S., and Dencher, N. A. (2005) Active oligomeric ATP synthases in mammalian mitochondria. *Biochem. Biophys. Res. Commun*. **329**, 583-590

167. Kraytsberg, Y., Kudryavtseva, E., McKee, A. C., Geula, C., Kowall, N. W., and Khrapko, K. (2006) Mitochondrial DNA deletions are abundant and cause functional impairment in aged human substantia nigra neurons. *Nat. Genet.* **38**, 518-520

168. Kremer, J. R., Mastronarde, D. N., and McIntosh, J. R (1996) Computer visualization of three-dimensional image data using IMOD. *J. Struct. Biol.* **116**, 71-76

169. Kügler, M., Jänsch, L., Kruft, V., Schmitz, U. K., Braun, H. P. (1997) Analysis of the chloroplast protein complexes by blue native polyacrylamide gelelectrophoresis. *Photosynth. Res.* **53**, 35-44

170. Kühlbrandt, W., and Williams, A. K. (1999) Analysis of macromolecular structure and dynamics by electron cryo-microscopy. *Curr. Opin. Chem. Biol.* **3**, 537-543

171. Kühlbrandt, W., Wang, D. N., and Fujiyoshi, Y. (1994) Atomic model of plant light harvesting complex by electron crystallography. *Nature* **367**, 614-621

172. Kukat, C., Wurm, C. A., Spåhr, H., Falkenberg, M., Larsson, N. G., and Jakobs, S. (2011) Super-resolution microscopy reveals that mammalian mitochondrial nucleoids have a uniform size and frequently contain a single copy of mtDNA. *Proc. Natl. Acad. Sci*. **108**, 13534-13539

173. Kuroiwa, T., Nishida, K., Yoshida, Y., Fujiwara, T., Mori, T., Kuroiwa, H., and Misumi, O. (2006) Structure, function and evolution of the mitochondrial division apparatus. *Biochim. Biophys. Acta* **1763**, 510-521

174. Kuroiwa, T. (1982) Mitochondrial nuclei. *Int. Rev. Cytol.* **75**, 1-59

175. Kuroiwa, T., Kitane, H., Watanabe, T., and Kawano, S. (1976) The general occurrence of mitochondrial nuclei in the true slime mold. *J. Electron Microsc. (Tokyo)* **25**, 103-105

176. Kushnareva, Y., Murphy, A. N., and Andreyev, A. (2002) Complex I-mediated reactive oxygen species generation: modulation by cytochrome *c* and NAD(P)$^+$ oxidation-reduction state. *Biochem. J.* **36**, 545-553

177. Kussmaul, L., and Hirst, J. (2006) The mechanism of superoxide production by NADH:ubiquinone oxidoreductase (complex I) from bovine heart mitochondria. *Proc. Natl. Acad. Sci. U. S. A.* **103**, 7607-7612

178. Laemmli, U. K. (1970) Cleavage of structural proteins during the assembly of the head of bacteriophage T4. *Nature* **227**, 680-685

179. Lange, C., Nett, J. H., Trumpower, B. L., and Hunte, C. (2001) Specific roles of protein-phospholipid interactions in the yeast cytochrome *bc$_1$* complex structure. *EMBO J.* **20**, 6591-6600

180. Larsson, N. G., Oldfors, A., Holme, E., and Clayton, D. A. (1994) Low levels of mitochondrial transcription factor A in mitochondrial DNA depletion. *Biochem. Biophys. Res. Commun.* **200**, 1374-1381

181. Larsson, N. G., Wang, J., Wilhelmsson, H., Oldfors, A., Rustin, P., Lewandoski, M., Barsh, G. S., and Clayton, D. A. (1998) Mitochondrial transcription factor A is necessary for mtDNA maintenance and embryogenesis in mice. *Nat. Genet*. **18**, 231-236

182. Lazar, I. M., Ramsey, R. S., Sundberg, S., and Ramsey, J. M. (1999) Subattomole-sensitivity microchip nanoelectrospray source with Time-of-flight mass spectrometry detection. *Anal. Chem.* **71**, 3627-3631

183. Legros, F., Malka, F., Frachon, P., Lombes, A., and Rojo, M. (2004) Organization and dynamics of human mitochondrial DNA. *J. Cell Sci*. **117**, 2653-2662

184. Lenaz, G., and Genova, M. L. (2009) Structural and functional organization of the mitochondrial respiratory chain: a dynamic super-assembly. *Int. J. Biochem. Cell Biol*. **41**, 1750-1772

185. Liesa, M., Palacin, M., and Zorzano, A. (2009) Mitochondrial dynamics in mammalian health and disease. *Physiol. Rev*. **89**, 799-845

186. Lin, M. T., and Beal, M. F. (2006) Mitochondrial dysfunction and oxidative stress in neurodegenerative diseases. *Nature* **443**, 787-795

187. Liu, T., Lu, B., Lee, I., Ondrovicova, G., Kutejova, E., and Suzuki, C. K. (2004) DNA and RNA binding by the mitochondrial LON protease is regulated by nucleotide and protein substrate. *J. Biol. Chem.* **279**, 13902-13910

188. Loo, J. A., Edmonds, C. G., and Smith, R. D. (1990) Primary sequence information from intact proteins by electrospray ionization tandem mass spectrometry. *Science* **248**, 201-204

189. Lottspeich, F., and Engels, J. W. (2006) *Bioanalytic* **2**. Auflage, 461

190. Lucič, V., Förster, F., and Baumeister, W. (2005) Structural studies by electron tomography: from cells to molecules. *Annu. Rev. Biochem.* **74**, 833-865

191. Lynch, A. S., and Wang, J. C. (1993) Anchoring of DNA to the bacterial cytoplasmic membrane through cotranscriptional synthesis of polypeptides encoding membrane proteins or proteins for export: a mechanism of plasmid hypernegative supercoiling in mutants deficient in DNA topoisomerase I. *J. Bacteriol.* **175**, 1645-1655

192. Malka, F., Lombès, A., and Rojo, M. (2006) Organization, dynamics and transmission of mitochondrial DNA: focus on vertebrate nucleoids. *Biochim. Biophys. Acta* **1763**, 463-472

193. Maniura-Weber, K., Goffart, S., Garstka, H. L., Montoya, J., and Wiesner, R. J. (2004) Transient overexpression of mitochondrial transcription factor A (TFAM) is sufficient to stimulate mitochondrial DNA transcription, but not sufficient to increase mtDNA copy number in cultured cells. *Nucl. Acids Res.* **32**, 6015-6027

194. Mannella, C. A. (2006) Structure and dynamics of the mitochondrial inner membrane cristae. *Biochim. Biophys. Acta* **1763**, 542-548

195. Margineantu, D. H., Cox, W. G., Sundell, L., Sherwood, S. W., Beechem, J. M., Capaldi, R. A. (2002) Cycle dependent morphology changes and associated mitochondrial DNA. *Mitochondrion* **1**, 425-435

196. Margulis, L. (1970) Origin of eukaryotic cells. Yale University Press, New Haven 349

197.   McKenzie, M., Lazarou, M., Thorburn, D. R., and Ryan, M. T. (2006) Mitochondrial respiratory chain supercomplexes are destabilized in Barth Syndrome patients. *J. Mol. Biol.* **361**, 462-469

198.   McLafferty, F. W., Breuker, K., Jin, M., Han, X., and Infusini, G., Jiang, H., Kong, X., and Begley, T. P. (2007) Top-down MS, a powerful complement to the high capabilities of proteolysis proteomics. *FEBS J.* **274**, 6256-6268

199.   Megraw, T. L., and Chae, C. B. (1993) Functional complementarity between the HMG1-like yeast mitochondrial histone HM and the bacterial histone-like protein HU. *J. Biol. Chem.* **268**, 12758-12763

200.   Meisinger, C., Pfannschmidt, S., Rissler, M., Milenkovic, D., Becker, T., Stojanovski, D., Youngman, M. J., Jensen, R. E., Chacinska, A., Guiard, B., Pfanner, N., and Wiedemann, N. (2007) The morphology proteins Mdm12/Mmm1 function in the major beta-barrel assembly pathway of mitochondria. *EMBO J.* **26**, 2229-2239

201.   Meisinger, C., Sommer, T., and Pfanner, N. (2000) Purification of *Saccharomcyes cerevisiae* mitochondria devoid of microsomal and cytosolic contaminations. *Anal. Biochem.* **287**, 339-342

202.   Merkwirth, C., Dargazanli, S., Tatsuta, T., Geimer, S., Lower, B., Wunderlich, F. T., von Kleist-Retzow, J. C., Waisman, A., Westermann, B., and Langer, T. (2008) Prohibitins control cell proliferation and apoptosis by regulating OPA1-dependent cristae morphogenesis in mitochondria. *Genes Dev.* **22**, 476-488

203.   Meyer, B., Wittig, I., Trifilieff, E., Karas, M., and Schägger, H. (2007) Identification of two proteins associated with mammalian ATP synthase. *Mol. Cell. Proteomics* **6**, 1690-1699

204.   Michel, H. (1998) The mechanism of proton pumping by cytochrome *c* oxidase. *Proc. Natl. Acad. Sci. U. S. A.* **95**, 12819-12824

205.   Minauro-Sanmiguel, F., Wilkens, S., García, J. J. (2005) Structure of dimeric mitochondrial ATP synthase: novel F_0 bridging features and the structural basis of mitochondrial cristae biogenesis. *Proc. Natl. Acad. Sci. U. S. A.* **102**, 12356-12358

206.   Mitchell, P. (1961) Coupling of phosphorylation to electron and hydrogen transfer by a chemi-osmotic type of mechanism. *Nature* **191**, 144-148

207. Mitchell, P. (2011) Chemiosmotic coupling in oxidative and photosynthetic phosphorylation. 1966. *Biochim. Biophys. Acta* **1807**, 1507-1538

208. Miyakawa, I., Fumoto, S., Kuroiwa, T., and Sando, N. (1995) Characterization of DNA-binding proteins involved in the assembly of mitochondrial nucleoids in the yeast *Saccharomyces cerevisiae. Plant Cell Physiol.* **36**, 1179-1188

209. Miyakawa, I., Sando, N., Kawano, S., Nakamura, S., and Kuroiwa, T. (1987) Isolation of morphologically intact mitochondrial nucleoids from the yeast, *Saccharomyces cerevisiae*. *J. Cell Sci.* **88**, 431-439

210. Mootha, V. K., Bunkenborg, J., Olsen, J. V, Hjerrild, M., Wisniewski, J. R, Stahl, E., Bolouri, M. S., Ray, H. N., Sihag, S., Kamal, M., Patterson, N., Lander, E. S., and Mann, M. (2003) Integrated analysis of protein composition, tissue diversity, and gene regulation in mouse mitochondria. *Cell* **115**, 629-640

211. Morgner, N., Zickermann, V., Kerscher, S., Wittig, I., Abdrakhmanova, A., Barth, H. D., Brutschy, B., and Brandt, U. (2008) Subunit mass fingerprinting of mitochondrial complex I. *Biochim. Biophys. Acta* **1777**, 1384-1391

212. Nass, M. M. (1966) The circularity of mitochondrial DNA. *Proc. Natl. Acad. Sci. U. S. A.* **56**, 1215-1222

213. Nass, M. M. (1969) Mitochondrial DNA. I. Intramitochondrial distribution and structural relations of single- and double-length circular DNA. *J. Mol. Biol*. **42**, 521-528

214. Nass, M. M., and Nass, S. (1963a) Intramitochondrial fibers with DNA characteristics. I. Fixation and electron staining reactions. *J. Cell Biol.* **19**, 593-611

215. Nass, S., and Nass, M. M. (1963b) Intramitochondrial fibers with DNA characteristics. II. Enzymatic and other hydrolytic treatments. *J. Cell Biol.* **19**, 613-629

216. Navratil, M., Poe, B. G., and Arriaga, E. A. (2007) Quantitation of DNA copy number in individual mitochondrial particles by capillary electrophoresis. *Anal. Chem*. **79**, 7691-7699

217. Neupert, W., and Brunner, M. (2002) The protein import motor of mitochondria. *Nat. Rev. Mol. Cell Biol.* **3**, 555-565

References

218. Newman, S. M., Zelenaya-Troitskaya, O., Perlman, P. S., and Butow, R. A. (1996) Analysis of mitochondrial DNA nucleoids in wild-type and a mutant strain of *Saccharomyces cerevisiae* that lacks the mitochondrial HMG box protein Abf2p. *Nucl. Acids Res.* **24**, 386-393

219. Ngo, H. B., Kaiser, J. T., and Chan, D. C. (2012) Tfam, a mitochondrial transcription and packaging factor, imposes a U-turn on mitochondrial DNA. *Nat. Struct. Mol. Biol.* **18**, 1290-1296

220. Nübel, E., Wittig, I., Kerscher, S., Brandt, U., and Schägger, H. (2009) Two-dimensional native electrophoretic analysis of respiratory supercomplexes from *Yarrowia lipolytica*. *Proteomics* **9**, 2408-2418

221. Oberto, J., Drlica, K., and Rouviere-Yaniv, J. (1994) Histones, HMG, HU, IHF: Meme combat. *Biochimie* **76**, 901-908

222. Olsen, J. V., de Godoy, L. M., Li, G. Q., Macek, B., Mortensen, P., Pesch, R., Makarov, A., Lange, O., Horning, S., and Mann, M. (2005) Parts per million mass accuracy on an orbitrap mass spectrometer via lock mass injection into a C-trap. *Mol. Cell. Proteomics* **4**, 2010-2021

223. Olsen, J. V., Macek, B., Lange, O., Makarov, A., Horning, S., and Mann, M. (2007) Higher-energy C-trap dissociation for peptide modification analysis. *Nat. Methods* **4**, 709-712

224. Olsen, J. V., Schwartz, J. C., Griep-Raming, J., Nielsen, M. L., Eduard, D. E., Denisov, E., Lange, O., Remes, P., Taylor, D., Splendore, M., Wouters, E. R., Senko, M., Makarov, A., Mann, M., and Horning, S. (2009) A dual pressure linear ion trap Orbitrap instrument with very high sequencing speed. *Mol. Cell. Proteomics* **8**, 2759-2769

225. Palade, G. (1952) The fine structure of mitochondria. *Anat. Rec.* **114**, 427-451

226. Pan, C., Park, B. H., McDonald, W. H., Carey, P. A., and Banfield, J. F., VerBerkmoes, N. C., Hettich, R. L., and Samatova, N. F. (2010) A high-throughput *de novo* sequencing approach for shotgun proteomics using high-resolution tandem mass spectrometry. *BMC Bioinformatics* **11**, 118

227. Parisi, M. A., and Clayton, D. A. (1991) Similarity of human mitochondrial transcription factor 1 to high mobility group proteins. *Science* **252**, 965-969

228. Parisi, M. A., Xu, B., and Clayton, D. A. (1993) A human mitochondrial transcriptional activator can functionally replace a yeast mitochondrial HMG-box protein both *in vivo* and *in vitro*. *Mol. Cell. Biol.* **13**, 1951-1961

229. Paschen, S. A., and Neupert, W. (2001) Protein import into mitochondria. *IUBMB Life* **52**, 101-112

230. Paumard, P., Vaillier, J., Coulary, B., Schaeffer, J., Soubannier, V., Mueller, D. M., Brethes, D., di Rago, J. P., and Velours, J. (2002) The ATP synthase is involved in generating mitochondrial cristae morphology. *EMBO J.* **21**, 221-230

231. Pellegrini, M., Asin-Cayuela, J., Erdjument-Bromage, H., Tempst, P., Larsson, N. G., and Gustafsson, C. M. (2009) MTERF2 is a nucleoid component in mammalian mitochondria. *Biochim. Biophys. Acta* **1787**, 296-302

232. Perry, A. J., Rimmer, K. A., Mertens, H. D., Waller, R. F., Mulhern, T. D., Lithgow, T., and Gooley, P. R. (2008) Structure, topology and function of the translocase of the outer membrane of mitochondria. *Plant Physiol. Biochem.* **46**, 265-274

233. Pfeiffer, K., Gohil, V., Stuart, R. A., Hunte, C., Brandt, U., Greenberg, M. L., and Schägger, H. (2003) Cardiolipin stabilizes respiratory chain supercomplexes, *J. Biol. Chem.* **278**, 52873-52880

234. Poe, B. G., Duffy, C. F., Greminger, M. A., Nelson, B. J., and Arriaga, E. A. (2010) Detection of heteroplasmy in individual mitochondrial particles. *Anal. Bioanal. Chem.* **397**, 3397-3407

235. Pohjoismäki, J. L., Wanrooij, S., Hyvärinen, A. K., Goffart, S., Holt, I. J., Spelbrink, J. N., and Jacobs, H. T. (2006) Alterations to the expression level of mitochondrial transcription factor A, TFAM, modify the mode of mitochondrial DNA replication in cultured human cells. *Nucl. Acids Res.* **34**, 5815-5828

236. Ponamarev, M. V., She, Y. M., Zhang, L., and Robinson, B. H. (2005) Proteomics of bovine mitochondrial RNA-binding proteins: HES1/KNP-I is a new mitochondrial resident protein. *J. Proteome Res.* **4**, 43-52

237. Prachar, J. (2010) Mouse and human mitochondrial nucleoid: detailed structure in relation to function. *Gen. Physiol. Biophys.* **29**, 160-174

238. Rais, I., Karas, M., and Schägger, H. (2004) Two-dimensional electrophoresis for the isolation of integral membrane proteins and mass spectrometric identification. *Proteomics* **4**, 2567-2571

239. Rehling, P., Pfanner, N., and Meisinger, C. (2003) Insertion of hydrophobic membrane proteins into the inner mitochondrial membrane-a guided tour. *J. Mol. Biol.* **326**, 639-657

240. Reyes, A., He, J., Mao, C. C., Bailey, L. J., Di Re, M., Sembongi, H., Kazak, L., Dzionek, K., Holmes, J. B., Cluett, T. J., Harbour, M. E., Fearnley, I. M., Crouch, R. J., Conti, M. A., Adelstein, R. S., Walker, J. E., and Holt, I. J. (2011) Actin and myosin contribute to mammalian mitochondrial DNA maintenance. *Nucl. Acids Res.* **39**, 5098-5108

241. Rizzuto, R., Pinton, P., Carrington, W., Fay, F. S., Fogarty, K. E., Lifshitz, L. M., Tuft, R. A., and Pozzan, T. (1998) Close contacts with the endoplasmic reticulum as determinants of mitochondrial Ca^{2+} responses. *Science* **280**, 1763-1766

242. Rorbach, J., Richter, R., Wessels, H. J., Wydro, M., Pekalski, M., Farhoud, M., Kuhl, I., Gaisne, M., Bonnefoy, N., Smeitink, J. A., Lightowlers, R. N., and Chrzanowska-Lightowlers, Z. M. A. (2008) The human mitochondrial ribosome recycling factor is essential for cell viability. *Nucl. Acids Res.* **36**, 5787-5799

243. Rubio-Cosials, A., Sidow, J. F., Jiménez-Menéndez, N., Fernández-Millán, P., Montoya, J., Jacobs, H. T., Coll, M., Bernadó, P., and Solà, M. (2011) Human mitochondrial transcription factor A induces a U-turn structure in the light strand promoter. *Nat. Struct. Mol. Biol.* **18**, 1281-1289

244. Ruprecht, J., and Nield. J. (2001) Determining the structure of biological macromolecules by transmission electron microscopy, single particle analysis and 3D reconstruction. *Prog. Biophys. Mol. Biol.* **75**, 121-164

245. Sambrook, J., Fritsch, E. F., and Maniatis, T. (1989) Molecular cloning. A laboratory manual. Cold Spring Harbor Laboratory Press, Cold Spring Harbor, NY.

246.   Saraste, M. (1999) Oxidative phosphorylation at the fin de siècle. *Science* **283**, 1488-1493

247.   Sasaki, N., Kuroiwa, H., Nishitani, C., Takano, H., Higashiyama, T., Kobayashi, T., Shirai, S., Sakai, A., Kawano, S., Murakami-Murofushi, K., and Kuroiwa, T. (2003) Glom is a novel mitochondrial DNA packaging protein in Physarum polycephalum and causes intense chromatin condensation without suppressing DNA functions. *Mol. Biol. Cell* **14**, 4758-4769

248.   Satoh, M., and Kuroiwa, T. (1991) Organization of multiple nucleoids and DNA molecules in mitochondria of a human cell. *Exp. Cell Res.* **196**, 137-140

249.   Schäfer, E., Seelert, H., Reifschneider, N. H., Krause, F., Dencher, N. A., and Vonck, J. (2006) Architecture of active mammalian respiratory chain supercomplexes. *J. Biol. Chem.* **281**, 15370-15375

250.   Schäfer, E., Dencher, N. A., Vonck, J., Parcej, D. N. (2007) Three-dimensional structure of the respiratory chain supercomplex $I_1III_2IV_1$ from bovine heart mitochondria. *Biochemistry* **46**, 12579-12585

251.   Schägger, H. (2002) Respiratory chain supercomplexes of mitochondria and bacteria. *Biochim. Biophys. Acta* **1555**, 154-159

252.   Schägger, H. (2006) Tricine-SDS-PAGE. *Nat. Protocols* **1**, 16-22

253.   Schägger, H., and Pfeiffer, K. (2000) Supercomplexes in the respiratory chains of yeast and mammalian mitochondria. *EMBO J.* **19**, 1777-1783

254.   Schägger, H., and Pfeiffer, K. (2001) The ratio of oxidative phosphorylation complexes I-V in bovine heart mitochondria and the composition of respiratory chain supercomplexes. *J. Biol. Chem.* **276**, 37861-37867

255.   Schägger, H., and von Jagow, G. (1987) Tricine-sodium dodecyl sulfate-polyacrylamide gel electrophoresis for the separation of proteins in the range from 1 to 100 kDa. *Anal. Biochem.* **166**, 368-379

256.   Schägger, H., and von Jagow, G. (1991) Blue native electrophoresis for isolation of membrane protein complexes in enzymatically active form. *Anal. Biochem.* **199**, 223-231

References

257. Schägger, H., Cramer, W. A., and von Jagow, G. (1994) Analysis of molecular masses and oligomeric states of protein complexes by blue native electrophoresis and isolation of membrane protein complexes by two-dimensional native electrophoresis. *Anal. Biochem.* **217**, 220-230

258. Schägger, H., de Coo, R., Bauer, M. F., Hofmann, S., Godinot, C., and Brandt, U. (2004) Significance of respirasomes for the assembly/stability of human respiratory chain complex I. *J. Biol. Chem.* **279**, 36349-36353

259. Schägger, H., Hagen, T., Roth, B., Brandt, U., Link, T. A., and von Jagow, G. (1990) Phospholipid specificity of bovine heart bc_1 complex. *Eur. J. Biochem.* **190**, 123-130

260. Shevchenko, A., Tomas, H., Havlis, J., Olsen, J. V., and Mann, M. (2006) In-gel digestion for mass spectrometric characterization of proteins and proteomes. *Nat. Protocols* **1**, 2856-2860

261. Schwartz, J. C., and Jardine, I. (1996) Quandrupole ion trap mass spectrometry. *Methods Enzymol.* **270**, 552-586

262. Schwerzmann, K., Cruz-Orive, L. M., Eggman, R., Sänger, A., and Weibel, E. R. (1986) Molecular architecture of the inner membrane of mitochondria from rat liver: a combined biochemical and stereological study. *J. Cell Biol.* **102**, 97-103

263. Shin, J. H., Weitzdoerfer, R., Fountoulakis, M., and Lubec, G. (2004) Expression of cystathionine beta-synthase, pyridoxal kinase, and ES1 protein homolog (mitochondrial precursor) in fetal Down syndrome brain. *Neurochem. Int.* **45**, 73-79

264. Silva, J., Kohler, M., Graff, C., Oldfors, A., Magnusson, M., Berggren, P., and Larsson, N. G. (2000) Impaired insulin secretion and β-cell loss in tissue-specific knockout mice with mitochondrial diabetes. *Nat. Genet.* **26**, 335-340

265. Slayter, E. M., and Slayter, H. S. (1992) Light and Electron Microscopy. Cambridge University Press 149-167

266. Smith, A. L. (1967) Preparation, properties, and conditions for assay of mitochondria: slaughterhouse material, small-scale. *Methods Enzymol.* **10**, 81-86

267.   Sogo, L. F., and Yaffe, M. P. (1994) Regulation of mitochondrial morphology and inheritance by Mdm10p, a protein of the mitochondrial outer membrane. *J. Cell Biol.* **126**, 1361-1373

268.   Solmaz, S. R., and Hunte, C. (2008) Structure of complex III with bound cytochrome *c* in reduced state and definition of a minimal core interface for electron transfer. *J. Biol. Chem.* **283**, 17542-17549

269.   Sone, N., Sekimachi, M., and Kutoh, E. (1987) Identification and properties of a quinol oxidase super-complex composed of a bc_1 complex and cytochrome oxidase in the thermophilic bacterium PS3. *J. Biol. Chem.* **262**, 15386-15391

270.   Spelbrink, J. N. (2010) Functional organization of mammalian mitochondrial DNA in nucleoids: history, recent developments, and future challenges. *IUBMB Life* **62**, 19-32

271.   Spelbrink, J. N., Li, F. Y., Tiranti, V., Nikali, K., Yuan, Q. P., Tariq, M., Wanrooij, S., Garrido, N., Comi, G., Morandi, L., Santoro, L., Toscano, A., Fabrizi, G. M., Somer, H., Croxen, R., Beeson, D., Poulton, J., Suomalainen, A., Jacobs, H. T., Zeviani, M., and Larsson, C. (2001) Human mitochondrial DNA deletions associated with mutations in the gene encoding Twinkle, a phage T7 gene 4-like protein localized in mitochondria. *Nat. Genet.* **28**, 223-231

272.   Stahlberg, H., and Walz, T. (2008) Molecular electron microscopy: state of the art and current challenges. *ACS Chem. Biol.* **3**, 268-281

273.   Starkov, A. A. (2008) The role of mitochondria in reactive oxygen species metabolism and signaling. *Ann. N. Y. Acad. Sci.* **1147**, 37-52

274.   Stevens, B. (1981) Mitochondrial structure. In: *The Molecular Biology of the Yeast Saccharomyces, Life Cycle and Inheritance*. Strathern, J. N., Jones, E. W., and Broach J. R. (Eds.). Cold Spring Harbor Laboratory Press, Cold Spring Harbor **1**, 471-504

275.   Stock, D., Leslie, A. G., and Walker, J. E. (1999) Molecular architecture of the rotary motor in ATP synthase. *Science* **286**, 1700-1705

276.   Strauss, M., Hofhaus, G., Schröder, R. R., and Kühlbrandt, W. (2008) Dimer ribbons of ATP synthase shape the inner mitochondrial membrane. *EMBO J.* **27**, 1154-1160

References

277. Strecker, V., Wumaier, Z., Wittig, I., and Schägger, H. (2010) Large pore gels to separate mega protein complexes larger than 10 MDa by blue native electrophoresis: isolation of putative respiratory strings or patches. *Proteomics* **18**, 3379-3387

278. Stroh, A., Anderka, O., Pfeiffer, K., Yagi, T., Finel, M., Ludwig, B., and Schägger, H., (2004) Assembly of respiratory complexes I, III, and IV into NADH oxidase supercomplex stabilizes complex I in *Paracoccus denitrificans*. *J. Biol. Chem.* **279**, 5000-5007

279. Suzuki, T., Kawano, S., and Kuroiwa, T. (1982) Structure of three-dimensionally rod-shaped mitochondrial nucleoids isolated from the slime mould *Physarum polycephalum. J. Cell Sci.* **58**, 241-261

280. Takamatsu, C., Umeda, S., Ohsato, T., Ohno, T., Abe, Y., Fukuoh, A., Shinagawa, H., Hamasaki, N., and Kang, D. (2002) Regulation of mitochondrial D-loops by transcription factor A and single-stranded DNA binding protein. *EMBO Rep.* **3**, 451-456

281. Takata, K., Yoshida, H., Hirose, F., Yamaguchi, M., Kai, M., Oshige, M., Sakimoto, I., Koiwai, O., and Sakaguchi, K. (2001) Drosophila mitochondrial transcription factor A: characterization of its cDNA and expression pattern during development. *Biochem. Biophys. Res. Commun.* **287**, 474-483

282. Taylor, R. W., and Turnbull, D. M. (2005) Mitochondrial DNA mutations in human disease. *Nat. Rev. Genet.* **6**, 389-402

283. Taylor, S. W., Fahy, E., Zhang, B., Glenn, G. M., Warnock, D. E., Wiley, S., Murphy, A. N., Gaucher, S. P., Capaldi, R. A., Gibson, B. W., and Ghosh, S. S. (2003) Characterization of the human heart mitochondrial proteome. *Nat. Biotechnol.* **21**, 281-286

284. Thornburn, D. R. (2004) Mitochondrial disorders: prevalence, myths and advances. *J. Inherit. Metab. Dis.* **27**, 349-362

285. Tisdale, H. D. (1967) Preparation and properties of succinic-cyctochrome *c* reductase (complex II-III). *Methods Enzymol.* **10**, 213-216

286.   Tominaga, K., Hayashi. J., Kagawa, Y., and Ohta, S. (1993) Smaller isoform of human mitochondrial transcription factor 1: its wide distribution and production by alternative splicing. *Biochem. Biophys. Res. Commun*. **194**, 544-550

287.   Trifunovic, A., Wredenberg, A., Falkenberg, M., Spelbrink, J. N., Rovio, A. T., Bruder, C. E., Bohlooly, Y. M., Gidlöf, S., Oldfors, A., Wibom, R., Törnell, J., Jacobs, H. T., and Larsson, N. G. (2004) Premature aging in mice expressing defective mitochondrial DNA polymerase. *Nature* **429**, 417-423

288.   Tsukihara, T., Aoyama, H., Yamashita, E., Tomizaki, T., Yamaguchi, H., Shinzawa-Itoh, K., Nakashima, R., Yaono, R., and Yoshikawa, S. (1996) The whole structure of the 13-subunit oxidized cytochrome *c* oxidase at 2.8 Å. *Science* **272**, 1136-1144

289.   Turrens, J. F., and Boveris, A. (1980) Generation of superoxide anion by the NADH dehydrogenase of bovine heart mitochondria. *Biochem. J.* **191**, 421-427

290.   Tyynismaa, H., Sembongi, H., Bokori-Brown, M., Granycome, C., Ashley, N., Poulton, J., Jalanko, A., Spelbrink, J. N., Holt, I. J, and Suomalainen, A. (2004) Twinkle helicase is essential for mtDNA maintenance and regulates mtDNA copy number. *Hum. Mol. Genet.* **13**, 3219-3227

291.   Ugalde, C., Janssen, R. J., van den Heuvel, L. P., Smeitink, J. A., and Nijtmans, L. G. J. (2004) Differences in assembly or stability of complex I and other mitochondrial OXPHOS complexes in inherited complex I deficiency. *Hum. Mol. Genet.* **13,** 659-667

292.   Van Tuyle, G. C., and McPherson, M. L. (1979) A compact form of rat liver mitochondrial DNA stabilized by bound proteins. *J. Biol. Chem*. **254**, 6044-6053

293.   Van Tuyle, G. C., and Pavco, P. A. (1985) The rat mitochondrial DNA–protein complex: displaced single strands of replicative intermediates are protein coated. *J. Cell Biol.* **100**, 251-257

294.   Venturi, M., Rimon, A., Gerchman, Y., and Hunte, C., Padan, E., and Michel, H. (2002) The monoclonal antibody 1F6 identifies a pH-dependent conformational change in the hydrophilic NH2 terminus of NhaA Na1/H1 antiporter of *Escherichia coli*. *J. Biol. Chem.* **275**, 4734-4742

295. Virgilio, De. C., Pousis, C., Bruno, S., and Gadaleta, G. (2011) New isoforms of human mitochondrial transcription factor A detected in normal and tumoral cells. *Mitochondrion* **11**, 287-295

296. Wang, J., Wilhelmsson, H., Graff, C., Li, H., Oldfors, A., Rustin, P., Bruning, J., Kahn, C., Clayton, D., Barsh, G., Thoren, P., and Larsson, N. G. (1999) Dilated cardiomyopathy and atrioventricular conduction blocks induced by heart-specific inactivation of mitochondrial DNA gene expression. *Nat. Genet.* **21**,133-137

297. Wang, Y., and Bogenhagen, D. F. (2006) Human mitochondrial DNA nucleoids are linked to protein folding machinery and metabolic enzymes at the mitochondrial inner membrane. *J. Biol. Chem.* **281**, 25791-25802

298. Wang, Z., Cotney, J., and Shadel, G. S. (2007) Human mitochondrial ribosomal protein MRPL12 interacts directly with mitochondrial RNA polymerase to modulate mitochondrial gene expression. *J. Biol. Chem.* **282**, 12610-12618

299. Wanrooij, S., Luoma, P., van Goethem, G., van Broeckhoven, C., Suomalainen, A., and Spelbrink, J. N. (2004) Twinkle and POLG defects enhance age-dependent accumulation of mutations in the control region of mtDNA. *Nucl. Acids Res.* **32**, 3053-3064

300. Watt, I. N., Montgomery, M. G., Runswick, M. J., Leslie, A. G., and Walker, J. E. (2010) Bioenergetic cost of making an adenosine triphosphate molecule in animal mitochondria. *Proc. Natl. Acad. Sci. U. S. A.* **107**, 16823-16827

301. Wenz, T., Hielscher, R., Hellwig, P., Schägger, H., Richers, S., and Hunte, C. (2009) Role of phospholipids in respiratory cytochrome bc_1 complex catalysis and supercomplex formation. *Biochim. Biophys. Acta* **1787**, 609-616

302. Wenz, T. (2004) Wechselwirkung des Cytochrom-bc_1-Komplexes aus *Saccharomyces cerevisiae* mit seinen Substraten sowie mit der Cytochrom-*c*-Oxidase. *Thesis*, Goethe University, Frankfurt am Main, Germany

303. Wikström, M. (1984) Two protons are pumped from the mitochondrial matrix per electron transferred between NADH and ubiquinone. *FEBS Lett.* **169**, 300-304

304.   Wikström, M., Krab, K., and Saraste, M. (1981) Proton-translocating cytochrome complexes. *Annu. Rev. Biochem.* **50**, 623-655

305.   Williamson, D. (2002) The curious history of yeast mitochondrial DNA. *Nat. Rev. Genet.* **3**, 475-481

306.   Wittig, I., and Schägger, H. (2005) Advantages and limitations of clear native polyacrylamide gel electrophoresis. *Proteomics* **5**, 4338-4346

307.   Wittig, I., and Schägger, H. (2008a) Features and applications of blue native and clear native electrophoresis. *Proteomics* **8**, 3974–3990

308.   Wittig, I., and Schägger, H. (2008b) Structural organization of mitochondrial ATP synthase. *Biochim. Biophys. Acta* **1777**, 592-598

309.   Wittig, I., and Schägger, H. (2009a) Supramolecular organization of ATP synthase and respiratory chain in mitochondrial membranes. *Biochim. Biophys. Acta* **1787**, 672-680

310.   Wittig, I., Beckhaus, T., Wumaier, Z., Karas, M., and Schägger, H. (2010a) Mass estimation of native proteins by blue native electrophoresis: principles and practical hints. *Mol. Cell. Proteomics* **9**, 2149-2161

311.   Wittig, I., Braun, H. P., and Schägger, H. (2006a) Blue-Native-PAGE. *Nat. Protocols* **1**, 416-428

312.   Wittig, I., Carrozzo, R., Santorelli, F. M., and Schägger, H. (2006b) Supercomplexes and subcomplexes of mitochondrial oxidative phosphorylation. *Biochim. Biophys. Acta* **1757**, 1066-1072

313.   Wittig, I., Carrozzo, R., Santorelli, F. M., and Schägger, H. (2007b) Functional assays in high-resolution clear native gels to quantify mitochondrial complexes in human biopsies and cell-lines. *Electrophoresis* **28**, 3811-3820

314.   Wittig, I., Karas, M., and Schägger, H. (2007a) High-resolution clear native electrophoresis for in-gel functional assays and fluorescence studies of membrane protein complexes. *Mol. Cell. Proteomics* **6**, 1215-1225

References

315. Wittig, I., Meyer, B., Heide, H., Steger, M., Bleier, L., Wumaier, Z., Karas, M., and Schägger, H. (2010b) Assembly and oligomerization of human ATP synthase lacking mitochondrial subunits a and A6L. *Biochim. Biophys. Acta* **1797**, 1004-1011

316. Wittig, I., Velours, J., Stuart, R., and Schägger, H. (2008) Characterization of domain-interfaces in monomeric and dimeric ATP synthase. *Mol. Cell. Proteomics* **7**, 995-1004

317. Wittig, I., and Schägger, H. (2009b) Native electrophoretic techniques to identify protein-protein interactions. *Proteomics* **9**, 5214-5223

318. Woldringh, C. L. (2002) The role of co-transcriptional translation and protein translocation (transertion) in bacterial chromosome segregation. *Mol. Microbiol.* **45**, 17-29

319. Wumaier, Z., Nübel, E., Wittig, I., and Schägger, H. (2009) Two-dimensional native electrophoresis for fluorescent and functional assays of mitochondrial complexes. *Methods Enzymol.* **456**, 153-168

320. Xie, J., Marusich, M. F., Souda, P., Whitelegge, J., and Capaldi, R. A. (2007) The mitochondrial inner membrane protein Mitofilin exists as a complex with SAM50, metaxins 1 and 2, coiled-coil-helix coiled-coil-helix domain-containing protein 3 and 6 and DnaJC11. *FEBS Lett.* **581**, 3545-3549

321. Yang, C., Curth, U., Urbanke, C., and Kang, C. (1997) Crystal structure of human mitochondrial single-stranded DNA binding protein at 2.4 Å resolution. *Nat. Struct. Biol.* **4**,153-157

322. Yankovskaya, V., Horsefield, R., Tornroth, S., Luna-Chavez, C., Leger, C., Byrne, B., Cecchini, G., and Iwata, S. (2003) Architecture of succinate dehydrogenase and reactive oxygen species generation. *Science* **299**, 700-704

323. Yoshikawa, S., Shinzawa-Itoh, K., Nakashima, R., Yaono, R., Yamashita, E., Inoue, N., Yao, M., Fei, M. J., Libeu, C. P., Mizushima, T., Yamaguchi, H., Tomizaki, T., and Tsukihara, T. (1998) Redox-coupled crystal structural changes in bovine heart cytochrome *c* oxidase. *Science* **280**, 1723-1729

324. Yost, R. A., and Enke, C. G. (1979) Triple quadrupole mass spectrometry for direct mixture analysis and structure elucidation. *Anal. Chem*. **51**, 1251-1264

325. Zelenaya-Troitskaya, O., Perlman, P. S., and Butow, R. A. (1995) An enzyme in yeast mitochondria that catalyzes a step in branched-chain amino acid biosynthesis also functions in mitochondrial DNA stability. *EMBO J.* **14**, 3268-3276

326. Zerbetto, E., Vergani, L., and Dabbeni-Sala, F. (1997) Quantification of muscle mitochondrial oxidative phosphorylation enzymes via histochemical staining of blue native polyacrylamide gels. *Electrophoresis* **18**, 2059-2064

327. Zhang, M., Mileykovskaya, E., and Dowhan, W. (2002) Gluing the respiratory chain together: cardiolipin is required for supercomplex formation in the inner mitochondrial membrane. *J. Biol. Chem.* **277**, 43553-43556

328. Zhang, Z., Huang, L., Shulmeister, V. M., Yi, Chi., Kim, K. K., Hung L. W., Crofts, A. R., Berry, E. A., and Kim, S. H. (1998) Electron transfer by domain movement in cytochrome *bc$_1$. Nature* **392**, 677-684

329. Zhou, Z. H., Liao, W., Cheng, R. H., Lawson, J. E., McCarthy, D. B., Reed, L. J., and Stoops, J. K. (2001) Direct evidence for the size and conformational variability of the pyruvate dehydrogenase complex revealed by three-dimensional electron microscopy. The "breathing" core and its functional relationship to protein dynamics. *J. Biol. Chem.* **276**, 21704-21713

330. Zhou, C., Huang, Y., and Przedborski, S. (2008) Oxidative stress in Parkinson's disease: a mechanism of pathogenic and therapeutic significance. *Ann. N. Y. Acad. Sci.* **1147**, 93-104

331. Zickermann, V., Bostina, M., Hunte, C., Ruiz, T., Radermacher, M., and Brandt, U. (2003) Functional implications from an unexpected position of the 49 kDa subunit of complex I. *J. Biol. Chem.* **276**, 29072-29078

332. Zickermann, V., Wumaier, Z., Wrzesniewska, B., Hunte, C., and Schägger, H. (2010) Native immunoblotting of blue native gels (NIBN) to identify conformation-specific antibodies. *Proteomics* **10**, 1959-1963

VII. Appendix I

LC-MS/MS spectrum of NUPM subunit of complex I
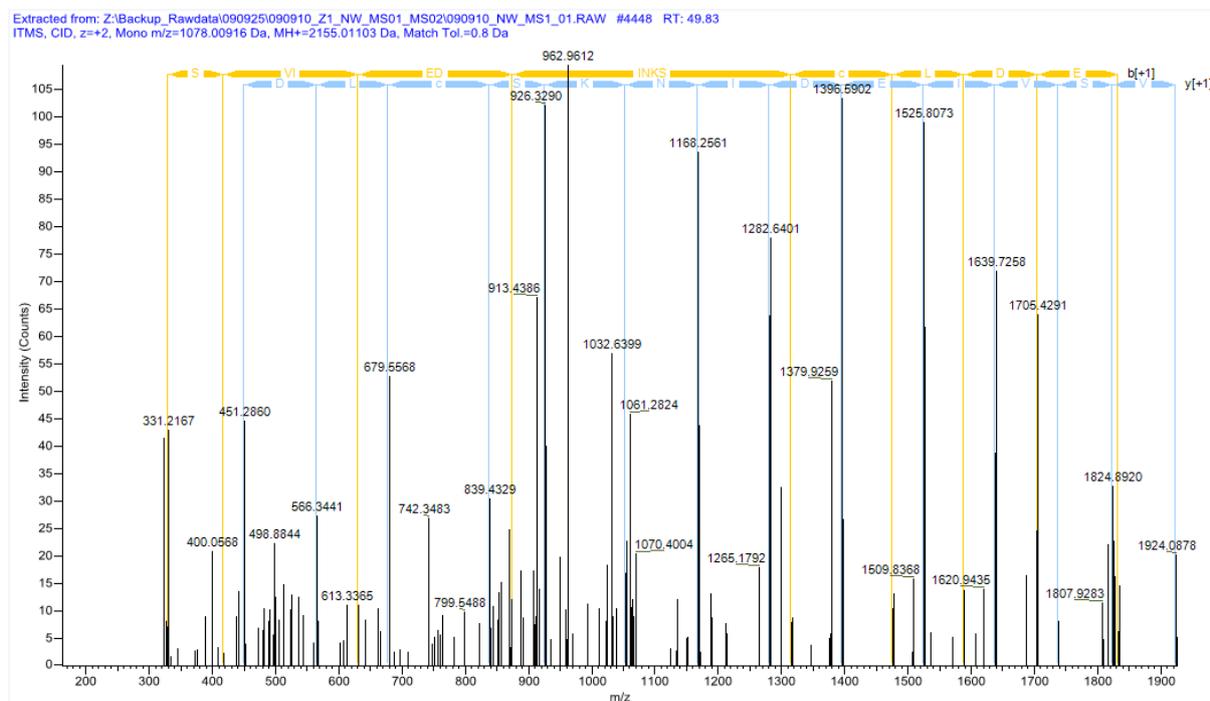
Figure 50. LC-MS/MS spectrum of NUPM subunit of complex I from *Y. lipolytica*. Monoclonal antibody 31A8 recognized a protein spot on a 3-D BN/dSDS gel (Fig. 21). The protein spot was excised for the protein identification by LC-MS/MS. 15 non-redundant peptides were found, which could be assigned with a sequence coverage of 83% to the NUPM subunit of complex I. A spectrum of one of these peptides with highst Mascot score (94) is exemplified here. The sequence of this peptide is: CAVSVIEDINKSCLDEFR; C1-Carbamidomethyl (57.02146 Da), C13-Carbamidomethyl (57.02146 Da); Charge: +2, Monoisotopic m/z: 1078.00916 Da (-2.27 ppm), MH+: 2155.01103 Da, RT: 49.83 min, Identified with Mascot; IonScore: 96, Fragment Match Tolerance: 0.8 Da; Reference: NUPM similar to uniprot|P21976 Neurospora crassa NADH:ubiquinone oxidoreductase 20.8 kDa subunit (*Y. lipolytica*) complete CDS.

Table 10. Protein composition of mitochondrial nucleoids at different preparative steps. Red lines indicate that human homologues have been identified by other groups (see Bogenhagen et al. 2008). Mass, the precursor mass is indicated; Pept, number of non-redundant peptides; Cov, sequence coverage; Rank, proteins were ranked according to the Mascot scores; mito, mitochondrial; DH, dehydrogenase; DHC, dehydrogenase complex

UniProt accession	Protein; Gene	Purified 33 MDa nucleoid band from blue native gel					Crude nucleoids from sucrose gradient	
		Mass (kDa)	Pept	Cov (%)	Mascot score	Rank	Mascot score	Rank
Q29RI0|ADCK3_BOVIN	Chaperone activity of bc_1 complex-like, mitochondrial; CABC1	72036	58	76.7	35580	1	16034	2
P49410|EFTU_BOVIN	Elongation factor Tu, mito; TUFM	49367	51	77.2	34370	2	14709	3
Q04467|IDHP_BOVIN	Isocitrate dehydrogenase [NADP], mitochondrial; IDH2	50707	36	72.3	30776	3	7507	15
Q148D5|SUCB1_BOVIN	Succinyl-CoA ligase [ADP-forming] subunit beta, mitochondrial; SUCLA2	50098	42	67.0	26266	4	11288	5
Q3T0U3|Q3T0U3_BOVIN	Es1 protein; ES1	28681	28	78.5	24145	5	12414	4
Q59HJ6|LONM_BOVIN	Lon protease homolog, mito; LONP1	106604	62	62.1	23367	6	16658	1
Q17QJ1|ACSF2_BOVIN	Acyl-CoA synthetase family member 2, mitochondrial; ACSF2	68157	47	70.7	21231	7	10752	6
P43896|EFTS_BOVIN	Elongation factor Ts, mito; TSFM	36579	27	74.6	15547	8	6828	18
P19483|ATPA_BOVIN	ATP synthase subunit alpha; ATP5A1	59683	43	64.6	14745	9	5682	23
Q3MHX5|SUCB2_BOVIN	Succinyl-CoA ligase [GDP-forming] subunit beta, mitochondrial; SUCLG2	46662	34	60.6	14335	10	6890	17
P15690|NDUS1_BOVIN	NADH-ubiquinone oxidoreductase 75 kDa subunit, mitochondrial; NDUFS1	79391	49	69.6	13848	11	7971	13
P00829|ATPB_BOVIN	ATP synthase subunit beta; ATP5B	56249	44	79.7	13508	12	9705	8
Q0III1|Q0III1_BOVIN	Methylmalonyl Coenzyme A mutase; MUT	83204	53	73.7	13308	13	9559	9
Q58DR8|SUCA_BOVIN	Succinyl-CoA ligase [GDP-forming] subunit alpha, mito; SUCLG1	36144	23	38.7	12923	14	7720	14
Q24JZ7|Q24JZ7_BOVIN	3-oxoacid CoA transferase 1; OXCT1	56417	32	57.9	12380	15	4199	31
Q58CP0|IDH3G_BOVIN	Isocitrate dehydrogenase [NAD] subunit gamma, mito; IDH3G	42836	27	50.3	12215	16	6067	22
P11181|ODB2_BOVIN	Lipoamide acyltransferase of branched-chain alpha-keto acid DHC, mito; DBT	53376	28	63.5	11954	17	6121	20
A4FUC5|A4FUC5_BOVIN	Acyl-CoA synthetase short-chain family member 1; ACSS1	74249	39	61.6	11380	18	8737	11
Q3ZBQ0|SIRT5_BOVIN	NAD-dependent deacetylase sirtuin-5; SIRT5	33966	19	59.0	11317	19	6114	21

A5D9G3|A5D9G3_BOVIN	Similar to Succinyl-CoA ligase [GDP-form.] beta-chain, mito; LOC283398	46635	34	60.6	10757	20	4496	27
Q2TBI4|TRAP1_BOVIN	Heat shock protein 75 kDa, mitochondrial; TRAP1	79331	49	59.5	9660	21	9053	10
A0JN67|A0JN67_BOVIN	Glutaminase; GLS	66169	35	61.2	8678	22	4393	29
Q07536|MMSA_BOVIN	Methylmalonate-semialdehyde DH [acylating], mitochondrial; ALDH6A1	58026	32	61.5	8455	23	5007	25
Q1RMM6|Q1RMM6_BOVIN	Coenzyme Q10 homolog A (*S. cerevisiae*); COQ10A	27094	18	58.4	8098	24	3281	37
Q2NL34|COQ9_BOVIN	Ubiquinone biosynthesis protein COQ9, mitochondrial; COQ9	35756	21	44.8	7230	25	4432	28
P20004|ACON_BOVIN	Aconitate hydratase, mito; ACO2	85306	44	54.4	7028	26	7477	16
A7YWE4|AL4A1_BOVIN	Delta-1-pyrroline-5-carboxylate de-hydrogenase, mito; ALDH4A1	61456	23	50.4	6744	27	1582	66
O77784|IDH3B_BOVIN	Isocitrate dehydrogenase [NAD] subunit beta, mitochondrial; IDH3B	42470	24	45.2	6124	28	3499	34
Q2KJB7|CPT2_BOVIN	Carnitine O-palmitoyltransferase 2, mitochondrial; CPT2	74436	33	48.2	6079	29	2431	45
Q3ZCH0|GRP75_BOVIN	Stress-70 protein, mito; HSPA9	73696	36	48.7	5997	30	9949	7
P11024|NNTM_BOVIN	NAD(P) transhydrogenase, mito; NNT	113780	27	27.8	5637	31	4236	30
Q3SZ00|Q3SZ00_BOVIN	HADHA protein; HADHA	83196	50	57.1	5543	32	6689	19
O46504|PDPR_BOVIN	Pyruvate dehydrogenase phosphatase regulatory subunit, mito; PDPR	98794	57	58.5	5466	33	2526	43
Q148N0|ODO1_BOVIN	2-oxoglutarate dehydrogenase, mitochondrial; OGDH	115734	38	46.4	5048	34	3150	39
Q3SZ73|ABHDB_BOVIN	Abhydrolase domain-containing protein 11; ABHD11	33527	29	79.9	4925	35	2387	46
Q3SZI8|IVD_BOVIN	Isovaleryl-CoA dehydrogenase, mitochondrial; IVD	46468	21	55.2	4907	36	1790	58
Q0P5A2|COQ5_BOVIN	Ubiquinone biosynthesis methyltrans-ferase COQ5, mitochondrial; COQ5	37567	23	71.2	4870	37	1781	59
A6QLZ6|A6QLZ6_BOVIN	GLRX5 protein; GLRX5	16765	8	47.5	4636	38	632	147
Q58DN7|ACSF3_BOVIN	Acyl-CoA synthetase family member 3, mitochondrial; ACSF3	64949	34	61.3	4443	39	3762	32
P11966|ODPB_BOVIN	Pyruvate dehydrogenase E1 component subunit beta, mitochondrial; PDHB	39101	31	67.1	4154	40	8624	12
Q2HJ97|PHB2_BOVIN	Prohibitin-2; PHB2	33337	28	80.9	4062	41	1008	98
Q29RK1|CISY_BOVIN	Citrate synthase, mitochondrial; CS	51739	22	43.8	4011	42	2153	50

P34942|NDUAA_BOVIN	NADH dehydrogenase 1 alpha sub-complex subunit 10, mito; NDUFA10	39239	15	76.1	3998	43	2569	42
A4FUH8|A4FUH8_BOVIN	Chromosome 1 open reading frame 93 ortholog; C16H1orf93	21467	28	85.6	3782	44	1037	96
P02722|ADT1_BOVIN	ADP/ATP translocase 1; SLC25A4	32946	34	66.1	3685	45	1136	86
A7E3V3|A7E3V3_BOVIN	Mitofilin; Inner membrane protein, mitochondrial; IMMT	83002	27	40.1	3642	46	5123	24
Q2HJI1|Q2HJI1_BOVIN	SDHA protein; SDHA	74360	15	36.0	3595	47	2113	51
Q3SZJ1|Q3SZJ1_BOVIN	IARS2 protein (Fragment); IARS2	56105	25	51.1	3525	48	3291	36
Q3T165|PHB_BOVIN	Prohibitin; PHB	29786	21	83.5	3317	49	1897	56
A6QNM2|RRF2M_BOVIN	Ribosome-releasing factor 2, mitochondrial; GFM2	85977	33	47.2	3309	50	2247	49
A5PKG4|A5PKG4_BOVIN	NFS1 protein; NFS1	50312	24	59.3	3217	51	1594	65
A7MB35|ODPA_BOVIN	Pyruvate dehydrogenase E1 subunit alpha, somatic form, mito; PDHA1	43360	26	61.3	3036	52	4520	26
A6QQ83|A6QQ83_BOVIN	THEM2 protein; THEM2	16846	14	62.6	3023	53	1900	55
P17694|NDUS2_BOVIN	NADH dehydrogenase [ubiquinone] iron-sulfur protein 2, mito; NDUFS2	52522	32	56.4	2798	54	1566	67
Q148J8|Q148J8_BOVIN	Isocitrate dehydrogenase 3 (NAD+) alpha; IDH3A	39672	24	52.7	2705	55	1407	75
Q2KIG0|ETFD_BOVIN	Electron transfer flavoprotein-ubiqui-none oxidoreductase, mito; ETFDH	68568	20	43.8	2674	56	1438	72
Q08DN5|Q08DN5_BOVIN	Carnitine acetyltransferase; MGC142781	70971	25	48.9	2602	57	1964	54
O46629|ECHB_BOVIN	Trifunctional enzyme subunit beta, mitochondrial; HADHB	51312	31	62.3	2594	58	2093	52
A1A4J9|A1A4J9_BOVIN	DnaJ (Hsp40) homolog, subfamily A, member 3; DNAJA3	49223	18	49.7	2592	59	2298	48
A5D954|A5D954_BOVIN	Solute carrier family 25, member 11 (Fragment); SLC25A11	33877	18	57.6	2588	60	827	115
P23709|NDUS3_BOVIN	NADH dehydrogenase [ubiquinone] iron-sulfur protein 3, mito; NDUFS3	30266	19	52.3	2564	61	719	132
P12234|MPCP_BOVIN	Phosphate carrier protein, mitochondrial; SLC25A3	40114	18	49.7	2561	62	1109	89
P22439|ODPX_BOVIN	Pyruvate dehydrogenase protein X component, mitochondrial; PDHX	53852	24	45.5	2446	63	2939	40
Q32KX0|ISOC2_BOVIN	Isochorismatase domain-containing protein 2, mitochondrial; ISOC2	22406	12	77.5	2390	64	790	119
Q3T0B6|C1QBP_BOVIN	Complement component 1 Q subcom-ponent-binding protein, mito; C1QBP	30587	11	57.2	2349	65	1331	78

Q2KI62|PTCD3_BOVIN	Pentatricopeptide repeat-containing protein 3, mitochondrial; PTCD3	77781	26	52.0	2322	66	1758	61
P31800|QCR1_BOVIN	Cytochrome bc_1 complex subunit 1, mitochondrial; UQCRC1	52702	17	47.3	2303	67		
Q5E9D3|CHCH3_BOVIN	Coiled-coil-helix-coiled-coil-helix domain-containing protein 3, mitochondrial; CHCHD3	26084	15	58.6	2236	68	702	135
Q01321|NDUA4_BOVIN	NADH DH 1 alpha subcomplex subunit 4; mitochondrial; NDUFA4	9319	6	59.8	2193	69	577	154
P48818|ACADV_BOVIN	Very long-chain specific acyl-CoA dehydrogenase; ACADVL	70604	24	49.6	2140	70	1558	68
P82649|RT22_BOVIN	28S ribosomal protein S22, mitochondrial; MRPS22	40639	32	63.5	2136	71	1267	79
Q8SQH5|ADT2_BOVIN	ADP/ATP translocase 2; SLC25A5	32934	15	44.6	2114	72		
Q0VC50|RT4I1_BOVIN	Reticulon-4-interacting protein 1, mitochondrial; RTN4IP1	43555	27	69.4	2093	73	1178	82
Q2KJI7|AFG32_BOVIN	AFG3-like protein 2; AFG3L2	89331	23	31.3	1999	74	1746	62
Q2KIW8|Q2KIW8_BOVIN	Glutathione S-transferase kappa 1; GSTK1	25660	11	38.9	1927	75	1118	88
Q148D3|Q148D3_BOVIN	Fumarate hydratase; FH	54656	21	53.5	1925	76	2050	53
P31081|CH60_BOVIN	60 kDa heat shock protein, mitochondrial, HSP 60; HSPD1	61069	24	46.2	1922	77	1136	85
Q3SZK4|TBRG4_BOVIN	Protein TBRG4; TBRG4	71596	26	61.1	1916	78	945	102
Q1JPF2|Q1JPF2_BOVIN	NADH DH 1 alpha subcomplex, 9, 39kDa (Fragment); NDUFA9	41634	19	55.3	1894	79	914	107
P25708|NDUV1_BOVIN	NADH dehydrogenase [ubiquinone] flavoprotein 1, mitochondrial; NDUFV1	50620	23	67.5	1880	80	778	121
Q3SZ27|APOOL_BOVIN	Apolipoprotein O-like; APOL	29096	12	59.5	1864	81	727	130
P23004|QCR2_BOVIN	Cytochrome bc_1 complex subunit 2, mitochondrial; UQCRC2	48119	19	51.7	1850	82	1823	57
P22600|HEMH_BOVIN	Ferrochelatase, mitochondrial; FECH	46905	20	49.3	1828	83	1186	81
P42028|NDUS8_BOVIN	NADH dehydrogenase [ubiquinone] iron-sulfur protein 8, mito; NDUFS8	23881	10	55.2	1827	84	1675	63
A5D9H9|A5D9H9_BOVIN	DNA polymerase delta interacting protein 2; POLDIP2	41916	16	53.3	1755	85	993	99
Q2KJG8|BCKD_BOVIN	[3-methyl-2-oxobutanoate DH [lipoamide]] kinase, mito; BCKDK	46409	20	58.0	1743	86	1428	74
Q3T179|Q3T179_BOVIN	HSPD1 protein (Fragment); HSPD1	42138	20	47.9	1742	87	1036	97
P46198|IF2M_BOVIN	Translation initiation factor IF-2, mitochondrial;	81713	20	30.1	1718	88	914	106

	MTIF2							
P82669|RT25_BOVIN	28S ribosomal protein S25, mitochondrial; MRPS25	20042	13	62.4	1692	89	730	129
Q2KJH7|Q2KJH7_BOVIN	Aldehyde dehydrogenase 18 family, member A1; ALDH18A1	87140	30	40.5	1657	90	1516	69
Q17QH8|D39U1_BOVIN	Epimerase family protein SDR39U1; SDR39U1	31315	19	64.6	1639	91	851	113
P54149|MSRA_BOVIN	Peptide methionine sulfoxide reductase; MSRA	25802	14	69.5	1626	92	1160	83
Q58D58|Q58D58_BOVIN	Cat eye syndrome chromosome region, candidate 5 isoform 2; CECR5	42522	17	53.8	1615	93	1640	64
Q3MHW4|Q3MHW4_BOVIN	SQRDL protein; SQRDL	49854	16	44.4	1601	94	1480	71
P25285|GCST_BOVIN	Aminomethyltransferase, mitochondrial; AMT	42841	20	62.0	1562	95	876	110
A7YVD7|CH038_BOVIN	UPF0551 protein C8orf38 homolog, mitochondrial	38079	19	54.7	1528	96	824	116
A4FV92|A4FV92_BOVIN	CYP27A1 protein; CYP27A1	60303	24	61.0	1526	97	457	189
Q3T0R7|THIM_BOVIN	3-ketoacyl-CoA thiolase, mitochondrial; ACAA2	42104	20	55.4	1523	98	1192	80
A6QQF5|QORL2_BOVIN	Quinone oxidoreductase-like protein 2	37644	17	68.2	1519	99	493	180
Q3ZBF6|ACADS_BOVIN	Short-chain specific acyl-CoA dehydrogenase, mito; ACADS	44524	13	44.9	1497	100	1078	91
A0JNB4|A0JNB4_BOVIN	Leucyl-tRNA synthetase 2, mitochondrial; LARS2	69767	21	43.3	1455	101	973	101
Q32LG3|MDHM_BOVIN	Malate dehydrogenase, mito; MDH2	35646	17	51.8	1451	102	2299	47
Q58DK1|CPT1B_BOVIN	Carnitine O-palmitoyltransferase 1, muscle isoform; CPT1B	88455	20	32.2	1436	103	1064	93
P21839|ODBB_BOVIN	2-oxoisovalerate dehydrogenase subunit beta, mito; BCKDHB	42908	11	55.4	1397	104	1356	77
P30404|PPIF_BOVIN	Peptidyl-prolyl cis-trans isomerase F, mitochondrial; PPIF	22234	10	44.5	1387	105	343	219
P23935|NDUA5_BOVIN	NADH dehydrogenase 1 alpha subcomplex subunit 5; NDUFA5	13307	10	64.7	1353	106	186	302
Q3T0G5|PROSC_BOVIN	Proline synthetase co-transcribed bacterial homolog protein; PROSC	29924	19	69.6	1348	107	556	162
A5D7G0|A5D7G0_BOVIN	YARS2 protein; YARS2	52959	15	43.1	1343	108	681	139
P13621|ATPO_BOVIN	ATP synthase subunit O, mito; ATP5O	23305	15	62.0	1293	109	409	200
Q2HJ73|HIBCH_BOVIN	3-hydroxyisobutyryl-CoA hydrolase, mitochondrial; HIBCH	43321	17	39.9	1268	110	1096	90
Q3SZ20|GLYM_BOVIN	Serine hydroxymethyltransferase, mitochondrial; SHMT2	55570	12	42.7	1241	111	795	118
Q3MHY7|RM10_BOVIN	39S ribosomal protein L10, mitochondrial; MRPL10	29309	10	53.1	1230	112	604	152

P82928|RT28_BOVIN	28S ribosomal protein S28, mitochondrial; MRPS28	21028	6	33.9	1220	113	736	128
P35705|PRDX3_BOVIN	Thioredoxin-dependent peroxide reductase, mitochondrial; PRDX3	28177	9	38.9	1205	114	941	104
Q1JPD3|D2HDH_BOVIN	D-2-hydroxyglutarate dehydrogenase, mitochondrial; D2HGDH	59018	9	21.7	1188	115	563	159
Q2YDI0|RM11_BOVIN	39S ribosomal protein L11, mitochondrial; MRPL11	20767	13	64.1	1169	116	394	202
Q08D87|Q08D87_BOVIN	Phenylalanyl-tRNA synthetase 2, mitochondrial; FARS2	51371	19	54.9	1169	117	786	120
Q58DQ5|RT09_BOVIN	28S ribosomal protein S9, mitochondrial; MRPS9	45202	18	48.2	1157	118	849	114
Q3SZD7|CBR1_BOVIN	Carbonyl reductase [NADPH] 1; CBR1	30514	14	57.0	1148	119	753	124
Q02337|BDH_BOVIN	D-beta-hydroxybutyrate dehydrogenase, mitochondrial; BDH1	38366	13	41.3	1147	120	1127	87
Q2KHU5|MACD1_BOVIN	MACRO domain-containing protein 1; MACROD1	35547	11	32.9	1119	121	618	150
C6K7D4|C6K7D4_BOVIN	Sirtuin 3 (Fragment); Sirt3	22782	7	33.7	1117	122	643	146
Q9BGI1|PRDX5_BOVIN	Peroxiredoxin-5, mito; PRDX5	23238	15	56.2	1086	123	666	143
P12344|AATM_BOVIN	Aspartate aminotransferase, mitochondrial; GOT2	47483	11	31.9	1082	124	756	123
Q05B74|Q05B74_BOVIN	Mitochondrial ribosomal protein L39; MRPL39	38435	21	61.8	1057	125	752	125
Q2KIS2|RM44_BOVIN	39S ribosomal protein L44, mitochondrial; MRPL44	37389	13	53.0	1039	126	687	137
Q3SWX4|Q3SWX4_BOVIN	Glioblastoma amplified sequence; GBAS	33398	13	36.7	1022	127	1436	73
Q2NL27|RT23_BOVIN	28S ribosomal protein S23, mitochondrial; MRPS23	21580	7	45.3	7477	128	401	201
P82925|RT31_BOVIN	28S ribosomal protein S31, mitochondrial; MRPS31	43648	16	52.3	1013	129	145	326
A6QPQ5|RM01_BOVIN	39S ribosomal protein L1, mitochondrial; MRPL1	36633	13	38.8	997	130	559	161
A4FUZ6|HSDL2_BOVIN	Hydroxysteroid dehydrogenase-like protein 2; HSDL2	45120	8	34.7	964	131	867	112
A6QQP1|A6QQP1_BOVIN	DAP3 protein (Fragment); DAP3	48413	19	50.0	960	132	688	136
A8WFQ0|A8WFQ0_BOVIN	NDUFS7 protein; NDUFS7	20108	10	55.3	956	133	1044	94
Q3SZ86|RT26_BOVIN	28S ribosomal protein S26, mitochondrial; MRPS26	23759	11	51.7	954	134	229	269
Q3ZC57|Q3ZC57_BOVIN	Peroxisomal D3,D2-enoyl-CoA isomerase; PECI	23502	7	37.3	948	135	241	262
Q2YDF6|RT35_BOVIN	28S ribosomal protein S35, mitochondrial; MRPS35	37046	13	45.5	947	136	560	160

A0JN95|ME5D1_BOVIN	Putative S-adenosyl-L-methionine-dependent methyltransferase; METT5D1	45739	12	38.1	944	137	983	100
A7YWC4|ATAD3_BOVIN	ATPase family AAA domain-containing protein 3; ATAD3	66066	19	40.1	934	138	717	133
P82920|RT21_BOVIN	28S ribosomal protein S21, mitochondrial; MRPS21	10668	9	43.7	900	139	510	174
Q2TBS2|RM21_BOVIN	39S ribosomal protein L21, mitochondrial; MRPL21	23168	7	44.5	887	140	566	158
Q2PC20|PPM1K_BOVIN	Protein phosphatase 1K, mitochondrial; PPM1K	41125	5	12.9	877	141	768	122
Q3T100|MGST3_BOVIN	Microsomal glutathione S-transferase 3; MGST3	16873	4	32.9	877	142		
Q2TBV3|ETFB_BOVIN	Electron transfer flavoprotein subunit beta; ETFB	27682	13	54.9	870	143	566	157
Q1JQB8|Q1JQB8_BOVIN	Coenzyme Q10 homolog B (S. cerevisiae); COQ10B	27737	8	34.4	848	144	227	272
Q0II87|TFAM_BOVIN	Transcription factor A, mito; TFAM	28888	10	32.1	844	145	301	239
A6QQK5|A6QQK5_BOVIN	MMAA protein; MMAA	46658	14	37.5	833	146	880	109
Q0V8J6|Q0V8J6_BOVIN	Branched-chain-amino-acid aminotransferase (Fragment); BCAT2	44245	14	60.9	830	147	344	218
P35816|PDP1_BOVIN	[Pyruvate DH [acetyl-trans-ferring]]-phosphatase 1, mito; PDP1	61146	13	31.8	812	148	612	151
Q02370|NDUA2_BOVIN	NADH DH [ubiquinone] 1 alpha subcomplex subunit 2; NDUFA2	11073	8	63.6	811	149	509	175
Q32LB9|CD014_BOVIN	Uncharacterized protein C4orf14 homolog	77195	9	23.8	801	150	575	156
A3KN05|CB047_BOVIN	Uncharacterized protein C2orf47 homolog, mitochondrial	32919	12	29.6	792	151	340	221
Q2HJ55|SAM50_BOVIN	Sorting and assembly machinery component 50 homolog; SAMM50	52009	13	33.0	792	152	679	140
A5PJA6|A5PJA6_BOVIN	Stomatin (EPB72)-like 2; STOML2	38709	11	37.1	791	153	330	229
Q3SZX5|RM22_BOVIN	39S ribosomal protein L22, mitochondrial; MRPL22	23537	10	42.6	789	154	497	179
Q2NL38|Q2NL38_BOVIN	Dodecenoyl-Coenzyme A delta isomerase; DCI	33123	8	27.7	789	155	286	246
Q2TBT9|Q2TBT9_BOVIN	BCKDHA protein (Fragment); BCKDHA	51401	13	37.1	787	156		
Q0P5H7|SYRM_BOVIN	Probable arginyl-tRNA synthetase, mitochondrial; RARS2	65590	13	39.1	784	157	265	252
P11179|ODO2_BOVIN	Dihydrolipoyllysine succinyl-transferase of 2-oxoglutarate DHC, mito; DLST	48942	9	21.5	765	158	1074	92
Q3SZG8|ISCA1_BOVIN	Iron-sulfur cluster assembly 1 homolog, mitochondrial; ISCA1	14170	10	64.3	758	159	85	391

P15246|PIMT_BOVIN	Protein-L-isoaspartate(D-aspartate) O-methyltransferase; PCMT1	24550	11	61.7	749	160	413	199
Q1JQB6|Q1JQB6_BOVIN	Mitochondrial translation optimization 1 homolog (S. cerevisiae); MTO1	77224	10	22.5	746	161	470	186
Q9N0F3|SYSM_BOVIN	Seryl-tRNA synthetase, mitochondrial; SARS2	58259	12	31.5	735	162	203	287
Q2TBG7|ISCA2_BOVIN	Iron-sulfur cluster assembly 2 homolog, mitochondrial; ISCA2	16425	7	50.7	734	163	360	209
P82911|RT11_BOVIN	28S ribosomal protein S11, mitochondrial; MRPS11	20825	5	33.0	724	164	303	238
A6QLJ3|A6QLJ3_BOVIN	GUF1 protein; GUF1	74719	8	17.8	712	165	347	217
A6QP28|A6QP28_BOVIN	Helicase; SUPV3L1 protein; SUPV3L1	58798	11	29.3	705	166	525	167
P82923|RT02_BOVIN	28S ribosomal protein S2, mitochondrial; MRPS2	31710	12	43.7	698	167	543	164
Q2TA12|RM02_BOVIN	39S ribosomal protein L2, mitochondrial; MRPL2	33323	12	41.2	684	168	623	148
A6QPR9|CQ042_BOVIN	UPF0629 protein C17orf42 homolog	40582	13	39.0	681	169	266	251
P13272|UCRI_BOVIN	Cytochrome bc_1 complex subunit Rieske, mitochondrial; UQCRFS1	29528	9	28.8	672	170	153	321
Q5EAD4|ACDSB_BOVIN	Short/branched chain specific acyl-CoA dehydrogenase, mito; ACADSB	47093	15	40.0	672	171	458	188
P00257|ADX_BOVIN	Adrenodoxin, mitochondrial; FDX1	19744	7	33.3	665	172	273	249
Q32L86|T126A_BOVIN	Transmembrane protein 126A; TMEM126A	21523	11	58.9	663	173	100	372
Q2HJF1|RM53_BOVIN	39S ribosomal protein L53, mitochondrial; MRPL53	11990	6	67.9	661	174	361	208
A5PJV9|A5PJV9_BOVIN	DTYMK protein; DTYMK	23760	11	42.9	658	175	333	227
Q2HJJ1|RM28_BOVIN	39S ribosomal protein L28, mitochondrial; MRPL28	30021	6	34.0	655	176	414	197
Q3T094|ETHE1_BOVIN	Protein ETHE1, mito; ETHE1	27882	6	40.2	649	177	524	168
Q32PI6|RM04_BOVIN	39S ribosomal protein L4, mitochondrial; MRPL4	33350	11	52.4	642	178	160	313
Q3T172|Q3T172_BOVIN	ECH1 protein (Fragment); ECH1	37548	9	32.0	636	179	1506	70
Q29RH8|Q29RH8_BOVIN	PDK2 protein (Fragment); PDK2	49402	13	39.0	636	180	679	141
Q29RZ5|CV025_BOVIN	Uncharacterized protein C22orf25 homolog	30810	8	48.9	631	181	137	334
Q0NXR6|ACAD8_BOVIN	Isobutyryl-CoA dehydrogenase, mitochondrial; ACAD8	45278	9	29.3	602	182	382	204
Q3T040|RT07_BOVIN	28S ribosomal protein S7, mitochondrial; MRPS7	28112	9	43.4	595	183	622	149
Q3ZCF5|OAT_BOVIN	Ornithine aminotransferase, mitochondrial; OAT	48045	10	32.6	591	184	890	108
Q2TBW6|ARL3_BOVIN	ADP-ribosylation factor-like protein 3; ARL3	20492	11	63.7	590	185	135	338

Q3SZC1|GRPE1_BOVIN	GrpE protein homolog 1, mitochondrial; GRPEL1	24291	10	55.8	573	186	133	341
Q58D49|MMAB_BOVIN	Cob(I)yrinic acid a,c-diamide adenosyl-transferase, mitochondrial; MMAB	26571	6	44.4	567	187	280	248
Q58DM8|ECHM_BOVIN	Enoyl-CoA hydratase, mito; ECHS1	31223	5	24.1	566	188	260	253
Q0VCK0|PUR9_BOVIN	Bifunctional purine biosynthesis protein PURH; ATIC	64442	10	29.7	566	189	746	127
Q2KIX6|Q2KIX6_BOVIN	Biphenyl hydrolase-like (Serine hydrolase); BPHL	32418	10	46.0	557	190	426	194
Q0P5M8|MPPA_BOVIN	Mitochondrial-processing peptidase subunit alpha; PMPCA	58097	7	17.0	555	191	394	203
Q0V8N7|Q0V8N7_BOVIN	Mitochondrial ribosomal protein L49 (Fragment); MRPL49	18676	8	43.1	548	192	213	281
A6QLL2|A6QLL2_BOVIN	Metaxin-2; MTX2 protein; MTX2	29660	6	32.2	546	193	105	363
A6QP05|DHR12_BOVIN	Dehydrogenase/reductase SDR family member 12; DHRS12	35043	9	41.6	543	194	441	191
Q3ZBN8|TIM14_BOVIN	Mitochondrial import inner membrane translocase subunit TIM14; DNAJC19	12491	7	60.3	541	195	333	228
Q3SZV6|TI21L_BOVIN	TIM21-like protein, mitochondrial	27920	6	25.4	541	196	236	264
Q3SZ55|PTCD2_BOVIN	Pentatricopeptide repeat-containing protein 2; PTCD2	43917	13	35.7	538	197	242	260
A0JNI7|A0JNI7_BOVIN	G-rich RNA sequence binding factor 1; GRSF1	53019	6	22.9	534	198	1038	95
Q32L81|MMP37_BOVIN	MMP37-like protein, mitochondrial	37396	10	30.1	527	199	439	192
Q2NKZ7|Q2NKZ7_BOVIN	Protein tyrosine phosphatase, mitochondrial 1; PTPMT1	29244	7	28.9	525	200	352	215
Q8SPJ1|PLAK_BOVIN	Junction plakoglobin; JUP	81769	9	16.6	522	201	644	145
O02691|HCD2_BOVIN	3-hydroxyacyl-CoA dehydrogenase type-2; HSD17B10	27123	10	51.3	520	202	504	177
A7YWQ8|A7YWQ8_BOVIN	DDX28 protein; DDX28	59964	11	31.7	512	203	507	176
P00366|DHE3_BOVIN	Glutamate dehydrogenase 1, mitochondrial; GLUD1	61473	13	30.5	510	204	429	193
Q0IIB7|Q0IIB7_BOVIN	C13H20ORF7 protein (Fragment); C13H20ORF7	39096	9	32.1	505	205	369	206
P05631|ATPG_BOVIN	ATP synthase subunit gamma; ATP5C1	33051	9	47.0	498	206	356	211
Q32PC3|RM27_BOVIN	39S ribosomal protein L27, mitochondrial; MRPL27	16024	5	37.8	496	207	141	329
P22027|ATP5S_BOVIN	ATP synthase subunit s; ATP5S	23278	11	51.5	495	208	241	261
Q2HJI2|NDUF3_BOVIN	NADH DH 1 alpha subcomplex assembly factor 3; NDUFAF3	20464	7	37.5	487	209	121	350

Q8SQ21|HINT2_BOVIN	Histidine triad nucleotide-binding protein 2, mitochondrial; HINT2	17136	5	44.2	486	210		
Q3SYS1|RM13_BOVIN	39S ribosomal protein L13, mitochondrial; MRPL13	20562	10	50.6	477	211	414	198
Q7YR75|RM12_BOVIN	39S ribosomal protein L12, mitochondrial; MRPL12	21387	11	60.6	474	212	81	396
Q02375|NDUS4_BOVIN	NADH dehydrogenase [ubiquinone] iron-sulfur protein 4, mito; NDUFS4	19799	6	37.1	450	213	84	394
Q32S21|Q32S21_BOVIN	FabG-like protein; HKE6	26452	5	28.2	447	214	481	181
A7MBI8|A7MBI8_BOVIN	NUDT9 protein; NUDT9	38588	9	21.5	440	215	474	182
Q6B860|RT14_BOVIN	28S ribosomal protein S14, mitochondrial; MRPS14	15034	4	33.6	432	216	232	265
P82916|RT17_BOVIN	28S ribosomal protein S17, mitochondrial; MRPS17	14465	5	46.9	430	217	281	247
P13620|ATP5H_BOVIN	ATP synthase subunit d; ATP5H	18681	6	47.8	427	218		
Q32LD4|TFB2M_BOVIN	Dimethyladenosine transferase 2, mitochondrial; TFB2M	44923	8	28.4	420	219	157	316
Q08DG6|COX15_BOVIN	Cytochrome *c* oxidase assembly protein COX15 homolog; COX15	46097	4	11.4	413	220		
O97725|NDUAC_BOVIN	NADH dehydrogenase 1 alpha subcomplex subunit 12; NDUFA12	17079	6	45.5	411	221	95	379
O77480|FMT_BOVIN	Methionyl-tRNA formyltransferase, mitochondrial; MTFMT	43592	7	24.9	411	222	460	187
Q2NKU1|Q2NKU1_BOVIN	Deoxyuridine triphosphatase; DUT	20005	3	21.1	409	223	224	273
Q2HJI0|RM19_BOVIN	39S ribosomal protein L19, mitochondrial; MRPL19	33314	10	36.0	407	224	338	223
Q2TBK7|RUSD3_BOVIN	RNA pseudouridylate synthase domain-containing protein 3; RPUSD3	36985	6	29.7	407	225	359	210
P46195|KGUA_BOVIN	Guanylate kinase; GUK1	21896	5	37.9	405	226	125	346
P82670|RT10_BOVIN	28S ribosomal protein S10, mitochondrial; MRPS10	23017	8	30.3	404	227	209	284
Q3SZ22|RM46_BOVIN	39S ribosomal protein L46, mitochondrial; MRPL46	31706	7	33.6	403	228	287	245
Q2TBQ0|TFB1M_BOVIN	Mitochondrial dimethyladenosine transferase 1; TFB1M	38859	8	38.1	402	229	191	297
Q2M2T7|RT24_BOVIN	28S ribosomal protein S24, mitochondrial; MRPS24	19067	8	34.7	400	230	160	312
Q0VC30|DPOG2_BOVIN	DNA polymerase subunit gamma-2, mitochondrial;	54628	6	12.4	398	231		

POLG2

Protein	Description							
Q29RZ0|THIL_BOVIN	Acetyl-CoA acetyltransferase, mitochondrial; ACAT1	44860	6	24.4	398	232	204	286
P82918|RT18B_BOVIN	28S ribosomal protein S18b, mitochondrial; MRPS18B	29156	7	39.1	391	233	132	342
P13619|AT5F1_BOVIN	ATP synthase subunit b; ATP5F1	28803	4	21.9	383	234	212	282
P82924|RT30_BOVIN	28S ribosomal protein S30, mitochondrial; MRPS30	49325	8	25.5	382	235	350	216
Q32P59|SLIRP_BOVIN	SRA stem-loop-interacting RNA-binding protein, mitochondrial; SLIRP	12485	6	70.3	381	236	224	274
P04394|NDUV2_BOVIN	NADH dehydrogenase [ubiquinone] flavoprotein 2; NDUFV2	27290	7	30.5	376	237	101	370
Q3ZBP1|KCRS_BOVIN	Creatine kinase S-type, mito; CKMT2	47201	8	32.5	375	238	943	103
A4FUC7|A4FUC7_BOVIN	Coiled-coil domain-containing protein 127; CCDC127 protein; CCDC127	30561	4	21.3	373	239	228	271
Q2TA37|ARL2_BOVIN	ADP-ribosylation factor-like protein 2; ARL2	20894	8	50.0	373	240	171	308
P00426|COX5A_BOVIN	Cytochrome *c* oxidase subunit 5A, mitochondrial; COX5A	16725	4	16.4	370	241	256	255
Q3T142|RM45_BOVIN	39S ribosomal protein L45, mitochondrial; MRPL45	35120	9	21.9	369	242	138	333
Q32PI8|RT27_BOVIN	28S ribosomal protein S27, mitochondrial; MRPS27	47925	9	25.8	367	243	301	240
Q2KID9|RT05_BOVIN	28S ribosomal protein S5, mitochondrial; MRPS5	47842	11	21.4	367	244	808	117
A5PK90|A5PK90_BOVIN	LYPLAL1 protein; LYPLAL1	25605	5	29.3	367	245		
Q0VC21|RM15_BOVIN	39S ribosomal protein L15, mitochondrial; MRPL15	33653	9	37.0	366	246	750	126
Q2KIF1|GATCL_BOVIN	GatC-like protein; GATC	15167	4	44.9	364	247		
Q05B52|COQ4_BOVIN	Ubiquinone biosynthesis protein COQ4 homolog; COQ4	16326	6	17.2	362	248	213	280
Q2YDI5|RM48_BOVIN	39S ribosomal protein L48, mitochondrial; MRPL48	24007	6	17.9	359	249	292	244
Q2TBT3|ECHD2_BOVIN	Enoyl-CoA hydratase domain-containing protein 2; ECHDC2	31584	6	32.4	357	250	575	155
A6QNL8|A6QNL8_BOVIN	MCAT protein (Fragment); MCAT	38344	8	23.8	357	251	550	163
Q2KJF7|GLCTK_BOVIN	Glycerate kinase; GLYCTK	54686	8	19.7	356	252	309	236
P82917|RT18C_BOVIN	28S ribosomal protein S18c, mitochondrial; MRPS18C	16203	2	21.7	354	253		

P82929|RT34_BOVIN	28S ribosomal protein S34, mitochondrial; MRPS34	25816	7	38.5	351	254	180	304
Q2M2S9|LYRM7_BOVIN	LYR motif-containing protein 7; LYRM7	11915	4	41.3	348	255		
A6QQA9|A6QQA9_BOVIN	Acyl-coenzyme A thioesterase 2, mito; ACOT2 protein; ACOT2	50893	6	25.4	346	256	82	395
Q32PB0|SSBP_BOVIN	Single-stranded DNA-binding protein, mitochondrial; SSBP1	17197	3	27.7	342	257		
P68002|VDAC2_BOVIN	Voltage-dependent anion-selective channel protein 2; VDAC2	31600	6	26.9	341	258	343	220
A6QNS9|AT5SL_BOVIN	ATP synthase subunit s-like protein; ATP5SL	33164	4	19.9	335	259	106	361
Q05AT5|Q05AT5_BOVIN	HIG1 domain family, member 2A ; HIGD2A	11568	2	50.0	334	260		
A8E657|AASS_BOVIN	Alpha-aminoadipic semialdehyde synthase, mitochondrial; AASS	102019	8	17.6	334	261	354	213
A4IFA7|CBR4_BOVIN	Carbonyl reductase family member 4; CBR4	25253	9	45.6	333	262	205	285
P42029|NDUA8_BOVIN	NADH DH [ubiquinone] 1 alpha subcomplex subunit 8; NDUFA8	20078	5	35.5	331	263	149	324
Q2TBR0|PCCB_BOVIN	Propionyl-CoA carboxylase beta chain, mitochondrial; PCCB	58274	6	14.8	330	264	379	205
A4FUC0|RM37_BOVIN	39S ribosomal protein L37, mitochondrial; MRPL37	48022	7	23.2	330	265	726	131
P82915|RT16_BOVIN	28S ribosomal protein S16, mitochondrial; MRPS16	15122	7	50.4	329	266	199	288
A6QP42|A6QP42_BOVIN	MGC151610 protein; MGC151610	78145	10	18.3	326	267	193	293
Q3SYS0|RM24_BOVIN	39S ribosomal protein L24, mitochondrial; MRPL24	24770	7	43.1	323	268	231	268
Q2KHU4|CLPP_BOVIN	Putative ATP-dependent Clp protease proteolytic subunit, mito; CLPP	29685	2	17.6	318	269		
Q02827|NDUC2_BOVIN	NADH dehydrogenase [ubiquinone] 1 subunit C2; NDUFC2	14087	3	35.8	317	270	105	362
A6QQH9|A6QQH9_BOVIN	C22H3ORF23 protein; C22H3ORF23	30816	6	33.8	316	271	117	352
Q1LZ96|ATPF2_BOVIN	ATP synthase mitochondrial F1 complex assembly factor 2; ATPAF2	32839	3	14.2	314	272	245	259
Q4PS77|MTG1_BOVIN	Mitochondrial GTPase 1; MTG1	36981	5	19.0	311	273	191	298
Q3SZ47|RM33_BOVIN	39S ribosomal protein L33, mitochondrial; MRPL33	7485	3	23.1	310	274		
A5D974|A5D974_BOVIN	Acyl-Coenzyme A dehydrogenase family, member 9; ACAD9	68164	7	14.7	309	275	312	233

Q95KE5|RM43_BOVIN	39S ribosomal protein L43, mitochondrial; MRPL43	17724	5	33.3	299	276	531	166
A7E3Q1|A7E3Q1_BOVIN	Threonyl-tRNA synthetase-like 1; TARSL1	80908	11	18.8	298	277	503	178
Q2KJF3|Q2KJF3_BOVIN	NFU1 iron-sulfur cluster scaffold homolog (S. cerevisiae); NFU1	28127	6	26.1	297	278	164	309
Q3T0L3|RM17_BOVIN	39S ribosomal protein L17, mitochondrial; MRPL17	19733	6	34.3	296	279	218	277
Q2TBK2|RM09_BOVIN	39S ribosomal protein L9, mitochondrial; MRPL9	30506	8	35.8	293	280	337	224
Q3T0N2|Q3T0N2_BOVIN	Lysyl-tRNA synthetase; KARS	71275	6	13.2	293	281	193	292
Q02366|NDUA6_BOVIN	NADH DH [ubiquinone] 1 alpha subcomplex subunit 6; NDUFA6	15044	4	28.9	292	282	180	306
P05630|ATPD_BOVIN	ATP synthase subunit delta; ATP5D	17601	3	19.0	290	283		
Q3SZ13|Q3SZ13_BOVIN	Inositol hexakisphosphate kinase 3; IP6K3 protein; IP6K3	15965	4	45.6	290	284		
Q3MHX4|Q3MHX4_BOVIN	MTERFD2 protein (Fragment); MTERFD2	38579	3	9.9	289	285	239	263
Q0V8R7|NSUN4_BOVIN	Putative methyltransferase NSUN4; NSUN4	43171	5	12.0	282	286	197	290
A5D7A7|A5D7A7_BOVIN	C26H10ORF2 protein, Twinkle; PEO1	76488	6	14.1	281	287	211	283
Q2KHW9|Q2KHW9_BOVIN	Ribonuclease H1 pseudogene 1; RNASEH1P1	31363	5	25.4	281	288	190	299
P82931|RT06_BOVIN	28S ribosomal protein S6, mitochondrial; MRPS6	14139	7	63.7	281	289	146	325
Q3T116|ICT1_BOVIN	Immature colon carcinoma transcript 1 protein; ICT1	23292	4	29.1	280	290	326	230
Q08DT6|RM47_BOVIN	39S ribosomal protein L47, mitochondrial; MRPL47	29562	7	26.6	280	291	312	234
P82927|RM42_BOVIN	39S ribosomal protein L42, mitochondrial; MRPL42	16626	4	20.4	280	292		
Q2HJ25|Q2HJ25_BOVIN	Methionine aminopeptidase; MAP1D	23791	3	18.4	278	293	159	315
P82908|RT36_BOVIN	28S ribosomal protein S36, mitochondrial; MRPS36	11536	4	28.2	275	294	73	401
Q17QE6|Q17QE6_BOVIN	Iron-sulfur cluster scaffold homolog (E. coli); ISCU	17841	4	26.3	275	295	64	403
Q2HJC0|NGRN_BOVIN	Neugrin; NGRN	23529	5	34.0	273	296	92	383
A7E2Z6|A7E2Z6_BOVIN	SPG7 protein; SPG7	86140	10	20.2	272	297	340	222
Q2KHV5|MIDA_BOVIN	Protein midA homolog, mitochondrial	49233	6	22.7	270	298	335	225
A6QNM9|A6QNM9_BOVIN	SLC25A12 protein; SLC25A12	74483	5	10.7	269	299	308	237
Q3ZBX6|RM03_BOVIN	39S ribosomal protein L3, mitochondrial; MRPL3	38575	5	21.8	269	300		
Q05B51|ADXL_BOVIN	Adrenodoxin-like protein, mitochondrial; FDX1L	19934	4	26.9	265	301		

Q4U0T9|CSRP3_BOVIN	Cysteine and glycine-rich protein 3; CSRP3	20939	4	32.5	264	302	140	330
Q5E948|OCAD1_BOVIN	OCIA domain-containing protein 1; Ociad1	27812	5	21.5	260	303	153	322
Q05B87|FRDA_BOVIN	Frataxin, mitochondrial; FXN	23552	4	19.8	259	304		
Q05752|NDUA7_BOVIN	NADH DH [ubiquinone] 1 alpha subcomplex subunit 7; NDUFA7	12669	3	29.2	257	305	52	410
A1L593|A1L593_BOVIN	Abhydrolase domain containing 4; ABHD4	38743	6	26.0	256	306	156	317
Q3ZBR7|RM18_BOVIN	39S ribosomal protein L18, mitochondrial; MRPL18	20384	5	26.1	256	307	713	134
Q2KIB0|FAHD2_BOVIN	Fumarylacetoacetate hydrolase domain-containing protein 2; FAHD2	34534	5	24.8	255	308	101	369
A7E358|A7E358_BOVIN	MTERFD3 protein (Fragment); MTERFD3	32909	3	17.3	250	309		
Q3ZBI7|USMG5_BOVIN	Up-regulated during skeletal muscle growth protein 5; USMG5	6430	3	44.8	245	310	164	310
A6QL68|A6QL68_BOVIN	CLYBL protein; CLYBL	37526	3	16.7	243	311		
Q148H0|APOO_BOVIN	Apolipoprotein O; APOO	22548	2	13.6	242	312		
Q862F9|Q862F9_BOVIN	Similar to vimentin (Fragment)	9501	2	39.3	239	313		
Q3T0J3|RM16_BOVIN	39S ribosomal protein L16, mitochondrial; MRPL16	28555	6	24.3	239	314	419	195
P23934|NDUS6_BOVIN	NADH dehydrogenase iron-sulfur protein 6, mitochondrial; NDUFS6	13405	3	37.1	235	315	160	311
Q2KJE4|ETFA_BOVIN	Electron transfer flavoprotein subunit alpha, mitochondrial; ETFA	34940	5	25.8	234	316		
Q1JQ99|RM14_BOVIN	39S ribosomal protein L14, mitochondrial; MRPL14	15905	5	41.4	234	317	326	231
Q862N3|Q862N3_BOVIN	Similar to B15 subunit of the NADH: ubiquinone oxidoreductase (Fragment)	11161	4	45.4	232	318	124	347
Q2KIL4|COQ6_BOVIN	Ubiquinone biosynthesis monooxygenase COQ6; COQ6	51116	6	19.0	226	319	334	226
P0C2B8|RM55_BOVIN	39S ribosomal protein L55, mitochondrial; MRPL55	14999	3	13.5	222	320	192	295
Q29RP9|QRSL1_BOVIN	Glutamyl-tRNA(Gln) amidotrans-ferase subunit A homolog; QRSL1	57264	7	20.0	221	321	221	275
Q2YDG5|Q2YDG5_BOVIN	Basic FGF-repressed Zic binding protein; C20orf44	34036	7	18.9	219	322	93	381
A6QR45|A6QR45_BOVIN	Magnesium transporter MRS2 homolog, mitochondrial; MRS2	50471	2	8.8	218	323		
Q0VCJ1|Q0VCJ1_BOVIN	Aurora kinase A interacting protein 1; AURKAIP1	22906	2	7.0	217	324		

196

P00428|COX5B_BOVIN	Cytochrome *c* oxidase subunit 5B, mitochondrial; COX5B	13825	6	39.5	215	325	657	144
Q8HXG6|NDUAB_BOVIN	NADH DH [ubiquinone] 1 alpha subcomplex subunit 1; NDUFA11	14749	4	34.8	215	326		
B1P072|B1P072_BOVIN	Cytochrome *c* oxidase subunit 2; COX2	25970	2	15.9	214	327	125	345
Q2KHU6|Q2KHU6_BOVIN	DHRS4 protein; DHRS4	29436	2	7.9	213	328		
Q2TA23|Q2TA23_BOVIN	Methicillin resistance mecR1 protein; MECR protein; MECR	34718	3	13.9	212	329		
Q3SZV8|ROMO1_BOVIN	Reactive oxygen species modulator 1; ROMO1	8177	2	24.1	209	330		
Q0VCA7|OXSM_BOVIN	3-oxoacyl-[acyl-carrier-protein] synthase, mitochondrial; OXSM	48586	4	14.6	208	331	143	328
A6QR49|A6QR49_BOVIN	Pyruvate dehydrogenase kinase isoform 4, PDK4 protein; PDK4	46129	4	17.9	207	332	192	296
Q17QB8|Q17QB8_BOVIN	Uracil-DNA glycosylase; UNG	33910	2	9.9	206	333		
Q3T061|COX7R_BOVIN	Cytochrome *c* oxidase subunit 7A-related protein, mito; COX7A2L	12535	2	40.4	206	334		
Q3ZBF3|RM38_BOVIN	39S ribosomal protein L38, mitochondrial; MRPL38	44594	6	23.2	205	335	521	170
Q0P5G9|Q0P5G9_BOVIN	SPRY domain containing 4; SPRYD4	22971	6	40.1	202	336		
P00586|THTR_BOVIN	Thiosulfate sulfurtransferase; TST	33275	8	38.7	201	337	136	336
Q2KI49|RM50_BOVIN	39S ribosomal protein L50, mitochondrial; MRPL50	18055	4	27.7	201	338		
Q3SZK3|Q3SZK3_BOVIN	Growth hormone inducible transmembrane protein; GHITM	37005	3	8.1	199	339	150	323
Q2KJC5|Q2KJC5_BOVIN	Hydroxyacyl-Coenzyme A dehydrogenase; HADH	34368	4	14.0	197	340	116	353
Q3MHG6|GTPBA_BOVIN	GTP-binding protein 10; GTPBP10	42905	3	12.7	196	341	216	278
P82919|RT18A_BOVIN	28S ribosomal protein S18a, mitochondrial; MRPS18A	22267	4	23.0	192	342	36	424
Q32KT5|CF136_BOVIN	Uncharacterized protein C6orf136 homolog	35549	2	8.3	191	343		
Q148I4|Q148I4_BOVIN	Acyl-CoA thioesterase 7; ACOT7	37344	4	16.3	191	344	88	390
Q3SZB4|ACADM_BOVIN	Medium-chain specific acyl-CoA dehydrogenase, mito; ACADM	46544	5	12.6	186	345	471	184
Q1LZ78|CA057_BOVIN	Nucleoside-triphosphatase C1orf57 homolog	20669	5	34.2	183	346	58	409
Q2KI15|RF1ML_BOVIN	Peptide chain release factor 1-like, mitochondrial; MTRF1L	43496	5	21.8	183	347	77	398
Q2KHZ9|GCDH_BOVIN	Glutaryl-CoA dehydrogenase, mitochondrial; GCDH	48441	3	8.7	181	348	310	235

Q24K16|ZADH2_BOVIN	Zinc-binding alcohol dehydrogenase domain-containing protein 2; ZADH2	40094	3	10.3	181	349	133	340
Q3T189|DHSB_BOVIN	Succinate dehydrogenase iron-sulfur subunit, mitochondrial; SDHB	31498	5	17.9	180	350	102	368
Q2KI45|MRRP1_BOVIN	Mitochondrial ribonuclease P protein 1; RG9MTD1	49753	4	17.4	180	351		
A6QP80|A6QP80_BOVIN	LOC532995 protein; LOC532995	45435	2	6.6	180	352		
A7MBD2|A7MBD2_BOVIN	Mitochondrial rRNA methyltransferase 1; MRM1 protein; MRM1	38898	7	22.8	179	353	90	387
Q29RJ1|AP4A_BOVIN	Bis(5~-nucleosyl)-tetraphosphatase [asymmetrical]; NUDT2	16765	5	56.5	178	354		
P79110|TXTP_BOVIN	Tricarboxylate transport protein, mitochondrial; SLC25A1	33855	4	12.9	177	355	98	375
A5PJ71|A5PJ71_BOVIN	Mitochondrial ribosomal protein L41; MRPL41 protein; MRPL41	15012	6	36.3	177	356	120	351
Q03763|DSG1_BOVIN	Desmoglein-1; DSG1	112173	2	3.4	175	357		
Q0VCX7|Q0VCX7_BOVIN	Malic enzyme; ME3	67168	2	6.6	174	358		
Q3MHR0|LYPA1_BOVIN	Acyl-protein thioesterase 1; lysophospholipase I; LYPLA1	24580	3	16.5	173	359	84	393
Q3ZBL5|PTH2_BOVIN	Bcl-2 inhibitor of transcription; BIT1; peptidyl-tRNA hydrolase 2, mitochondrial; PTRH2	19278	4	33.5	172	360		
Q08DF7|PDE12_BOVIN	2~,5~-phosphodiesterase 12; PDE12	67222	3	6.4	170	361	246	258
A8YXY6|A8YXY6_BOVIN	MTPAP protein (Fragment); MTPAP	46076	4	16.8	170	362	232	266
P20000|ALDH2_BOVIN	Aldehyde dehydrogenase, mito; ALDH2	56617	5	8.7	164	363	198	289
Q2NKY8|DHX30_BOVIN	Putative ATP-dependent RNA helicase DHX30; DHX30	135861	7	7.8	162	364	64	404
P02510|CRYAB_BOVIN	Alpha-crystallin B chain; CRYAB	20024	5	26.3	162	365	298	242
Q24K02|IDE_BOVIN	Insulin-degrading enzyme; IDE	118026	5	6.8	162	366		
Q95108|THIOM_BOVIN	Thioredoxin, mitochondrial; TXN2	18405	2	27.7	160	367	42	421
A6QPU5|SYDM_BOVIN	Aspartyl-tRNA synthetase, mitochondrial; DARS2	73641	3	6.6	160	368	353	214
P45879|VDAC1_BOVIN	Voltage-dependent anion-selective channel protein 1; VDAC1	30722	4	15.9	159	369	136	337
Q95KV7|NDUAD_BOVIN	NADH dehydrogenase 1 alpha subcomplex subunit 13; NDUFA13	16662	4	22.2	159	370	40	422
Q58DV5|RM30_BOVIN	39S ribosomal protein L30, mitochondrial; MRPL30	18486	2	13.7	158	371		
A6QQD0|A6QQD0_BOVIN	LOC100125578 protein; LOC100125578	47684	4	18.5	155	372	189	300

Q2KIJ6|UBXN6_BOVIN	UBX domain-containing protein 6; UBXN6	49702	2	9.8	155	373	134	339
Q3T099|SYWM_BOVIN	Tryptophanyl-tRNA synthetase, mitochondrial; WARS2	40179	4	15.6	152	374	123	348
Q17QJ7|P5CR2_BOVIN	Pyrroline-5-carboxylate reductase 2; PYCR2	33609	4	18.1	147	375	299	241
Q3SZ07|OVCA2_BOVIN	Ovarian cancer-associated gene 2 protein homolog; OVCA2	24152	3	18.1	147	376		
Q5E9H9|ABHDA_BOVIN	Abhydrolase domain-containing protein 10, mitochondrial; ABHD10	33961	3	13.1	146	377	70	402
Q5E9D6|HDHD3_BOVIN	Haloacid dehalogenase-like hydrolase domain-containing protein 3; HDHD3	27865	3	18.3	146	378		
Q28851|ATPK_BOVIN	ATP synthase subunit f, mitochondrial; ATP5J2	10290	2	27.3	146	379		
A6QLS9|A6QLS9_BOVIN	RAB10 protein; RAB10	22527	2	11.0	146	380		
Q0P5E7|GTPB8_BOVIN	GTP-binding protein 8; GTPBP8	32545	5	21.5	144	381	76	399
Q5EA45|FXRD1_BOVIN	FAD-dependent oxidoreductase do-main-containing protein 1; FOXRED1	54047	6	16.9	143	382	93	382
Q02369|NDUB9_BOVIN	NADH dehydrogenase [ubiquinone] 1 beta subcomplex subunit 9; NDUFB9	21775	6	36.9	137	383	91	386
Q0P5G4|KAT3_BOVIN	Kynurenine-oxoglutarate transaminase 3; CCBL2	51438	4	14.5	137	384	363	207
A1L503|A1L503_BOVIN	Chromobox homolog 4 (Fragment); CBX4	38492	2	3.7	137	385	193	294
P38447|NUCG_BOVIN	Endonuclease G, mito; ENDOG	32242	4	22.1	135	386	62	405
Q0MRP5|Q0MRP5_9CETA	Lysozyme C; LZ	16790	2	20.9	134	387		
P41976|SODM_BOVIN	Superoxide dismutase [Mn], mitochondrial; SOD2	24623	2	12.6	134	388	129	343
Q3SZA4|Q3SZA4_BOVIN	Solute carrier family 25, member 20; SLC25A20	32906	3	8.3	133	389		
A3KN46|LTMD1_BOVIN	LETM1 domain-containing protein 1; LETMD1	41885	3	12.8	130	390		
Q3SZA2|CG055_BOVIN	UPF0562 protein C7orf55 homolog	12844	2	17.7	129	391		
A4FV90|A4FV90_BOVIN	PCCA protein; PCCA	81666	2	4.0	129	392	215	279
Q3T057|RL23_BOVIN	60S ribosomal protein L23; RPL23	14856	2	27.1	129	393		
Q58DH4|Q58DH4_BOVIN	GS2 gene; PNPLA4	28074	4	24.5	128	394	104	366
P61603|CH10_BOVIN	10 kDa heat shock protein, mito; HSPE1	10925	2	25.5	127	395	184	303
A8R4B3|A8R4B3_BOVIN	LOC782657 protein; LOC782657	17857	3	32.1	124	396		
Q2TBW2|COQ7_BOVIN	Ubiquinone biosynthesis protein COQ7 homolog; COQ7	24346	3	21.2	122	397	85	392
Q17QY3|Q17QY3_BOVIN	Nipsnap homolog 3A (C. elegans); NIPSNAP3A	28522	3	13.4	120	398	100	371
Q08DW1|Q08DW1_BOVIN	RAB9A, member RAS oncogene family; RAB9A	22895	3	21.2	119	399		
A6QQZ5|A6QQZ5_BOVIN	MGC165715 protein; MGC165715	37972	4	18.4	115	400		

Q00361|ATP5I_BOVIN	ATP synthase subunit e; ATP5I	8315	2	32.4	114	401	172	307
A6QQY8|A6QQY8_BOVIN	FASTKD1 protein; FASTKD1	96201	5	6.0	111	402	258	254
Q0IIJ8|Q0IIJ8_BOVIN	2,4-dienoyl CoA reductase 1, mitochondrial; DECR1	35358	2	10.0	107	403	113	357
A6QPX8|A6QPX8_BOVIN	RAB12 protein; RAB12	27268	3	17.6	106	404		
Q1LZE3|Q1LZE3_BOVIN	MTERF domain containing 1; MTERFD1	47504	4	9.4	102	405	114	355
Q3MHI7|RF1M_BOVIN	Peptide chain release factor 1, mitochondrial; MTRF1	52515	3	10.5	102	406	229	270
Q0P562|Q0P562_BOVIN	Hypothetical LOC509253; MGC152190	26087	2	4.7	99	407		
Q3SX05|ECSIT_BOVIN	Evolutionarily conserved signaling intermediate in Toll pathway, mitochondrial; ECSIT	49220	2	9.5	99	408	297	243
A7YWQ4|A7YWQ4_BOVIN	Beta-2-syntrophin; SNTB2 protein; SNTB2	57920	2	4.6	98	409	139	332
Q02380|NDUB5_BOVIN	NADH dehydrogenase 1 beta sub-complex subunit 5, mito; NDUFB5	21576	3	7.9	98	410		
Q2KHV4|PARL_BOVIN	Presenilins-associated rhomboid-like protein, mitochondrial; PARL	42274	2	10.1	98	411		
A6H7I3|ANGE2_BOVIN	Carbon catabolite repressor protein 4 homolog 1; CCR4. Protein angel homolog 2; ANGEL2	62308	3	10.7	96	412	105	365
Q5E9N4|AADAT_BOVIN	Kynurenine/alpha-aminoadipate aminotransferase, mito; AADAT	47871	2	6.1	94	413	252	256
B1NZ26|B1NZ26_BOVIN	NADH-ubiquinone oxidoreductase chain 5; ND5	68225	2	4.8	94	414		
Q2KIF8|SYCM_BOVIN	Cysteinyl-tRNA synthetase, mitochondrial; CARS2	61160	2	5.2	94	415	180	305
Q3T131|COQ3_BOVIN	Hexaprenyldihydroxybenzoate methyltransferase, mito; COQ3	41464	2	8.6	93	416		
P00125|CY1_BOVIN	Cytochrome c_1, heme protein, mitochondrial; CYC1	35274	2	8.6	90	417		
Q6TNF3|Q6TNF3_BOVIN	Tranglutaminase 1; TGM1	93047	2	3.3	90	418		
Q58DH2|PISD_BOVIN	Phosphatidylserine decarboxylase proenzyme; PISD	47214	2	7.5	90	419	75	400
Q0VCZ8|Q0VCZ8_BOVIN	Acyl-CoA synthetase long-chain family member 1; ACSL1	78230	2	4.3	86	420	523	169
B1P0I6|B1P0I6_BOVIN	NADH-ubiquinone oxidoreductase chain 1; ND1	35628	2	6.3	85	421		
Q17QW3|Q17QW3_BOVIN	Retinol dehydrogenase 14 (All-trans/9-cis/11-cis); RDH14	36602	2	7.4	83	422		
P82926|RT33_BOVIN	28S ribosomal protein S33, mitochondrial; MRPS33	12445	2	19.8	80	423	51	411
Q2NKR7|F162A_BOVIN	Protein FAM162A; FAM162A	17725	3	8.3	79	424		

Q7YS70|MECR_BOVIN	Trans-2-enoyl-CoA reductase, mitochondrial; MECR	40249	3	13.1	78	425		
Q0IIG8|RAB18_BOVIN	Ras-related protein Rab-18; RAB18	22977	2	12.6	78	426		
Q2KIH9|Q2KIH9_BOVIN	Lipoyl synthase, mitochondrial; LIAS protein; LIAS	33420	3	14.1	77	427		
Q3MHM1|Q3MHM1_BOVIN	Calsequestrin; CASQ2	49884	3	8.1	76	428	89	389
Q2TBP8|M11D1_BOVIN	Protein RSM22 homolog, mitochondrial; METT11D1	51525	2	4.5	76	429	122	349
P00423|COX41_BOVIN	Cytochrome *c* oxidase subunit 4 isoform 1, mitochondrial; COX4I1	19559	3	19.5	75	430		
Q0IIE2|SHC1_BOVIN	SHC-transforming protein 1; SHC1	51599	2	8.7	74	431	107	360
P62998|RAC1_BOVIN	Ras-related C3 botulinum toxin substrate 1; RAC1	21436	2	12.5	73	432		
A5PK43|A5PK43_BOVIN	ERAL1 protein; ERAL1	48537	3	8.2	70	433	415	196
A6H7E1|SYMM_BOVIN	Methionyl-tRNA synthetase, mitochondrial; MARS2	66606	2	4.6	68	434	195	291
Q08DC2|Q08DC2_BOVIN	RAB31, member RAS oncogene family; RAB31	21501	2	12.8	68	435	96	376
A6QLE2|A6QLE2_BOVIN	RMND1 protein; RMND1	51752	2	5.1	67	436		
Q1RMI2|Q1RMI2_BOVIN	Ras homolog gene family, member G (Rho G); RHOG	21267	2	19.9	66	437		
Q3SYV3|OXA1L_BOVIN	Mitochondrial inner membrane protein OXA1L; OXA1L	48956	2	8.8	59	438		
Q3SZ85|CB079_BOVIN	Uncharacterized protein C2orf79 homolog	15962	2	15.0	59	439		
Q32PA7|Q32PA7_BOVIN	Mitochondrial ribosomal protein L23; MRPL23	12307	2	30.2	58	440		
Q04232|Q04232_BVDV	Viral diarrhea virus CP1 putative helcase/protease (Fragment)	210031	2	0.9	57	441		
A6H751|FOLC_BOVIN	Folylpolyglutamate synthase, mitochondrial; FPGS	64859	2	7.0	57	442	113	356
Q2TBI6|RM32_BOVIN	39S ribosomal protein L32, mitochondrial; MRPL32	21310	3	13.3	55	443		
A7MBF7|A7MBF7_BOVIN	LOC616332 protein; LOC616332	22892	2	10.5	54	444	35	425
Q3SZA9|RM35_BOVIN	39S ribosomal protein L35, mitochondrial; MRPL35	21637	2	10.6	51	445		
Q32L67|GLRX2_BOVIN	Glutaredoxin-2, mitochondrial; GLRX2	17191	2	22.3	51	446		
Q0IIM2|ARL6_BOVIN	ADP-ribosylation factor-like protein 6; ARL6	21042	2	11.8	46	447		
Q0VCG0|LYRM4_BOVIN	LYR motif-containing protein 4; LYRM4	10705	2	24.2	44	448		

201

B0JYQ0|B0JYQ0_BOVIN	ALB protein; ALB	69248	3518	33
B0JYN6|B0JYN6_BOVIN	Alpha-2-HS-glycoprotein; AHSG	38394	3417	35
P48616|VIME_BOVIN	Vimentin; VIM	53695	3267	38
P02769|ALBU_BOVIN	Serum albumin; ALB	69248	2927	41
Q3MI02|Q3MI02_BOVIN	UQCRC1 protein (Fragment); UQCRC1	52487	1777	60
P11178|ODBA_BOVIN	2-oxoisovalerate dehydrogenase subunit alpha, mitochondrial; BCKDHA	51646	1368	76
Q32PH8|EF1A2_BOVIN	Elongation factor 1-alpha 2; EEF1A2	50438	1141	84
Q76LV2|HS90A_BOVIN	Heat shock protein HSP 90-alpha; HSP90AA1	84678	923	105
Q76LV1|HS90B_BOVIN	Heat shock protein HSP 90-beta; HSP90AB1	83201	875	111
Q58DU3|Q58DU3_BOVIN	Sulfide dehydrogenase like; SQRDL	39196	684	138
P34955|A1AT_BOVIN	Alpha-1-antiproteinase; SERPINA1	46075	666	142
Q3MHM5|TBB2C_BOVIN	Tubulin beta-2C chain; TUBB2C	49799	603	153
Q2KJD0|TBB5_BOVIN	Tubulin beta-5 chain; TUBB5	49639	535	165
Q0VD56|Q0VD56_BOVIN	Myosin binding protein C, cardiac; MYBPC3	139606	511	171
P81947|TBA1B_BOVIN	Tubulin alpha-1B chain;	50120	511	172
Q2TBR2|RM20_BOVIN	39S ribosomal protein L20, mitochondrial; MRPL20	17524	510	173
P82920|RT21_BOVIN	28S ribosomal protein S21, mitochondrial; MRPS21	10668	510	174
Q9XSC6|KCRM_BOVIN	Creatine kinase M-type; CKM	42962	472	183
Q2HJ86|TBA1D_BOVIN	Tubulin alpha-1D chain; TUBA1D	50251	470	185
P02081|HBBF_BOVIN	Hemoglobin fetal subunit beta;	15849	454	190
Q3ZC07|ACTC_BOVIN	Actin, alpha cardiac muscle 1; ACTC1	41992	356	212
Q0MRP5|Q0MRP5_9CETA	Lysozyme C; LZ	16790	323	232
Q9BE39|MYH7_BOVIN	Myosin-7; MYH7	223091	272	250
Q3T149|HSPB1_BOVIN	Heat shock protein beta-1; HSPB1	22379	251	257
Q3SZ71|MPPB_BOVIN	Mitochondrial-processing peptidase subunit beta; PMPCB	54202	231	267
A5PJC5|A5PJC5_BOVIN	MLYCD protein; MLYCD	55381	218	276
A4FV36|A4FV36_BOVIN	SPATA20 protein; SPATA20	88303	189	301
Q02373|NDUBA_BOVIN	NADH dehydrogenase [ubiquinone] 1 beta subcomplex subunit 10; NDUFB10	20952	160	314
Q1JP98|Q1JP98_BOVIN	ATP synthase subunit d isoform a (Fragment);	14022	155	318

	ATP5H			
Q58CX2|FAKD3_BOVIN	FAST kinase domain-containing protein 3; FASTKD3	75438	154	319
P19120|HSP7C_BOVIN	Heat shock cognate 71 kDa protein; HSPA8	71196	153	320
P06623|CN37_BOVIN	2',3'-cyclic-nucleotide 3'-phosphodiesterase; CNP	44847	145	327
P04272|ANXA2_BOVIN	Annexin A2; ANXA2	38588	139	331
Q29RK2|PYC_BOVIN	Pyruvate carboxylase, mito; PC	129616	137	335
Q5E9Z1|RUSD4_BOVIN	RNA pseudouridylate synthase domain-containing protein 4; RPUSD4	41974	115	354
Q0IIG5|K6PF_BOVIN	6-phosphofructokinase, muscle type; PFKM	85239	111	358
Q9N2I8|TRXR2_BOVIN	Thioredoxin reductase 2, mitochondrial; TXNRD2	54636	108	359
Q3ZC04|RT63_BOVIN	Ribosomal protein 63, mitochondrial; MRP63	11859	105	364
A0ERA7|A0ERA7_BOVIN	Solute carrier family 27 member 1 isoform; SLC27A1	39483	103	367
A5PJL7|A5PJL7_BOVIN	MGC160092 protein; MGC160092	45970	99	373
Q1LZC4|Q1LZC4_BOVIN	Hypothetical LOC506205; MGC138976	39214	99	374
Q0PHT2|Q0PHT2_BOVIN	LOC533186 (Fragment);	25187	96	377
A8WFL6|A8WFL6_BOVIN	DMD protein; DMD	68864	96	378
A5D7V9|SYHM_BOVIN	Probable histidyl-tRNA synthetase, mitochondrial; HARS2	56878	94	380
Q32PA7|Q32PA7_BOVIN	Mitochondrial ribosomal protein L23; MRPL23	12307	92	384
Q08DN3|Q08DN3_BOVIN	CDK5 regulatory subunit associated protein 1; CDK5RAP1	66395	91	385
P15497|APOA1_BOVIN	Apolipoprotein A-I; APOA1	30258	90	388
Q08DU7|Q08DU7_BOVIN	MTERF protein (Fragment); MTERF	50623	79	397
Q3MHH6|PYRD2_BOVIN	Pyridine nucleotide-disulfide oxidoreductase domain-containing protein 2; PYROXD2	62948	60	406
Q2HJF8|MIRO1_BOVIN	Mitochondrial Rho GTPase 1; RHOT1	72032	58	407
A6H783|A6H783_BOVIN	VDAC5P protein; VDAC5P	30850	58	408
A5D7E8|A5D7E8_BOVIN	PDIA3 protein; PDIA3	56894	51	412
Q3T0D0|HNRPK_BOVIN	Heterogeneous nuclear ribonucleoprotein K; HNRNPK	50987	50	413
Q02368|NDUB7_BOVIN	NADH dehydrogenase [ubiquinone] 1 beta subcomplex subunit 7; NDUFB7	16387	50	414
Q0P5K8|Q0P5K8_BOVIN	Nipsnap homolog 1 (C. elegans); NIPSNAP1	33139	50	415

203

B0JYK6|B0JYK6_BOVIN	Phosphorylase; PYGM	97227	48	416
O62654|DESM_BOVIN	Desmin; DES	53499	48	417
A4IF72|A4IF72_BOVIN	CHCHD10 protein; CHCHD10	14215	46	418
P62935|PPIA_BOVIN	Peptidyl-prolyl cis-trans isomerase A; PPIA	17858	45	419
Q05B66|OPA3_BOVIN	Optic atrophy 3 protein homolog; OPA3	21247	43	420
Q7YRA7|Q7YRA7_BOVIN	Cytochrome c_1 (Fragment); CYC1	20408	37	423

Table 11. Classification and possible functional roles of the bovine heart mitochondrial nucleoid proteins. Mitochondrial nucleoid proteins were sorted into the following groups: **NAbm**, group of nucleic acid binding or modifying proteins; **Reg**, other regulatory proteins; **RiPS**, protein constituents of mitochondrial ribosomes and other proteins involved in protein synthesis; **OxPh**, proteins associated with the mitochondrial system of oxidative phosphorylation; **Redox**, proteins catalyzing redox reactions other than OXPHOS proteins; **PMD**, protein modification and degradation group; **Chap**, chaperones; **Imp**, mitochondrial protein import components; **Carb**, carbohydrate metabolic group; **Lip**, lipid metabolic group; **Keto**, ketone body metabolic group; **AA**, amino acid metabolic group; **Nucl**, nucleotide metabolic group; **TCC**, transporters, carriers and channels; **OM**, components of the outer mitochondrial membrane; **X**, mostly uncharacterized and previously hypothetical proteins; **Cyto**, subunit of cytosolic ribosomes and cytoskeletal and intercellular adhesion proteins. Mito, mitochondrial; DH, dehydrogenase; DHC, dehydrogenase complex.

No.	Protein Accession	Protein; Gene	Group	Description, function
1	Q29RI0|ADCK3_BOVIN	Chaperone activity of bc1 complex-like, mitochondrial; CABC1	OxPh	May be a chaperone-like protein for the proper conformation of respiratory chain complexes. Belongs to the aarF domain-containing protein kinase 3 (ADCK) protein kinase family.
2	P49410|EFTU_BOVIN	Elongation factor Tu, mitochondrial; TUFM	RiPS	Translational elongation factor promoting the GTP-dependent binding of aminoacyl-tRNA to the A-site of ribosomes.
3	Q04467|IDHP_BOVIN	Isocitrate dehydrogenase [NADP], mitochondrial; IDH2	Carb	Isocitrate dehydrogenase may tightly associate or interact with the pyruvate dehydrogenase complex.
4	Q148D5|SUCB1_BOVIN	Succinyl-CoA ligase [ADP-forming] subunit beta, mitochondrial; SUCLA2	Carb	Tricarboxylic acid cycle. ATP-specific succinyl-CoA synthetase subunit beta.
5	Q3T0U3|Q3T0U3_BOVIN	Es1 protein; ES1	NAbm	RNA-protein interaction regulation; thiamine biosynthesis; Ras-related signal transduction; protease.
6	Q59HJ6|LONM_BOVIN	Lon protease homolog, mitochondrial; LONP1	PMD	ATP-dependent serine protease catalyzing the first steps of intramitochondrial protein degradation. Binds to single-stranded but not to double-stranded DNA.
7	Q17QJ1|ACSF2_BOVIN	Acyl-CoA synthetase family member 2, mitochondrial; ACSF2	Lip	Acyl-CoA synthases catalyze the initial thioester formation with CoA in fatty acid metabolism.
8	P43896|EFTS_BOVIN	Elongation factor Ts, mitochondrial; TSFM	RiPS	Associates with EF-Tu/GDP; induces exchange of GDP to GTP; remains bound to aminoacyl-tRNA.
9	P19483|ATPA_BOVIN	ATP synthase subunit alpha; ATP5A1	OxPh	Oxidative phosphorylation; mitochondrial ATP synthase.
10	Q3MHX5|SUCB2_BOVIN	Succinyl-CoA ligase [GDP-forming] subunit beta, mitochondrial; SUCLG2	Carb	Belongs to the succinate/malate CoA ligase beta subunit family.
11	P15690|NDUS1_BOVIN	NADH-ubiquinone oxidoreductase 75 kDa subunit, mitochondrial; NDUFS1	OxPh	Oxidative phosphorylation; respiratory complex I.

12	P00829|ATPB_BOVIN	ATP synthase subunit beta, mito; ATP5B	OxPh	Oxidative phosphorylation; mitochondrial ATP synthase.
13	Q0III1|Q0III1_BOVIN	Methylmalonyl Coenzyme A mutase; MUT	AA	Degradation of amino acids, odd- chain fatty acids and cholesterol via propionyl-CoA to the Krebs cycle.
14	Q58DR8|SUCA_BOVIN	Succinyl-CoA ligase [GDP-forming] subunit alpha, mito; SUCLG1	Carb	Carbohydrate metabolism; tricarboxylic acid cycle; GTP + succinate + CoA = GDP + phosphate + succinyl-CoA.
15	Q24JZ7|Q24JZ7_BOVIN	3-oxoacid CoA transferase 1; OXCT1	Keto	Transferase; ketone body catabolic process.
16	Q58CP0|IDH3G_BOVIN	Isocitrate dehydrogenase [NAD] subunit gamma, mitochondrial; IDH3G	Carb	Citric acid cycle; isocitrate + NAD+ = 2-oxoglutarate + CO2 + NADH
17	P11181|ODB2_BOVIN	Lipoamide acyltransferase of branched-chain alpha-keto acid DHC, mito; DBT	AA	Lipoamide acyltransferase component of branched-chain alpha-keto acid dehydrogenase complex.
18	A4FUC5|A4FUC5_BOVIN	Acyl-CoA synthetase short-chain family member 1; ACSS1	Lip	Acyl-CoA synthetase.
19	Q3ZBQ0|SIRT5_BOVIN	NAD-dependent deacetylase sirtuin-5; SIRT5	PMD	Deacetylase that activates CPS1 and regulates blood ammonia levels during prolonged fasting.
20	A5D9G3|A5D9G3_BOVIN	Similar to Succinyl-CoA ligase [GDP-forming] beta-chain, mito; LOC283398	Carb	Belongs to the succinate/malate CoA ligase beta subunit family.
21	Q2TBI4|TRAP1_BOVIN	Heat shock protein 75 kDa, mitochondrial; TRAP1	Chap	Protein folding; chaperone with ATPase activity. Binds to tumor necrosis factor type 1 receptor.
22	A0JN67|A0JN67_BOVIN	Glutaminase; GLS	AA	Glutaminase.
23	Q07536|MMSA_BOVIN	Methylmalonate-semialdehyde dehydro-genase [acylating], mito; ALDH6A1	AA	Plays a role in valine and pyrimidine metabolism.
24	Q1RMM6|Q1RMM6_BOVIN	Coenzyme Q10 homolog A (S. cerevisiae); COQ10A	Lip	Ubiquinone biosynthesis?
25	Q2NL34|COQ9_BOVIN	Ubiquinone biosynthesis protein COQ9, mitochondrial; COQ9	Lip	Ubiquinone biosynthesis; interaction of COQ3-4-6-7-9.
26	P20004|ACON_BOVIN	Aconitate hydratase, mitochondrial; ACO2	Carb	Carbohydrate metabolism; tricarboxylic acid cycle; isocitrate from oxaloacetate.
27	A7YWE4|AL4A1_BOVIN	Delta-1-pyrroline-5-carboxylate dehydrogenase, mitochondrial; ALDH4A1	AA	Amino-acid degradation; irreversible conversion of delta-1-pyrroline-5-carboxylate (from proline or ornithine) to glutamate. Step in the pathway interconnecting the urea and tricarboxylic acid cycles.
28	O77784|IDH3B_BOVIN	Isocitrate dehydrogenase [NAD] subunit beta, mitochondrial; IDH3B	Carb	Tricarboxylic acid cycle; isoform A is predominant in heart muscle; isoform B is present in kidney and liver.
29	Q2KJB7|CPT2_BOVIN	Carnitine O-palmitoyltransferase 2, mitochondrial; CPT2	Lip	Lipid metabolism.
30	Q3ZCH0|GRP75_BOVIN	Stress-70 protein, mitochondrial, Mortalin-2; HSPA9	Chap	Protein folding. Control of cell proliferation and cellular aging. May also act as a chaperone.
31	P11024|NNTM_BOVIN	NAD(P) transhydrogenase, mitochondrial; NNT	OxPh	NADH/NADP transhydrogenation is coupled to respiration and ATP hydrolysis; pumps proton across the membrane.
32	Q3SZ00|Q3SZ00_BOVIN	HADHA protein; HADHA	Lip	Beta oxidation.

33	O46504|PDPR_BOVIN	Pyruvate dehydrogenase phosphatase regulatory subunit, mito; PDPR	Carb	Pyruvate dehydrogenase complex.
34	Q148N0|ODO1_BOVIN	2-oxoglutarate dehydrogenase, mitochondrial; OGDH	Carb	Tricarboxylic acid cycle; E1 component of 2-oxoglutarate dehydrogenase complex; conversion of 2-oxoglutarate to succinyl-CoA and CO_2.
35	Q3SZ73|ABHDB_BOVIN	Abhydrolase domain-containing protein 11; ABHD11	PMD	Hydrolase.
36	Q3SZI8|IVD_BOVIN	Isovaleryl-CoA dehydrogenase, mitochondrial; IVD	AA	Amino-acid degradation; L-leucine degradation; (S)-3-hydroxy-3-methylglutaryl-CoA from 3-isovaleryl-CoA.
37	Q0P5A2|COQ5_BOVIN	Ubiquinone biosynthesis methyltransferase COQ5, mitochondrial; COQ5	Lip	Ubiquinone biosynthesis.
38	A6QLZ6|A6QLZ6_BOVIN	GLRX5 protein; GLRX5	Redox	Redox homeostasis; protein disulfide oxidoreductase.
39	Q58DN7|ACSF3_BOVIN	Acyl-CoA synthetase family member 3, mitochondrial; ACSF3	Lip	Acyl-CoA synthetase.
40	P11966|ODPB_BOVIN	Pyruvate dehydrogenase E1 component subunit beta, mitochondrial; PDHB	Carb	Pyruvate dehydrogenase complex.
41	Q2HJ97|PHB2_BOVIN	Prohibitin-2; PHB2	Reg	Mediator of transcriptional repression by nuclear hormone receptors. Estrogen receptor-selective coregulator potentiating the inhibitory activities of antiestrogens and repressing the activity of estrogens. Interacts with PHB.
42	Q29RK1|CISY_BOVIN	Citrate synthase, mitochondrial; CS	Carb	Citric acid cycle.
43	P34942|NDUAA_BOVIN	NADH dehydrogenase 1 alpha subcomplex subunit 10, mito; NDUFA10	OxPh	Oxidative phosphorylation; respiratory complex I.
44	A4FUH8|A4FUH8_BOVIN	Chromosome 1 open reading frame 93 ortholog; C16H1orf93	X	Localized in thioredoxin-like cluster.
45	P02722|ADT1_BOVIN	ADP/ATP translocase 1; SLC25A4	TCC	Exchange of ADP and ATP across the mitochondrial inner membrane.
46	A7E3V3|A7E3V3_BOVIN	Inner membrane protein, mitochondrial, Mitofilin; IMMT	X	Mitofilin seems to control cristae morphology of mitochondria.
47	Q2HJI1|Q2HJI1_BOVIN	SDHA protein; SDHA	OxPh	Oxidative phosphorylation; respiratory complex II; succinate dehydrogenase complex.
48	Q3SZJ1|Q3SZJ1_BOVIN	IARS2 protein (Fragment); IARS2	RiPS	Aminoacyl-tRNA synthetase; hypothetical protein in bos taurus.
49	Q3T165|PHB_BOVIN	Prohibitin; PHB	Reg	Prohibitin inhibits DNA synthesis and regulates proliferation. May play a role in regulating mitochondrial respiration and in aging. Interacts with PHB2.
50	A6QNM2|RRF2M_BOVIN	Ribosome-releasing factor 2, mito; GFM2	RiPS	Mitochondrial ribosome.
51	A5PKG4|A5PKG4_BOVIN	Cysteine desulfurase, mitochondrial; NFS1 protein; NFS1	RiPS	Aminotransferase; L-cysteine + [enzyme]-cysteine = L-alanine + [enzyme]-S-sulfanylcysteine.
52	A7MB35|ODPA_BOVIN	Pyruvate dehydrogenase E1 subunit alpha, somatic form, mitochondrial; PDHA1	Carb	Pyruvate dehydrogenase complex.
53	A6QQ83|A6QQ83_BOVIN	Thioesterase superfamily member 2; THEM2 protein; THEM2	Lip	Thioesterase superfamily member 2; Acyl-CoA thioesterases are a group of enzymes that catalyze the hydrolysis of acyl-CoAs.
54	P17694|NDUS2_BOVIN	NADH dehydrogenase [ubiquinone] iron-	OxPh	Oxidative phosphorylation; respiratory complex I.

		sulfur protein 2, mito; NDUFS2		
55	Q148J8|Q148J8_BOVIN	Isocitrate dehydrogenase 3 (NAD+) alpha; IDH3A	Carb	Tricarboxylic acid cycle. Isoform A is predominant in heart muscle; also found in brain, kidney and liver. Isoform B is present in kidney and liver.
56	Q2KIG0|ETFD_BOVIN	Electron transfer flavoprotein-ubiquinone oxidoreductase, mito; ETFDH	OxPh	ETFDH transfers electrons from ETF to ubiquinone.
57	Q08DN5|Q08DN5_BOVIN	Carnitine acetyltransferase; MGC142781	Lip	Lipid metabolism.
58	O46629|ECHB_BOVIN	Trifunctional enzyme subunit beta, mitochondrial; HADHB	Lip	Beta oxidation.
59	A1A4J9|A1A4J9_BOVIN	DnaJ (Hsp40) homolog, subfamily A, member 3; DNAJA3	Chap	Chaperone, assciated with heat shock 70kDa protein 9B (HSPA9 or mortalin-2) that is implicated in the control of cell proliferation.
60	A5D954|A5D954_BOVIN	Solute carrier family 25, member 11 (Fragment); SLC25A11	TCC	Mitochondrial carrier; oxoglutarate carrier.
61	P23709|NDUS3_BOVIN	NADH dehydrogenase [ubiquinone] iron-sulfur protein 3, mito; NDUFS3	OxPh	Oxidative phosphorylation; respiratory complex I.
62	P12234|MPCP_BOVIN	Phosphate carrier protein, mitochondrial; SLC25A3	TCC	Phosphate transport.
63	P22439|ODPX_BOVIN	Pyruvate dehydrogenase protein X component; PDHX	Carb	Pyruvate dehydrogenase complex.
64	Q32KX0|ISOC2_BOVIN	Isochorismatase domain-containing protein 2, mitochondrial; ISOC2	AA	Amino-acid degradation.
65	Q3T0B6|C1QBP_BOVIN	Complement component 1 Q subcomponent-binding protein, mito; C1QBP	Reg	Complement activation.
66	Q2KI62|PTCD3_BOVIN	Pentatricopeptide repeat-containing protein 3, mitochondrial; PTCD3	NAbm	Some PPR proteins play a role in post-transcriptional processes and are thought to be sequence-specific RNA-binding proteins. PPR proteins contain tandem 35 amino acid repeats.
67	P31800|QCR1_BOVIN	Cytochrome bc_1 complex subunit 1, mitochondrial; UQCRC1	OxPh	Oxidative phosphorylation; respiratory complex III.
68	Q5E9D3|CHCH3_BOVIN	Coiled-coil-helix-coiled-coil-helix domain-containing protein 3, mito; CHCHD3	X	Contains 1 CHCH domain. Interacts with DNA helicase.
69	Q01321|NDUA4_BOVIN	NADH dehydrogenase 1 alpha subcomplex subunit 4; mito; NDUFA4	OxPh	Oxidative phosphorylation; respiratory complex I.
70	P48818|ACADV_BOVIN	Very long-chain specific acyl-CoA dehydrogenase, mitochondrial; ACADVL	Lip	Lipid metabolism; mitochondrial fatty acid beta-oxidation.
71	P82649|RT22_BOVIN	28S ribosomal protein S22, mito; MRPS22	RiPS	Mitochondrial ribosome.
72	Q8SQH5|ADT2_BOVIN	ADP/ATP translocase 2; SLC25A5	TCC	Exchange of ADP and ATP across the mitochondrial inner membrane.
73	Q0VC50|RT4I1_BOVIN	Reticulon-4-interacting protein 1, mitochondrial; RTN4IP1	Redox	Oxidoreductase; interacts with Core proteins I and II of respiratory complex III.
74	Q2KJI7|AFG32_BOVIN	AFG3-like protein 2; AFG3L2	PMD	AAA ATPase; metallo protease.
75	Q2KIW8|Q2KIW8_BOVIN	Glutathione S-transferase kappa 1; GSTK1	Redox	Protein disulfide oxidoreductase.

76	Q148D3|Q148D3_BOVIN	Fumarate hydratase; FH	Carb	Glucose metabolism; tricarboxylic acid cycle.
77	P31081|CH60_BOVIN	60 kDa heat shock protein, mito; HSPD1	Chap	Implicated in mitochondrial protein import and macromolecular assembly.
78	Q3SZK4|TBRG4_BOVIN	Transforming growth factor beta regulator 4; TBRG4	Reg	TBRG4 may play a role in cell cycle progression; belongs to FAST kinase (forkhead activin signal transducer) family.
79	Q1JPF2|Q1JPF2_BOVIN	NADH dehydrogenase1 alpha subcomplex, 9, 39kDa (Fragment); NDUFA9	OxPh	Oxidative phosphorylation; respiratory complex I.
80	P25708|NDUV1_BOVIN	NADH dehydrogenase [ubiquinone] flavoprotein 1, mitochondrial; NDUFV1	OxPh	Oxidative phosphorylation; respiratory complex I.
81	Q3SZ27|APOOL_BOVIN	Apolipoprotein O-like; APOL	Lip	Belongs to the apolipoprotein O family.
82	P23004|QCR2_BOVIN	Cytochrome bc_1 complex subunit 2, mitochondrial; UQCRC2	OxPh	Oxidative phosphorylation; respiratory complex III.
83	P22600|HEMH_BOVIN	Ferrochelatase, mitochondrial; FECH	OxPh	Protoheme ferro-lyase; heme synthase; protoheme from protoporphyrin-IX.
84	P42028|NDUS8_BOVIN	NADH dehydrogenase [ubiquinone] iron-sulfur protein 8, mito; NDUFS8	OxPh	Oxidative phosphorylation; respiratory complex I.
85	A5D9H9|A5D9H9_BOVIN	DNA polymerase delta interacting protein 2; POLDIP2	NAbm	Potential interaction with TFAM.
86	Q2KJG8|BCKD_BOVIN	[3-methyl-2-oxobutanoate dehydrogenase [lipoamide]] kinase, mito; BCKDK	AA	Amino-acid metabolism.
87	Q3T179|Q3T179_BOVIN	HSPD1 protein (Fragment); HSPD1	Chap	Belongs to the chaperonin (HSP60) family. Implicated in mitochondrial protein import and macromolecular assembly.
88	P46198|IF2M_BOVIN	Translation initiation factor IF-2, mitochondrial; MTIF2	RiPS	Mitochondrial ribosome.
89	P82669|RT25_BOVIN	28S ribosomal protein S25, mito; MRPS25	RiPS	Mitochondrial ribosome.
90	Q2KJH7|Q2KJH7_BOVIN	Aldehyde dehydrogenase 18 family, member A1; ALDH18A1	AA	Oxidoreductase; proline biosynthesis.
91	Q17QH8|D39U1_BOVIN	Epimerase family protein SDR39U1; SDR39U1	Carb	Belongs to the sugar epimerase family. SDR39U1 subfamily.
92	P54149|MSRA_BOVIN	Peptide methionine sulfoxide reductase; MSRA	Redox	Repairs proteins inactivated by oxidation. Reversible reduction of methionine sulfoxide to methionine.
93	Q58D58|Q58D58_BOVIN	Cat eye syndrome chromosome region, candidate 5 isoform 2; CECR5	X	Candidate gene for the Cat Eye Syndrome (CES) associated with the duplication of a 2 Mb region of 22q11.2.
94	Q3MHW4|Q3MHW4_BOVIN	Sulfide:quinone oxidoreductase, mitochondrial; SQRDL protein; SQRDL	Redox	Oxidoreductase; catalyzes the oxidation of hydrogen sulfide, with the help of a quinone.
95	P25285|GCST_BOVIN	Aminomethyltransferase, mito; AMT	AA	Amino-acid degradation; catalyzes the degradation of glycine.
96	A7YVD7|CH038_BOVIN	UPF0551 protein C8orf38 homolog, mito;	OxPh	Required for the function of respiratory complex I.
97	A4FV92|A4FV92_BOVIN	Cytochrome P450 27; CYP27A1 protein; CYP27A1	Redox	Oxidoreductase; cytochrome P450, sterol 26-hydroxylase, mitochondrial.
98	Q3T0R7|THIM_BOVIN	3-ketoacyl-CoA thiolase, mito; ACAA2	Lip	Lipid metabolism; fatty acid metabolism.
99	A6QQF5|QORL2_BOVIN	Quinone oxidoreductase-like protein 2;	Redox	Oxidoreductase.

100	Q3ZBF6|ACADS_BOVIN	Short-chain specific acyl-CoA dehydrogenase, mitochondrial; ACADS	Lip	Lipid metabolism; mitochondrial fatty acid beta-oxidation.
101	A0JNB4|A0JNB4_BOVIN	Leucyl-tRNA synthetase 2, mitochondrial; LARS2	RiPS	Protein biosynthesis.
102	Q32LG3|MDHM_BOVIN	Malate dehydrogenase, mitochondrial; MDH2	Carb	Glucose metabolism.
103	Q58DK1|CPT1B_BOVIN	Carnitine O-palmitoyltransferase 1, muscle isoform; CPT1B	Lip	Lipid metabolism; fatty acid beta-oxidation.
104	P21839|ODBB_BOVIN	2-oxoisovalerate dehydrogenase subunit beta, mitochondrial; BCKDHB	AA	Amino acid metabolism.
105	P30404|PPIF_BOVIN	Peptidyl-prolyl cis-trans isomerase F, mitochondrial; PPIF	RiPS	PPIases accelerate protein folding by cis-trans isomerization of proline bonds.
106	P23935|NDUA5_BOVIN	NADH dehydrogenase 1 alpha subcomplex subunit 5; NDUFA5	OxPh	Oxidative phosphorylation; respiratory complex I.
107	Q3T0G5|PROSC_BOVIN	Proline synthetase co-transcribed bacterial homolog protein; PROSC	AA	Amino-acid metabolism.
108	A5D7G0|A5D7G0_BOVIN	Tyrosyl-tRNA synthetase, mitochondrial; YARS2 protein; YARS2	RiPS	Belongs to the class-I aminoacyl-tRNA synthetase family.
109	P13621|ATPO_BOVIN	ATP synthase subunit O, mito; ATP5O	OxPh	Oligomycin sensitivity conferral protein.
110	Q2HJ73|HIBCH_BOVIN	3-hydroxyisobutyryl-CoA hydrolase, mitochondrial; HIBCH	AA	Amino-acid degradation.
111	Q3SZ20|GLYM_BOVIN	Serine hydroxymethyltransferase, mitochondrial; SHMT2	AA	Interconversion of serine and glycine.
112	Q3MHY7|RM10_BOVIN	39S ribosomal protein L10, mito; MRPL10	RiPS	Mitochondrial ribosome.
113	P82928|RT28_BOVIN	28S ribosomal protein S28, mito; MRPS28	RiPS	Mitochondrial ribosome.
114	P35705|PRDX3_BOVIN	Thioredoxin-dependent peroxide reductase, mitochondrial; PRDX3	Redox	Protects radical-sensitive enzymes from oxidative damage.
115	Q1JPD3|D2HDH_BOVIN	D-2-hydroxyglutarate dehydrogenase, mito; D2HGDH	AA	Amino-acid degradation.
116	Q2YDI0|RM11_BOVIN	39S ribosomal protein L11, mito; MRPL11	RiPS	Mitochondrial ribosome.
117	Q08D87|Q08D87_BOVIN	Phenylalanyl-tRNA synthetase 2, mitochondrial; FARS2	RiPS	Aminoacyl-tRNA synthetase; protein biosynthesis.
118	Q58DQ5|RT09_BOVIN	28S ribosomal protein S9, mito; MRPS9	RiPS	Mitochondrial ribosome.
119	Q3SZD7|CBR1_BOVIN	Carbonyl reductase [NADPH] 1; CBR1	Redox	Reductase of carbonyl compounds like quinones, prostaglandins, menadiones.
120	Q02337|BDH_BOVIN	D-beta-hydroxybutyrate dehydrogenase, mitochondrial; BDH1	Keto	Ketone body metabolism.
121	Q2KHU5|MACD1_BOVIN	MACRO domain-containing protein 1; MACROD1	Reg	Estrogen signaling. Amplifies the transactivation function of AR in response to androgen binding.
122	C6K7D4|C6K7D4_BOVIN	Sirtuin 3 (Fragment); Sirt3	Reg	Protein amino acid deacetylation; chromatin silencing.
123	Q9BGI1|PRDX5_BOVIN	Peroxiredoxin-5, mitochondrial; PRDX5	Redox	Intracellular redox signaling. Reduces hydrogen peroxide and alkyl

				hydroperoxides through the thioredoxin system.
124	P12344|AATM_BOVIN	Aspartate aminotransferase, mito; GOT2	AA	Amino acid exchange between mitochondria and cytosol.
125	Q05B74|Q05B74_BOVIN	Mitochondrial ribosomal protein L39; MRPL39	RiPS	Mitochondrial ribosome.
126	Q2KIS2|RM44_BOVIN	39S ribosomal protein L44, mito; MRPL44	RiPS	Mitochondrial ribosome.
127	Q3SWX4|Q3SWX4_BOVIN	Glioblastoma amplified sequence; GBAS	X	Similarity to the NIPSNAP family putatively involved in vesicular transport.
128	Q2NL27|RT23_BOVIN	28S ribosomal protein S23, mito; MRPS23	RiPS	Mitochondrial ribosome.
129	P82925|RT31_BOVIN	28S ribosomal protein S31, mito; MRPS31	RiPS	Mitochondrial ribosome.
130	A6QPQ5|RM01_BOVIN	39S ribosomal protein L1, mito; MRPL1	RiPS	Mitochondrial ribosome.
131	A4FUZ6|HSDL2_BOVIN	Hydroxysteroid dehydrogenase-like protein 2; HSDL2	Redox	Oxidoreductase; has apparently no steroid dehydrogenase activity.
132	A6QQP1|A6QQP1_BOVIN	DAP3 protein (Fragment); DAP3	RiPS	Component of the mitochondrial ribosome small subunit (28S).
133	A8WFQ0|A8WFQ0_BOVIN	NDUFS7 protein; NDUFS7	OxPh	Oxidative phosphorylation. Respiratory complex I.
134	Q3SZ86|RT26_BOVIN	28S ribosomal protein S26, mito; MRPS26	RiPS	Mitochondrial ribosome.
135	Q3ZC57|Q3ZC57_BOVIN	Peroxisomal D3,D2-enoyl-CoA isomerase; PECI	Lip	Lipid metabolism; isomerase.
136	Q2YDF6|RT35_BOVIN	28S ribosomal protein S35, mito; MRPS35	RiPS	Mitochondrial ribosome.
137	A0JN95|ME5D1_BOVIN	Putative S-adenosyl-L-methionine-dependent methyltransferase; METT5D1	PMD	Probable S-adenosyl-L-methionine-dependent methyltransferase.
138	A7YWC4|ATAD3_BOVIN	ATPase family AAA domain-containing protein 3; ATAD3	PMD	AAA ATPase.
139	P82920|RT21_BOVIN	28S ribosomal protein S21, mito; MRPS21	RiPS	Mitochondrial ribosome.
140	Q2TBS2|RM21_BOVIN	39S ribosomal protein L21, mito; MRPL21	RiPS	Mitochondrial ribosome.
141	Q2PC20|PPM1K_BOVIN	Protein phosphatase 1K, mito; PPM1K	PMD	Regulates the mitochondrial permeability transition pore.
142	Q3T100|MGST3_BOVIN	Microsomal glutathione S-transferase 3; MGST3	Redox	Also functions as a glutathione peroxidase. RX + glutathione = HX + R-S-glutathione.
143	Q2TBV3|ETFB_BOVIN	Electron transfer flavoprotein subunit beta; ETFB	OxPh	Oxidative phosphorylation.
144	Q1JQB8|Q1JQB8_BOVIN	Coenzyme Q10 homolog B (S. cerevisiae); COQ10B	Chap	Required for the function of coenzyme Q in the respiratory chain. May serve as a chaperone or may be involved in the transport of Q6 from its site of synthesis to the catalytic sites of the respiratory complexes.
145	Q0II87|TFAM_BOVIN	Transcription factor A, mitochondrial; TFAM	NAbm	Mitochondrial transcription regulation. Required for promoter recognition by the mitochondrial RNA polymerase. Is able to unwind and bend DNA. Interacts with TFB1M and TFB2M.
146	A6QQK5|A6QQK5_BOVIN	Methylmalonic aciduria type A protein, mitochondrial; MMAA	TCC	May be involved in the transport of cobalamin into mitochondria for the final steps of adenosylcobalamin synthesis.
147	Q0V8J6|Q0V8J6_BOVIN	Branched-chain-amino-acid aminotransferase (Fragment); BCAT2	AA	Amino-acid biosynthesis; branched-chain amino acid biosynthesis.
148	P35816|PDP1_BOVIN	[Pyruvate dehydrogenase [acetyl-	Carb	Pyruvate dehydrogenase complex.

		transferring]]-phosphatase 1, mito; PDP1		
149	Q02370|NDUA2_BOVIN	NADH dehydrogenase [ubiquinone] 1 alpha subcomplex subunit 2; NDUFA2	OxPh	Oxidative phosphorylation; respiratory complex I.
150	Q32LB9|CD014_BOVIN	Uncharacterized protein C4orf14 homolog	X	?
151	A3KN05|CB047_BOVIN	Uncharacterized protein C2orf47 homolog, mitochondrial	X	?
152	Q2HJ55|SAM50_BOVIN	Sorting and assembly machinery component 50 homolog; SAMM50	Imp	May be required for the assembly pathway of mitochondrial outer membrane proteins.
153	A5PJA6|A5PJA6_BOVIN	Stomatin (EPB72)-like 2; STOML2	Cyto	Associated with the cytoskeleton.
154	Q3SZX5|RM22_BOVIN	39S ribosomal protein L22, mito; MRPL22	RiPS	Mitochondrial ribosome.
155	Q2NL38|Q2NL38_BOVIN	Dodecenoyl-Coenzyme A delta isomerase (3,2 trans-enoyl-CoA isomerase); DCI	Lip	Lipid metabolism; fatty acid beta-oxidation. Isomerizes 3-cis and 3-trans double bonds into the 2-trans form in enoyl-CoA species.
156	Q2TBT9|Q2TBT9_BOVIN	BCKDHA protein (Fragment); BCKDHA	AA	Amino acid metabolism; branched-chain alpha-keto acid dehydrogenase E1 component, alpha chain.
157	Q0P5H7|SYRM_BOVIN	Probable arginyl-tRNA synthetase, mitochondrial; RARS2	RiPS	Aminoacyl-tRNA synthetase; protein biosynthesis.
158	P11179|ODO2_BOVIN	Dihydrolipoyllysine-residue succinyltrans-ferase component of 2-oxoglutarate DHC, mitochondrial; DLST	Carb	Glucose metabolism; E2 component of 2-oxoglutarate dehydrogenase complex.
159	Q3SZG8|ISCA1_BOVIN	Iron-sulfur cluster assembly 1 homolog, mitochondrial; ISCA1	OxPh	Involved in the assembly of mitochondrial iron-sulfur proteins.
160	P15246|PIMT_BOVIN	Protein-L-isoaspartate(D-aspartate) O-methyltransferase; PCMT1	PMD	Methyl esterification of L-isoaspartyl and D-aspartyl residues in damaged proteins. Repair and/or degradation of damaged proteins.
161	Q1JQB6|Q1JQB6_BOVIN	Mitochondrial translation optimization 1 homolog (S. cerevisiae); MTO1	RiPS	tRNA wobble uridine modification.
162	Q9N0F3|SYSM_BOVIN	Seryl-tRNA synthetase, mito; SARS2	RiPS	Aminoacyl-tRNA synthetase; protein biosynthesis.
163	Q2TBG7|ISCA2_BOVIN	Iron-sulfur cluster assembly 2 homolog, mitochondrial; ISCA2	OxPh	Involved in the assembly of mitochondrial iron-sulfur proteins.
164	P82911|RT11_BOVIN	28S ribosomal protein S11, mito; MRPS11	RiPS	Mitochondrial ribosome.
165	A6QLJ3|A6QLJ3_BOVIN	GUF1 protein; GUF1	X	Belongs to the GTP-binding elongation factor family.
166	A6QP28|A6QP28_BOVIN	SUPV3L1 protein; SUPV3L1	RiPS	ATP-dependent DNA/RNA helicase.
167	P82923|RT02_BOVIN	28S ribosomal protein S2, mito; MRPS2	RiPS	Mitochondrial ribosome.
168	Q2TA12|RM02_BOVIN	39S ribosomal protein L2, mito; MRPL2	RiPS	Mitochondrial ribosome.
169	A6QPR9|CQ042_BOVIN	UPF0629 protein C17orf42 homolog	X	?
170	P13272|UCRI_BOVIN	Cytochrome bc_1 complex subunit Rieske, mitochondrial; UQCRFS1	OxPh	Oxidative phosphorylation; respiratory complex III.
171	Q5EAD4|ACDSB_BOVIN	Short/branched chain specific acyl-CoA dehydrogenase, mito; ACADSB	Lip	Lipid metabolism; mitochondrial fatty acid beta-oxidation.
172	P00257|ADX_BOVIN	Adrenodoxin, mitochondrial; FDX1	Redox	Adrenodoxin transfer electrons from adrenodoxin reductase to the cholesterol

				side chain cleavage cytochrome P450.
173	Q32L86|T126A_BOVIN	Transmembrane protein 126A; TMEM126A	X	Defects in TMEM126A are the cause of optic atrophy type 7 (OPA7).
174	Q2HJF1|RM53_BOVIN	39S ribosomal protein L53, mito; MRPL53	RiPS	Mitochondrial ribosome.
175	A5PJV9|A5PJV9_BOVIN	DTYMK protein; DTYMK	Nucl	dTDP biosynthesis; deoxythymidylate kinase.
176	Q2HJJ1|RM28_BOVIN	39S ribosomal protein L28, mito; MRPL28	RiPS	Mitochondrial ribosome.
177	Q3T094|ETHE1_BOVIN	Protein ETHE1, mitochondrial; ETHE1	Reg	May function as a nuclear-cytoplasmic shuttling protein that binds transcription factor RELA/NFKB3 in the nucleus and exports it to the cytoplasm. Suppresses p53-induced apoptosis by preventing nuclear localization of RELA.
178	Q32PI6|RM04_BOVIN	39S ribosomal protein L4, mito; MRPL4	RiPS	Mitochondrial ribosome.
179	Q3T172|Q3T172_BOVIN	ECH1 protein (Fragment); ECH1	Lip	Belongs to the enoyl-CoA hydratase/isomerase family.
180	Q29RH8|Q29RH8_BOVIN	Pyruvate dehydrogenase kinase isoform 2; PDK2 protein (Fragment); PDK2	Carb	Inhibits the mitochondrial pyruvate dehydrogenase complex by phosphorylating the E1 alpha subunit.
181	Q29RZ5|CV025_BOVIN	Uncharacterized protein C22orf25 homolog	X	?
182	Q0NXR6|ACAD8_BOVIN	Acyl-CoA dehydrogenase family member 8; ACAD8	AA	Amino-acid degradation. Isobutyryl-CoA dehydrogenase, mitochondrial.
183	Q3T040|RT07_BOVIN	28S ribosomal protein S7, mito; MRPS7	RiPS	Mitochondrial ribosome.
184	Q3ZCF5|OAT_BOVIN	Ornithine aminotransferase, mito; OAT	AA	Amino-acid synthesis.
185	Q2TBW6|ARL3_BOVIN	ADP-ribosylation factor-like protein 3; ARL3	Cyto	Required for normal cytokinesis. Present on the mitotic spindle.
186	Q3SZC1|GRPE1_BOVIN	GrpE protein homolog 1, mitochondrial; GRPEL1	Imp	Component of the PAM complex for the import of proteins into mitochondria. Controls the binding of mitochondrial HSP70 to substrate proteins.
187	Q58D49|MMAB_BOVIN	Cob(I)yrinic acid a,c-diamide adenosyltransferase, mitochondrial; MMAB	PMD	Cofactor biosynthesis; adenosylcobalamin biosynthesis.
188	Q58DM8|ECHM_BOVIN	Enoyl-CoA hydratase, mitochondrial; ECHS1	Lip	Lipid metabolism; beta-oxidation of C4 to C16 enoyl-CoA thioesters.
189	Q0VCK0|PUR9_BOVIN	Bifunctional purine biosynthesis protein PURH; ATIC	Nucl	Purine biosynthesis.
190	Q2KIX6|Q2KIX6_BOVIN	Biphenyl hydrolase-like (Serine hydrolase); BPHL	Nucl	Serine hydrolase that catalyzes the hydrolytic activation of amino acid ester prodrugs of nucleoside analogs.
191	Q0P5M8|MPPA_BOVIN	Mitochondrial-processing peptidase subunit alpha; PMPCA	PMD	Caution: Does not seem to cleave mitochondrial protein precursors as it lack the zinc-binding site.
192	Q0V8N7|Q0V8N7_BOVIN	Mitochondrial ribosomal protein L49 (Fragment); MRPL49	RiPS	Mitochondrial ribosome.
193	A6QLL2|A6QLL2_BOVIN	Metaxin-2; MTX2 protein; MTX2	OM	Mitochondrial outer membrane import complex protein 2.
194	A6QP05|DHR12_BOVIN	Dehydrogenase/reductase SDR family member 12; DHRS12	Lip	Belongs to the short-chain dehydrogenases/reductases (SDR) family.
195	Q3ZBN8|TIM14_BOVIN	Mitochondrial import inner membrane translocase subunit TIM14; DNAJC19	Imp	Probable component of the PAM complex, at least composed of HSP70 protein, GRPEL1 or GRPEL2, TIMM44, TIMM16/MAGMAS and TIMM14/DNAJC19.
196	Q3SZV6|TI21L_BOVIN	TIM21-like protein, mitochondrial;	Imp	Translocation of transit peptide-containing proteins across the MIM.
197	Q3SZ55|PTCD2_BOVIN	Pentatricopeptide repeat-containing protein 2;	NAbm	PPR proteins play a role in post-transcription and are thought to be sequence-

		PTCD2		specific RNA-binding proteins. PPR proteins are characterized by 35 amino acid tandem repeats.
198	A0JNI7|A0JNI7_BOVIN	G-rich RNA sequence binding factor 1; GRSF1	NAbm	Nucleic acid binding.
199	Q32L81|MMP37_BOVIN	MMP37-like protein, mitochondrial;	Imp	Translocation of proteins across the mitochondrial inner membrane?
200	Q2NKZ7|Q2NKZ7_BOVIN	Protein tyrosine phosphatase 1, mitochondrial; PTPMT1	PMD	Protein tyrosine/serine/threonine phosphatase activity.
201	Q8SPJ1|PLAK_BOVIN	Junction plakoglobin; JUP	Cyto	The presence of plakoglobin in desmosomes and intermediate junctions suggests that it plays a central role in the structure and function of submembranous plaques.
202	O02691|HCD2_BOVIN	3-hydroxyacyl-CoA dehydrogenase type-2; HSD17B10	NAbm	Mitochondrial tRNA maturation. Oxidoreductase part of mitochondrial ribonuclease P, which cleaves tRNA molecules in their 5'-ends?
203	A7YWQ8|A7YWQ8_BOVIN	Mitochondrial DEAD box protein 28; DDX28 protein; DDX28	NAbm	Helicase.
204	P00366|DHE3_BOVIN	Glutamate dehydrogenase 1, mito; GLUD1	AA	Amino acid metabolism. Oxidoreductase.
205	Q0IIB7|Q0IIB7_BOVIN	C13H20ORF7 protein (Fragment); C13H20ORF7	OxPh	Oxidative phosphorylation; respiratory complex I assembly.
206	P05631|ATPG_BOVIN	ATP synthase subunit gamma, mito; ATP5C1	OxPh	Oxidative phosphorylation.
207	Q32PC3|RM27_BOVIN	39S ribosomal protein L27, mito; MRPL27	RiPS	Mitochondrial ribosome.
208	P22027|ATP5S_BOVIN	ATP synthase subunit s, mito; ATP5S	OxPh	Oxidative phosphorylation.
209	Q2HJI2|NDUF3_BOVIN	NADH dehydrogenase 1 alpha subcomplex assembly factor 3; NDUFAF3	OxPh	Oxidative phosphorylation; respiratory complex I.
210	Q8SQ21|HINT2_BOVIN	Histidine triad nucleotide-binding protein 2, mitochondrial; HINT2	PMD	Hydrolase in steroid biosynthesis? May play a role in apoptosis. Has adenosine phosphoramidase activity. The histidine triad (HIT motif) forms part of the binding loop for the alpha-phosphate of purine mononucleotide.
211	Q3SYS1|RM13_BOVIN	39S ribosomal protein L13, mito; MRPL13	RiPS	Mitochondrial ribosome.
212	Q7YR75|RM12_BOVIN	39S ribosomal protein L12, mito; MRPL12	RiPS	Mitochondrial ribosome.
213	Q02375|NDUS4_BOVIN	NADH dehydrogenase [ubiquinone] iron-sulfur protein 4, mito; NDUFS4	OxPh	Oxidative phosphorylation; respiratory complex I.
214	Q32S21|Q32S21_BOVIN	Estradiol 17-beta-dehydrogenase 8; FabG-like protein; HKE6	Lip	Steroid biosynthesis; estrogen biosynthesis. May play a role in biosynthesis of fatty acids in mitochondria.
215	A7MBI8|A7MBI8_BOVIN	NUDT9 protein; NUDT9	Nucl	NDP-ribose pyrophosphatase.
216	Q6B860|RT14_BOVIN	28S ribosomal protein S14, mito; MRPS14	RiPS	Mitochondrial ribosome.
217	P82916|RT17_BOVIN	28S ribosomal protein S17, mito; MRPS17	RiPS	Mitochondrial ribosome.
218	P13620|ATP5H_BOVIN	ATP synthase subunit d, mito; ATP5H	OxPh	Oxidative phosphorylation.
219	Q32LD4|TFB2M_BOVIN	Dimethyladenosine transferase 2, mitochondrial; TFB2M	NAbm	DNA-dependent regulation of transcription; S-adenosyl-L-methionine-dependent methyltransferase specifically dimethylates mitochondrial 12S rRNA at the conserved stem loop. Also required for basal transcription of mtDNA, probably via its interaction with POLRMT and TFAM.

220	Q08DG6|COX15_BOVIN	Cytochrome *c* oxidase assembly protein COX15 homolog; COX15	OxPh	Oxidative phosphorylation; respiratory complex IV assembly.
221	O97725|NDUAC_BOVIN	NADH dehydrogenase 1 alpha subcomplex subunit 12; NDUFA12	OxPh	Oxidative phosphorylation; respiratory complex I.
222	O77480|FMT_BOVIN	Methionyl-tRNA formyltransferase, mitochondrial; MTFMT	NAbm	Formylates methionyl-tRNA in mitochondria. A single tRNA(Met) gene gives rise to both an initiator and an elongator species.
223	Q2NKU1|Q2NKU1_BOVIN	Deoxyuridine triphosphatase; DUT	Nucl	The protein produces dUMP, the immediate precursor of thymidine nucleotides and it decreases the intracellular concentration of dUTP so that uracil cannot be incorporated into DNA.
224	Q2HJI0|RM19_BOVIN	39S ribosomal protein L19, mito; MRPL19	RiPS	Mitochondrial ribosome.
225	Q2TBK7|RUSD3_BOVIN	RNA pseudouridylate synthase domain-containing protein 3; RPUSD3	NAbm	Pseudouridine synthase activity. RNA binding.
226	P46195|KGUA_BOVIN	Guanylate kinase; GUK1	Nucl	ATP + GMP = ADP + GDP. Essential for recycling GMP and indirectly, cGMP.
227	P82670|RT10_BOVIN	28S ribosomal protein S10, mito; MRPS10	RiPS	Mitochondrial ribosome.
228	Q3SZ22|RM46_BOVIN	39S ribosomal protein L46, mito; MRPL46	RiPS	Mitochondrial ribosome.
229	Q2TBQ0|TFB1M_BOVIN	Mitochondrial dimethyladenosine transferase 1; TFB1M	NAbm	Regulation of transcription. S-adenosyl-L-methionine-dependent methyltransferase specifically dimethylates mitochondrial 12S rRNA at the conserved stem loop. Also required for basal transcription of mitochondrial DNA, probably via its interaction with POLRMT and TFAM.
230	Q2M2T7|RT24_BOVIN	28S ribosomal protein S24, mito; MRPS24	RiPS	Mitochondrial ribosome.
231	Q0VC30|DPOG2_BOVIN	DNA polymerase subunit gamma-2, mitochondrial; POLG2	NAbm	Mitochondrial DNA polymerase accessory subunit PolG-beta, MtPolB.
232	Q29RZ0|THIL_BOVIN	Acetyl-CoA acetyltransferase, mito; ACAT1	Lip	Ketone body metabolism.
233	P82918|RT18B_BOVIN	28S ribosomal protein S18b, mito; MRPS18B	RiPS	Mitochondrial ribosome.
234	P13619|AT5F1_BOVIN	ATP synthase subunit b, mito; ATP5F1	OxPh	Oxidative phosphorylation.
235	P82924|RT30_BOVIN	28S ribosomal protein S30, mito; MRPS30	RiPS	Mitochondrial ribosome.
236	Q32P59|SLIRP_BOVIN	SRA stem-loop-interacting RNA-binding protein, mitochondrial; SLIRP	NAbm	RNA-binding protein that acts as a nuclear receptor corepressor. Binds the STR7 loop of SRA RNA. Also able to repress glucocorticoid, androgen, thyroid and VDR-mediated transactivation.
237	P04394|NDUV2_BOVIN	NADH dehydrogenase [ubiquinone] flavoprotein 2, mitochondrial; NDUFV2	OxPh	Oxidative phosphorylation; respiratory complex I.
238	Q3ZBP1|KCRS_BOVIN	Creatine kinase S-type, mito; CKMT2	PMD	Phosphate transfer between ATP and phosphogens, e.g., creatine phosphate.
239	A4FUC7|A4FUC7_BOVIN	Coiled-coil domain-containing protein 127; CCDC127 protein; CCDC127	X	?
240	Q2TA37|ARL2_BOVIN	ADP-ribosylation factor-like protein 2; ARL2	Reg	Required for normal progress through the cell cycle. Small GTPase mediated signal transduction. Regulates formation of new microtubules.
241	P00426|COX5A_BOVIN	Cytochrome *c* oxidase subunit 5A, mitochondrial; COX5A	OxPh	Oxidative phosphorylation; respiratory complex IV.

242	Q3T142|RM45_BOVIN	39S ribosomal protein L45, mito; MRPL45	RiPS	Mitochondrial ribosome.
243	Q32PI8|RT27_BOVIN	28S ribosomal protein S27, mito; MRPS27	RiPS	Mitochondrial ribosome.
244	Q2KID9|RT05_BOVIN	28S ribosomal protein S5, mito; MRPS5	RiPS	Mitochondrial ribosome.
245	A5PK90|A5PK90_BOVIN	LYPLAL1 protein; LYPLAL1	Lip	Lysophospholipase-like protein 1; lysophospholipase activity.
246	Q0VC21|RM15_BOVIN	39S ribosomal protein L15, mito; MRPL15	RiPS	Mitochondrial ribosome.
247	Q2KIF1|GATCL_BOVIN	Glutamyl-tRNA(Gln) amidotransferase subunit C like; GatC-like protein; GATC	RiPS	Regulation of translational fidelity
248	Q05B52|COQ4_BOVIN	Ubiquinone biosynthesis protein COQ4 homolog, mitochondrial; COQ4	Lip	Ubiquinone biosynthesis.
249	Q2YDI5|RM48_BOVIN	39S ribosomal protein L48, mito; MRPL48	RiPS	Mitochondrial ribosome.
250	Q2TBT3|ECHD2_BOVIN	Enoyl-CoA hydratase domain-containing protein 2, mitochondrial; ECHDC2	Lip	Lipid metabolism.
251	A6QNL8|A6QNL8_BOVIN	MCAT protein (Fragment); MCAT	Lip	Malonyl CoA:ACP acyltransferase?
252	Q2KJF7|GLCTK_BOVIN	Glycerate kinase; GLYCTK	Carb	ATP + (R)-glycerate = ADP + 3-phospho-(R)-glycerate.
253	P82917|RT18C_BOVIN	28S ribosomal protein S18c, mitochondrial; MRPS18C	RiPS	Mitochondrial ribosome.
254	P82929|RT34_BOVIN	28S ribosomal protein S34, mito; MRPS34	RiPS	Mitochondrial ribosome.
255	Q2M2S9|LYRM7_BOVIN	LYR motif-containing protein 7; LYRM7	X	LYR motif (also found in respiratory complexes).
256	A6QQA9|A6QQA9_BOVIN	Acyl-coenzyme A thioesterase 2, mitochondrial; ACOT2 protein; ACOT2	Lip	Lipid metabolism.
257	Q32PB0|SSBP_BOVIN	Single-stranded DNA-binding protein, mitochondrial; SSBP1	NAbm	Binds preferentially and cooperatively to ssDNA. Probably involved in mitochondrial DNA replication.
258	P68002|VDAC2_BOVIN	Voltage-dependent anion-selective channel protein 2; VDAC2	OM	Channel through the cell membrane for diffusion of small hydrophilic molecules.
259	A6QNS9|AT5SL_BOVIN	ATP synthase subunit s-like protein; ATP5SL	OxPh	Oxidative phosphorylation.
260	Q05AT5|Q05AT5_BOVIN	HIG1 domain family, member 2A; HIGD2A	Redox	Hypoxia-inducible gene 2 protein.
261	A8E657|AASS_BOVIN	Alpha-aminoadipic semialdehyde synthase, mitochondrial; AASS	AA	Catalyzes the first two steps in lysine degradation.
262	A4IFA7|CBR4_BOVIN	Carbonyl reductase family member 4; CBR4	Lip	Fatty acid biosynthesis in mitochondria. The heteroteramer with HSD17B8 has NADH-dependent 3-ketoacyl-acyl carrier protein reductase activity. The homotetramer may act as NADPH-dependent quinone reductase.
263	P42029|NDUA8_BOVIN	NADH dehydrogenase [ubiquinone] 1 alpha subcomplex subunit 8; NDUFA8	OxPh	Oxidative phosphorylation; respiratory complex I.
264	Q2TBR0|PCCB_BOVIN	Propionyl-CoA carboxylase beta chain, mitochondrial; PCCB	Lip	Propanoyl-CoA degradation; succinyl-CoA from propanoyl-CoA.
265	A4FUC0|RM37_BOVIN	39S ribosomal protein L37, mito; MRPL37	RiPS	Mitochondrial ribosome.
266	P82915|RT16_BOVIN	28S ribosomal protein S16, mito; MRPS16	RiPS	Mitochondrial ribosome.
267	A6QP42|A6QP42_BOVIN	MGC151610 protein; MGC151610	Reg	Apoptosis; protein kinase; related to FAST (forkhead activin signal transducer).
268	Q3SYS0|RM24_BOVIN	39S ribosomal protein L24, mito; MRPL24	RiPS	Mitochondrial ribosome.

269	Q2KHU4|CLPP_BOVIN	Putative ATP-dependent Clp protease proteolytic subunit, mito;	PMD	Clp cleaves peptides in various proteins in a process that requires ATP hydrolysis.
270	Q02827|NDUC2_BOVIN	NADH dehydrogenase [ubiquinone] 1 subunit C2; NDUFC2	OxPh	Oxidative phosphorylation; respiratory complex I.
271	A6QQH9|A6QQH9_BOVIN	C22H3ORF23 protein; C22H3ORF23	X	?
272	Q1LZ96|ATPF2_BOVIN	ATP synthase mitochondrial F1 complex assembly factor 2; ATPAF2	OxPh	Oxidative phosphorylation.
273	Q4PS77|MTG1_BOVIN	Mitochondrial GTPase 1; MTG1	RiPS	Mitochondrial GTPase. Assembly of the large ribosomal subunit?
274	Q3SZ47|RM33_BOVIN	39S ribosomal protein L33, mito; MRPL33	RiPS	Mitochondrial ribosome.
275	A5D974|A5D974_BOVIN	Acyl-Coenzyme A dehydrogenase family, member 9; ACAD9	Lip	Lipid metabolism; oxidoreductase.
276	Q95KE5|RM43_BOVIN	39S ribosomal protein L43, mito; MRPL43	RiPS	Mitochondrial ribosome.
277	A7E3Q1|A7E3Q1_BOVIN	Threonyl-tRNA synthetase-like 1; TARSL1	RiPS	Protein biosynthesis. Aminoacyl-tRNA synthetase.
278	Q2KJF3|Q2KJF3_BOVIN	NFU1 iron-sulfur cluster scaffold homolog (S. cerevisiae); NFU1	PMD	Iron-sulfur cluster scaffold protein, which can assemble [4Fe-2S] clusters and deliver them to target proteins. Interacts with HIRA and EPM2A/laforin.
279	Q3T0L3|RM17_BOVIN	39S ribosomal protein L17, mito; MRPL17	RiPS	Mitochondrial ribosome.
280	Q2TBK2|RM09_BOVIN	39S ribosomal protein L9, mito; MRPL9	RiPS	Mitochondrial ribosome.
281	Q3T0N2|Q3T0N2_BOVIN	Lysyl-tRNA synthetase; KARS	RiPS	Protein biosynthesis. Aminoacyl-tRNA synthetase.
282	Q02366|NDUA6_BOVIN	NADH dehydrogenase [ubiquinone] 1 alpha subcomplex subunit 6; NDUFA6	OxPh	Oxidative phosphorylation.
283	P05630|ATPD_BOVIN	ATP synthase subunit delta, mito; ATP5D	OxPh	Oxidative phosphorylation.
284	Q3SZ13|Q3SZ13_BOVIN	Inositol hexakisphosphate kinase 3; IP6K3 protein; IP6K3	PMD	Converts inositol hexakisphosphate to diphosphoinositol pentakisphosphate and 1,3,4,5,6-pentakisphosphate to PP-InsP4.
285	Q3MHX4|Q3MHX4_BOVIN	MTERFD2 protein (Fragment); MTERFD2	NAbm	Mitochondrial transcription termination factor D2 protein.
286	Q0V8R7|NSUN4_BOVIN	Putative methyltransferase NSUN4; NSUN4	PMD	Methyltransferase?
287	A5D7A7|A5D7A7_BOVIN	Twinkle; C26H10ORF2 protein; C26H10ORF2	NAbm	Twinkle-helicase; single-stranded DNA-binding; 5'-3' DNA helicase activity; mitochondrial DNA replication
288	Q2KHW9|Q2KHW9_BOVIN	Ribonuclease H1 pseudogene 1; RNASEH1P1	NAbm	Nucleic acid binding; ribonuclease H activity.
289	P82931|RT06_BOVIN	28S ribosomal protein S6, mito; MRPS6	RiPS	Mitochondrial ribosome.
290	Q3T116|ICT1_BOVIN	Immature colon carcinoma transcript 1 protein; ICT1	RiPS	Translational termination. Translation release factor activity.
291	Q08DT6|RM47_BOVIN	39S ribosomal protein L47, mito; MRPL47	RiPS	Mitochondrial ribosome.
292	P82927|RM42_BOVIN	39S ribosomal protein L42, mito; MRPL42	RibPS	Mitochondrial ribosome.
293	Q2HJ25|Q2HJ25_BOVIN	Methionine aminopeptidase; MAP1D	RiPS	Removes the amino-terminal methionine from nascent proteins.
294	P82908|RT36_BOVIN	28S ribosomal protein S36, mito; MRPS36	RiPS	Mitochondrial ribosome.
295	Q17QE6|Q17QE6_BOVIN	Iron-sulfur cluster scaffold homolog (E. coli); ISCU	OxPh	Mitochondrial iron-sulfur cluster assembly enzyme ISCU.
296	Q2HJC0|NGRN_BOVIN	Neugrin; NGRN	Reg	May be involved in neuronal differentiation.
297	A7E2Z6|A7E2Z6_BOVIN	SPG7 protein; SPG7	PMD	Putative ATP dependent protease; defects in SPG7 are the cause of spastic

				paraplegia autosomal recessive type 7.
298	Q2KHV5|MIDA_BOVIN	Protein midA homolog, mito;	X	midA = Mitochondrial dysfunction gene A.
299	A6QNM9|A6QNM9_BOVIN	SLC25A12 protein; SLC25A12	TCC	Mitochondrial carrier. Contains 3 Solcar (solute carrier) repeats.
300	Q3ZBX6|RM03_BOVIN	39S ribosomal protein L3, mito; MRPL3	RiPS	Mitochondrial ribosome.
301	Q05B51|ADXL_BOVIN	Adrenodoxin-like protein, mito; FDX1L	Redox	Electron transport. Binds 1 2Fe-2S cluster.
302	Q4U0T9|CSRP3_BOVIN	Cysteine and glycine-rich protein 3; CSRP3	Cyto	Cell differentiation. Positive regulator of myogenesis. Could play a role in mechanical stretch sensing. The nuclear protein associates with actin.
303	Q5E948|OCAD1_BOVIN	OCIA domain-containing protein 1; Ociad1	X	OCIA (ovarian carcinoma immunoreactive antigen).
304	Q05B87|FRDA_BOVIN	Frataxin, mitochondrial; FXN	TCC	Involved in iron homeostasis. Anti-apoptotic protein, which prevents mitochondrial damage and ROS production.
305	Q05752|NDUA7_BOVIN	NADH dehydrogenase [ubiquinone] 1 alpha subcomplex subunit 7; NDUFA7	OxPh	Oxidative phosphorylation; respiratory complex I.
306	A1L593|A1L593_BOVIN	Abhydrolase domain containing 4; ABHD4	PMD	Abhydrolase domain containing protein 4.
307	Q3ZBR7|RM18_BOVIN	39S ribosomal protein L18, mito; MRPL18	RiPS	Mitochondrial ribosome.
308	Q2KIB0|FAHD2_BOVIN	Fumarylacetoacetate hydrolase domain-containing protein 2; FAHD2	PMD	May have hydrolase activity.
309	A7E358|A7E358_BOVIN	MTERFD3 protein (Fragment); MTERFD3	NAbm	Mitochondrial transcription termination factor-like protein.
310	Q3ZBI7|USMG5_BOVIN	Up-regulated during skeletal muscle growth protein 5; USMG5	OxPh	Oxidative phosphorylation.
311	A6QL68|A6QL68_BOVIN	Citrate lyase subunit beta-like protein, mitochondrial; CLYBL protein; CLYBL	X	Even though this protein has clear similarity to citrate lyase beta subunit, it lacks the other subunits that are necessary for ATP-independent citrate lyase activity and is expected to have a somewhat different enzyme activity.
312	Q148H0|APOO_BOVIN	Apolipoprotein O; APOO	Lip	Promotes cholesterol efflux from macrophage cells. VLDL-associated protein that is subsequently transferred to HDL. Detected in HDL, LDL and VLDL.
313	Q862F9|Q862F9_BOVIN	Similar to vimentin (Fragment)	Cyto	Vimentins are class-III intermediate filaments.
314	Q3T0J3|RM16_BOVIN	39S ribosomal protein L16, mito; MRPL16	RiPS	Mitochondrial ribosome.
315	P23934|NDUS6_BOVIN	NADH dehydrogenase iron-sulfur protein 6, mitochondrial; NDUFS6	OxPh	Oxidative phosphorylation; respiratory complex I.
316	Q2KJE4|ETFA_BOVIN	Electron transfer flavoprotein subunit alpha, mitochondrial; ETFA	OxPh	ETF alpha.
317	Q1JQ99|RM14_BOVIN	39S ribosomal protein L14, mito; MRPL14	RiPS	Mitochondrial ribosome.
318	Q862N3|Q862N3_BOVIN	Similar to B15 subunit of the NADH: ubiquinone oxidoreductase (Fragment)	OxPh	Oxidative phosphorylation; respiratory complex I.
319	Q2KIL4|COQ6_BOVIN	Ubiquinone biosynthesis monooxygenase COQ6; COQ6	Lip	Ubiquinone biosynthesis.
320	P0C2B8|RM55_BOVIN	39S ribosomal protein L55, mito; MRPL55	RiPS	Mitochondrial ribosome.
321	Q29RP9|QRSL1_BOVIN	Glutamyl-tRNA(Gln) amidotransferase subunit A homolog; QRSL1	NAbm	Amidase; ATP + L-glutamyl-tRNA(Gln) + L-glutamine = ADP + phosphate + L-glutaminyl-tRNA(Gln) + L-glutamate.
322	Q2YDG5|Q2YDG5_BOVIN	Basic FGF-repressed Zic binding protein;	OxPh	Oxidative phosphorylation. Respiratory complex III. Ubiquinol-cytochrome *c*

		C20orf44		reductase complex chaperone CBP3 homolog.
323	A6QR45|A6QR45_BOVIN	Magnesium transporter MRS2 homolog, mitochondrial; MRS2 protein; MRS2	TCC	Magnesium transporter that may mediate the influx of magnesium into the mitochondrial matrix.
324	Q0VCJ1|Q0VCJ1_BOVIN	Aurora kinase A interacting protein 1; AURKAIP1	PMD	Negative regulator of Aurora-A kinase? by proteasome-dependent degradation.
325	P00428|COX5B_BOVIN	Cytochrome *c* oxidase subunit 5B; COX5B	OxPh	Oxidative phosphorylation; respiratory complex IV.
326	Q8HXG6|NDUAB_BOVIN	NADH dehydrogenase [ubiquinone] 1 alpha subcomplex subunit 1; NDUFA11	OxPh	Oxidative phosphorylation; respiratory complex I.
327	B1P072|B1P072_BOVIN	Cytochrome *c* oxidase subunit 2; COX2	OxPh	Oxidative phosphorylation; respiratory complex IV.
328	Q2KHU6|Q2KHU6_BOVIN	DHRS4 protein; DHRS4	Lip	Short-chain dehydrogenase/reductase family member 4. R-CHOH-R' + NADP+ = R-CO-R' + NADPH.
329	Q2TA23|Q2TA23_BOVIN	Methicillin resistance mecR1 protein; MECR protein; MECR	Lip	Nuclear receptor-binding factor 1. Role in mitochondrial synthesis of fatty acids?
330	Q3SZV8|ROMO1_BOVIN	Reactive oxygen species modulator 1; ROMO1	Redox	Cellular response to reactive oxygen species. Positive regulation of cell proliferation.
331	Q0VCA7|OXSM_BOVIN	3-oxoacyl-[acyl-carrier-protein] synthase, mitochondrial; OXSM	Lip	Lipid metabolism; fatty acid biosynthesis. Acyl-[acyl-carrier-prot] + malonyl-[acyl-carrier-prot] = 3-oxoacyl-[acyl-carrier-prot] + CO2 + [acyl-carrier-prot].
332	A6QR49|A6QR49_BOVIN	Pyruvate dehydrogenase kinase isoform 4, PDK4 protein; PDK4	Carb	Inhibits the mitochondrial pyruvate dehydrogenase complex by phosphorylation of the E1 alpha subunit, thus regulating glucose metabolism.
333	Q17QB8|Q17QB8_BOVIN	Uracil-DNA glycosylase; UNG	NAbm	Excises uracil residues from the DNA (due to deamination of cytosine).
334	Q3T061|COX7R_BOVIN	Cytochrome *c* oxidase subunit 7A-related protein, mitochondrial; COX7A2L	OxPh	Oxidative phosphorylation; respiratory complex IV.
335	Q3ZBF3|RM38_BOVIN	39S ribosomal protein L38, mito; MRPL38	RiPS	Mitochondrial ribosome.
336	Q0P5G9|Q0P5G9_BOVIN	SPRY domain containing 4; SPRYD4	X	Contains SPRY (sprouty) domain.
337	P00586|THTR_BOVIN	Thiosulfate sulfurtransferase; TST	OxPh	Thiosulfate + CN- = sulfite + SCN-. Protein subunit of respiratory complex I.
338	Q2KI49|RM50_BOVIN	39S ribosomal protein L50, mito; MRPL50	RiPS	Mitochondrial ribosome.
339	Q3SZK3|Q3SZK3_BOVIN	Growth hormone inducible transmembrane protein; GHITM	Reg	Transmembrane BAX inhibitor motif-containing protein.
340	Q2KJC5|Q2KJC5_BOVIN	Hydroxyacyl-Coenzyme A dehydrogenase; HADH	RiPS	Mitochondrial ribosome. May be a component of the 28S subunit.
341	Q3MHG6|GTPBA_BOVIN	GTP-binding protein 10; GTPBP10	RiPS	Ribosome biogenesis.
342	P82919|RT18A_BOVIN	28S ribosomal protein S18a, mito; MRPS18A	RiPS	Mitochondrial ribosome.
343	Q32KT5|CF136_BOVIN	Uncharacterized protein C6orf136 homolog	X	?
344	Q148I4|Q148I4_BOVIN	Acyl-CoA thioesterase 7; ACOT7	Lip	Lipid metabolism; hydrolysis of acyl-CoA to the free fatty acid and CoA.
345	Q3SZB4|ACADM_BOVIN	Medium-chain specific acyl-CoA dehydrogenase, mito; ACADM	Lip	Lipid metabolism; mitochondrial fatty acid beta-oxidation.
346	Q1LZ78|CA057_BOVIN	Nucleoside-triphosphatase C1orf57 homolog	Nucl	Nucleoside triphosphate phosphohydrolase. NTP + H2O = NDP + phosphate.
347	Q2KI15|RF1ML_BOVIN	Peptide chain release factor 1-like, mitochondrial; MTRF1L	RiPS	Mitochondrial ribosome. Release factor that directs the termination of translation in response to the peptide chain termination codons UAA and UAG.

219

348	Q2KHZ9|GCDH_BOVIN	Glutaryl-CoA dehydrogenase, mitochondrial; GCDH	AA	Oxidative decarboxylation of glutaryl-CoA in the degradative pathway of L-lysine, L-hydroxylysine, and L-tryptophan. Uses ETF as electron acceptor.
349	Q24K16|ZADH2_BOVIN	Zinc-binding alcohol DH domain-containing protein 2; ZADH2	Redox	Zinc-containing alcohol dehydrogenase; quinone oxidoreductase subfamily.
350	Q3T189|DHSB_BOVIN	Succinate dehydrogenase iron-sulfur subunit, mitochondrial; SDHB	OxPh	Oxidative phosphorylation; respiratory complex II.
351	Q2KI45|MRRP1_BOVIN	Mitochondrial ribonuclease P protein 1; RG9MTD1	NAbm	Methyltransferase; mitochondrial tRNA maturation. Part of mitochondrial ribonuclease P, which cleaves tRNA in their 5'-ends.
352	A6QP80|A6QP80_BOVIN	LOC532995 protein; LOC532995	X	?
353	A7MBD2|A7MBD2_BOVIN	Mitochondrial rRNA methyltransferase 1; MRM1	NAbm.	Mitochondrial rRNA methyltransferase 1.
354	Q29RJ1|AP4A_BOVIN	Bis(5~-nucleosyl)-tetraphosphatase [asymmetrical]; NUDT2	Nucl	Asymmetrically hydrolyzes Ap4A (diadenosine 5',5'''-P1,P4-tetraphosphate) to yield AMP and ATP.
355	P79110|TXTP_BOVIN	Tricarboxylate transport protein, mitochondrial; SLC25A1	TCC	Citrate/malate exchange.
356	A5PJ71|A5PJ71_BOVIN	Mitochondrial ribosomal protein L41; MRPL41 protein; MRPL41	RiPS	Mitochondrial ribosome. 39S ribosomal protein L41.
357	Q03763|DSG1_BOVIN	Desmoglein-1; DSG1	Cyto	Interaction of plaque proteins and intermediate filaments in cell-cell adhesion.
358	Q0VCX7|Q0VCX7_BOVIN	Malic enzyme; ME3		(S)-malate + NADP+ = pyruvate + CO2 + NADPH.
359	Q3MHR0|LYPA1_BOVIN	Acyl-protein thioesterase 1; lysophospholipase I; LYPLA1	Lip	Hydrolyzes fatty acids from S-acylated cysteine residues in proteins. Also has low lysophospholipase activity.
360	Q3ZBL5|PTH2_BOVIN	Bcl-2 inhibitor of transcription; BIT1; peptidyl-tRNA hydrolase 2, mitochondrial; PTRH2	Reg	The natural substrate for this enzyme may be peptidyl-tRNAs, which drop off the ribosome during protein synthesis. Promotes caspase-independent apoptosis by regulating the function of two transcriptional regulators, AES and TLE1.
361	Q08DF7|PDE12_BOVIN	2~,5~-phosphodiesterase 12; PDE12	Nucl	Cleaves 3',5'-phosphodiester bond. Negative regulator of the 2-5A system, a major pathway for antiviral and antitumor functions induced by interferons.
362	A8YXY6|A8YXY6_BOVIN	MTPAP protein (Fragment); MTPAP	NAbm	Poly(A) RNA polymerase, mitochondrial.
363	P20000|ALDH2_BOVIN	Aldehyde dehydrogenase, mito; ALDH2	PMD	Ethanol degradation; acetate from ethanol.
364	Q2NKY8|DHX30_BOVIN	Putative ATP-dependent RNA helicase DHX30; DHX30	NAbm	Belongs to the DEAD box helicase family. DEAH box protein 30. Identified in a complex with TFAM and SSBP1.
365	P02510|CRYAB_BOVIN	Alpha-crystallin B chain; CRYAB	Chap	Small heat shock protein (HSP20). May contribute to the transparency and of the lens. Anti-apoptosis; negative regulation of intracellular transport.
366	Q24K02|IDE_BOVIN	Insulin-degrading enzyme; IDE	PMD	Degradation of insulin, glucagon and other polypeptides.
367	Q95108|THIOM_BOVIN	Thioredoxin, mitochondrial; TXN2	Redox	Anti-apoptotic. Regulation of mitochondrial membrane potential. Dithiol-reducing activity.
368	A6QPU5|SYDM_BOVIN	Aspartyl-tRNA synthetase, mito; DARS2	RiPS	Belongs to the class-II aminoacyl-tRNA synthetase family.
369	P45879|VDAC1_BOVIN	Voltage-dependent anion-selective channel protein 1; VDAC1	OM	Channel through the mitochondrial outer membrane and the plasma membrane. Cell volume regulation and apoptosis. Component of the permeability transition pore that triggers apoptosis?

370	Q95KV7|NDUAD_BOVIN	NADH dehydrogenase 1 alpha subcomplex subunit 13; NDUFA13	OxPh	Oxidative phosphorylation; respiratory complex I.
371	Q58DV5|RM30_BOVIN	39S ribosomal protein L30, mito; MRPL30	RiPS	Mitochondrial ribosome.
372	A6QQD0|A6QQD0_BOVIN	LOC100125578 protein; LOC100125578	X	?
373	Q2KIJ6|UBXN6_BOVIN	UBX domain-containing protein 6; UBXN6	PMD	Ubiquitination protein degradation pathway.
374	Q3T099|SYWM_BOVIN	Tryptophanyl-tRNA synthetase, mitochondrial; WARS2	RiPS	ATP + L-trp + tRNA(Trp) = AMP + diphosphate + L-tryptophyl-tRNA(Trp).
375	Q17QJ7|P5CR2_BOVIN	Pyrroline-5-carboxylate reductase 2; PYCR2	AA	Amino-acid biosynthesis; L-proline from L-glutamate 5-semialdehyde.
376	Q3SZ07|OVCA2_BOVIN	Ovarian cancer-associated gene 2 protein homolog; OVCA2	Reg	Response to retinoic acid.
377	Q5E9H9|ABHDA_BOVIN	Abhydrolase domain-containing protein 10, mitochondrial; ABHD10	PMD.	Serin-protease.
378	Q5E9D6|HDHD3_BOVIN	Haloacid dehalogenase-like hydrolase domain-containing protein 3; HDHD3	PMD	Phosphoglycolate phosphatase activity.
379	Q28851|ATPK_BOVIN	ATP synthase subunit f, mito; ATP5J2	OxPh	Oxidative phosphorylation.
380	A6QLS9|A6QLS9_BOVIN	Ras-related protein Rab-10; RAB10	Reg	May be involved in vesicular trafficking and neurotransmitter release.
381	Q0P5E7|GTPB8_BOVIN	GTP-binding protein 8; GTPBP8		?
382	Q5EA45|FXRD1_BOVIN	FAD-dependent oxidoreductase domain-containing protein 1; FOXRED1	Redox	Oxidoreductase.
383	Q02369|NDUB9_BOVIN	NADH dehydrogenase [ubiquinone] 1 beta subcomplex subunit 9; NDUFB9	OxPh	Oxidative phosphorylation; respiratory complex I.
384	Q0P5G4|KAT3_BOVIN	Kynurenine-oxoglutarate transaminase 3; CCBL2	AA	Class-I pyridoxal-phosphate-dependent aminotransferase. Irreversible transamination of the L-tryptophan metabolite L-kynurenine to form kynurenic acid.
385	A1L503|A1L503_BOVIN	Chromobox homolog 4 (Fragment); CBX4	PMD	Protein sumoylation. E3 SUMO-protein ligase CBX4.
386	P38447|NUCG_BOVIN	Endonuclease G, mitochondrial; ENDOG	NAbm	Cleaves double- and single-stranded DNA. Has also RNase and RNase H activities. Generating the RNA primers required by DNA polymerase gamma.
387	Q0MRP5|Q0MRP5_9CETA	Lysozyme C; LZ	PMD	Hydrolysis of (1->4)-beta-linkages between N-acetylmuramic acid and N-acetyl-D-glucosamine residues in a peptidoglycan.
388	P41976|SODM_BOVIN	Superoxide dismutase [Mn], mito; SOD2	Redox	Destroys superoxide radicals.
389	Q3SZA4|Q3SZA4_BOVIN	Solute carrier family 25, member 20; SLC25A20	TCC	Carnitine/acylcarnitine translocase.
390	A3KN46|LTMD1_BOVIN	LETM1 domain-containing protein 1; LETMD1	Reg	May function as a negative regulator of the TP53/p53.
391	Q3SZA2|CG055_BOVIN	UPF0562 protein C7orf55 homolog	X	?
392	A4FV90|A4FV90_BOVIN	PCCA protein; PCCA	Lip	Propionyl-CoA carboxylase alpha chain. ATP + propanoyl-CoA + HCO3- = ADP + Pi+ (S)-methylmalonyl-CoA.
393	Q3T057|RL23_BOVIN	60S ribosomal protein L23; RPL23	Cyto	60S ribosome.
394	Q58DH4|Q58DH4_BOVIN	GS2 gene; PNPLA4	Lip	Lipid degradation.

395	P61603|CH10_BOVIN	10 kDa heat shock protein, mitochondrial; HSPE1	Chap	Eukaryotic CPN10 homolog, which is essential for mitochondrial protein biogenesis, together with CPN60.
396	A8R4B3|A8R4B3_BOVIN	LOC782657 protein; LOC782657	X	?
397	Q2TBW2|COQ7_BOVIN	Ubiquinone biosynthesis protein COQ7 homolog; COQ7	Lip	Ubiquinone biosynthesis.
398	Q17QY3|Q17QY3_BOVIN	Nipsnap homolog 3A (C. elegans); NIPSNAP3A	X	May be part of some vesicular structure distinct from lysosomal vesicles.
399	Q08DW1|Q08DW1_BOVIN	RAB9A, member RAS oncogene family; RAB9A	Reg	Small GTPase mediated signal transduction.
400	A6QQZ5|A6QQZ5_BOVIN	MGC165715 protein; MGC165715	X	?
401	Q00361|ATP5I_BOVIN	ATP synthase subunit e, mito; ATP5I	OxPh	Oxidative phosphorylation.
402	A6QQY8|A6QQY8_BOVIN	FASTKD1 protein; FASTKD1	Reg	Apoptosis; protein kinase; forkhead activin signal transducer.
403	Q0IIJ8|Q0IIJ8_BOVIN	2,4-dienoyl CoA reductase 1, mitochondrial; DECR1	Lip	Beta-oxidation. Metabolism of fatty enoyl-CoA esters with double bonds in even- and odd-numbered positions.
404	A6QPX8|A6QPX8_BOVIN	RAB12 protein; RAB12	Reg	May be involved in vesicular trafficking and neurotransmitter release. Small GTPase mediated signal transduction.
405	Q1LZE3|Q1LZE3_BOVIN	MTERF domain containing 1; MTERFD1	NAbm	Mitochondrial transcription termination factor D1.
406	Q3MHI7|RF1M_BOVIN	Peptide chain release factor 1, mito; MTRF1	RiPS	Mitochondrial peptide chain release factor for the termination of translation.
407	Q0P562|Q0P562_BOVIN	Hypothetical LOC509253; MGC152190	X	?
408	Q3SX05|ECSIT_BOVIN	Evolutionarily conserved signaling intermediate in Toll pathway, mito; ECSIT	Reg	Adapter protein in Toll-like receptor signaling, activation of NF-kappa-B via MAP3K1. Required for efficient assembly of respiratory complex I.
409	A7YWQ4|A7YWQ4_BOVIN	Beta-2-syntrophin; SNTB2 protein; SNTB2	Cyto	Adapter protein that binds to a variety of membrane proteins. May link various receptors to the actin cytoskeleton and the dystrophin glycoprotein complex.
410	Q02380|NDUB5_BOVIN	NADH dehydrogenase 1 beta subcomplex subunit 5, mito; NDUFB5	OxPh	Oxidative phosphorylation; respiratory complex I.
411	Q2KHV4|PARL_BOVIN	Presenilins-associated rhomboid-like protein, mitochondrial; PARL	Reg	Control of apoptosis. Interacts with PSEN1 and PSEN2. Binds OPA1.
412	A6H7I3|ANGE2_BOVIN	Carbon catabolite repressor protein 4 homolog 1 (CCR4). Protein angel homolog 2; ANGEL2	NAbm	Glucose-repressible alcohol dehydrogenase transcriptional effector. The major mRNA deadenylase involved in mRNA turnover.
413	Q5E9N4|AADAT_BOVIN	Kynurenine/alpha-aminoadipate aminotransferase, mitochondrial; AADAT	AA	L-2-aminoadipate + 2-oxoglutarate = 2-oxoadipate + L-glutamate. Transaminase with broad substrate specificity.
414	B1NZ26|B1NZ26_BOVIN	NADH-ubiquinone oxidoreductase chain 5; ND5	OxPh	Oxidative phosphorylation; respiratory complex I.
415	Q2KIF8|SYCM_BOVIN	Cysteinyl-tRNA synthetase, mito; CARS2	RiPS	ATP + L-cysteine + tRNA(Cys) = AMP + diphosphate + L-cysteinyl-tRNA(Cys).
416	Q3T131|COQ3_BOVIN	Hexaprenyldihydroxybenzoate methyltransferase, mitochondrial; COQ3	Lip	Ubiquinone biosynthesis.
417	P00125|CY1_BOVIN	Cytochrome c_1, heme protein, mito; CYC1	OxPh	Oxidative phosphorylation; respiratory complex III.
418	Q6TNF3|Q6TNF3_BOVIN	Tranglutaminase 1; TGM1	PMD	Protein-glutamine gamma-glutamyltransferase K; catalyzes the cross-linking of

222

				proteins and the conjugation of polyamines to proteins.
419	Q58DH2|PISD_BOVIN	Phosphatidylserine decarboxylase proenzyme; PISD	Lip	Phospholipid metabolism; phosphatidyl-L-serine>phosphatidylethanolamine+CO2.
420	Q0VCZ8|Q0VCZ8_BOVIN	Acyl-CoA synthetase long-chain family member 1; ACSL1	Lip	Lipid metabolism.
421	B1P0I6|B1P0I6_BOVIN	NADH-ubiquinone oxidoreductase chain 1; ND1	OxPh	Oxidative phosphorylation; respiratory complex I.
422	Q17QW3|Q17QW3_BOVIN	Retinol dehydrogenase 14 (All-trans/9-cis/11-cis); RDH14	Redox	Oxidoreductase acting on retinal and retinoids.
423	P82926|RT33_BOVIN	28S ribosomal protein S33, mito; MRPS33	RiPS	Mitochondrial ribosome.
424	Q2NKR7|F162A_BOVIN	Protein FAM162A; FAM162A	Reg	Induction by 17-beta-estradiol.
425	Q7YS70|MECR_BOVIN	Trans-2-enoyl-CoA reductase, mito; MECR	Lip	Fatty acid degradation; Acyl-CoA + NADP+ = trans-2,3-dehydroacyl-CoA + NADPH.
426	Q0IIG8|RAB18_BOVIN	Ras-related protein Rab-18; RAB18	Reg	Small GTPase mediated signal transduction. Apical endocytosis/recycling.
427	Q2KIH9|Q2KIH9_BOVIN	Lipoyl synthase, mitochondrial; LIAS protein; LIAS	Lip	Catalyzes the radical-mediated insertion of two sulfur atoms into the C-6 and C-8 positions of the octanoyl moiety bound to the lipoyl domains of enzymes, thereby converting the octanoylated domains into lipoylated derivatives.
428	Q3MHM1|Q3MHM1_BOVIN	Calsequestrin; CASQ2	Reg	Calsequestrin is a calcium-binding protein and acts as an internal calcium store in muscle. The release of calcium bound to calsequestrin through a calcium release channel triggers muscle contraction.
429	Q2TBP8|M11D1_BOVIN	Protein RSM22 homolog, mitochondrial; METT11D1	RiPS	May be a component of the mitochondrial small ribosomal subunit.
430	P00423|COX41_BOVIN	Cytochrome *c* oxidase subunit 4 isoform 1, mitochondrial; COX4I1	OxPh	Oxidative phosphorylation; respiratory complex IV.
431	Q0IIE2|SHC1_BOVIN	SHC-transforming protein 1; SHC1	Reg	Signaling adapter that couples activated growth factor receptors to signaling pathway. Regulation of growth.
432	P62998|RAC1_BOVIN	Ras-related C3 botulinum toxin substrate 1; RAC1	Reg	Plasma membrane-associated small GTPase, which binds to a variety of effector proteins to regulate cellular responses.
433	A5PK43|A5PK43_BOVIN	ERAL1 protein; ERAL1	NAbm	RNA binding protein.
434	A6H7E1|SYMM_BOVIN	Methionyl-tRNA synthetase, mitochondrial; MARS2	NAbm	ATP + L-methionine + tRNA(Met) = AMP + diphosphate + L-methionyl-tRNA(Met).
435	Q08DC2|Q08DC2_BOVIN	RAB31, member RAS oncogene family; RAB31	Reg	Ras-related protein; belongs to the Rab family.
436	A6QLE2|A6QLE2_BOVIN	RMND1 protein; RMND1	Reg	Required for meiotic nuclear division protein 1 homolog.
437	Q1RMI2|Q1RMI2_BOVIN	Ras homolog gene family, member G (Rho G); RHOG	Reg	Required for the formation of membrane ruffles during macropinocytosis. Required for the formation of cup-like structures during trans-endothelial migration of leukocytes.
438	Q3SYV3|OXA1L_BOVIN	Oxidase assembly 1-like protein OXA1L; OXA1L	OxPh	Required for the insertion of integral membrane proteins into the mitochondrial inner membrane. Essential for the assembly of cytochrome oxidase.

223

439	Q3SZ85|CB079_BOVIN	Uncharacterized protein C2orf79 homolog	X	?
440	Q32PA7|Q32PA7_BOVIN	Mitochondrial ribosomal protein L23; MRPL23	RiPS	Mitochondrial ribosome.
441	Q04232|Q04232_BVDV	Viral diarrhea virus CP1 putative helicase/protease (Fragment)	X	?
442	A6H751|FOLC_BOVIN	Folylpolyglutamate synthase, mitochondrial; FPGS	PMD	Tetrahydrofolate synthesis: ATP + tetrahydropteroyl-(γ-Glu)(n) + L-Glu = ADP + Pi + tetrahydropteroyl- γ-Glu)(n+1).
443	Q2TBI6|RM32_BOVIN	39S ribosomal protein L32, mito; MRPL32	RiPS	Mitochondrial ribosome.
444	A7MBF7|A7MBF7_BOVIN	LOC616332 protein; LOC616332	X	Hydrolase?
445	Q3SZA9|RM35_BOVIN	39S ribosomal protein L35, mito; MRPL35	RiPS	Mitochondrial ribosome.
446	Q32L67|GLRX2_BOVIN	Glutaredoxin-2, mitochondrial; GLRX2	Redox	Glutathione-dependent oxidoreductase for the maintenance of mitochondrial redox homeostasis. Catalyzes both glutathionylation and deglutathionylation of mitochondrial complex I, which in turn regulates the superoxide production by the complex. Overexpression decreases the susceptibility to apoptosis and prevents loss of cardiolipin and cytochrome *c* release.
447	Q0IIM2|ARL6_BOVIN	ADP-ribosylation factor-like protein 6; ARL6	PMD	May be involved in protein transport, membrane trafficking, or cell signaling during hematopoietic maturation.
448	Q0VCG0|LYRM4_BOVIN	LYR motif-containing protein 4; LYRM4	X	?

Abbreviations

2-D BN/ BNE	Two-dimensional blue native/modified blue native (DDM in cathode buffer) polyacrylamide gel electrophoresis
2-D BN/hrCNE	Two-dimensional blue native/high-resolution clear native polyacrylamide gel electrophoresis
2-D BN/SDS PAGE	Two-dimensional blue native/sodium dodecyl sulfate polyacrylamide gel electrophoresis
2-D IEF/SDS	Two-dimensional isoelectric focusing/sodium dodecyl sulfate polyacrylamide gel electrophoresis
A6	ATP synthase gene 6
A8	ATP synthase gene 8
ADP	Adenosine-5'-diphosphate
Ag+	Silver ion
APS	Ammoniumpersulfate
ATP	Adenosine-5'- triphosphate
b_H	High potential heme b
b_L	Low potential heme b
BNE	Blue native electrophoresis
BN-PAGE	Blue native polyacrylamide gel electrophoresis
bp	Base pair
BSA	Bovine serum albumin
CI	Complex I, NADH:ubiquinone oxidoreductase
CII	Complex II, succinate:ubiquinone oxidoreductase
CIII	Complex III, ubiquinol:cytochrome *c* oxidoreductase
CIV	Complex IV, cytochrome *c* oxidase
CNE	Clear native electrophoresis
COB	Cytochrome *b* of QCR
COR1	Core 1 protein of QCR
COR2	Core 2 protein of QCR
COX	Cytochrome *c* oxidase (complex IV) gene
Cox1	Subunit 1 of complex IV

Cox12	Subunit 12 of complex IV
Cox13	Subunit 13 of complex IV
Cox2	Subunit 2 of complex IV
Cox26	Subunit 26 of complex IV
Cox3	Subunit 3 of complex IV
Cox4	Subunit 4 of complex IV
Cox5	Subunit 5 of complex IV
Cox7	Subunit 7 of complex IV
Cox8	Subunit 8 of complex IV
Cox9	Subunit 9 of complex IV
CV	Complex V, F_1F_0-ATP synthase
Cyt b	Cytochrome b gene
Cyt *c*	Cytochrome *c*
CYT1	Cytochrome c_1 of QCR
DAB	Diaminobenzidine
DAPI	4'-6-Diamidino-2-phenylindole
DDM	Dodecylmaltoside
DMSO	Dimethylsulfoxide
DNA	Deoxyribonucleic acid
DOC	Sodium desoxycholate
ds	Double-stranded
dSDS-PAGE	Doubled sodium dodecylsulfate-polyacrylamide gel electrophoresis
DTT	Dithioerythreitol
EDTA	Ethylendiamine tetraacetic acid
ELISA	Enzyme-linked immunosorbent assay
EM	Electrone microscopy
ERMES	Endoplasmatic reticulum (ER)-mitochondria encounter structure
Es1	Bovine mitochondrial Es1 protein
ES1	Human, mouse, rat mitochondrial ES1 protein homolog
ESI-MS	Electrospray ionization mass spectrometry
FAD	Flavine-adenine-dinucleotide
$FADH_2$	Flavine-adenine-dinucleotide, reduced form
FMN	Flavine-mononucleotide
g	Acceleration of gravity

g/g	Gram per gram
GFP	Green fluorescent protein
HEPES	4-(2-hydroxyethyl)-1-piperazineethanesulfonic acid
HMG-box	High mobility group box
HMW	High molecular weight
HPLC	High-performance liquid chromatography
hrCNE	High-resolution clear native electrophoresis
iPALM	Three-dimensional photoactivated localization microscopy
IAA	Iodoacetamide
IMM	Inner mitochondrial membrane
kb	Kilobasepairs
kDa	Kilodalton
LC-MS/MS	Liquid-chromatography mass spectrometry
LILBID	Laser-induced liquid bead desorption
LM	Light microscopy
M	Molarity in mol/l
MALDI	Matrix-assisted laser desorption/ionisation
MDa	Megadalton
MELAS	Mitochondrial encephalomyopathy, lactic acidosis, stroke-like episodes
MERFF	Myoclonus epilepsy with ragged-red fibers
min	Minutes
Mops	3-(N-morpholino) propanesulfonic acid
MS	Mass spectrometry
mtDNA	Mitochondrial deoxyribonucleic acid
MW	Molecular weight
NAD^+	Nicotinamide-adenine-dinucleotide, oxidized form
NADH	Nicotinamide-adenine-dinucleotide, reduced form
ND	NADH dehydrogenase genes
NESM	One of the accessory subunit of CI
NHS	N-hydroxysuccinimide
NIBN	Native immunoblotting of blue native gels
nm	Nanometer
NMR	nuclear magnetic resonance spectroscopy

NR	Non-reliable
NTB	Nitrotetrazoliumblue
NUPM	One of the accessory subunit of complex I
$O_2^{\cdot-}$	Superoxide anion
OXPHOS	Oxidative phosphorylation
PAGE	Polyacrylamide gel electrophoresis
PALM	Two-dimensional photoactivated localization microscopy
PCR	Polymerase chain reaction
PE	Phosphatidylethanolamine
PEG	Polyethyleneglycol
Pi	Inorganic phosphate
PMF	Proton motive force
PMSF	Phenylmehylsulfonylfluoride
PVDF	Polyvinylidendifluoride
Q	Ubiquione
QCR	Ubiquinol:cytochrome *c* oxidoreductase (complex III)
QCR6	Subunit 6 of QCR
QCR7	Subunit 7 of QCR
QCR8	Subunit 8 of QCR
QCR9	Subunit 9 of QCR
QH_2	Ubiquinol
RIP1	Rieske iron-sulfur protein of QCR
ROS	Reactive oxygen species
rpm	Rounds per minute
rRNA	Ribosomal ribonucleic acid
RT	Room temperature
SAM	Sorting and assembly machinery of the mitochondrial outer membrane
SDS	Sodium dodecyl sulfate
SH mitochondria	Super-heavy mitochondria
SS	Start sample
ssDNA	Single-stranded deoxyribonucleic acid
STED	Stimulated emission depletion microscopy
TAE	Tris-acetate-EDTA

TEMED	Tetramethylethylendiamid
TIM	Translocase of the mitochondrial inner membrane
TOF	Time-of-flight
TOM	Translocase of the mitochondrial outer membrane
Tricine	N-(tri(hydroxymethyl)methyl)glycine
Tris	Tris-(hydroxymethyl)-aminomethan
tRNA	Transfer ribonucleic acid
V_D	ATP synthase dimer
w/v	Weight per volume
WT	Wildtype

List of Figures

List of Tables

234

VIII. Appendix II on CD

Original Mascot-search results of MS-identified proteins in this work are listed only on CD. The CD contains also some control experiments to section 4, Structure and composition of native nucleoids from bovine heart mitochondria (chapter IV, Results).

Curriculum Vitae

Personal informations

Name	Zibirnisa Kadeer*
Maiden Name	Omar
Place of Birth	Kashgar, Xinjiang, China
Date of Birth	March 1, 1978
Gender	Female
Family Status	Married, One child

Education

Since Sept. 2007	Ph.D. under the supervision of Prof. Dr. Hermann Schägger in the Molecular Bioenergetics Group, University of Frankfurt
Sept. 2006 – Aug. 2007	Student at the University of Mainz
Sept. 2001 – Jul. 2004	Master of Science, Department of Biology, Xinjiang University, Ürümqi, China
Sept. 1996 – Jul. 2001	Bachelor of Science, Department of Biology, Xinjiang University,Ürümqi, China
Sept. 1993 – Jul. 1996	No. 3 High School, Kashgar, Xinjiang, China
Sept. 1990 – Jul. 1993	No. 3 Middle School, Kashgar, Xinjiang, China
Sept. 1984 – Jul. 1990	No. 3 Primary School, Kashgar, Xinjiang, China

* My name was Wumaier Zibiernisha till 16.02.2012.